Fall 2021

Sex Differences and Neuroimmune Effects of Microglial Response in the Mesolimbic Reward Pathway in Nicotine Substance Use Disorder

Erin Leigh Anderson

Sex differences and neuroimmune effects of microglial response in the mesolimbic reward pathway in nicotine substance use disorder

by

Erin Leigh Anderson

Bachelor of Science
North Carolina State University 1994

Bachelor of Arts
North Carolina State University 1994

_____

Submitted in Partial Fulfilment of the Requirements

For the Degree of Doctor of Philosophy in

Pharmaceutical Sciences

College of Pharmacy

University of South Carolina

2021

Accepted by:

Jill Turner, Major Professor

Michael Wyatt, Committee Member

Douglas Pittman, Committee Member

Shannon Davis, Committee Member

Deanna Smith, Committee Member

James Chou, Committee Member

Tracey L. Weldon, Interim Vice Provost and Dean of the Graduate School

Dedication

To my partner in crime, Kevin, who inspires me to reach beyond anything I thought I could achieve, all my love always.

To my graduate school confidant, Dave, who knew what I was facing in graduate school and walked beside me while I went through it. I am forever thankful for the shared journey.

To my dad (notice I didn't call you Homer), who offered both sympathy and encouragement, whichever I needed at the time. You taught me that my learning disability meant I needed new tools but that I could find a way to succeed. I would not have made it this far without you.

To the Landing family, your support and love mean absolutely everything, and I am forever grateful.

To Dr. Roger Nicholl, the only neuroscientist I had heard of with learning disabilities, I am indebted to you for the encouragement.

Finally, to Wil Wheaton, who taught me in *Just a Geek* that a "9th grade Mrs. Lee" has no power over you, and for saying exactly what I'd like to say about it. It was a constant source of inspiration.

May my science stand as a testament to those with disabilities succeeding in STEM and may the knowledge be put to good use in the world.

Acknowledgements

I had not expected to return to graduate school when I moved to Columbia, but I found a collaborative science community that I wanted to become a part of. I appreciate the support and encouragement from Dr. Doug Pittman and Dr. Michael Wyatt when I applied to graduate school.

I am also exceptionally thankful for Dr. Jill Turner, who took a huge chance on a biochemist with a cancer background to join her lab. As a mentor she helped me through a steep initial learning curve and provided continual support amid all the peaks and valleys. I am quite appreciative of the support and knowledge shared by my USC Turner lab mates and colleagues, Dr. Luyi Zhou, Dr. Miranda Fisher, Dr. Adewale Adeluyi, and Dr. Rob Cole. I have learned so much from each of you. I also appreciate the PharmD students who rotated in our lab and at various points helped on this project; Micah Drew, Hunter Laag, Rachel Marsh, Andy Montgomery, and Josh Turowski.

When Dr. Turner moved to the University of Kentucky, I gained a lab of amazingly supportive colleagues, and I would like to thank them: Ms. Marissa Hessing-Alpers, Jack Keady, Anthony Marcelletti, Dr. Lilian Gonçalves Custódio, and Dr. Mohit Kumar.

I would also like to thank the mentor of my adopted lab home, Dr. Shannon Davis. I went for the microscopy, found a second home in the Biology Department as an

adoptee, and benefitted from amazing advice and support, all through a surprise pandemic.

To Ms. Elizabeth Thames, technical expert extraordinaire, sharing your knowledge with me helped me jumpstart my neuroscience. Your friendship and support continue to be a gift. Thank you.

From my graduate program cohort, Jake Massey, Danda Chapagai, and Dr. Qi Zhang, I cannot thank you all enough for the support, friendship, and laughter.

First and foremost amongst our collaborators is Dr. Georgia Hodes, who I want to thank for her expertise in individual differences and neuroimmunology. Your assistance and advice with obtaining my R36 grant was invaluable. I am also grateful for the assistance of Dr. Jennifer Rainville, also of Virginia Tech, and her expertise on the Luminex® assay system and analysis.

I want to thank Micah Johnston for his invaluable programming expertise.

I would like to thank and recognize Dr. Chad Beneker (USC) and Dr. Linnea Freeman (Furman) for their technical support and advice.

I would also like to acknowledge the Functional Genomics Core, COBRE Center for targeted Therapeutics, University of South Carolina, College of Pharmacy.

I appreciate the visual communication tools provided by BioRender.com for the generation of figures used throughout this dissertation.

I would like to acknowledge the data acquisition in the University of Kentucky Light Microscopy Core, which is supported in part by the Office of the Vice President for Research at UK. I would also like to recognize and thank my collaborators from UK, Dr.

James Pauly and Ms. Deann Hopkins for their assistance in autoradiography, Dr. Richard Charnigo for assistance in biostatistics, and Dr. Penni Black for her assistance in the human data aspect of the research and for aid in coordinating samples from The Kentucky Registry and Specimen Bank. I appreciate you all being part of the scientific community on this project.

Abstract

Smoking remains the leading cause of morbidity and mortality in the United States, with less than 5% of smokers attempting to quit succeeding. This is due to the unpleasant withdrawal symptomology, which includes affective symptoms, such as irritability, weight gain, anxiety, and severe craving among others, as well as the cognitive effects, such as difficulty concentrating. This low smoking cessation success rate is also thought to be due to the long-lasting sensitization of nicotinic acetylcholine receptors (nAChRs) leading to long-term neuroadaptations in the brain's reward system and alterations in synaptic plasticity that occur following chronic nicotine exposure and withdrawal. Glial cells, consisting of microglia, astrocytes, and oligodendrocytes, have recently emerged as active players in the development of dependence phenotypes. This is due to their roles in modulating neuronal functions and synaptic plasticity, both developmentally and postnatally [1-4], and increasing evidence indicates their role in drug dependence and its associated behavioral manifestations (see review [5]). There is also a role for neuroinflammation in drugs of abuse and the alterations of cytokines, small signaling proteins affecting cell signaling. Gaps remain in current literature as to the role of nicotine in altering the neuroimmune signaling within the brain's mesocorticolimbic reward circuitry. In addition, it is unknown how if nicotine affects the reward pathway of males and females differently. Utilizing morphological analysis and biochemical techniques for mRNA and protein analysis, we analyzed the role of

microglial cells as molecular driver of nicotine dependence and withdrawal-associated phenotypes. The sex differences found between males and females at the transcription and translational level within the various brain regions provide new insights to nicotine substance use disorder and may provide new pharmacological targets for future drug discovery.

Table of Contents

List of Figures

List of Tables

Chapter 1. General Introduction

1.1. Introduction

Globally, over 7 million premature and preventable deaths are attributable to tobacco smoking every year, and nearly 7% – about 480,000 of these deaths occur in the United States [6, 7], where 45 million Americans smoke and account for a total economic cost of approximately $289 billion (USD) [8]. Despite decreased smoking prevalence in the United States over the last decade, the disease burden attributable to tobacco smoking continues to rise. While this is due in part to population growth, it is also due to the high failure rate in quit attempts made by current smokers [9]. Even though cessation would decrease the risk of smoking-related disease and death and the majority (70%) of US smokers report a desire to quit smoking, nearly 80% have made serious quit attempts without success [9-11]. However, successful smoking cessation in the United States remains a major challenge with the success rate in quit attempts each year hovering at 8% [9, 10]. Former smokers are also vulnerable to relapse due to stimuli that these individuals associate with the rewarding effects of nicotine [9]. Studies in behavior and reward have made it clearer that nicotine and its withdrawal (during smoking cessation) have complex effects in the brain, affecting not only receptors for nicotine on neurons, but also glial cells, especially microglia, or the immune cells within the brain, and their signaling cascades. While this new information may lead to new therapeutic development, unknowns regarding sex differences in this withdrawal

response potentially complicate smoking cessation efforts. This introduction summarizes the molecular effects of nicotine in reward pathway circuitry and explores the role of glial cells in nicotine dependence.

1.2. Neurobiology of Nicotine Dependence

1.2.1. Nicotine and neuronal nicotinic acetylcholine receptors (nAChRs)

Following intake of nicotine and pulmonary venous absorption, nicotine will reach the brain in approximately 7 seconds [12], where it binds and activates nicotinic acetylcholine receptors (nAChRs). These ionotropic receptors are pentamers, composed of α and β subunits (α2–α10 and β2–β4) [13]. Neuronal nAChRs pentamers occur as homomeric nAChR subtypes, in which all subunits are the same (e.g., α7 nAChRs), or as heteromeric nAChR subtypes, which are a mix of different subunits (e.g., α4β2 nAChRs). The most abundant nAChR subtypes in the mammalian brain are the α4β2* heteromeric and the α7 homomeric subunit combinations. The varying subunit composition influences the pharmacological features of nAChRs and ultimately their responses to nicotine stimulation ([14, 15] and reviews [16, 17]). Activation of nAChRs opens a cationic channel, allowing passage of potassium, sodium, and calcium ions. Because nAChRs are preferentially located at the presynaptic terminal, their effects are primarily modulatory, rapidly increasing calcium and/or sodium channel conductance resulting in the release of nearly every major neurotransmitter ([18] and reviews [19, 20]).

For example, dopamine release is increased during nicotine administration, where it is proportional to the hedonic (affective rewarding response) to cigarette smoking in humans ([21] and review [16]), and dopamine concentrations are decreased

during nicotine withdrawal [22]. Other neurotransmitters modulated by nAChRs include γ-aminobutyric acid (GABA), β-endorphin, glutamate, serotonin, acetylcholine, and norepinephrine [23], which all have effects on behavior. The release of GABA or β-endorphins results in attenuation of anxiety and depression [24-26]. Acetylcholine release enhances cognition, while increased norepinephrine levels suppress appetite [27]. Glutamate levels are associated with learning and memory [28] and serotonin release is connected to mood change [29]. The ability of nAChRs to promote release of myriad neurotransmitters provides a functional basis for nicotine's modulation of a wide variety of behaviors, contributing to the difficulty of developing efficacious smoking cessation aids [19, 30, 31].

1.2.2. Nicotinic modulation of the dopamine reward pathway

The mesocorticolimbic pathway, also known as the dopamine reward pathway, is the critical neural pathway for reinforcing rewarding behaviors, including those behaviors underlying nicotine dependence (see reviews [20, 32, 33]). All drugs of abuse, including nicotine, are believed to enhance the effect of dopaminergic function in the mesocorticolimbic pathway. This is particularly true at dopaminergic nerve terminals arising from the ventral tegmental area (VTA) and terminating in the nucleus accumbens (NAc) – a key neural substrate of motivation and reward (see reviews [16, 32, 34, 35]). For example, nicotine activates the dopaminergic VTA-NAc pathway either (1) directly via stimulation of nAChRs on VTA dopaminergic terminals in the NAc or (2) indirectly

through stimulation of nAChRs on glutamatergic nerve terminals innervating dopaminergic neurons in the VTA (see Figure 1.1 and reviews [16, 36]).

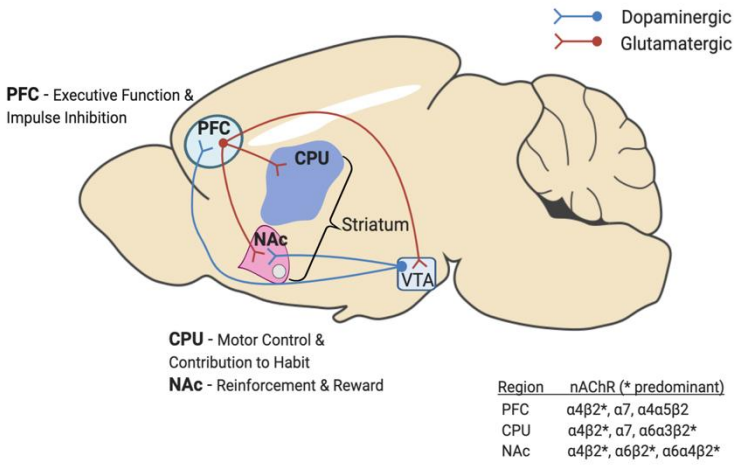

Figure 1.1. Mesocorticolimbic system with predominant nAChRs and dopaminergic and glutamatergic denotations.

This dopaminergic neurotransmission (increased firing of midbrain dopaminergic neurons) terminates in the NAc on the GABAergic medium spiny neurons, which account for ~95% of the NAc neuronal population [37]. Nicotine increases glutamate release by activating the α7 nAChR on presynaptic glutamatergic terminals leading to calcium-mediated glutamate release [38] as well as postsynaptic AMPA/NMDA receptor-mediated neurotransmission at glutamatergic–dopaminergic synapses in the VTA [39]. In addition to dopaminergic input, medium spiny neurons also receive glutamatergic input from the prefrontal cortex (PFC), where these dopaminergic and glutamatergic inputs interact physically at different sites on the dendritic spines of these GABAergic cells (review by [40] and [41, 42]). The PFC glutamatergic terminals also possess nAChRs, further increasing the complex actions of the nicotine in this circuit.

However, studies investigating how these interactions impact nicotine dependence have shown that inhibition of glutamatergic neurotransmission or stimulation of GABAergic neurotransmission attenuates nicotine intake and nicotine-seeking behavior in rodents [43]. Overall, these mechanisms of the mesocorticolimbic pathway are appropriated by nicotine and account for its rewarding effect.

1.2.3. Neurobiology of nicotine tolerance and withdrawal

Repeated exposure of nicotine leads to desensitization or ligand induced closure effects an upregulation of high affinity nAChRs like α4β2, via a debated mechanism [44] which is stoichiometrically predominated by the heteromeric (α4)2(β2)3 at about ~60% [45]. During the day, nicotine users maintain a fairly steady state of nicotine in the blood stream by their smoking rates balances desensitized receptor number and active receptors. The continual use of nicotine causes some nicotinic receptors to always be desensitized [46]. This desensitization leads to distinct neuronal adaptations, such as increased extracellular dopamine and decreased dopamine binding potential [47], major factors contributing to the development of nicotine tolerance and withdrawal effects following smoking cessation ([48-50] and reviews [51, 52]). Exposure to chronic nicotine produces tolerance to most of its aversive pharmacological effects such as sedation, nausea, anxiety, and tension but not its effects on memory and attention [53]. Furthermore, nicotine withdrawal symptoms manifest a few hours after discontinuation of nicotine use, and the collection of these negative symptoms during abstinence from nicotine is the major determinant preventing smokers from successful quitting [54]. In humans, symptoms of nicotine withdrawal encompass affective, cognitive, and somatic

domains. Affective symptoms include anxiety, depression, irritability, anhedonia, hyperalgesia, dysphoria, severe craving for nicotine, insomnia, increased appetite, and weight gain [53], while memory impairment and difficulty concentrating are cognitive manifestations [54]. Together, the biological basis of nicotine addiction can be regarded as a mix of positive reinforcement, such as mood enhancement, and avoidance of negative effects associated with nicotine withdrawal (see reviews [19, 20, 55]). Similar behavioral phenotypes are also observed in rodents that have undergone chronic nicotine exposure and withdrawal [56-59]. Rodent model investigation has highlighted the importance of multiple brain regions and their contribution to mechanisms underlying nicotine withdrawal-induced behavioral deficits, including the medial habenula [60], interpeduncular nucleus [61], central amygdala [62, 63], PFC [64, 65] and NAc [50, 58, 66, 67]. These studies have characterized the neuronal contributions to withdrawal-related behaviors, but the contribution of glial cell involvement needs greater study. Extra neuronal cells may provide an untapped therapeutic target for new front-line pharmacotherapeutic treatments.

1.3. Neuroimmunity and Nicotine

1.3.1. Smoking and the immune system

Nicotine is the major psychoactive component in tobacco that drives the neurobiological effects underlying the sustainment and reinforcement of tobacco smoking (see reviews [19, 68]). Smoke particles containing nicotine are inhaled into the lungs, where about 90% of nicotine present in the inhaled smoke is immediately absorbed into the pulmonary venous circulation [69, 70]. Smoking triggers an

inflammatory response in the lung, contributing to the development of lung cancer, chronic obstructive pulmonary disease (COPD), asthma, cardiovascular disease [71], and alteration of the immune response. The lung inflammatory response stimulates the release of proinflammatory signaling molecules known as cytokines [72, 73]. In tandem with these peripheral effects, the same inhalation of nicotine, as an acute dose, travels to the brain within seconds and binds to its receptor. This institutes changes in the immune response and can alter cytokine signaling, the acute nicotine also generates alterations in genes involved in mitochondrial function and synaptic transmission[74, 75]. It is this CNS response that this project will focus on.

1.3.2. Cytokines

Cytokines are a large family of small proteins, peptides, and glycoproteins that act as immune signaling molecules or chemical mediators to affect cell communication (see review [76]). This family is further divided into subdomains, such as chemokines (secreted chemoattractant cytokines), growth factors, tumor necrosis factors (TNF family), interferons (IFN α, β, and ɣ), and interleukins (secreted molecules and signal molecules secreted by leukocytes or white blood cells). Cytokines then bind to their target cognate surface receptors found on specific cell types to initiate specific cell signaling pathways. Cytokines target glia, among other cells, and can function as the targets as well as the producers of further downstream cytokine signaling. The cytokines can act at the same cell or a cell of a similar type (autocrine), may act locally (paracrine), or it can act within the system at an endocrine level. Cytokines mediate innate and

adaptive immune response as well as inflammatory response in both the peripheral and central nervous systems as immunoregulators and neuromodulators.

1.3.2.1 Cytokines in the healthy brain

In the healthy brain, cytokines are typically found at very low (pg/mL) levels. These low levels are sufficient to maintain homeostasis through immune surveillance, stimulate the HPA axis [77], regulate sleep [78], and affect brain plasticity and modulate learning (see review [79]). Studies of cytokines are heavily dependent on the region of the brain studied and the health of the brain, as cytokine levels change during psychological stress, aging, drug use, and disease.

1.3.2.2 Cytokines in disease or substance use

Cytokines within the brain may be affected by cytokines from the periphery, which may signal and/or transport across the BBB (for example TNF, interleukins 1 α and β, and 6 are transportable); brain cytokines may also be affected by neural signals, both synaptic signals and action potentials. Cytokines, and alterations in their levels, induce signaling cascades, both proinflammatory and anti-inflammatory signaling which help the microglia to respond to injury and disease and maintain homeostasis. It is when the inflammatory response becomes chronic that homeostasis is disrupted causing harmful effects. By analyzing cytokines in the reward system regions of the brain as well as the periphery, the signaling cascades and the subsequent changes may provide targets which could be used as potential biomarkers for predictors of disease or treatment, as well as for new targets for new therapeutics.

Two cytokines are being investigated as peripheral biomarkers for Alzheimer's Disease (AD), interleukin 12 (IL-12) and interferon gamma (IFN-γ). Increases in these cytokines in patients exhibiting high levels of amyloid beta, as characterized by positron emission tomography (PET) brain-imaging scans, correlated to low levels of cognitive decline, providing a minimally invasive method to monitor cognitive decline. It is hypothesized that this may be due to the proinflammatory cytokines in the periphery warding off infections before they contribute to the AD pathology [80]. Proinflammatory peripheral cytokines are also being investigated in major depressive disorder (MDD), which affects women approximately 1.7 fold higher than men (see reviews [81, 82] and [83]). Interleukin 6 (IL-6) peripheral levels are being investigated for correlation to suicidality [84]. During malnutrition induced inflammation and seizure susceptibility was connected to interleukin-1 beta (IL-1β) and its receptor [85], which may intensify inflammation. Other cytokines, such as CCL2, CLL3, and CXCL10, are also being investigated for their role in brain excitability [86]. Along with malnutrition, the cytokine fractalkine (CX3CL1) has been found to determine obesity susceptibility in male mice leading to weight gain on a high fat diet through decreases in mRNA expression of both CX3CL1 and its receptor CX3CR1 [87]. The next consideration is whether cytokines are only involved locally or whether cytokines in the periphery affect the brain.

1.3.2.3 Cytokines and the blood brain barrier

The blood-brain barrier (BBB) is a specialized CNS interface that enforces homeostasis and the brain itself was once considered immune privileged. Under normal conditions, cytokines typically do not cross the BBB, although small amounts of

interleukin 1 alpha(IL-1α), interleukin 1 beta (IL-1β), IL-1 receptor antagonist (IL-1ra), interleukin 6 (IL-6), and tumor necrosis factor-alpha (TNFα) may cross from the periphery via saturable transport systems [88]. It is also known that drugs of abuse alter the barrier by promoting inflammation and immune system dysfunction ([89, 90] and see review [91]). The barrier is also affected via alterations in the tight junction protein complex made up of integral membrane proteins, occludins and claudins, junction adhesion molecules, and both cytoskeleton and scaffolding proteins (see Figure 1.2 and review [92]).

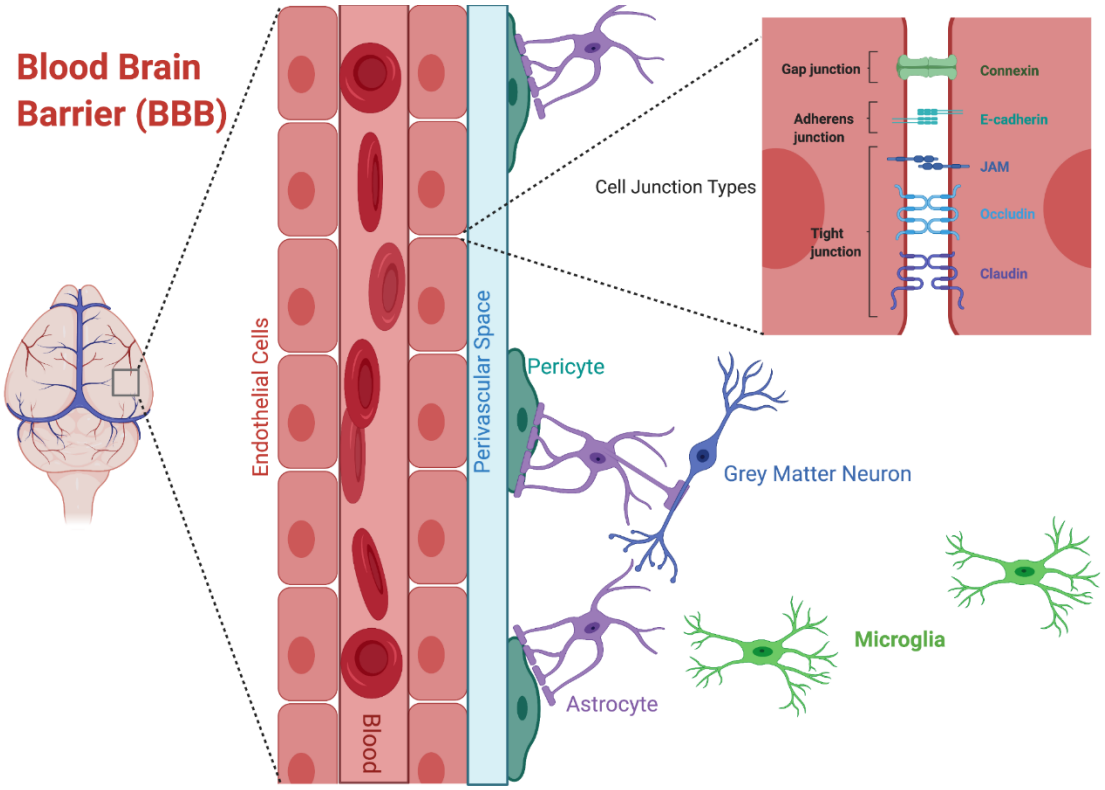

Figure 1.2. Schematic of the blood brain barrier noting the inter-endothelial connections and junctions denoted along with a sample of cells that communicate readily with the interface.

Chronic social stress has been found to affect BBB integrity by loss of claudin-5 (CLDN5) in male mice, allowing for more circulating peripheral proinflammatory

cytokines to cross and causing depression-like behaviors [93]. In disease, peripheral cytokines such as interferon alpha (IFNα) can cross the blood-brain barrier. IFNα, used to treat viral infections such as hepatitis C and various cancers, has been correlated to depression and cognitive impairment (see review [94]). In aging, sex differences in the BBB integrity were seen in non-demented subjects [95]. Drugs of abuse are known to affect the BBB and cytokines are being investigated as therapeutic targets to decrease neuroinflammation (see review [96]). Chronic nicotine, as a drug of abuse, is known to disrupt the BBB [97] and our lab has demonstrated that this effect is more prevalent in female than male mice (Kumar et al. unpublished data).

Understanding how the immune system, and any differences in treatment by sex, functionally contribute to chronic nicotine use and withdrawal may allow for development of possible biomarker assays and effective new therapeutics.

1.4. Novel Targets for Smoking Cessation: Glial Cells in Nicotine Dependence

Much of our mechanistic understanding of nicotine dependence pertains exclusively to neurons, particularly in the mesocorticolimbic neurocircuitry. However, while much less is understood regarding glial cells and their contribution to these processes, recent work has highlighted a prominent role of microglia in drug dependence. For example, recent studies have shown that microglial activation and microglia mediated inflammatory responses and alterations in proinflammatory cytokines following chronic nicotine treatment and withdrawal are major contributing factors for nicotine withdrawal-induced behavioral deficits [56, 98]. These findings suggest that impaired interplay amongst these brain cell-types as a consequence of

nicotine dependence may be a major determinant underlying high relapse rates among smokers.

1.4.1. Microglia: Morphology and physiology

Microglia are the resident innate immune cells in the brain, accounting for ~10% of the CNS cell population in the healthy brain (see review [99]), and are both self-renewing and long-lived [100, 101]. Microglia are highly branched, dynamic cells in their "resting" or surveilling state, with relatively rapid movement compared to other brain cell-types. Nimmerjahn et al in 2005 using two-photon microscopy found that resting microglia can surveil the entire brain within a few hours and that processes extend and retract at a rate of ~1.47 μm/min for surveillance increasing to ~1.8 μm/min when responding to insult [102]. These features, in addition to their fine motile processes, allow them to constantly scan the brain parenchyma to maintain homeostasis. Further, as CNS surveillance elements, microglia can sense and respond rapidly to extracellular signals. Developmentally, microglia are critical for pruning and phagocytosis to guide neuronal circuit development [103-105], as well as for brain sex differentiation (specifically masculinization [106]), and they may be involved in diseases such as schizophrenia, which exhibit developmentally reduced synapses [107]. Postnatally, microglial are important for promoting learning-dependent synapse formation [108] and modulate both special learning and social behavior [109]. In adult microglia, their process motility and neuronal monitoring of synaptic terminals is modulated by neuronal activity [110, 111] and use receptors such as P2Y(6) as a sensor for phagocytosis [112].

In terms of their developmental origin and functions, microglia are a unique population among the other brain cell-types. Like peripheral myeloid cells, microglia are derived from the mesoderm lineage, and are unlike other brain cell-types such as neurons and macroglia (astrocytes and oligodendrocytes), which are derived from neuroectodermal progenitors. Recent lineage-tracing studies provided additional characterization of microglia origin, showing they are derived from the yolk-sac progenitors – an embryonic origin distinct from that of the peripheral myeloid populations solving a decades long debate as to their origin [113-115] and populating the brain around E9.5. This discovery has been important in establishing microglia that have unique characteristics, such as their ability to self-renew and unique gene signatures allowing for the possibility of targeting the cells as therapeutic targets. Microglia cells contain the most numerous and varied receptor types in the CNS, expressing a variety of pattern recognition receptors (PRRs), scavenger receptors such as receptors for advanced glycation end-products (RAGE), and receptors for damage associated molecular patterns (DAMPs). These DAMPS, along with pathogen-associated molecular receptors (PAMPS), may also be recognized by Toll-like receptors (TLRs) and calcitonin receptor-like receptors (CLRs), many of which are upregulated in neuroinflammation [116-127]. This wide array of receptors (see Figure 1.3 inspired and modified from [128]) allow for microglia to surveil the brain with receptors to detect an abundance of possible brain insults and trigger the cell's activation.

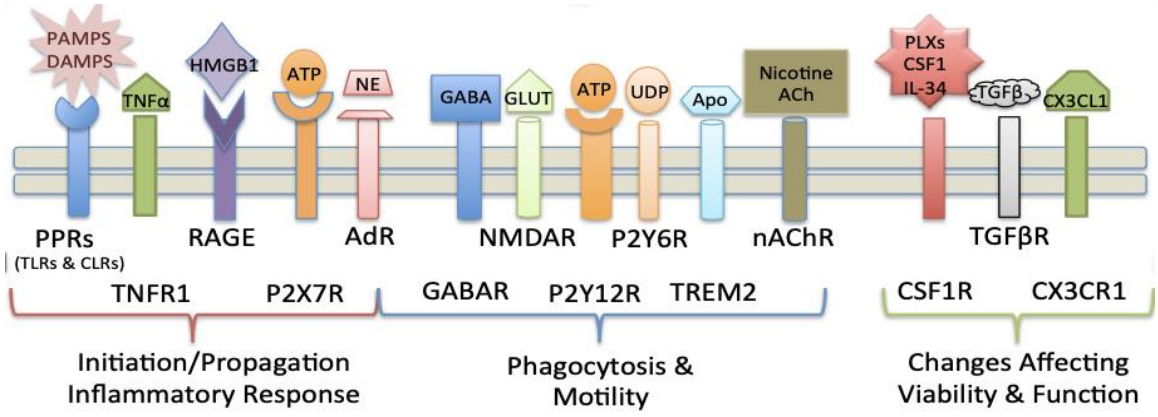

Figure 1.3. Schematic of a variety of receptors found on microglia with their cognate ligand or ligand class.

The microglia may be both a target and a major source of cytokines and chemokines in their local environment [129]. In a healthy brain, microglia rely on receptors such as CX3CR1 to detect neuronal damage by sensing the neuron's downregulation of CX3CL1 (see review [130]). Studies have shown microglial involvement through the IFNAR membrane receptor signaling and demonstrate that IFNα affects microglial morphology and pruning, verifying cytokine receptors on microglia as a target of endogenous cytokines [129, 131, 132].

1.4.1.1 Microglial activation and polarization

Microglia, as the primary immune cell of the brain, rapidly respond to insults to the brain and activate to secrete effector molecules such as cytokines and chemokines. Microglial release of cytotoxic and neuroprotective signaling factors allows the microglia to carry out a range of functions that support tissue health, affect cell-to-cell signaling, and limit damage from inflammation and injury [133]. As such, glial modulators are moving to the forefront as a potential therapeutic target for nicotine use.

Historically, microglia have been classified into a pro-inflammatory activation phenotype (M1) or an anti-inflammatory activation type (M2) [134]. This simplistic characterization of microglia activation phenotypes is based on the presence of particular cell surface molecules and the expression of specific sets of cytokines (see review [135]). For example, M1 microglia were once associated with mediators of proinflammatory response factors, such as tumor necrosis factor alpha (TNFα), interleukin-1-beta (IL-1β), interleukin 6 (IL-6), nitric oxide and reactive oxygen species (ROS) (see reviews [136-139] and [140, 141]). While M2 microglia were typified by mediators of repair and homeostasis, including interleukin-10 (IL-10), insulin like growth factor 1 (IGF1) and TGF-β (see reviews [135, 138]). However, evidence from more recent genome wide expression studies have refined and recharacterized microglial diversity (see review [142] and [133]) and evinced that this simplistic view of microglial phenotype does not sufficiently represent the intricate physiology of microglial cells [85-89]. Single cell sequencing has been instrumental in studying diseased or injured brains to identify whether an M1 and M2 population existed in a mixed population or a spectrum of morphologies and genetic phenotypes[135, 143-148]. It has been used in a cohort of 76,000 individual mice to characterize nine different distinct subpopulations with unique transcriptional and spatial signatures across age and disease [145] and datamining from these databases has elucidated more information on morphology and models of disease [149]. Genes which were found to be unique in homeostatic microglial gene signatures, such as TMEM119, have been combined with antibody panning for very specific microglial RNA seq in both mouse and humans [150]. Indeed,

transcriptomic, and proteomic data underscore the need for better functional understanding of these sub-categorizations.

In studying the physical microglial cell characteristics regardless of cell surface molecule expression, the cell morphology varies based on environmental signals. Early studies in non-diseased brain tissue revealed homeostatic microglia as cells with small, rounded soma (cell body containing the nucleus) with delicate branching processes (see review[151]). While in diseased tissue, the processes are retracted, branching is decreased, and the soma is enlarged, at times taking on an amoeboid appearance. This change in morphology is indicative of the microglial reactive response to environmental stimuli and reflects an “activated” morphology.

In addition to the phenotypic complexities of microglia, there are microglia which stably interact with brain capillaries, capillary-associated microglia (CAMs) [152]. It has also been demonstrated that microglia are largely heterogeneous across diverse neural circuits and brain regions [133]. For example, a recent study that examined microglial phenotypes among subcortical nuclei revealed that microglia across the basal ganglia are very diverse in terms of their density and morphology, metabolic and activation state, and transcriptome [133, 153]. This implicates local cues as a critical mediator of microglia phenotype across neural circuits (see review [154]). Further, regional microglial heterogeneity may also indicate that diverse functional phenotypes are required for the sustained integrity of the various local CNS environments.

1.4.1.2 Effect of nicotine on microglia

Microglia were once considered simply as support cells in the brain [129], but recent evidence demonstrates they are active players in both brain function and dysfunction [99]. In addition to their immune functions, microglia are critical elements in synaptic remodeling and plasticity [204], placing them as potential participants in the neuroplasticity underlying drug addiction. Nicotine and many other drugs of abuse can directly modulate microglial morphology and function via interaction with nAChRs on microglia.

Currently, the α7-nAChR is the only nAChR subtype reportedly found on microglia whose functionality is inhibited [155]. Studies in immortalized microglia lines and primary cell culture have reported α7-nAChR expression [156-160], and Shytle et al., observed α7 expression both in primary murine microglial cortical culture and brain slices [160]. The Shytle lab also examined the α7 microglial role in vivo and in vitro and described that physiologically relevant levels of nicotine had a protective or anti-inflammatory effect of nicotine in a model of evoked microglia activation. This activation was initiated following treatment with a neuroinflammatory substance, lipopolysaccharide (LPS), resulting in the release of TNFα. This release of the anti-inflammatory TNFα effect could be attenuated by adding the nAChR α7 selective nicotinic antagonist α-bungarotoxin. These anti-inflammatory effects were subsequently confirmed using both methyllycaconitine (MLA), another α7-nAChR antagonist, and NS6740, a very weak α7 partial agonist [161-163] demonstrating the TNFα release was evoked by LPS through the activation of α7 nAChRs and supporting the role for nAChRs

for cognitive impairments[164]. This neuroprotective effect on microglia activation was also observed in rat models of ischemia, where nicotine treatment prevented both microglial proliferation and thrombin-induced microglial activation [165, 166]. Interestingly, this neuroprotective effect of nicotine can be observed in vivo reducing microglial activation in adult brains but increasing microglial activation in the adolescent brain [167].

In addition to playing a role in nicotine-mediated neuroprotection, microglia's direct involvement in nicotine withdrawal-related behaviors has been demonstrated in two recent in vivo studies in rodents [56, 98]. Adeluyi and colleagues demonstrated that withdrawal from chronic nicotine treatment induced microglial morphological changes in the ventral striatum or NAc, promoting microglial activation via Nox2-mediated increases in ROS [56]. Furthermore, these activated microglia released pro-inflammatory cytokines (TNFα and IL-1) in the NAc, which were correlated with exaggerated withdrawal behavior, and are absent in mice with microglial depletion by the PLX5622 compound (a colony stimulating factor receptor 1 (CSFR1) inhibitor that is requisite for microglial survival). When microglia were depleted in the study, the anxiogenic response of mice, spending less time in the center of open field arena, was reverted by loss of the microglia. These findings were complementary with a study from Saravia et al. [98], which linked nicotine withdrawal- induced cognitive deficits to microglial activation that were prevented by treatment with an anti-inflammatory agent.

While microglia may actively contribute to nicotine dependence, research investigating the role of microglia in nicotine dependence is still in the early stages.

Because of their role in immune surveillance and inflammation, microglia potentially represent an untapped opportunity to develop more potent and specific drugs to treat nicotine dependence and withdrawal.

1.5. Conclusion

There are currently only three FDA-approved first-line smoking cessation medications: Nicotine Replacement Therapy (NRT), Chantix (varenicline tartrate) and Zyban (bupropion hydrochloride); see review and clinical practice guidelines [168, 169]. Interventions such as nicotine specific vaccines continue in the research and development pipeline [170-172], though to date clinical trials have failed to show efficacy in vaccine vs control. Despite years of work in behavioral intervention strategies and pharmacological intervention with smoking cessation medications, a large population of smokers who attempt to quit still fail. This may be largely attributable to the inability of current smoking cessation therapies to address previously unaddressed critical aspects of nicotine dependency. For instance, the three FDA-approved smoking cessation medications were each developed to mechanistically target neuronal nAChRs, neglecting the possible contributions of targets on glial cells like microglia. To advance nicotine dependence research, studies exploring microglia, both form and function, will be explored in detail in this dissertation. In the long term, microglia, and the inflammation cascade from their cytokines, may represent an untapped therapeutic avenue for smoking cessation.

Chapter 2. Experimental Design and Microglial Morphology in the mesolimbic system

2.1. Introduction

Nicotine is the primary psychoactive component of tobacco and the compound that is responsible for the rewarding effect in the brain. Nicotine dependence is a chronic and relapsing use disorder where 50-75% of smokers who attempt to quit will relapse in the first month [173, 174]. To date, a large population of smokers is unable to quit with current cessation therapies that are mostly centered on nAChR receptor antagonists (outside of bupropion) and may not be addressing critical aspects of nicotine dependence. As nicotine levels decrease within the brain during smoking cessation, dopamine levels are reduced along with other neurotransmitters and withdrawal symptomology sets in. Repeated exposure to nicotine the development of both tolerance and the subsequent nAChR upregulation, along with neuronal adaptations all lead directly to nicotine withdrawal symptomology that makes quitting difficult [16, 44, 48]. Nicotine has been reported to have neuroprotective effects against neurodegeneration in diseases such as Parkinson's Disease (PD) and Alzheimer's Disease (AD) [175, 176]. Thus, withdrawal from nicotine could, in itself, be inflammatory to the brain. The fact that increased inflammation is an aspect in many pathological states which affects women more than men (depression, AD, autoimmune disease), the need for adding sex as a biological variable in the experimental design becomes judicious.

Microglial inflammation during chronic nicotine withdrawal has been linked to induced morphological changes in the ventral striatum, or nucleus accumbens, portion of the mesolimbic reward pathway [56]. As the brain's resident immune cell, these changes in morphology may be indicative of microglial activation and alterations in cytokines inducing a neuroinflammatory event. The cytokines and products of their signaling cascades may provide a new non-nicotinic receptor approach to discovering a new therapeutic that could be beneficial in nicotine withdrawal.

2.2. Materials and Methods

2.2.1. Animal use

An initial pilot study used adult male B6/129 F1 mice purchased from Taconic Biosciences (#B6129; Rensselaer, NY, 7 weeks of age; 17-28 g and allowed a week to acclimate). As per a change in University of South Carolina Animal Care and Use Committee guidance, adult male and female B6/129 F1/J mice were purchased from the Jackson Laboratory (#101043, Bar Harbor, ME, 7 weeks of age; males 22.9–30.8 g and females 17.2-24.4 g, one week acclimation after arrival). B6/129 F1 mouse strain is a hybrid of C57BL/6 and 129SvEv strains that are commonly used for the development of knockout mouse models; therefore, information regarding nicotine response in a variety of behaviors in this strain is of value for future studies aimed at investigating underlying genetic mechanisms. The F1 generation of mice provides hybrid vigor, minimizes founders' effects and genetic drift and, as shown in previous studies, provides more and more reliable reproducibility across laboratories [177]. Mouse work was done in 3 stages: first, the pilot experiment; second, the first ½ of scaled experiment performed at

the University of South Carolina; third, the final (second) ½ of the scaled experiment performed at the University of Kentucky. Mice were sorted by sex then by weight in ascending order and randomly assigned to treatment conditions (chronic nicotine with subgroups of 24Hr WD and 48Hr WD and control saline group) to ensure random cage assignment. Subjects were group-housed in a colony room where they were maintained on a 12-hour light/dark cycle with lights on at 0700 and ad libitum food and water access. This was in accordance with the University of South Carolina Animal Care and Use Committee and under guidance of the University of Kentucky Animal Welfare Assurance.

2.2.2. Osmotic drug delivery and administration

Doses of (-)-nicotine tartrate (MP Biomedicals, Solon, OH, USA) are reported as free base weight. The (−)-nicotine tartrate was dissolved in sterile 0.9% saline solution and then infused subcutaneously via osmotic minipumps (Alzet model 2002; DURECT Corporation, Cupertino, CA, USA) at a dose of 18 mg/kg/day for 14 days. This dose, based on prior work [58, 178, 179] and corresponds to a concentration similar to human smokers consuming 17 cigarettes a day on average ~0.31μM [70] in the mouse and is indicative of nicotine dependence. The nicotine concentration was adjusted to compensate for differences in mice body weight. The nicotine solution in the osmotic minipumps was not adjusted from the acidic at pH 4, as neutralized nicotine solutions are known to become unstable and degrade at a faster rate [70] and the minipumps deliver only ~0.5ul of solution/hour without negative consequences to the animal.

Withdrawal groups were assigned in the initial Control animals were implanted with osmotic minipumps filled with only sterile 0.9% sodium chloride solution.

2.2.3. Osmotic minipump surgeries

Before the start of surgery, mice were anesthetized with isoflurane/oxygen mixture (1–3%), and osmotic minipumps were inserted subcutaneously using aseptic techniques. Minipumps were placed parallel to the spine at shoulder level with the flow moderator directed away from the wound. The surgical wound was closed with 7-mm stainless steel wound clips (Reflex; Cellpoint Scientific, Gaithersburg, MD) and mice were left to recover on the warmed recovery pad before returning to their home cages. After 12-13 days of chronic administration of either saline or nicotine via osmotic minipumps, nicotine withdrawal syndrome was precipitated in mice withdrawal groups or saline controls similar techniques were used to remove the osmotic minipumps (48-hour withdrawal group on day 12, and 24-hour withdrawal on day 13). Animals in the chronic nicotine or chronic saline treatment groups underwent sham surgery, where an incision was made and restapled without removal of the pump.

2.2.4. Tissue processing

At the end of treatment, animals were sacrificed, blood was collected, and one hemisphere of the brain was collected for immunohistochemistry (IHC). The second brain half was microdissected for the appropriate brain regions (cortex, mPFC, CPU, and NAc and other regions for future experiments) for biochemistry; all tissue was frozen on dry ice and stored at -80°C until further use.

One brain hemisphere from each mouse was collected and fixed overnight in 4% paraformaldehyde (PFA) in phosphate-buffered saline (PBS) at 4°C. Fixed brains were cryoprotected stepwise first in a 15% sucrose solution overnight, then 30% sucrose solution overnight, followed by a second 30% sucrose incubation overnight all at 4°C. Post cryoprotection, the single brain hemispheres were stored at -80°C until sectioning. Before sectioning, the single brain hemispheres were moved to -20°C overnight, and then 45 µM coronal sections were prepared using OCT and a cryostat microtome (Leica, Wetzlar, Germany). Systematic sampling of sections was taken from ~Interaural 5.48mm/Bregma 1.69mm [180], which contains the cingulate cortex 24a, 24b, and 25 as well as the CPU and NAc core and shell. Slicing continued through to ~Interaural 4.52 mm/Bregma 0.73mm with each successive slice stored into 1 of 6 wells of a standard 12 well plate in a phosphate buffered saline (PBS) + 0.01% sodium azide solution such that each well contained 1/6th of the region of interest. The plate was covered with a lid and sealed with parafilm until IHC processing.

2.2.5. Receptor binding

Dissected cerebral cortex samples of approximately 10 mg (~400 ug) was homogenized in 50 mM Tris–HCl (Sigma-Aldrich) buffer, pH 7.4 at 24°C, and centrifuged twice at 30,000 × g for 15 min in fresh buffer at 4°C. After centrifugation, membrane pellets were resuspended in fresh buffer and transferred to tubes containing a saturating concentration (2 nM) of (+/-)Epibatidine, [5,6-Bicycloheptyl-3H] ([^{3}H]EB, PerkinElmer, Waltham, MA), an agonist with high-affinity binding to all heteromeric nAChRs extremely low nonspecific binding to muscarinic and serotonin 5-HT3 receptors.

The homogenates in [^{3}H]EB and Tris buffer (pH 7.4) were incubated for 2 hours at 24°C. Post incubation, vacuum filtration over 0.5% polyethyleneimine (MilliporeSigma, Burlington, MA) pretreated Whatman GF/C glass fiber filters mounted on a Brandel Cell Harvester (Brandel, Gaithersburg, MD) separated the bound receptors from free ligand. A liquid scintillation counter was used to count the filters. Nicotine at 300 uM concentration was present in the solution to determine the nonspecific binding. Specific binding was defined by subtracting the difference between total binding and nonspecific binding. The specific binding was then normalized to the total protein in the binding assay as measured by Pierce™ BCA Protein Assay Kit (Thermo Fisher Scientific, Waltham, MA) following manufacturer's instructions.

2.2.6. Immunohistochemistry for ionized calcium-binding adapter molecule 1 (IBA1)

IHC was performed on the cell slices above in one of two formats, "in-well" or "on-slide," as chosen by the degree of curling of the tissue. If the brain slice was very flat with little curling, the "in-well" method was used. If the brain slice was very curled, then the "on-slide" process was used.

2.2.6.1 In-well IBA1 IHC

Cryosectioned 45 uM slices were transferred via eyelash brush (an eyelash melted into a glass Pasteur pipette) into 12-well, 74 μM mesh Netwell™ plates (Corning Cat. 3477, Corning, NY) containing 0.3% hydrogen peroxide in PBS. After 15 minutes, the plates were transferred to 12-well plates containing PBS to rinse, 3 x 10 minutes, and placed in 5% NGS block (5% normal goat serum (MilliporeSigma Cat. G9023, Burlington, MA), 0.1% Triton X-100, in PBS) for 2 hours at room temperature (RT). Tissues were then

moved to wells containing 2.5 mL of rabbit anti-IBA1 (C-terminus) primary antibody overnight (1:1000; Wako Chemicals USA. Cat. 019–19741, Richmond, VA) in 3% NGS block (as 5% NGS above but containing only 3% normal goat serum). Plates were placed at 4°C overnight. Tissues were rinsed, 3 by 10 minutes, in PBS + 0.1% Tween 20 (PBST). This was followed by a 2-hour incubation in a biotin-sp-conjugated goat anti-rabbit secondary (1:500, Jackson ImmunoResearch Laboratories Cat. 111-065-003, West Grove, PA, USA) in PBST at RT and a PBST wash (3 x 10 minutes). The signal was amplified with the avidin/biotinylated complex Vectastain ABC HRP method (2 drops each A & B reagent into 5 mL PBST) (Vector Laboratories Cat PK-4000, Burlingame, CA) for 1.5 hours at RT and washed 3x 10 minutes in PBST. ImmPACT VIP peroxidase substrate (Vector Laboratories Cat SK-4605, Burlingame, CA) was used for 1.5 hours at RT followed by a 3X 10-minute PBST wash. Tissues were transferred out of the Transwell™ plates via eyelash brush and placed in VIP peroxidase substrate (3 drops each reagent in 5ml diluent using 1.5 ml per well) and incubated until IBA1 is stained purple (7-15 minutes). The reaction is stopped by transferring the tissue to a plate containing PBS alone (3x 5-minute PBS wash). Tissues were then moved to floating solution (30% ethanol in PBS) onto Histobond or Superfrost Plus glass slides, dried slightly, and sealed with 70 μl Prolong Gold antifade mounting medium (no DAPI) (ThermoFisher Scientific Cat. P36934, Waltham, MA) and stored in the dark at RT until imaging.

2.2.6.2 On-slide IBA1 IHC

Cryosectioned and curled 45 uM slices were transferred via eyelash brush into floating solution onto Histobond or Superfrost Plus glass slides (3 slices per slide) and dried for 5-10 minutes at RT (3 slices per slide). Slides were transferred to a Coplin jar containing 4% paraformaldehyde (PFA made from 16% stock vials in PBS) for 10-minutes. Slides were transferred to a new Coplin jar with PBS and washed 3X for 10-minutes each. Tissues were quenched in 0.3% hydrogen peroxide solution in PBS for 15 minutes and washed in PBS 2X for 5-minutes. The slides were transferred to a glass beaker on a heat block containing barely boiling 10mM citrate buffer for 15 minutes. The beaker was moved to RT and allowed to cool for 20-minutes then slides transferred to PBS for 2X 5-minute washes. Slides were removed, dried on the edges with a Kimwipe™, and a pap pen used to draw a hydrophobic barrier around the tissues. The tissues were blocked with a solution of 5% BSA, 5% normal goat serum, and 0.5% Triton X-100 in a humidified chamber for 2 hours at RT.

Post incubation, the slides were tilted, hydrophobic barrier replaced as needed, and primary antibody added to the tissue. The rabbit anti-IBA1 (C-terminus) primary antibody (1:1000; Wako Chemicals USA. Cat. 019–19741, Richmond, VA) was prepared at 1:1000 in Tween block (5% BSA, 5% normal goat serum, and 0.5% Tween-20) and enough added to fill the slide, and incubated in a humidified chamber overnight at 4°C. The next day, slides were washed 3X 10-minutes in PBST (Coplin jar), and placed back into the humidified chamber, replacing hydrophobic barrier as needed by pap pen. Secondary antibody, biotin-sp-conjugated goat anti-rabbit secondary (1:500, Jackson

ImmunoResearch Laboratories Cat. 111-065-003, West Grove, PA, USA), in Tween block was added directly to the slides using enough to cover the tissue and incubated for 2 hours at RT. Slides were washed 3X 10-minutes in PBST and the signal amplified with the avidin/biotin complex Vectastain ABC HRP prepared as above and added for 1.5 hours in a humidified incubator at RT. Slides were washed 3X 10-minutes in PBST and VIP peroxidase substrate prepared as above and added to the tissue on the slides and allowed to react until the IBA1 is a deep purple stained color (6-12 minutes). The reaction is halted by a 3X 5-minute wash in PBS, the slides dried, 70 μl Prolong Gold antifade mounting medium (ThermoFisher Scientific Cat. P36934, Waltham, MA) and stored in the dark at RT until imaging.

2.2.7. Blinding and randomization of slides for image analysis

Slides of IBA1 stained mouse coronal slices, by both methods, were randomized using numbers between 1-1000. Labels containing the newly randomized blinded number were created and applied by an impartial researcher. Slides were unblinded after analysis was complete (as described below).

2.2.8. Stereology

Slides were sent to the UK Light Microscopy Core (University of Kentucky, Lexington, KY) for imaging. The tissue slides were digitalized using an AxioScan.Z1 light-microscopic slide scanner (Carl Zeiss Microscopy GmbH). They were imaged at 40X using default brightfield protocols (objective Plan-Apochromat 40X/0.95 Korr M27) with a Hitachi HV-F203SCL camera and saved as individual files labelled with blinded label notation. Digitized images were explored with Zen Blue 3.0 software (Carl Zeiss

Microscopy GmbH). A digitized file was opened and each slice compared to the mouse brain atlas to identify ROIs which were then digitally outlined [180]. The image was magnified until the scale bar was at 100 microns, a box drawn around a representative portion of microglia within the area, and the image exported as an individual tif file. The image was further magnified to 20 micron and 5 random microglia were selected and exported individually as tif files for morphology analysis. A total of 5 mice per treatment group per sex (40 total) were included in the tif analysis.

2.2.8.1 Microglial density manual cell counting

The density tif files from above, one per coronal slice or 3 per slide (for 40 mice), were analyzed by each of 3 separate researchers. This was done using FIJI software with the cell_counter.jar plugin where individual microglia (as defined by visible soma and connected processes on a single plane) were counted [181, 182]. The data was recorded, and the median count calculated with the area as cells/mm^2.

2.2.8.2 Individual microglia tracing in Neurolucida

The individual 2D microglia tif files were imported into Neurolucida 360 version 2020.1.1 neuron tracing software (MBF Bioscience, Williston, VT). Upon import, the 40X digitized images were scaled to 0.111 x 0.111 μM/pixel. The microglia were traced using the “cell body” tracing for the soma and “dendrite” tracing for the processes. The soma and branches for each individual microglia were manually outlined to construct a skeletal representation of the cell (saved as a dat file). Neurolucida Explorer version 2021.1.1 (MBF Bioscience, Williston, VT) was used to batch analyze the dat files for the neuron summary, which calculates the perimeter of the soma, and length of the

processes as well as their complexity, and the number of branches and endings. Batch analysis was also used for an XY Convex Hull analysis for the approximate perimeter of the microglial area, as if a ribbon or rubber band was wrapped around the distal points of the processes. This data was transferred to GraphPad Prism for further analysis.

2.2.9. Data analysis and statistics

Statistical analysis was performed and graphed in GraphPad Prism 9 for macOS version 9.2.0 (GraphPad Software, LLC., San Diego, CA) with results presented as mean +/- SEM. The GraphPad online calculator was used to Grubbs' test or extreme studentized deviate (ESD) (https://www.graphpad.com/quickcalcs/grubbs1/) for each treatment condition removing at most 1 outlier per group based on the Alpha=0.05. Receptor binding data were analyzed by two-way ANOVA using treatment and sex as primary variables. Post hoc analysis for male and female comparisons was completed using Šídák's multiple comparisons test post hoc analysis and treatment while differences within sex were completed using Dunnett's multiple comparisons test post hoc analysis. Microglial density analysis between male and female data (saline control) was done by parametric unpaired two-tailed t-test. Microglial density data was analyzed by two-way ANOVA using Tukey's multiple comparisons test post hoc analysis to compare across all conditions or within sex and Šídák's multiple comparisons test for differences between males and females. Microglial morphology data was analyzed by two-way ANOVA for main effects of sex and treatment. Tukey's multiple comparison test was used as a post hoc when comparing all the data as a set or comparing within

sex. Šídák's multiple comparisons test was used for post hoc when comparing males and females.

2.3. Results and Discussion

2.3.1. Animal model of nicotine dependence

Rodents have long been a model for studies of nicotinic receptors (nAChRs) and nicotine use disorder. In the early 90's, scientists began to question whether an acute dose of nicotine was as translational a model as a chronic dosing would be, given that smokers and tobacco users maintained a regular usage schedule throughout a day. Dependent smokers self-maintained a fairly constant blood plasma level of nicotine (between 20-50 ng/ml) during waking hours, with a half-life of 4-10 minutes and an elimination half-life of 120 minutes [183]. Fung and Lao of the University of Nebraska Medical Center & Creighton University School of Medicine, with the Seidler Pharmacology lab at Duke University, were some of the earliest adopters of an osmotic minipump model for dosing of nicotine in rats [184-187]. These studies validated and recapitulated the upregulation of nAChR binding sites in brain regions such as the striatum, and specifically the ventral striatum or nucleus accumbens, the midbrain, hippocampus, and hypothalamus and regions similarly seen in humans. Chronic nicotine has also been shown to produce long-term changes in the mesolimbic reward circuitry related to nAChR level alterations [49, 188, 189]. Rodent models of nicotine withdrawal symptomology have been successful in recapitulating affective withdrawal symptoms such as anxiety-like behavior and depressive-like symptoms (open field test and novelty induced hypophagia) [56, 58, 190].

With our model and delivery method well validated, see Figure 2.1 (A), the nicotine dose is a crucial component. In their seminal 2007 paper, Dr. Shannon Matta and colleagues created a guideline of nicotine dose selection for in vivo research considering the pharmacokinetics and pharmacodynamics of nicotine. This is critical, as mice, for example, have a much higher metabolism of nicotine than humans, necessitating a higher dosage in rodents to achieve similar human plasma levels. Our dose of 18 mg/kg/day in a continuous osmotic minipump system has effective face validity with clinical withdrawal symptomology and produces a blood plasma level similar to a pack a day smoking habit [58, 70, 178, 179]. The 24-hour and 48-hour withdrawal time points were used as translational to symptomology seen in human smoking cessation where 80% of smoking cessation attempts fail in the first 24 hours and had increased stress induced analgesia at 48 hours [10, 191].

2.3.2. Validation of animal model by receptor binding up-regulation assay

Chronic nicotine has been shown to upregulate $a4b2$ nAChRs and increase dopamine release via the dopaminergic terminals [49, 59, 175, 192-194]. To validate our model, we evaluated heteromeric nAChR regulation via tritiated epibatidine, [3H]epibatidine, binding following cessation of chronic nicotine to verify upregulation of nAChRs. Epibatidine, a toxic alkaloid originally isolated from poisonous tree frogs, binds with high affinity (Kd ~1-10 pmol) to all heteromeric nAChRs [58, 194-196]. We use the cortex tissue for the assay, a tissue well-described as having chronic nicotine receptor upregulation in human and mouse [197-199]. In Figure 2.1 (B), the validation for the chronic nicotine mouse model can be seen by the upregulation of tritiated epibatidine

binding in the nicotine, 24Hr WD, and 48Hr WD groups as compared to saline in both males and females.

(A) Experimental design of osmotic minipump implantation with saline or 18 mg/kg nicotine for 14 days with subgroup receiving surgical pump removal and a 24- and 48-hour withdrawal timepoint and tissue collection. (B) Homogenate-binding in cortex tissue with saturating concentration of [^{3}H]epibatidine ([^{3}H]EB, 2 nM) as analyzed by two-way ANOVA with treatment and sex as main effects and Šídák's multiple comparisons

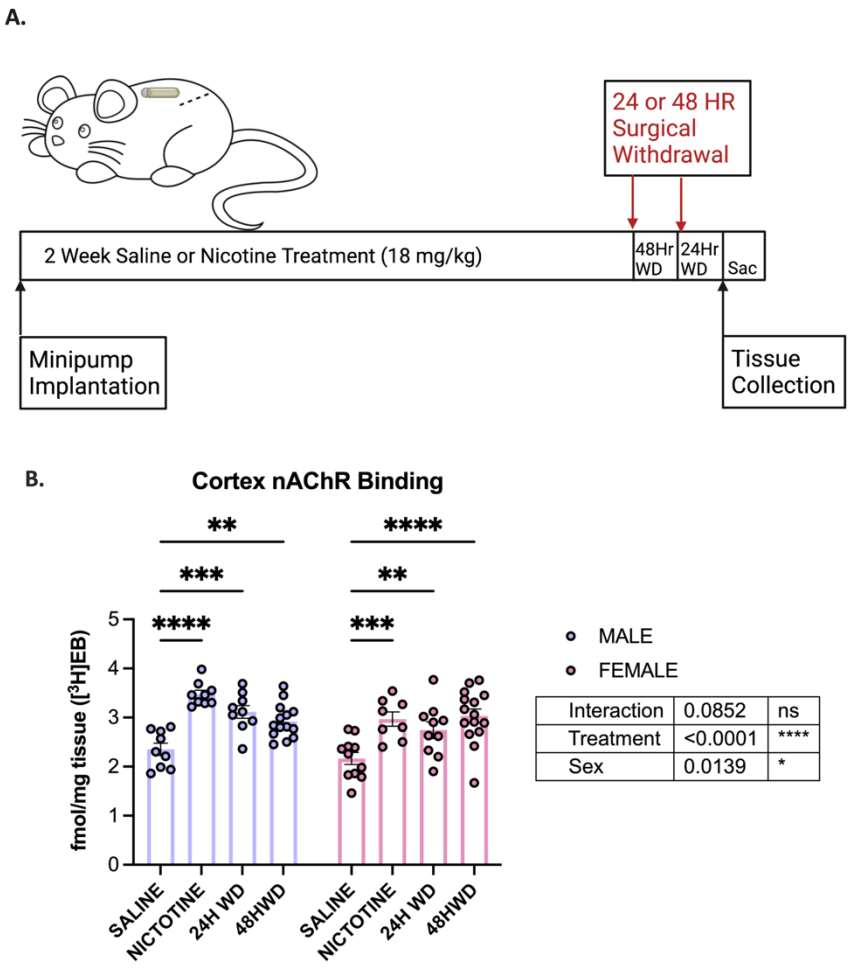

Figure 2.1. Chronic nicotine administration, experimental model, and validation.

test for post hoc analysis within sex, *$P < 0.05$, **$P < 0.01$, ****$P < 0.0001$, n =8-15. There are significantly higher levels of [^{3}H]EB binding relative to saline-treated controls, which persisted in the 48Hr WD group.

2.3.3. Neuroinflammation, nicotine withdrawal, and microglial morphology

Microglia are the neuroimmune cell of the brain, making up ~10% of the cells; as such, their primary role is to surveil the brain, covering its entirety every few hours with its numerous ramified processes. This surveilling state is often referred to as the "resting state," though this is a misnomer when considering its activity and the fact that they are key cellular mediators of neuroinflammation [200]. As noted in Figure 1.3, the microglia have a plethora of receptors capable of detecting multiple classes of signals caused by environmental changes. The microglia become "activated" by environmental cues from insult such as drugs, pathogens, or disease. This response triggers the activation and may lead to increased microglial propagation, density alterations, increased motility, and phagocytosis, leading to migration of microglia to the site of damage and altering their gene expression to secrete various chemokines and cytokines [99]. Chronic inflammation and microglial activation is also implicated in the aberrant release of neurotoxic factors like tumor necrosis alpha, nitric oxide, and reactive oxygen species which can drive neuronal damage [201]. Many drugs of abuse, such as alcohol, cocaine, and methamphetamine, have been shown to activate microglia and exhibit pro-inflammatory cytokines [200, 202, 203]. In analyzing our chronic nicotine and withdrawal model, nicotine tends to exhibit neuroprotective effects, and the "drug of abuse" is then withdrawal from nicotine. It is important to examine microglia not only

for their link to neuroinflammation and immune response but also for their role in neuroplasticity. Substance use disorders affect neuroplasticity and remodeling of neurocircuits, and as microglia are critical constituents in these processes, they are an important contributor to molecular changes found in the reward pathway [109, 204].

The activated microglia alter their morphology where long complex branched processes become foreshortened and retracted, sometimes to the point the cell is amoeboid in shape, and the size of the soma, the cell body, becomes increased (see Figure 2.2). While microglial morphology changes can be indicative of alterations in the neuroenvironment due to outside environmental changes, the local environment of a microglial cell establishes and maintains region-specific microglial phenotypes making analysis within our region of interest essential [133].

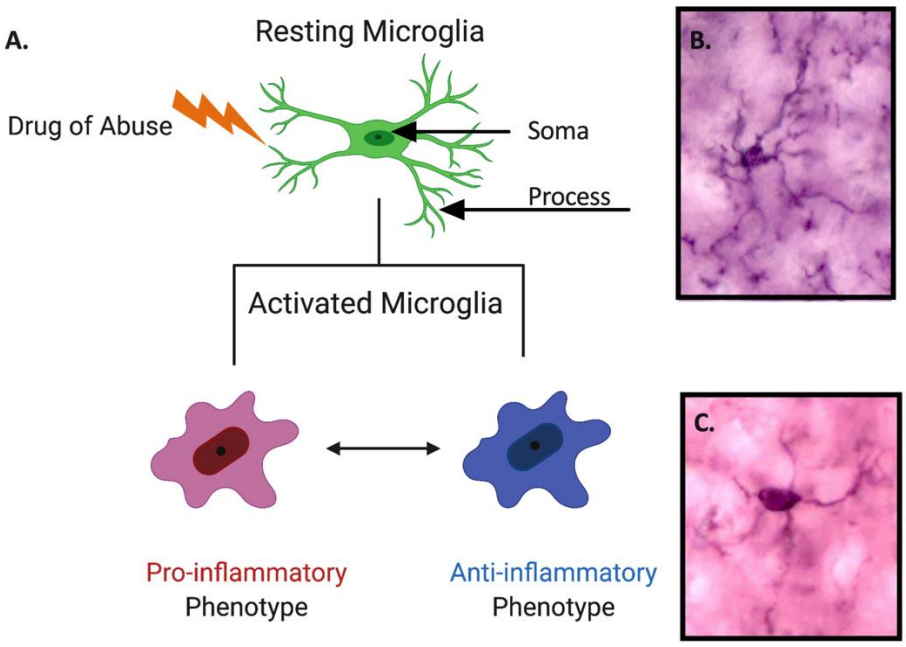

Figure 2.2. (A) A schematic of resting microglia becoming activated by drug of abuse, or in our case, removing the drug via chronic nicotine withdrawal and noting the soma and a process arm. An example of an IBA1 IHC stained surveilling or resting microglia cell (B) while an activated microglial cell example is in panel (C) demonstrating the retracted, less complex processes and larger soma.

Analysis of microglia centered on the mesolimbic reward system brain regions. Nicotinic receptors are concentrated in the ventral tegmental area (VTA) and the nucleus accumbens (NAc) and reinforce rewarding behavior via an increase in dopaminergic neuronal firing in the VTA. Dopaminergic terminals project from the VTA (VTA-DA) to the nucleus accumbens and prefrontal cortex where increased neuronal firing in response to nicotine releases increases extracellular dopamine in the PFC and NAc shell [205-207]. Reciprocally, there is glutamatergic or excitatory signaling from the PFC to both the NAc and VTA which may mediate an inhibitory feedback mechanism. Recently, microglia have been proposed to also control negative feedback of neuronal

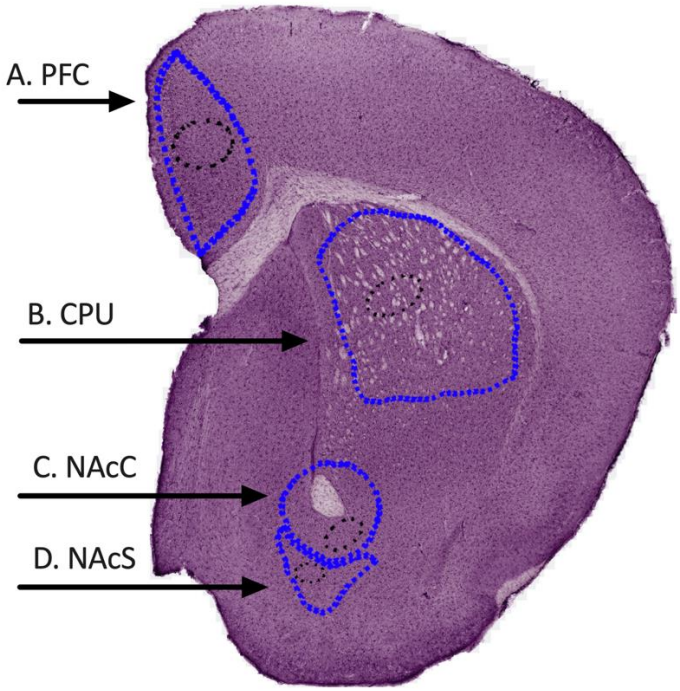

Figure 2.3. A coronal slice of one hemisphere of a mouse brain for IHC. Purple stained dots are the microglia as stained with the IBA1 microglial marker and SA-HRP VIP peroxidase. The blue dotted areas denote the regions of interest, (A) PFC, (B) CPU, (C) NAcC, and (D) NAcS and the smaller black dotted areas are example regions sampled for microglial density and individual microglia.

activity within the striatum [208]. The striatum is subdivided into caudate putamen dorsally, which is involved in motor control and contribution to habit, and ventrally in the nucleus accumbens, which is involved in reinforcement and reward; thus, both are regions are of interest. Nucleus accumbens is divided into subregions of interest, the core, which is responsive to aversive effects of nicotine, and the shell, which is responsive to rewarding effects of nicotine [209, 210]. From our frozen single hemisphere coronal slices, these regions of interest were sampled for microglial density as well as for individual microglia, see Figure 2.3.

2.3.3.1 Microglial density

To analyze the microglia, the single hemisphere coronal slices were processed by IHC with an antibody to the cell surface expression molecule, ionized calcium-binding adapter molecule or IBA1. IBA1 will bind cells of myeloid lineage and thus would bind both microglia and brain macrophages. In our previous cell sorting work, the myeloid marker Ccr2 revealed very low levels of macrophages across treatments, and provided confidence that there was little infiltration of these myeloid derived cells [56]. While a specific microglial marker, transmembrane protein 119 (Tmem119) has been discovered for the adult brain, alterations in its level have been found in models of ischemic injury and neurodegeneration and was not used for IHC [150, 211, 212]. The stained coronal slices (see example Figure 2.3) were analyzed for density by FIJI using manual cell counting of somas as described in the Materials and Methods section.

Microglia density was first analyzed for possible sex differences in our regions of interest. Figure 2.4 demonstrates that there tended to be an increased density in the PFC and the NAc Core for females (upward trend), though the spread of data was larger in the females as compared to the males. There was a significant sex difference in the microglial density, with females significantly increased over males in both the CPU and the NAc Shell. While not significant in all regions, the increasing female density trend is worth considering when analyzing nicotine treatment and withdrawal treatment groups.

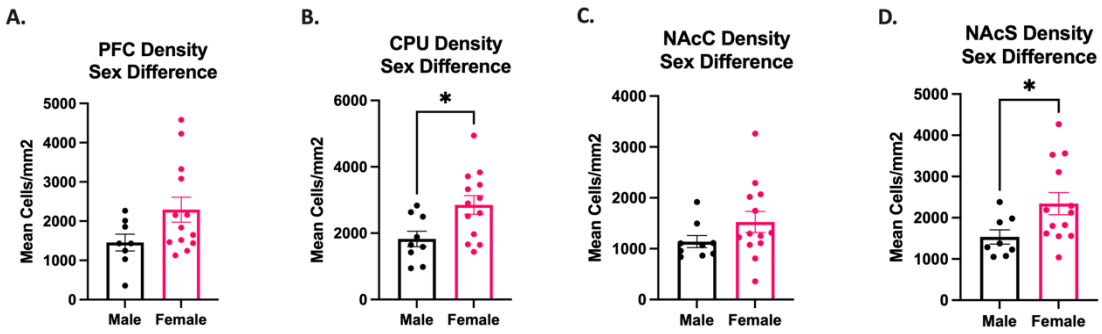

Figure 2.4. Sex differences in microglial density by brain region of interest. This is the saline control group comparing males and females of (A) PFC, (B) CPU, (C) NAc Core, (D) NAc Shell, 3-7 mice, 2-3 sections per region with mean and SEM graphed, n=8-16 as analyzed by parametric unpaired two-tailed t-test. There is a trending increase in females in all brain regions to have higher microglial density, but significance is only reached in the CPU and the NAc Shell —$*P < 0.05$, $**P < 0.01$, $**P < 0.001$, $****P < 0.0001$.

Microglia density across all regions with all treatment groups in both sexes is graphed in Figure 2.5 by counting the IBA1 stained microglia (3 images per mouse) within each region. When analyzed by two-way ANOVA and Tukey's post hoc multiple comparison, sex and treatment were significant main effects only in the PFC and the CPU. Sex differences found analyzing saline treatment alone not found by post hoc analysis when all data was analyzed together. However, the PFC and CPU each exhibited significant differences in male saline, nicotine, and 24Hr WD groups as compared to the female 48Hr WD group, and the CPU also having a significant difference between the male 48Hr WD group and the female one. Within the females in the PFC, the nicotine group is significantly different from this 48Hr WD group, which has a very high density. This high density in the 48Hr WD group is also seen in the CPU. There is post hoc significance between both nicotine and 24Hr WD as compared to the 48Hr WD treatment group. While density differences exist both in sex and treatment, they do not

appear to be so extreme that analysis of possible gene expression changes would be entirely due to density.

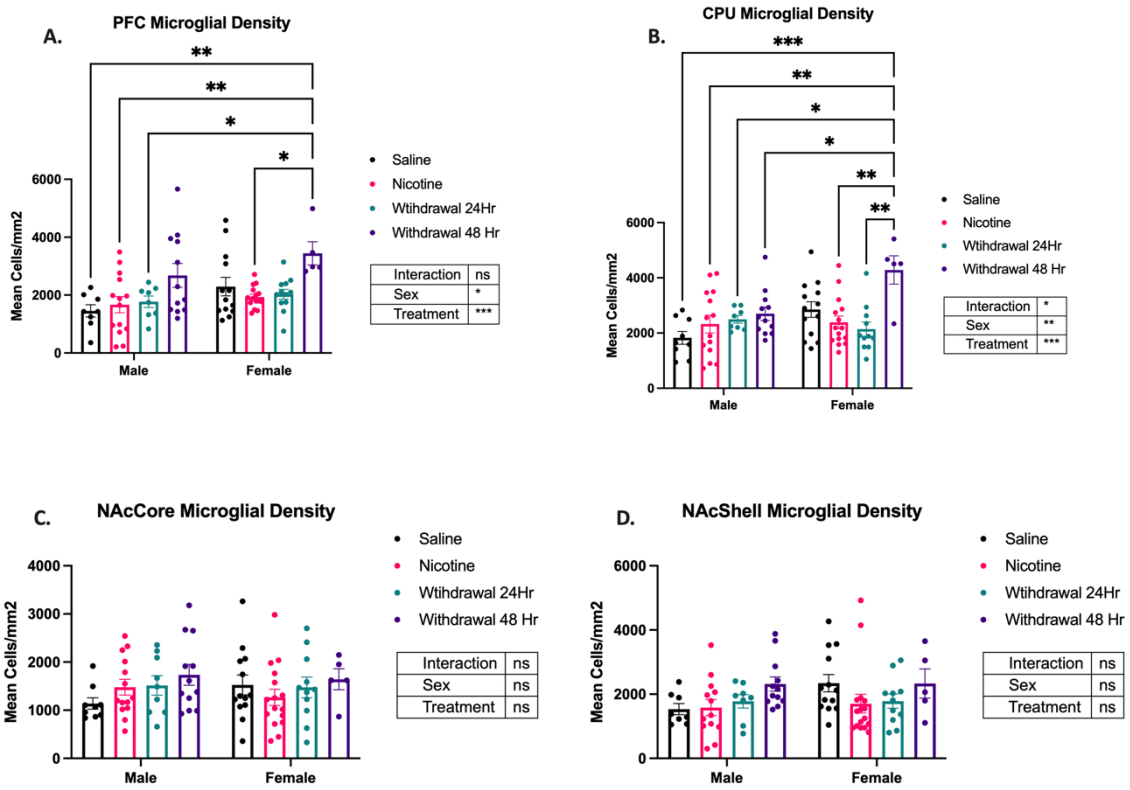

Figure 2.5. Microglial density by brain region. Data is reported in mean cells/mm2 (A) PFC, (B) CPU, (C) NAc Core, (D) NAc Shell, 3-7 mice, 2-3 sections per region, n=8-16 as analyzed by in two-way ANOVA for main effects of sex and treatment and with Tukey's multiple comparison post hoc analysis (*P<0.05, **P<0.01, ***P<0.001,****P<0.0001) after two-way ANOVA.

2.3.3.2 Microglial process length

Proceeding to analysis of the individual microglia, the microglia were manually skeletonized and measured using Neurolucida tracing and analysis software (MBF Bioscience, Williston, VT). This software allows for multiple morphology measurements, beginning with process length reported in micrometer. As mentioned, as microglial are

activated, the processes begin to retract and decrease in length. Figure 2.6 is the analysis for microglia within the PFC, the CPU, and the NAc core and shell. There are very significant main effects of interaction and sex in both the PFC and the CPU (Figure 2.6 A & B). By sex, this is largely due to the process length of females being much lower than in the males, in all treatment groups other than saline. In the females, small changes in process length would make a larger difference than it would in males. This is an interesting find, as females have stronger neuroinflammatory response in neurodegeneration conditions and autoimmune response [213-215]. In the PFC, as compared to the saline control group, chronic nicotine, 24Hr WD and 48Hr WD all have significantly increased process length. This demonstrates that all the microglial processes are longer and, rather than exhibiting activation, appear as resting microglia where longer processes would be more efficient at surveilling the brain. The females have decreased microglia process length in nicotine and withdrawal as compared to the female saline control, though the changes between groups is not significant. This process length decrease is indicative of activated microglia in the nicotine, 24Hr WD, and 48Hr WD groups.

The CPU (Figure 2.6 B) has very significant main effects of both interaction and sex. The pattern of overall increased process length in males over saline control (though the nicotine group is slightly decreased), and decreased process length in females as compared to the saline control. The males had significant post hoc differences between the nicotine and 24Hr WD groups only. The females displayed a significant decrease in 24Hr WD as compared to saline, and between nicotine and 24Hr WD. The 24Hr WD

group is also significantly different from the 48Hr WD group where process length increases but not does not return to the saline control level. These changes demonstrate that, within the CPU, the brain region that contributes to habit formation, female microglia are exhibiting activation in all the treatment groups compared with saline with the 24Hr WD time point appearing most activated as per process length. This is opposite to male microglia, which have longer processes in 24Hr WD and 48Hr WD groups and do not exhibit activation.

In the NAc, both core and shell (Figure 2.6 C & D) exhibit significant main effects of interaction, treatment, and sex for process length. There are also significant differences between male and female microglial process length, where males microglial process length is increased at saline baseline 5.5-fold higher than the female saline process length. However, in the females, the treatment groups of nicotine and withdrawal are increased as compared to their saline baseline much like the male microglial process length. Thus, while the overall process lengths are lower in the NAc for females, both sexes appear more like resting microglia and not activated. Within NAc core, in the male mice there are significant process length increases between nicotine and both the 24Hr WD and 48Hr WD groups, again demonstrating no treatment activation. In the NAc core females, there are significant increases in process length between saline both nicotine and 24Hr WD. Again, increased process length denotes that treatment is more consistent with resting microglia. Finally, within the NAc shell, there are significant differences (increases) between saline baseline and nicotine and

withdrawal groups in both males and females, again pointing more toward resting microglia than activated.

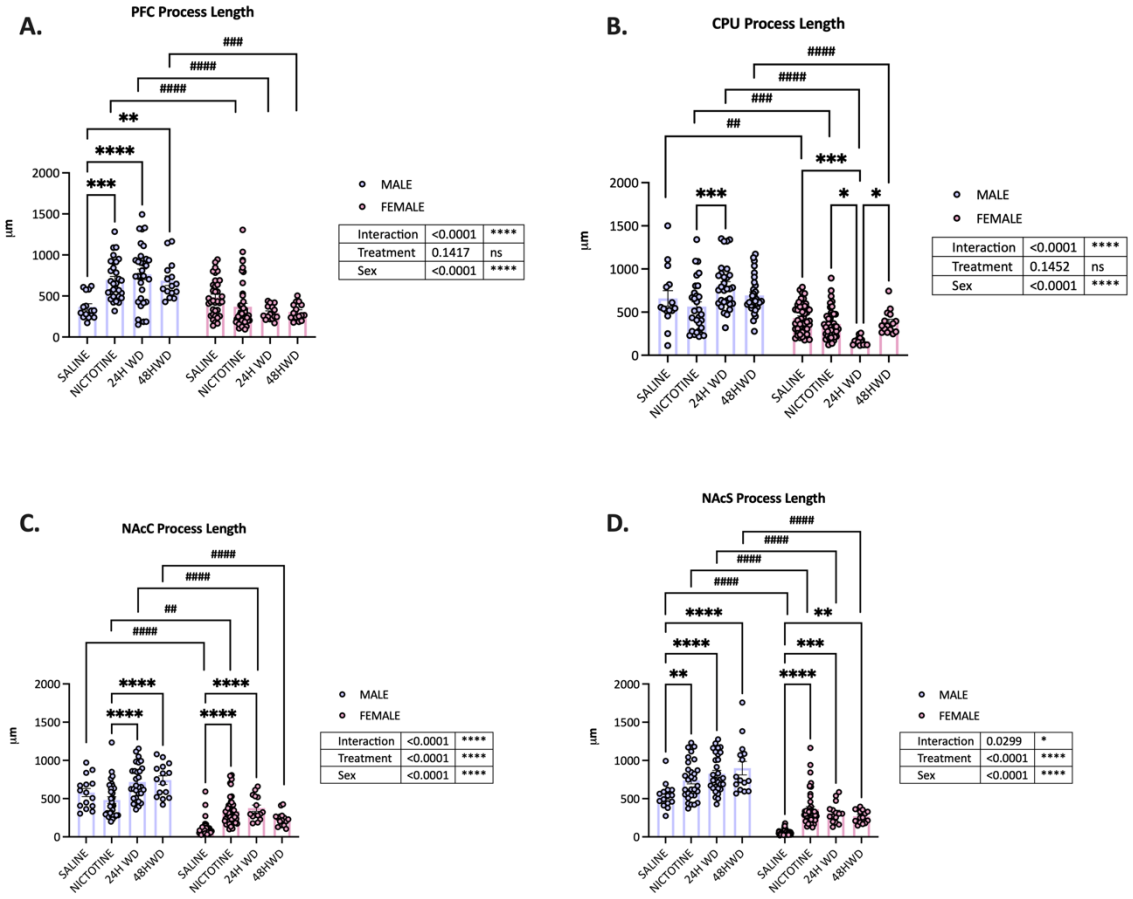

Figure 2.6. Microglial morphology comparing process length. Data is reported in μm for the (A) PFC, (B) CPU, (C) NAc Core, (D) NAc Shell, 4-5 mice, 4 regions per each of 3 slices with 5 microglia traced, roughly an n=60-75 cells/treatment. There are very strong sex effects with females having an overall lower process length than males. Only the females in the PFC do not exhibit a significant change between treatment groups. Analyzed by two-way ANOVA for main effects of sex and treatment and with Tukey's multiple comparison post hoc analysis (*P<0.05, **P<0.01, ***P<0.001, ****P<0.0001) within sex and Šídák's multiple comparisons test for post hoc of differences between sexes ($^{\#}$P<0.05, $^{\#\#}$P<0.01, $^{\#\#\#}$P<0.001,$^{\#\#\#\#}$P<0.0001).

2.3.3.3 Microglial soma area

Another measurement that alters in microglial activation is the size of the soma, which becomes enlarged as processes retract. The PFC, CPU, NAc core and NAc shell soma area are graphed in Figure 2.7 and reported as μm^2. In the PFC (Figure 2.7 A), there is a main effect of both treatment and sex. In the males, the only significant individual difference is found between saline and nicotine treatment. This is unexpected as the process length does not indicate any microglial activation but there is an increased soma size which is found in activated microglia. In comparing the males to the females in the PFC, only the 48Hr WD condition demonstrates a significant difference where the females exhibit larger soma increases. Within the females, there are significant soma area increases in nicotine and 48Hr WD as compared to saline. Based on the decreased process length seen in females in the PFC indicating activation, an increased soma size is an expected result for these conditions, again indicating activation of microglia.

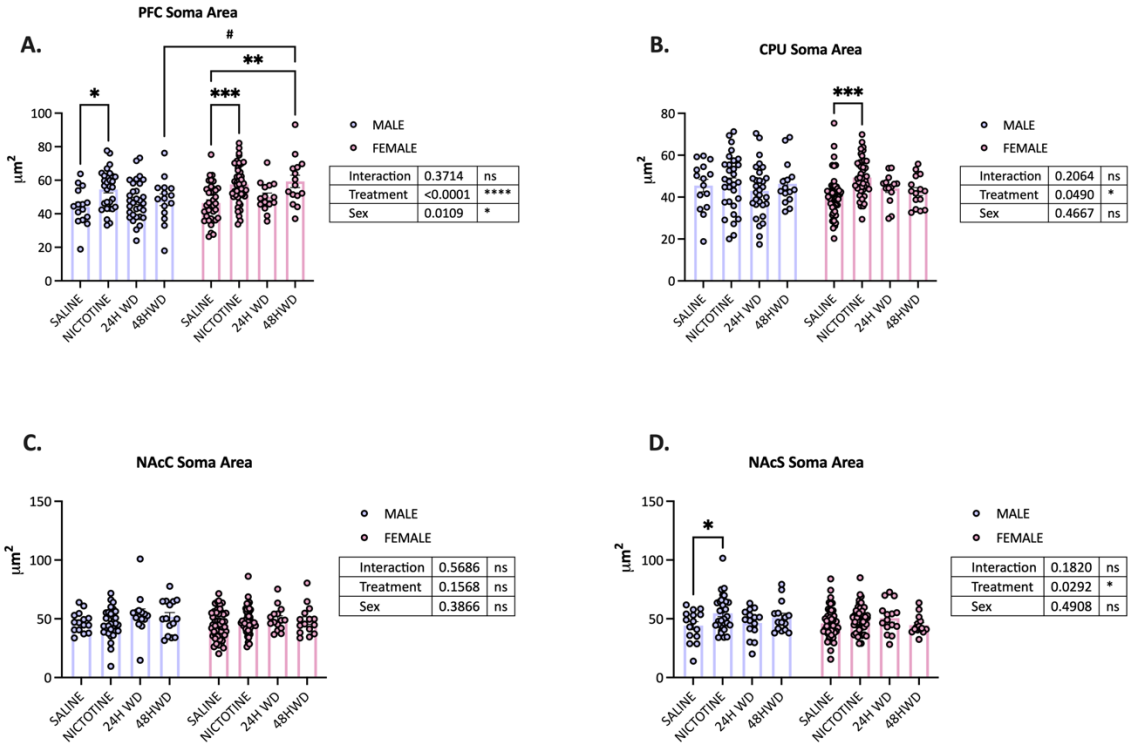

Figure 2.7. Microglial morphology comparing soma area. Data is reported in μm^2 for the (A) PFC, (B) CPU, (C) NAc Core, (D) NAc Shell, 4-5 mice per treatment group, 4 regions per each of 3 slices with 5 microglia traced, roughly an n=60-75 cells/treatment. Analyzed by in two-way ANOVA for main effects of sex and treatment and with Tukey's multiple comparison post hoc analysis for changes within sex (*P<0.05, **P<0.01, ***P<0.001,****P<0.0001). Changes between males and females were analyzed by Šídák's multiple comparisons test ($^{\#}$P<0.05, $^{\#\#}$P<0.01, $^{\#\#\#}$P<0.001,$^{\#\#\#\#}$P<0.0001).

In the CPU (Figure 2.7 B), there is a main effect of treatment and only one treatment condition significant by post hoc analysis, an increase in soma for nicotine treatment as compared to saline in females. This is, again, more expected, based on process length in this region in females, which was decreased and signifying microglial activation, as does increased soma area.

In the NAc core, there are no significant differences in main effect or by post hoc analysis (Figure 2.7 C). In the NAc shell (Figure 2.7 D), there is a significant main effect for treatment. The post hoc significance is only in males with a soma area increase in

nicotine as compared to saline. Again, this would not have been expected based on the increased process length in males in this brain region, which is aligned more with resting microglia, while the increased soma area is more indicative of activation.

2.3.3.4 Microglial process complexity

As microglia become activated and processes begin to retract, there is also a decrease in the amount of branching along the processes. A way to represent this process is to calculate the microglial complexity, a unitless measurement.

Process complexity = *(# of sister branches + # of process endings) * (Total process length)/ (# of primary processes)*

In Figure 2.8, overall, the process complexity in males is far greater than the process complexity of females, the only exception being an increase in female saline treatment in the PFC (Figure 2.8 A). This difference may be driving the very significant main effect of sex (****) in all the brain regions. Within the PFC, significant main effect in interaction and treatment as well as sex. The only significant post hoc differences are found in the males, which have increased complexity in all nicotine and 24Hr WD groups as compared to saline. This again correlates to the microglia as resting or surveilling as opposed to activated. In the PFC of the females, all treatment groups exhibit a downward trend as compared to saline control, but none rises to the level of significance.

In the CPU (Figure 2.8 B), the process complexity is significant in the main effects of interaction, treatment, and sex. There is a significant decrease in this complexity in females as compared to males in the 24Hr WD and 48Hr WD groups. Within sex, only

the males demonstrate a significant increase in the microglial process complexity in the 24Hr and 48Hr WD groups and significance between nicotine treatment and the 24Hr

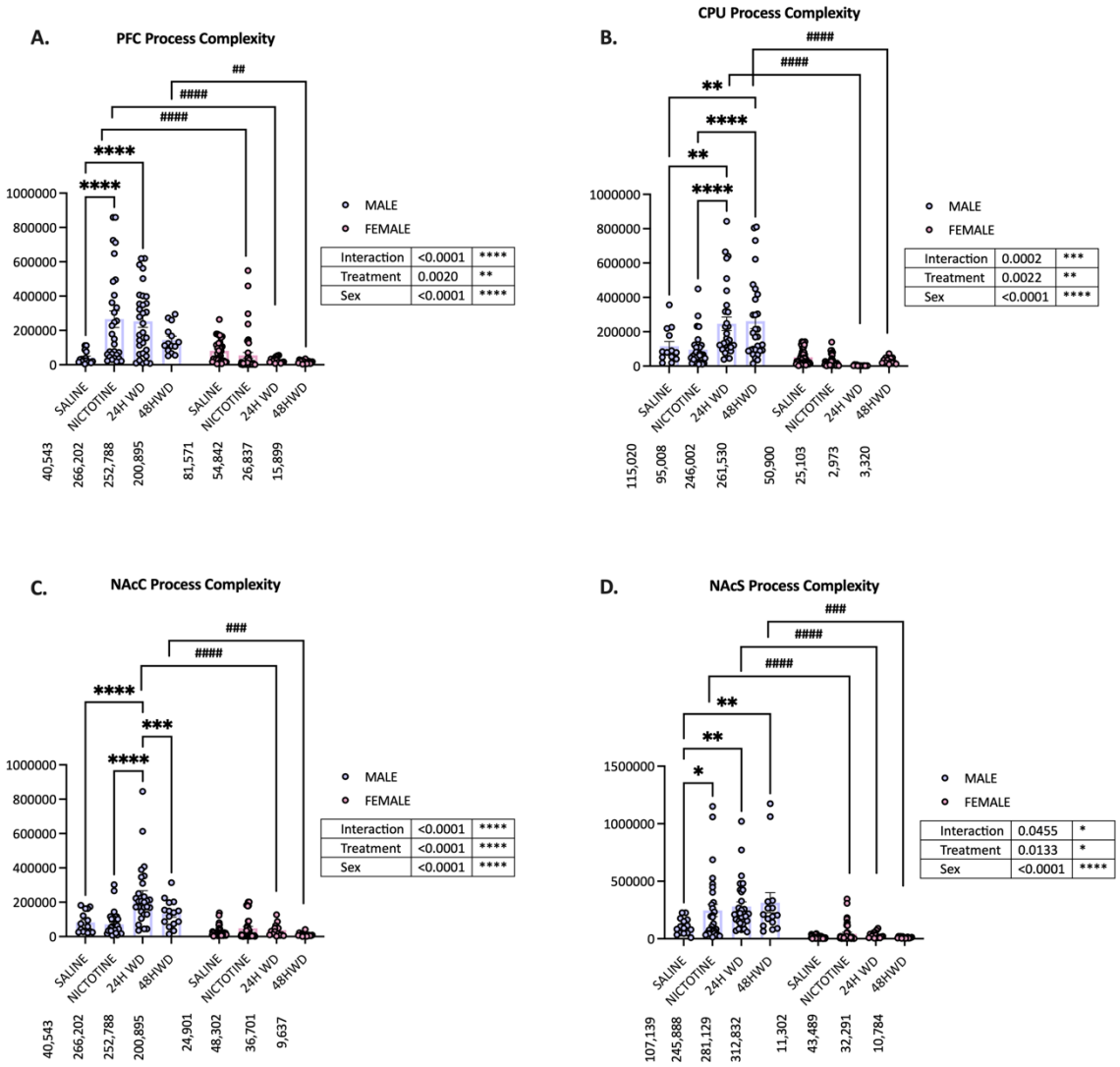

Figure 2.8. Microglial morphology comparing process complexity. Measurements are in the (A) PFC, (B) CPU, (C) NAc Core, (D) NAc Shell regions, 4-5 mice per treatment group, 4 regions per each of 3 slices with 5 microglia traced, roughly an n=60-75 cells/treatment. Overall, there is decreased process complexity in females as compared to males during both 24Hr WD and 48Hr WD in all brain regions. Analyzed by two-way ANOVA for main effects of sex and treatment and with Tukey's multiple comparison post hoc analysis for changes within sex (*P<0.05, **P<0.01, ***P<0.001,****P<0.0001). Changes between males and females were analyzed by Šídák's multiple comparisons test ($^{\#}$P<0.05, $^{\#\#}$P<0.01, $^{\#\#\#}$P<0.001,$^{\#\#\#\#}$P<0.0001). The numeric mean value is denoted on the x-axis due for clarity due to large spread of data.

and 48Hr WD groups. While not significant, there is again a large downward trend in the females in process complexity in all the treatment groups which correlates again to activated microglia.

In the NAc (Figure 2.8 C & D), both core and shell, there are significant main effects in interaction, treatment, and sex. The core exhibits a significant decrease in process complexity in the females as compared to the males in the 24Hr and 48Hr WD groups. While in the males, there is a significant increased process complexity of the 24Hr WD group as compared to the saline control. Also, within the males is a significant increase in complexity between the nicotine group and the higher complexity 24Hr WD group and the 24Hr WD group as compared to the 48Hr WD group, where complexity drops but remains higher than the saline control. In the shell, there is again a significant decrease in process complexity in the males as compared to the males in the nicotine, 24Hr, and 48Hr WD groups. While in the males, there are significant increases in all the treatment groups as compared to the saline control. The patterns for the process complexity in the females differ in the NAc shell, though again not significantly. Still, it is interesting to note that this region demonstrates increases in complexity as compared to the saline control for both nicotine treatment and 24Hr WD. Only in the NAc shell is there increased process complexity which, had it reached significance, would have implied surveilling, and not activated microglia.

2.3.3.5 Microglial convex hull analysis

The last set of microglial morphology measurements analyzed was convex hull analysis, a measurement of the size of the entire microglial field as reported in μm^2. It is a measurement that mimics a ribbon surrounding and touching the distal points of each of the processes. Microglial with large convex hull areas are the resting or surveilling microglia, while those with smaller convex hull areas are activated microglia.

In Figure 2.9 A, the PFC exhibits a significant main effect of interaction, treatment, and sex and a significant decrease in convex hull area in females of 24Hr WD as compared to the male 24Hr WD. Within the males, there is a significant increase in convex hull area in nicotine and 24Hr WD groups as compared to the saline control. In females, there is an increased convex hull area in the nicotine group as compared to the saline control. These increases are in line with microglia that are surveilling or resting. Also in the PFC females, there is a significant decrease in the convex hull area comparing the 24Hr and 48Hr WD groups. This suggests that in the PFC females in nicotine withdrawal have activated microglia.

Within the CPU (Figure 2.9 B), there is a significant main effect of interaction and sex with significance in post hoc analysis only in the males with an increase in convex hull area in the 24Hr WD group as compared to saline. Between males and females, the males have a higher complex hull area in the 24Hr and 48Hr WD as compared to their female counterparts for these treatment groups. This again suggests that, within the CPU, females have activated microglia when in nicotine withdrawal.

The NAc core region (Figure 2.9 C) there is a significant main effect of both interaction and sex for convex hull area. In this region, the only significance is between males and females. There is a decrease in the convex hull area in the female 48Hr WD group as compared to the males. Again, this decrease, which is below the female saline control, denotes a smaller area and is more consistent with microglial activation.

Lastly, within the NAc shell (Figure 2.9 D), there is a significant main effect of both treatment and sex. The convex hull area in the males is significantly increased over the females in each of the groups. Within the males, there are significant increase in the convex hull area in both nicotine and 24Hr WD as compared to the saline control, recapitulating previous published data [56]. This increase in convex hull area is significant in the females only in the nicotine group as compared to the saline control and, while not significant, the 24Hr and 48Hr WD groups are trending upward as compared to saline. Increases in convex hull area are more consistent with resting microglia than activated.

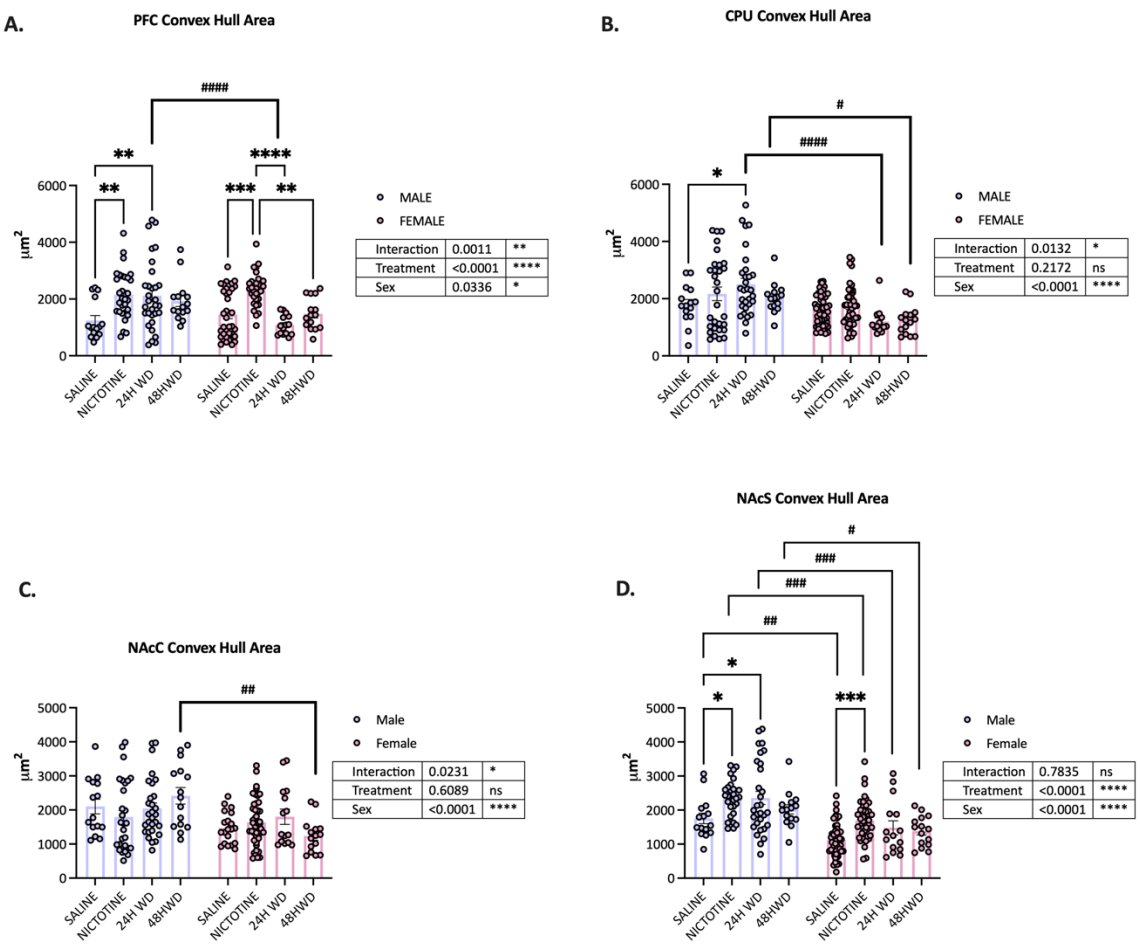

Figure 2.9. Microglial morphology for Convex Hull analysis (μm^2). In the (A) PFC, (B) CPU, (C) NAc Core, (D) NAc Shell brain regions, 4-5 mice per treatment group, 4 regions per each of 3 slices with 5 microglia traced, roughly an n=60-75 cells/treatment. Analyzed by in two-way ANOVA for main effects of sex and treatment and with Tukey's multiple comparison post hoc analysis for changes within sex (*P<0.05, **P<0.01, ***P<0.001, ****P<0.0001). Changes between males and females were analyzed by Šídák's multiple comparisons test ($^{\#}$P<0.05, $^{\#\#}$P<0.01, $^{\#\#\#}$P<0.001,$^{\#\#\#\#}$P<0.0001).

2.3.3.6 Microglia morphology activation summary

Most male microglia morphology measurement tend toward resting microglia; see Table 2.1. The microglia morphology data for the females are more variable and differ overall from the males. The females lean heavily toward activation as compared

to the males, but no concise conclusion can be drawn at this time. The morphology in both does change, which means a change in the local environment and a phenotypic response to the changes whether they are classically activated to an ameboid shape or not. The experiment was performed on non-ovariectomized females, and the estrous cycle was not accounted for in morphology variability. Nicotine has been shown to decrease aromatase enzyme activity, which is critical for the conversion of testosterone to 17B-estradiol (E2), and women who smoke have been shown to begin menopause 1-2 years earlier [216-218]. The effect of E2, which is known to affect synaptic plasticity, memory and learning, and neurodegenerative diseases, has also been shown to have an anti-inflammatory effect on microglia [219-223]. Variations of E2 in the estrous cycle could be accounted for in future experiments to see if the variability in morphology is E2-driven [224].

Table 2.1. Summation of Morphology Data. The data are presented as to whether the microglia morphology data trend towards resting or activated microglia.

	Males				Females			
	PFC	CPU	NAcC	NAcS	PFC	CPU	NAcC	NAcS
Process Length	R	R	R	R	A	A	R	R
Soma Area	Nic A	N/A	N/A	Nic A	Nic & 48Hr WD A	Nic A	N/A	N/A
Complexity	R	R	R	R	R	A	48Hr WD A	48Hr WD A
Convex Hull Area	R	R	R	R	R	R	R	R

Key: Resting microglia (R), active microglia (A), no discernable difference (N/A)

2.4. Conclusion

The mouse model for chronic nicotine and withdrawal, using osmotic minipumps for nicotine delivery (at an appropriate dose), is a well-validated system and is ideal for studying microglia and neuroinflammation. The receptor binding assay verified this validity in our hands with upregulation of nicotinic receptors by nicotine treatment. The density of microglia had significant baseline increase in females in the CPU and in the NAc shell, while the PFC and NAc core had nonsignificant values but a similar trend. Finally, the microglial morphology demonstrated that, in males, the microglia tended to

be in a resting state, while the females exhibited more activation. These morphology changes may denote neuroinflammatory alterations to the local environment and thus alterations in gene expression and protein expression of cytokines found in the microglia. The next two chapters will explore each of these topics.

Chapter 3. Transcriptional Changes in Response to Chronic Nicotine and Nicotine Withdrawal

3.1. Introduction

Neuroinflammation is associated with many substance use disorders though the inflammation occurs with use while in nicotine use disorder. Nicotine use has been shown to be involved in both inflammatory and oxidative stress events in mice and humans [47, 56, 98, 225-227]. As the neuroimmune cell of the brain, microglia are at the forefront of candidates for investigation of cytokines that may be involved in inflammatory cascades. Local cues are implicated in mediating the specific role of microglia in a specific brain region [133]. Part of the regulation involved in the local cues would be the regulation of gene expression, which would control the timing and amount of product produced by any given gene. This regulation could also be affected by nicotine's binding to the $\alpha 7$ nAChRs found on microglia, which could alter the gene signature in a specific region. Transcriptome analysis of human and mouse genes show a high degree of gene orthology where 80% of human genes and 72% of mouse genes have a one-to-one relationship [228]. RNA-seq has been used to analyze the gene signature of microglia and found distinct differences in the RNA signature in health and disease [135, 211]. For example, in a mouse model of amyotrophic lateral sclerosis (ALS) the gene signature included genes known to suppress neurodegeneration (*Igf1*and progranulin (*Gm*)) as well as factors upregulated in neurotoxicity such as Nox2 [143].

Thus, it behooves us to analyze the RNA in the reward system, which could be affected by chronic nicotine or nicotine withdrawal. Notwithstanding the NIH guidance use both sexes, we can compound the need with knowledge that neuroinflammatory and neurodegenerative conditions such as depression, Multiple Sclerosis (MS), and Alzheimer's Disease are much more prevalent in women than men (see reviews [229, 230]). Based on microglial information gleaned in Chapter 2, this study aimed to elucidate the applicability and significance of both sex and treatment in evaluating genes involved in inflammation and assess cytokine mRNA expression levels in the brain regions of the reward system; the prefrontal cortex (PFC), caudate putamen (CPU) and nucleus accumbens (NAc) during chronic nicotine use withdrawal.

3.2. Materials and Methods

3.2.1. Animal use

See Chapter 2 for Animal Use and Experimental Design (Figure 2.1 A). The half of the brain kept for biochemistry was microdissected for the following regions: cortex (for receptor binding validation, see Chapter 2, Figure 2.1 B), the PFC, 2mm punches from the CPU and NAc (core region) of the striatum, the dorsal and ventral hippocampus (future experiments) and cerebellum (future experiments) frozen on dry ice and stored at -80°C for biochemistry.

3.2.2. Qiagen RT^2 Profiler PCR Array

A mouse chemokine and cytokine expression array (RT^2 Profiler PCR Array PAMM150-Z, Format E; Qiagen, Valencia, CA) was used for the pilot animal group to detect chemokine expression patterns from a pilot set of experiments using male mice,

n=4 per treatment groups (saline, nicotine, and 24Hr nicotine withdrawal) with 2mm punches taken from the NAc. Total RNA was extracted from punches using the RNeasy Mini kit (Qiagen Cat74106, Valencia, CA) according to manufacturer instructions. Quantitation of mRNA was performed via a Nanodrop 2000 (ThermoFisher Scientific, Waltham, MA) and verified for accuracy and quality via an Agilent BioAnalyzer (Santa Clara, CA) by the Functional Genomics Core, COBRE Center for Targeted Therapeutics, UofSC College of Pharmacy (Columbia, SC). Total RNA (400 ng) was converted to cDNA following manufacturer's instructions using the RT^2 First Strand Kit (Qiagen Cat330404; Valencia, CA). A 102µL cDNA synthesis reaction volume was mixed with 2 × RT^2 SYBR Green qPCR Mastermix (Qiagen Cat330502; Valencia, CA) and RNase-free water to obtain a total volume of 1,300 µL. Next, 25 µL of the PCR component mix was placed into each well of the PCR array (a 96-well array using format E) using the RT^2 SYBR Green qPCR Mastermix. Samples were run in quadruplicate with 5 housekeeping genes (*Actb, B2m, Gapdh, Gusb, Hsp90ab1*), a genomic DNA control, reverse transcription controls, and positive PCR controls on each of 4 plates. The mouse genes assayed on the qPCR plate are listed in Table 3.1. Plates were processed in a Bio-Rad C1000 Touch CFX384 Thermo Cycler (Bio-Rad, Hercules, California) as per manufacturer directions. The expression levels were quantified relative to the values obtained for housekeeping genes and the relative abundance of gene transcripts calculated as $\log^{2\triangle CT}$. Subsequently, gene expression by fold change was calculated as fold over untreated control, the saline group. This data was calculated via the Qiagen GeneGlobe Data Analysis Center (https://geneglobe.qiagen.com/ch/analyze). Lastly, the data was

visualized via non-supervised hierarchical clustering of the data sets with dendrograms indicating co-regulated genes across treatments to analyze changes in gene expression in a clustergram.

Table 3.1. Qiagen RT2 Profiler PCR Array Mouse Chemokines & Cytokines Genes.

Chemokines	*Ccl1 (I-309), Ccl11 (Eotaxin), Ccl12 (MCP-5, Scya12), Ccl17 (Tarc), Ccl19, Ccl2 (MCP-1), Ccl20 (Mip-3a), Ccl22 (Mdc), Ccl24 (Mpif-2, Eotaxin-2), Ccl3 (Mip-1a), Ccl4 (Mip-1b), Ccl5 (Rantes), Ccl7 (mcp3), Cx3cl1, Cxcl1 (Gro1), Cxcl10 (Inp10), Cxcl11 (Itac, Ip9), Cxcl12, Cxcl13, Cxcl16, Cxcl3, Cxcl5 (Ena-78, Lix), Cxcl9 (Mig), Pf4, Ppbp, Xcl1*
Interleukins	*Il10, Il11, Il12a, Il12b, Il13, Il15, Il16, Il17a, Il17f, Il18, Il1a, Il1b, Il1rn, Il2, Il21, Il22, Il23a, Il24, Il27, Il3, Il4, Il5, Il6, Il7, Il9*
Interferons	*Ifna2, Ifng*
Growth Factors	*Bmp2, Bmp4, Bmp6, Bmp7, Cntf, Csf1 (Mcsf), Csf2 (GMCSF), Csf3 (Gcsf), Gpi1, Lif, Mstn, Nodal, Osm, Thpo, Vegfa*
TNF Receptor Superfamily Members	*Cd40lg, Cd70, Fasl, Lta (Tnfb), Ltb, Tnf, Tnfrsf11b (Opg), Tnfsf10 (Trail), Tnfsf11 (Rankl), Tnfsf13b*
Other Cytokines	*Adipoq, Ctf1, Hc, Mif, Spp1, Tgfb2*
Anti-Inflammatory Cytokines	*Ccl19, Il10, Il11, Il12a, Il12b, Il13, Il18, Il2, Il22, Il23a, Il24, Il4, Il6, Tgfb2*

3.2.3. Quantitative PCR

mRNA from specified brain regions (PFC, CPU punch, NAc punch) was isolated from frozen samples using TRIzol (ThermoFisher Scientific Cat 15596026, Waltham, MA), chloroform (ThermoFisher Scientific Cat 423555000, Waltham, MA), and phase lock gel heavy tubes (Quantabio Cat2302830, Beverly, MA), in conjunction with the RNeasy Mini

Kit (Qiagen Cat74106, Valencia, CA). Complimentary DNA (cDNA) was prepared using 500ng of the above mRNA (quantitated by Nanodrop 2000 (ThermoFisher Scientific, Waltham, MA)), adding Oligo (dT)15 primer (Promega CatC1101, Madison, WI), and dNTPs (ThermoFisher Scientific CatR0192, Waltham, MA), with nuclease free water incubating at 65°C for 5 minutes then placed on ice for 2minutes. To this reaction 1µL SuperScript™ II Reverse Transcriptase (ThermoFisher Scientific Cat18064014, Waltham, MA), DTT, and RNasin (ThermoFisher Scientific CatN2615, Waltham, MA) were added and incubated at 42°C for 5 minutes and the reaction stopped at 70°C incubation for 15 minutes (cDNA was diluted and stored at 1:2 dilution). qPCR reactions were assembled using 1ul of a 1:6 dilution of above cDNA, Maxima SYBR Green master mix (ThermoFisher Scientific CatK0253, Waltham, MA), and 100nM primers (Integrated DNA Technologies Inc., Coralville, IA, USA) diluted to 4.3nM final concentration in nuclease free water. Cycling parameters were 95°C for 10 minutes followed by 40 cycles of 95°C (30 s) and 60°C (1 min), ending with a melting curve analysis to control for the amplification of a single gene product. The mRNA levels were determined using the 2−ΔΔCT method [231]. All samples were tested in triplicate, the median cycle threshold was used for analysis, and the relative expression values normalized to the expression value of housekeeping gene Mus musculus TATA box binding protein (*Tbp*). All gene expression values were normalized to saline male controls. Primers were designed using NCBI [232]and Primer3Plus [233], validated before use, and are listed in Table 3.2.

3.2.4. Data analysis and statistics

The qPCR data was divided first by sex and brain region. The qPCR data was then normalized by setting the male saline treatment group to 100% and comparing the other treatment groups to this control. Statistical analysis was performed and graphed in GraphPad Prism 9 for macOS version 9.2.0 (GraphPad Software, LLC., San Diego, CA) with results presented as mean +/- SEM. The GraphPad online calculator was used to Grubbs' test or extreme studentized deviate (ESD) (https://www.graphpad.com/quickcalcs/grubbs1/) for each treatment condition removing at most 1 outlier per group based on the Alpha=0.05). Baseline analysis comparing male and female data (saline control) was done by parametric unpaired two-tailed t-test. Analysis of qPCR normalized samples (to saline male) were analyzed by two-way ANOVA for male and female comparisons using Šídák's multiple comparisons test post hoc analysis. Normalized samples analyzing mRNA expression changes across the treatment groups were analyzed by two-way ANOVA using Dunnett's multiple comparisons test post hoc analysis.

Table 3.2. qPCR primers for individual genes of interest.

Primer Name	Primer Sequence	Target Template
Bmp4_F	TCTCTGAGCCTTTCCAGCAAG	NM_007554.3
Bmp4_R	AAAGCAGAGCTCTCACTGGTC	
Ccl2_F	ACCTGCTGCTACTCATTCACC	NM_011333.3
Ccl2_R	TGCTGGTGATCCTCTTGTAGC	
Ccl3_F	CCTGACTAAGAGAAACCGGCA	NM_011337.2
Ccl3_R	CAGGCATTCAGTTCCAGGTCA	
Ccl4_F	AAACCTAACCCCGAGCAACA	NM_013652.2
Ccl4_R	CCATTGGTGCTGAGAACCCT	
Cd68_F	CTTGGGGCATATCTGTTTTGA	NM_001291058
Cd68_R	ATTGTATTCCACCGCCATGTA	
Cxcl10_F	TCCCCATCAGCACCATGAAC	NM_021274.2
Cxcl10_R	CCACTTGAGCGAGGACTCAG	
Cxcl12_F	TCTCTGAGTAGTGGCTCCCC	NM_013655.4
Cxcl12_R	GCAGGGCTCTTTCCATGACT	
Cxcr4_F	GCCATGGCTGACTGGTACTT	NM_009911.3
Cxcr4_R	AGGGCCTCTGTGATGGAGAT	
Iba1_L	GTTCCCAAGACCCACCTAGAG	NM_001361501.1
Iba1_R	GTGTGACATCCACCTCCAATC	
Il10_F	TCTATTCTAAGGCTGGCCACA	NM_010548.2
Il10_R	GCAGGAATGATCATCAAAGGA	
Il1a_F	GAAGCTCGTCAGGCAGAAGT	NM_010554.4
Il1a_R	GTGCAAGTGACTCAGGGTGA	
Il1b_F	CATGGAATCCGTGTCTTCCTA	NM_008361.4
Il1b_R	CAGAATGTGCCATGGTTTCTT	
Nox2_F	CCAACTGGGATAACGAGTTCA	NM_007807.5
Nox2_R	GGACATTTGGCAGCATACACT	
Ocln_F	TACTCCTCCAATGGCAAAGTG	NM_008756.2
Ocln_R	CCCACCTGTCGTGTAGTCTGT	
Tbp_F	GCACAGGACTTACTCCACAGC	NM_013684.3
Tbp_R	GTGGGTTGCTGAGATGTTGAT	
Tlr4_F	AACAAAACTCTGGGGCCTAAA	NM_021297.3
Tlr4_R	AGGCCTTAGCCTCTTCTCCTT	
Tmem119_F	GGATGCCTCACAGCTACAAAG	NM_146162
Tmem119_R	AGGGTTGCTTGACACTTGAGA	
Tnfa_F	CCCACTCTGACCCCTTTACTC	NM_013693.3
Tnfa_R	AAGCCCATTTGAGTCCTTGAT	
Trem2_F	CTCAATCCAGGAGCACAGTTC	NM_001272078.1
Trem2_R	GTGATCAGCAGCAGGAGAAAC	

3.3. Results and Discussion

3.3.1. Clustergram analysis yields distinct treatment affected gene groups

From the pilot experiment, total mRNA from the nucleus accumbens (NAc punch) was extracted and converted to cDNA for qPCR. Male mice, n=4 per treatment groups (saline, nicotine, and 24-hour withdrawal) were used to verify that the treatment conditions would alter gene expression. The data clustered into 3 large clusters, which have been separated for ease of viewing below in Figure 3.1. (Full unmodified clustergram image Appendix Figure A.1). The goal was to see if there were variations in the genes between the treatment groups corresponding to any literature for various cytokines studied for their role in neuroinflammation. As a regulatory molecule, the levels of cytokines remain low until activated by states of disease or aging (see review [234]). The 3 clustergram group data was analyzed, compared to literature for genes that might be involved with neuroinflammation, and investigated in the Brain RNA-seq database (https://www.brainrnaseq.org/) [235, 236] only for mouse genes with human orthologs, and brought forward if they were found mostly in microglia, and their general expression level as per fragments per kilobase per million (FKPM) was reasonable. Finally, the genes of interest were validated in mouse mRNA samples. The final list of genes to be investigated moving forward along with information about their function and location in the brain can be found in Table 3.3 and primers can be found in Table A.2.

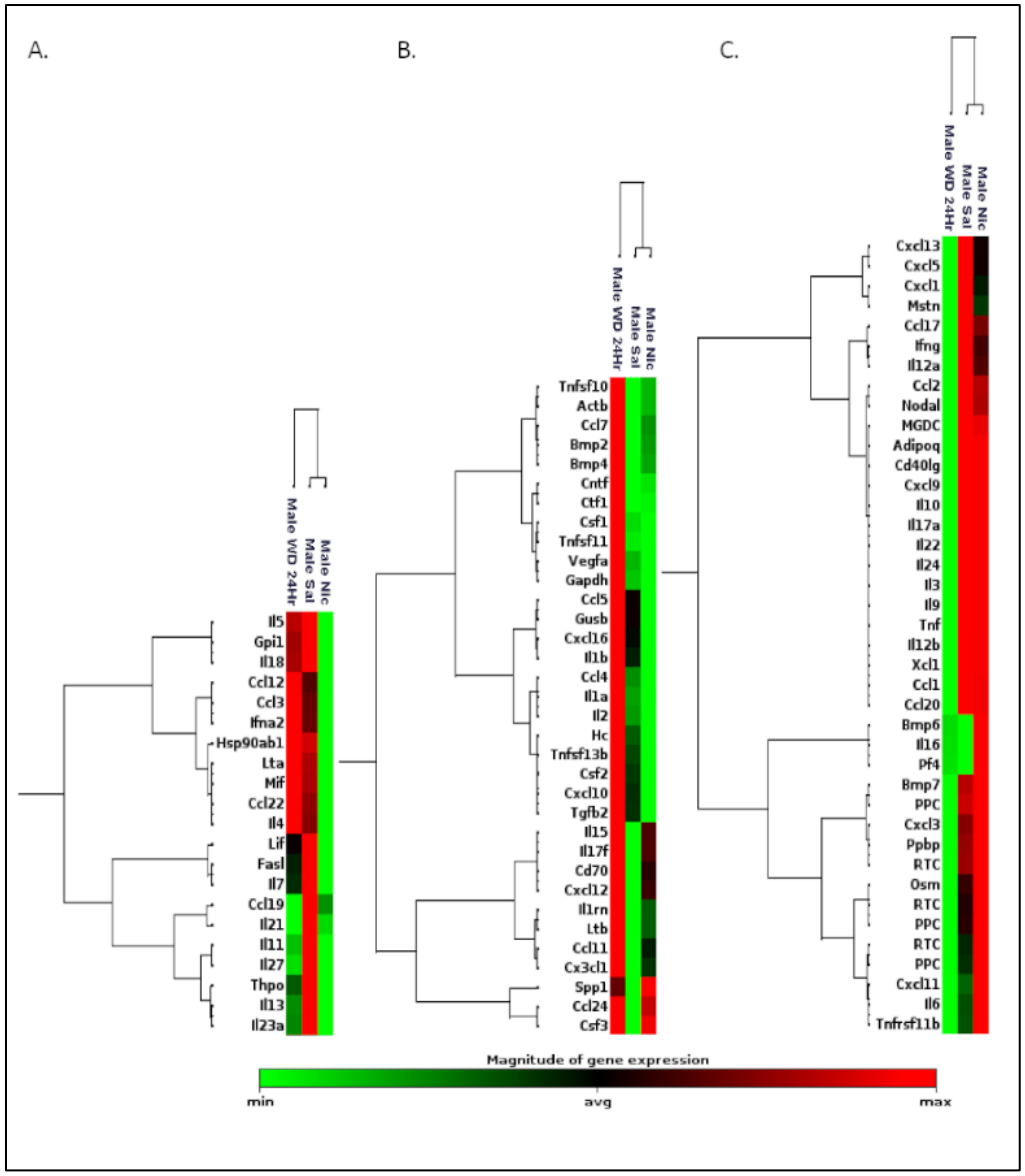

Figure 3.1. Qiagen clustergram, with dendrograms indicating co-regulated genes across treatment groups. Pilot data comparing qPCR fold change averaged results of male nicotine 24Hr WD, male saline, and male nicotine samples (n=4). A. Cluster with high expression of saline and some 24Hr WD B. Cluster with low expression of saline and nicotine as compared with a large group of cytokines with high expression in 24Hr WD. C. Cluster with low expression of 24Hr WD as compared to both saline and nicotine.

Table 3.3. Pilot study genes identified for further investigation. Pro- and Anti- denote if the genes have a proinflammatory or anti-inflammatory phenotype.

Gene	Name	Role in CNS	Cell Type Expression	Pro	Anti
Ccl2	Monocyte chemotactic protein 1	BBB Integrity & cytokine production	Microglia (mus) / Neurons (hu)	X	
Ccl3	Macrophage Inflammatory protein 1 alpha	Chemokine/immune recruitment	Microglia	X	
Ccl4	Macrophage inflammatory protein 1 beta	Chemokine/immune recruitment	Microglia	X	
Cxcl10	C-X-C Motif Chemokine Ligand 10	Lymphocyte regulation	Microglia	X	
Il1α	Interleukin 1 alpha	Inflammation/pyrogen	Microglia	X	
Il1ß	Interleukin 2 beta	Inflammation	Microglia	X	
Il10	Interleukin 10	Inhibit inflammatory cytokines	Microglia		X
Tnfα	Tumor necrosis factor alpha	Homeostasis	Microglia	X	
Bmp4	Bone morphogenetic protein 4	Member of *Tgfβ* superfamily	Oligo/OPC – low in hu	N/A	N/A
Cxcr4	C-X-C Motif Chemokine Ligand 4	Chemokine & Co-receptor for HIV	Endoth/Neuron (mus) & Microglia (hu)	N/A	N/A
Cxcl12	C-X-C Motif Chemokine Ligand 12	Chemokine regulating BBB	Endoth/Neuron (mus) & Microglia/Endoth (hu)	N/A	N/A
Lif	Leukemia inhibitory factor (Il6 family)	Growth & Differentiation	Microglia/Astrocyte – low in hu		X
Trem2	Triggering receptor expressed on myeloid cells 2	Stimulate phagocytosis	Microglia	N/A	N/A
Il2	Interleukin 2	BBB and alterations of brain microcirculation	Low in brain	X	
Aif1 (Iba1)	ionized calcium binding adaptor molecule 1	Microglia and Macrophage marker	Myeloid lineage	N/A	N/A
Tmem 119	Transmembrane protein 119	Surface marker for microglia	Microglia	N/A	N/A
Cd68	Cluster of differentiation 68	Lysosomal storage marker	Myeloid lineage	N/A	N/A
Ocln	Occludin	Tight Junction protein	Endothelial	N/A	N/A
Tgfb1	Transforming growth factor-beta	Regulates pericyte inflammation processes	Microglia & some Endoth in mus		X
Cybb (Nox2)	NADPH oxidase 2	Key enzyme activating ROS	Myeloid lineage	N/A	N/A

The pilot experiment provided strong evidence to move forward into the full-scale experiment which would include both male and female adult animals to see if nicotine effects would vary in the cytokine response and gauge sex as a biological variable (SABV) without estrous cycle identification. The full-scale experiment also included a second withdrawal timepoint (48Hr WD), as unpublished lab data from cell specific sequencing of microglia suggested a gene change at the 48Hr withdrawal timepoint.

3.3.2. Sex as a biological variable in cytokine mRNA expression saline control

The full-scale experiment was analyzed and genes with significant changes as compared to male saline control group are listed in Table 3.4. Of the 20 genes tested, only 5 genes exhibited any significance by a two-tailed t-test (see example graph Figure 3.2).

The chemokine *Ccl4* has been classified as sexually dimorphic perinatally in mice where the mRNA expression is noted to be 50 times higher in males than females in development of the hippocampus and cortex [106]. These levels are found to fluctuate between males and females dependent upon age and brain region postnatally [237]. In our data, there is a significant decrease in the female *Ccl4* cytokine mRNA expression in the CPU with no change in the levels between males and females in either the PFC or NAc.

Table 3.4. Sex differences as normalized and compared to male saline mRNA gene expression between genes in PFC, CPU, and NAc. Analysis by unpaired two-tailed t-test. P < 0.05, **P < 0.01, ****P < 0.0001, n = 9-12.

A. PFC						
Gene	**Male**	**Female**	**Significant**	**P value**	**t, df**	**Mice/group**
Ccl4	100.00	107.10	ns	0.5903	t=0.5468, df=21	11-12
Cxcl10	100.00	53.30	*	0.0465	t=2.123, df=20	11
Cxcl12	100.00	133.50	**	0.0050	t=3.132, df=21	11-12
Lif	100.00	136.10	ns	0.4212	t=0.8205, df=21	11-12
$Tnf\alpha$	100.00	141.00	*	0.0372	t=2.232, df=20	11-12
B. CPU						
Gene	**Male**	**Female**	**Significant**	**P value**	**t, df**	**Mice/group**
Ccl4	100.00	59.44	*	0.0240	t=2.464, df=18	10
Cxcl10	100.00	66.54	ns	0.1669	t=2.123, df=20	9
Cxcl12	100.00	127.40	ns	0.0407	t=2.188, df=20	10-12
Lif	100.00	81.67	ns	0.3365	t=0.9875, df=18	10
$Tnf\alpha$	100.00	68.26	ns	0.1165	t=1.649, df=18	10
C. NAc						
Gene	**Male**	**Female**	**Significant**	**P value**	**t, df**	**Mice/group**
Ccl4	100.00	109.80	ns	0.6375	t=0.4788, df=19	9-12
Cxcl10	100.00	79.77	ns	0.5312	t=0.6378, df=19	10-11
Cxcl12	100.00	119.60	*	0.0407	t=2.188, df=20	10-12
Lif	100.00	146.00	*	0.0166	t=2.628, df=19	10-11
$Tnf\alpha$	100.00	129.80	ns	0.3497	t=0.9588, df=19	9-12

Cxcl10 has also been evaluated in brain developmental in mice, where the endotoxin LPS was injected to induce an inflammatory response and alterations in cytokines studied. These studies found no sex differences in the expression of *Cxcl10* [238]. When these animals were assessed as adults, however, there was an increased *Cxcl10* expression in females across the PFC, amygdala, or hypothalamus [238]. *Cxcl10* in the saline control group here was found to be significantly decreased in the PFC, with a trend towards lower expression in the CPU and NAc of females.

In mouse and rat development, *Cxcl12* is critical for migration of neural progenitor cells in the cortex [239, 240]. In humans, gene expression studies in adult brains have found that *CXCL12* was significantly dysregulated in progressive supranuclear palsy (PSP) and Parkinson's disease (PD) [241], both of which are more common in men than women. In Alzheimer's disease, which is more prevalent in women, the expression of Cxcl12 was found to be lower in females though remained the same in men and women in aging (see review [242] and [243]). In this study, *Cxcl12* exhibits increased gene expression in females in both the PFC and the NAc and an insignificant increase in the CPU.

The brain RNA-seq database presents *Lif* gene expression as very low within a healthy brain. There are few studies addressing the role of *Lif* mRNA, but it is shown to be expressed in the adult visual cortex of rats [244]. Other research into the adult gene expression has also shown it to be increased in various human brain regions in both Alzheimer's disease (AD) and Parkinson's disease (PD) over healthy levels. At baseline in our regions of interest, the mouse *Lif* gene expression was found to be increased in females as compared to males in the NAc at significant levels and at non-significant levels in the PFC. In the CPU, the expression levels were decreased in females but not significantly [245, 246].

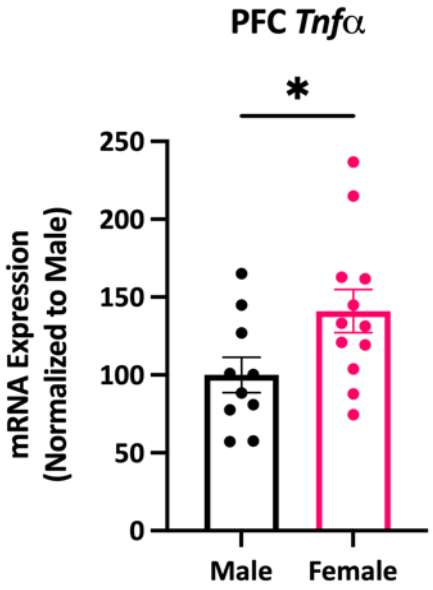

Figure 3.2. Example of mRNA expression of males compared to females in the saline control group (baseline mRNA expression) two-tailed t-test, *P<0.05, n=9-11. Increased Tnfα expression in the PFC of females as compared to males.

Some cytokines are also known to vary in an age specific matter. In aging studies using a mouse with a lifespan of only 6-7 months, the mutant Ercc1$^{\Delta/-}$ mouse (DNA repair abnormalities in nucleotide excision repair, interstrand crosslink repair, and double strand break repair) [247], the aged microglia increased their secretion of *Tnf*∝ after LPS stimulation [248]. This sexual dimorphism is seen in traumatic brain injury (TBI) in *Tnf*∝ gene expression where females had higher levels at 4 hours after injury with males having higher expression by day 3 post injury [249]. This may be due to circulating estrogen levels in the mice where in ischemic injury lower circulating levels of estrogen correlated to an increase in *Tnf*∝ gene expression [250]. In our baseline data, we also

have an increase in *Tnf*∝ mRNA levels that is significant (See Figure 3.2) and a similar increase in the NAc though it does not reach significance. The mRNA expression levels in the CPU were lower in females as compared to males, but this was not significant.

3.3.3. Sex and treatment effects on cytokine mRNA in brain regions of interest

Of the 20 genes chosen for investigation at the mRNA level between the treatment groups and between males and females, 16 genes were found to exhibit significance by main effect (interaction, sex, treatment) or via post hoc analysis (Šídák's or Dunnett's multiple comparisons). The data and the statistics for the two-way ANOVAs can be found in the following tables, PFC Table 3.5, CPU Table 3.6, and NAc Table 3.7, while an example of the individual graphs demonstrating significant post hoc analysis can be found in Figure 3.3 with the individual graphs available in the Appendix Figure A.3-Figure A.10. It is also important to note this data is generated from the same animals that were examined above to highlight the baseline sex differences with saline treatment alone.

As discussed in the introduction, cytokines, and indeed other genes found in Table 3.3, are involved in many dysregulated brain functions in substance use disorders other than nicotine, neurodegenerative disease, injury, and aging. Generating data on the mRNA transcriptional landscape of the reward system involved in nicotine use disorder and at early stages of withdrawal is critical to begin understanding changes in the gene expression patterns among the various regions involved (here the PFC, CPU, and NAc). While gene expression may be high within specific tissue, a healthy homeostatic brain will try and maintain the levels. Information about perturbations

within the reward system will help to identify gene patterns leading to different functions that lead to changes in behavior so new interventions can be investigated.

Table 3.5. qPCR sex and treatment effects in the prefrontal cortex (PFC).

PFC												
Gene	**Sex**	**Sal**	**Nic**	**24Hr WD**	**48Hr WD**	**Mice n**	**Interaction**	**Sig**	**Main Effect: Sex**	**Sig**	**Main Effect: Treatment**	**Sig**
Bmp4	M	100.00	108.09	94.21	111.22	10-13	F (3, 82) = 1.789	ns	F (1, 82) = 0.0682	ns	F (3, 82) = 0.875	ns
	F	101.81	114.23	110.03	92.90		P=0.1557		P=0.7946		P=0.4579	
Ccl2	M	100.00	107.77	85.07	121.48	10-11	F (3, 77) = 1.808	ns	F (1, 77) = 3.200	ns	F (3, 77) = 1.264	ns
	F	96.41	117.49	140.90	129.41		P=0.1528		P=0.0776		P=0.2926	
Ccl3	M	100.00	77.11	93.82	142.49	10-17	F (3, 82) = 1.374	ns	F (1, 82) = 2.404	ns	F (3, 82) = 2.922	*
	F	126.14	113.94	116.63	127.30		P=0.2564		P=0.1249		P=0.0388	
Ccl4	M	100.00	88.88	88.58	130.30	10-12	F (3, 79) = 2.756	*	F (1, 79) = 1.277	ns	F (3, 79) = 1.345	ns
	F	107.10	102.61	128.15	105.07		P=0.0479		P=0.2619		P=0.2660	
Cxcr4	M	100.00	105.05	69.29	145.48	10-13	F (2, 61) = 1.876	ns	F (1, 61) = 0.0812	ns	F (2, 61) = 0.175	ns
	F	90.68	87.56	106.77	108.77		P=0.1620		P=0.7767		P=0.8402	
Cxcl10	M	100.00	70.15	55.70	133.80	10-12	F (3, 78) = 3.350	*	F (1, 78) = 3.608	ns	F (3, 78) = 4.023	*
	F	53.30	46.51	91.60	86.78		P=0.0232		P=0.0612		P=0.0103	
Cxcl12	M	100.00	101.40	95.22	183.70	10-12	F (3, 80) = 5.766	**	F (1, 80) = 0.255	ns	F (3, 80) = 14.51	****
	F	133.50	94.32	104.40	133.60		P=0.0013		P=0.6151		P<0.0001	
Iba1	M	100.00	113.00	90.58	110.10	10-12	F (3, 81) = 1.817	ns	F (1, 81) = 2.62e-6	ns	F (3, 81) = 1.256	ns
	F	105.10	92.43	102.90	113.30		P=0.1507		P=0.9987		P=0.2950	
Il2	M	100.00	104.30	84.11	125.80	9-12	F (3, 76) = 0.717	ns	F (1, 76) = 1.527	ns	F (3, 76) = 0.543	ns
	F	132.70	146.80	111.20	103.80		P=0.5452		P=0.2204		P=0.6544	
Lif	M	100.00	172.20	99.03	374.50	9-12	F (3, 78) = 1.945	ns	F (1, 78) = 0.759	ns	F (3, 78) = 5.261	**
	F	136.10	160.60	129.80	200.50		P=0.1292		P=0.3863		P=0.0023	
Nox2	M	100.00	98.17	82.91	77.25	10-13	F (3, 82) = 0.423	ns	F (1, 82) = 1.119	ns	F (3, 82) = 0.954	ns
	F	79.90	86.03	87.72	70.04		P=0.7364		P=0.2932		P=0.4186	
Tgfb1	M	100.00	120.80	100.00	128.20	10-13	F (3, 81) = 5.694	**	F (1, 81) = 7.064	**	F (3, 81) = 0.979	ns
	F	118.10	92.44	94.11	85.84		P=0.0014		P=0.0095		P=0.4068	
Tlr4	M	100.00	84.69	80.80	118.80	10-13	F (3, 82) = 1.395	ns	F (1, 82) = 0.5863	ns	F (3, 82) = 3.801	*
	F	104.50	94.96	97.11	104.40		P=0.2503		P=0.4460		P=0.0132	
Tmem119	M	100.00	108.90	109.00	111.60	10-12	F (3, 81) = 1.915	ns	F (1, 81) = 0.9549	ns	F (3, 81) = 0.507	ns
	F	118.60	88.17	99.93	98.13		P=0.1337		P=0.3314		P=0.6785	

Tnfα	M	100.00	103.70	99.53	144.30	10-13	F (3, 81) = 1.253	ns	F (1, 81) = 1.693	ns	F (3, 81) = 1.354	ns
	F	141.00	102.20	136.40	130.80		P=0.2960		P=0.1968		P=0.2627	
Trem2	M	100.00	110.60	99.26	122.10	10-13	F (3, 81) = 3.122	*	F (1, 81) = 0.0154	ns	F (3, 81) = 3.812	*
	F	108.00	91.36	112.70	117.80	10-13	P=0.0304		P=0.9015		P=0.0131	

Table 3.6. qPCR sex and treatment effects in the caudate putamen (CPU).

CPU												
Gene	**Sex**	**Sal**	**Nic**	**24Hr WD**	**48Hr WD**	**Mice n**	**Interaction**	**Sig**	**Main Effect: Sex**	**Sig**	**Main Effect: Treatment**	**Sig**
Bmp4	M	100.00	112.80	97.30	68.47	10-13	F (3, 72) = 1.024	ns	F (1, 72) = 0.8395	ns	F (3, 72) = 5.845	**
	F	92.49	88.84	108.30	62.98		P=0.3871		P=0.3626		P=0.0012	
Ccl2	M	100.00	92.84	64.47	82.99	8-13	F (3, 72) = 2.718	ns	F (1, 72) = 4.303	*	F (3, 72) = 1.960	ns
	F	65.79	54.49	64.11	94.02		P=0.0509		P=0.0416		P=0.1277	
Ccl3	M	100.00	78.17	61.96	64.40	8-12	F (3, 70) = 1.906	ns	F (1, 70) = 2.846	ns	F (3, 70) = 0.733	ns
	F	58.88	58.20	67.63	66.93		P=0.1365		P=0.0961		P=0.5355	
Ccl4	M	100.00	76.13	62.30	77.71	8-13	F (3, 70) = 1.600	ns	F (1, 70) = 3.493	ns	F (3, 70) = 1.291	ns
	F	59.44	46.06	64.48	80.41		P=0.1972		P=0.0658		P=0.2844	
Cxcr4	M	100.00	90.65	57.29	52.37	9-13	F (3, 73) = 3.029	*	F (1, 73) = 1.293	ns	F (3, 73) = 5.526	**
	F	63.70	164.80	94.23	42.51		P=0.0348		P=0.2591		P=0.0018	
Cxcl10	M	100.00	113.70	128.60	181.70	8-12	F (3, 66) = 1.140	ns	F (1, 66) = 0.718	ns	F (3, 66) = 0.785	ns
	F	66.54	140.10	144.80	79.64		P=0.3393		P=0.3998		P=0.5066	
Cxcl12	M	100.00	93.30	89.61	85.27	9-13	F (3, 72) = 0.0693	ns	F (1, 72) = 0.6172	ns	F (3, 72) = 0.458	ns
	F	113.00	99.72	90.87	98.18		P=0.9761		P=0.4347		P=0.7126	
Iba1	M	100.00	116.30	86.42	82.62	9-12	F (3, 73) = 0.5022	ns	F (1, 73) = 5.183	*	F (3, 73) = 1.876	ns
	F	81.45	85.68	68.64	79.09		P=0.6819		P=0.0257		P=0.1411	
Il2	M	100.00	83.52	131.40	88.94	8-10	F (3, 67) = 1.456	ns	F (1, 67) = 1.557	ns	F (3, 67) = 0.572	ns
	F	42.92	88.57	68.37	113.00		P=0.2346		P=0.2164		P=0.6358	
Lif	M	100.00	77.31	62.65	100.50	9-12	F (3, 71) = 0.2067	ns	F (1, 71) = 1.189	ns	F (3, 71) = 4.825	**

	F	81.67	71.79	58.69	95.54		P=0.8914		P=0.2793		P=0.0041	
Nox2	M	100.00	71.02	86.82	73.56	9-12	F (3, 73) = 1.527	ns	F (1, 73) = 6.995	*	F (3, 73) = 0.734	ns
	F	60.90	58.82	46.79	75.87		P=0.2146		P=0.0100		P=0.5349	
Tgfb1	M	100.00	107.50	265.30	90.83	9-12	F (3, 74) = 21.59	****	F (1, 74) = 36.89	****	F (3, 74) = 17.61	****
	F	97.03	78.20	77.93	83.28		P<0.0001		P<0.0001		P<0.0001	
Tlr4	M	100.00	94.58	87.51	104.20	9-13	F (3, 74) = 0.1950	ns	F (1, 74) = 0.3240	ns	F (3, 74) = 2.202	ns
	F	97.13	85.04	81.77	107.90		P=0.8995		P=0.5709		P=0.0950	
Tmem119	M	100.00	105.90	110.70	83.62	9-12	F (3, 75) = 1.821	ns	F (1, 75) = 8.786	**	F (3, 75) = 1.220	ns
	F	96.08	79.20	70.38	78.14		P=0.1505		P=0.0041		P=0.3085	
Tnfα	M	100.00	72.94	65.13	64.46	9-13	F (3, 74) = 0.9563	ns	F (1, 74) = 3.866	ns	F (3, 74) = 1.916	ns
	F	68.26	45.28	55.95	67.64		P=0.4180		P=0.0530		P=0.1344	
Trem2	M	100.00	95.43	105.30	83.49	9-13	F (3, 72) = 1.229	ns	F (1, 72) = 8.766	**	F (3, 72) = 0.772	ns
	F	78.19	79.77	83.75	84.96		P=0.3055		P=0.0042		P=0.5137	

Table 3.7. qPCR sex and treatment effects in the nucleus accumbens (NAc)

NAc												
Gene	**Sex**	**Sal**	**Nic**	**24Hr WD**	**48Hr WD**	**Mice n**	**Interaction**	**Sig**	**Main Effect: Sex**	**Sig**	**Main Effect: Treatment**	**Sig**
Bmp4	M	100.00	102.00	96.27	76.27	10-13	F (3, 78) = 1.515	ns	F (1, 78) = 0.8294	ns	F (3, 78) = 9.459	****
	F	121.80	98.30	100.90	71.75		P=0.2171		P=0.3652		P<0.0001	
Ccl2	M	100.00	106.20	104.20	46.33	9-12	F (3, 74) = 1.969	ns	F (1, 74) = 1.309	ns	F (3, 74) = 1.495	ns
	F	122.60	79.30	107.60	105.40		P=0.1260		P=0.2563		P=0.2228	
Ccl3	M	100.00	146.70	77.79	15.71	10-12	F (3, 78) = 1.143	ns	F (1, 78) = 1.148	ns	F (3, 78) = 8.037	****
	F	101.60	91.90	51.59	32.22		P=0.3369		P=0.2873		P<0.0001	
Ccl4	M	100.00	111.80	106.10	51.29	9-12	F (3, 77) = 1.751	ns	F (1, 77) = 0.0177	ns	F (3, 77) = 4.085	**
	F	109.80	79.37	98.92	76.08		P=0.1636		P=0.8945		P=0.0095	
Cxcr4	M	100.00	95.51	76.28	127.80	10-12	F (3, 78) = 0.1430	ns	F (1, 78) = 2.174	ns	F (3, 78) = 3.873	*
	F	86.94	67.38	65.97	115.20		P=0.9339		P=0.1444		P=0.0123	
Cxcl10	M	100.00	60.81	68.37	114.10	9-11	F (3, 73) = 2.296	ns	F (1, 73) = 2.147	ns	F (3, 73) = 0.288	ns
	F	79.77	126.40	156.00	91.99		P=0.0848		P=0.1472		P=0.8339	
Cxcl12	M	100.00	78.97	79.53	98.84	9-12	F (3, 77) = 0.4122	ns	F (1, 77) = 7.179	**	F (3, 77) = 4.342	**
	F	119.60	97.38	94.34	103.00		P=0.7447		P=0.0090		P=0.0070	
Iba1	M	100.00	100.90	108.20	100.90	9-13	F (3, 76) = 0.4361	ns	F (1, 76) = 6.522	*	F (3, 76) = 1.142	ns
	F	117.00	121.70	150.50	117.40		P=0.7278		P=0.0127		P=0.3377	
Il2	M	100.00	61.47	111.40	23.24	8-12	F (3, 70) = 0.7451	ns	F (1, 70) = 0.0280	ns	F (3, 70) = 3.377	*
	F	79.89	71.98	84.03	50.36		P=0.5288		P=0.8675		P=0.0230	
Lif	M	100.00	129.80	105.70	154.50	10-12	F (3, 76) = 0.5170	ns	F (1, 76) = 5.100	*	F (3, 76) = 2.159	ns
	F	146.00	143.60	140.70	165.40		P=0.6718		P=0.0268		P=0.0999	
Nox2	M	100.00	77.66	106.60	104.20	10-13	F (3, 77) = 2.375	ns	F (1, 77) = 0.2227	ns	F (3, 77) = 1.884	ns
	F	78.66	102.30	117.30	74.56		P=0.0766		P=0.6383		P=0.1393	
Tgfb1	M	100.00	111.80	106.30	111.10	9-13	F (3, 74) = 0.8641	ns	F (1, 74) = 1.542	ns	F (3, 74) = 0.319	ns
	F	139.10	108.50	108.90	124.30		P=0.4637		P=0.2183		P=0.8118	
Tlr4	M	100.00	100.40	96.37	90.42	9-12	F (3, 77) = 0.3623	ns	F (1, 77) = 0.0002	ns	F (3, 77) = 1.926	ns
	F	103.40	96.79	101.90	84.83		P=0.7804		P=0.9897		P=0.1323	
Tmem119	M	100.00	101.20	133.50	74.96	9-13	F (3, 76) = 1.106	ns	F (1, 76) = 0.0789	ns	F (3, 76) = 2.377	ns
	F	106.60	118.50	105.60	90.30		P=0.3521		P=0.7796		P=0.0765	

Tnfα	M	100.00	145.40	83.86	73.98	9-11	F (3, 73) = 4.323	**	F (1, 73) = 0.1303	ns	F (3, 73) = 0.639	ns
	F	116.10	76.24	91.88	138.10		P=0.0073		P=0.7191		P=0.5927	
Trem2	M	100.00	108.30	113.90	110.00	9-12	F (3, 78) = 0.6118	ns	F (1, 78) = 3.463	ns	F (3, 78) = 0.372	ns
	F	120.30	114.50	114.60	126.60		P=0.6094		P=0.0665		P=0.7734	

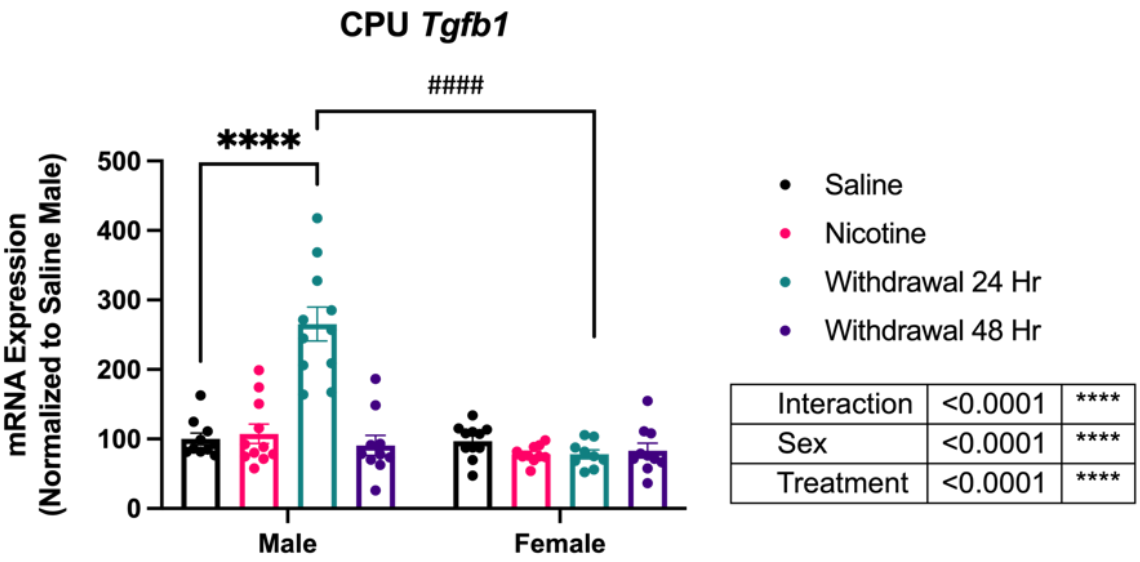

Figure 3.3. Cytokine mRNA expression levels in the PFC, CPU, and NAc of chronic nicotine and 24Hr and 48Hr WD animals. A bar chart illustrates *Tgfb1* mRNA expression in the CPU with a main effect of interaction, sex, and treatment with an n=9-12. Individual significance is noted in males between the saline and 48Hr WD group which is significantly increased (****). Individual significance is also found between the males and females at the 24Hr WD group, which is diminished in females as compared to males. All qPCR data is normalized to the male saline group at 100%. Post hoc analysis between sexes by Šídák's ($^{\#}$P<0.05, $^{\#\#}$P<0.01, $^{\#\#\#\#}$P<0.0001) and within sex Dunnett's multiple comparisons test (*P<0.05, **P<0.01, ****P<0.0001) after two-way ANOVA.

3.3.4. Both main effects and post hoc analysis in gene expression data

This data can be further summarized with genes whose mRNA expression shows both a significant main effect (interaction (I), sex (S), or treatment (T)) and a significant effect in post hoc analysis either between males and females or within the treatment groups for their sex (See Table 3.8).

Table 3.8. Genes with significant gene expression in main effect and post hoc analysis.

	Main Effect and post hoc significance
PFC	*CCl3 (T), Ccl4 (I), Cxcl12 (I,T), Lif (T), Tgfb1 (I,S), Tlr4 (T)*
CPU	*Ccl2 (S), Cxcr4 (I,T), Lif (T), Tgfb1 (I,S,T), Tmem119 (S)*
NAc	*Bmp4 (T), Ccl3 (T), Ccl4 (T), Cxcl12 (S,T), Il2 (T), Tnfα (I)*

Key: Interaction (I), Sex (S), or Treatment (T) main effects

3.3.5. Neither main effects nor post hoc analysis in gene expression data

However, in each of the brain regions of interest, there are cytokines with mRNA gene expression exhibiting neither significant main effect nor post hoc with significant individual effects between groups. The genes and the brain regions of interest are found in Table 3.9.

Table 3.9. Gene expression that had no significance in their statistics.

	No Significance in ANOVA and post hoc
PFC	*Bmp4, Cxcr4, Iba1, Il2, Nox2, Tnfα*
CPU	*Ccl2, Cxcl10, Cxcl12, Il2, Tlr4, Tnfα*
NAc	*Ccl2, Cxcl10, Tgfb1, Tlr4, Tmem119, Trem2*

3.3.6. Gene expression data with significant main effect only (no significant post hoc)

In the PFC, two cytokines have mRNA expression which exhibits a significant main effect, *Cxcl10* for interaction and treatment, and *Tlr4* for treatment with no significance within their post hoc analysis. Upon examination of the data for these cytokines and recognizing that the ANOVA indicates differences across the means, the spread of the data may be biasing the means toward global significance. *Cxcl10* is also

important for initiating chemotaxis in the inflammatory process and *Tlr4* has also been implicated in inflammation from AUD; therefore, both are of interest in our model [251, 252].

In the CPU, there are 4 genes that show this pattern of a significant main effect finding with no individual differences of significance between treatment groups or sex. The only gene with a significant treatment main effect is *Bmp4*, a gene critical in neurodevelopment but with little information described in the adult outside of the hippocampus. There are 3 genes with significant sex effect; of the three, *Iba1* and Nox2, have been previously described. *Trem2*, a gene studied in AD, has an important role in microglial phagocytosis of debris in neuronal death (ATP release) [253] and demyelination induced by cuprizone and described in models of Multiple Sclerosis (MS). Thus in 2 different diseases of neuroinflammation, illustrating its role may be important in the neuroinflammatory state of nicotine withdrawal [254].

Lastly, in the NAc, 3 genes exhibit this significant main effect without post hoc significance: *Cxcr4* (treatment), *Iba1* (sex), and *Lif* (sex). *Cxcr4* is the receptor for the cytokine *Cxcl12* and is also important for cortex development but is heavily implicated in neuroinflammation and neurodegenerative disease such as in AD [240, 241, 243]. The microglial marker *Iba1* is again of note, and, finally, *Lif,* was previously discussed for its association with neuroinflammation in neurodegenerative disease in section 3.3.2.

3.3.7. Gene expression data with significant individual post hoc data only (no significant main effects)

Beginning with mRNA expression data from the PFC (Table 3.5), cytokines *Ccl2* (Appendix Figure A.3) and *Tmem119* (Appendix Figure A.10) exhibit no significant main effects but have significance in their individual post hoc analysis. Thus, the difference between the groups is significant even though the global effect is not. The *Ccl2* cytokine is also referred to as a chemokine and is known to induce chemotaxis. The gene expression has been studied in alcohol use disorder (AUD), a disorder that also involves the mesolimbic reward pathway and may have strong applicability to nicotine use and withdrawal inflammation. In 2005, Blednov et al discovered that when *Ccl2* was knocked out in female mice, the mice had a reduced preference for and consumption of ethanol, while a male knock out did not [255]. In our data, *Ccl2* expression was increased in females when compared to males in the 24Hr WD group. The second cytokine, *Tmem119,* was first described as gene specific to microglia that was stable, developmentally regulated, and robustly expressed marker in 2016 [150]. This gene is often used as a microglial marker. In our microglial morphology analysis in Chapter 2, we instead used an antibody to the membrane protein Iba1 as *Tmem119* has been found to be unstable in ischemic stroke [212] and may not be stable in all contexts. In the PFC, there was a significant decrease in *Tmem119* expression in the females between saline and the nicotine group. However, the spread is wider in the saline than some genes, and this may be biasing this significance.

Continuing in the CPU (Table 3.6), *Ccl3* mRNA expression once again exhibits no significant main effects (no global effect) but has significance in their individual post hoc analysis (Appendix Figure A.4). There is a significant difference between the males and females at the baseline saline level not previously significant by t-test for sex alone. There is also a significant change within the male treatment groups where the saline to 24Hr Wd group *Ccl3* expression decreases. Also, within the CPU, the *Bmp4, Iba1,* and *Nox2* mRNA expression each exhibit a significant main effect. For *Bmp4,* the main effect is in treatment, and, for *Iba1* and *Nox2*, the main effect is in sex. With *Bmp4* (Figure A.3), the only post hoc significance is in female NAc mice with a drop in expression between saline and the 48Hr Wd group. Like *Ccl2, Ccl3* has been investigated in the reward system in AUD where knockout females exhibited a significant decrease in alcohol preference and amount consumed [255] and could have implications in other substance use disorders.

Finally, there is one gene in the NAc, *Nox2*, that exhibited no significant main effect but, in the females, has a significant increase in the 24Hr WD group as compared to saline control. Adeluyi et al. in 2019 reported the finding that *Nox2*, enriched in microglia, was the source of excess ROS in the NAc during nicotine withdrawal [56].

3.3.8. Interesting male expression pattern in the PFC 48Hr WD group

The last pattern of interest to point out is that of a consistent trend in the PFC in male mice. While not all are significant increases, numerous genes trend upward in mRNA expression in the 48Hr WD group over saline. These include *Ccl3, Ccl4, Cxcr4, Cxcl10*, *Cxcl12, Lif*, and *Tgfb1*. Gene expression patterns this consistent amongst so

many genes may signal that this 48-hour withdrawal timepoint is a critical one, which shows a sex-based bias in males. This treatment group should be further investigated at a protein level to see if the trend continues and if there is a possible signaling cascade that is very particular to this group. Another reason why sex differences should also be taken into consideration is the fact that men and women both begin and quit smoking for different reasons, and women have a 31% lower chance of quitting than men without pharmacotherapies [256]. When given varenicline, women's quit rates went up to match that of men [257], though the success rates remain around 20% at one year [258] and there is still need for more successful cessation treatments. When searching for new targets in the arena of neuroinflammation, having both sexes included may help tease out the molecular differences for these behaviors.

Our data show that there are genes (*Ccl4, Cxcl10, Cxcl12,* Lif, and *Tnfα*) known for their role in inflammation that exhibit a significant increased expression baseline in females as compared to males. As described in Chapter 2, this could be due to the increased microglial density found in these regions (all trending higher in females and at significance in the CPU and NacS). The mRNA expression was not normalized to microglial number as other genes of interest in the inflammatory process were examined. Of note, this experimental design did not account for monitoring sex hormone levels in the animals or the stage of estrus for the females. We used 7–8-week-old mice which would correlate to adult humans in their 20s.

We also described the analysis of the effect of treatment and sex upon 16 target genes within our brain regions of interest and ascertained significant findings in all

regions and in many of the genes. The pattern of mRNA expression in males, which increases in the 48HR WD over saline, is a very interesting find and should be examined to see if the gene expression correlates to significant changes at a protein level.

3.4. Conclusion

When examining sex as a biological variable (SABV), we found 5 cytokines which had variable RNA expression between males and females with significance in differing brain regions. There were patterns of gene expression that also varied both by sex and/or treatment. One striking example was the 48Hr WD treatment group of the PFC, in which a number of genes had increased RNA expression only within males. We were able to identify genes important in substance use disorder and in neuroinflammatory genes which were altered by sex and/or treatment, alterations which could be involved in the local cues affecting gene signatures. Lastly, while the transcription profile is the best beginning to associate genotype to phenotype with nicotine treatment and nicotine withdrawal, it must be followed up at the translational level.

Chapter 4. Translational Changes in Response to Chronic Nicotine and Withdrawal Timepoints

4.1. Introduction

Inflammation and neuroinflammation are composed of multiple components involved in signaling as well as triggering complex immune cascades. These components are important in allowing the body or brain to restore homeostasis, clear disease, or infection, and ultimately to attempt to repair damage from insult. Our mouse model of chronic nicotine involves a prolonged exposure of nicotine, which crosses over the blood brain barrier (BBB), hijacking the reward system. While nicotine is known to cause inflammation in the body and biomarkers for inflammation and oxidative stress rise in the periphery [259], it has also been found to have anti-inflammatory effects in conditions such as obesity, ulcerative colitis, MS, PD, and provide neurocognitive protection through the $a4b2$ nAChRs [163, 260-263]. Nicotine's pro-inflammatory effects have been documented in damaging the BBB and there is conflicting information on the harmful effects in ulcerative colitis [264-266]. As cytokines such as IL1A, IL1B, IL1, IL6, TNFA, and LIF are known to transport across the blood brain barrier, the shift in their levels could be altered with a damaged BBB [267, 268]. While there is typically a positive correlation between mRNA and protein expression, it is critical to analyze not just the RNA expression, as we accomplished in Chapter 3, since measurements have suggested that only ~40% of proteins correlate to high mRNA expression be variable for

downregulated genes [269]. Changes in the cytokine protein levels in the reward system could affect neuronal firing, plasticity, and behavior in a system that has already been usurped by nicotine. In this portion of the study, we aimed to profile the cytokine profiles of both peripheral serum and specific brain regions for absolute values and analyze the data for sex and treatment differences in hopes of furthering the study of nicotine's pro- and anti-inflammatory effects.

4.2. Materials and Methods

Animals and experimental design - see Chapter 2 Materials and Methods.

4.2.1. Mouse serum peripheral cytokine measurement

Circulating levels of cytokines following nicotine treatment and withdrawal were performed using a MILLIPLEX® MAP mouse cytokine/chemokine magnetic bead panel (MilliporeSigma Cat. MCYTOMAG-70K-PX32, Burlington, MA) to measure serum levels of 32 cytokines/chemokines. Blood was collected at the time of animal sacrifice and was allowed to clot for 30 minutes at room temperature. The tubes were then centrifuged at 2000 x g for 10 minutes at 4°C to separate the cells and the cleared serum supernatant transferred to a new tube and stored at -80°C until testing. Across the animal treatment groups, there were n=15-18 mice per treatment. Samples of 25 µl were run on a ® MAGPIX Multiplex ELISA system (LED) and quantified using MILLIPLEX® Analyst 5.1 software. The assays were calibrated using duplicate 8-point standard curves, and raw intensity measurements were converted to absolute protein concentrations using proprietary software [270].

Table 4.1. MILLIPLEX® MAP Mouse Cytokine/Chemokine Magnetic Bead Panel.

Chemokines	Eotaxin (CCL11), MCP1 (CCL2), MIP1A (CCL3), MIP1B (CCL4), MIP2 (CXCL2), RANTES (CCL5), MIG (CXCL9), CXCL5 (LIX), IP10(CXCL10), CXCL1 (KC)
Interleukins	IL1α, IL1β, IL2, IL3, IL4, IL5, IL6, IL7, IL9, IL10, IL12B, IL12 (p70), IL13, IL15, IL17
Interferons	IFNG
Growth Factors	GMCSF (CSF2), GCSF(CSF3), VEGF, LIF, MCSF (CSF1)
TNF Receptor Superfamily Members	TNFA

4.2.2. Cytokine measurement protein

Sex and brain region specific neuroimmune differences were examined in brain tissue using the previously described MILLIPLEX® MAP mouse cytokine/chemokine Panel (MilliporeSigma Cat. MCYTOMAG-70K-PX32, Burlington, MA) and Table 4.1. The NAc and CPU tissue samples (2mm punches previously stored at -80°C) were homogenized in 34 µl of lysis buffer (100 mM PIPES; pH 7.0, 500 mM NaCl, 2 mM EDTA, 0.1% (w/v) sodium azide, 2% (w/v) bovine serum albumin, 0.2% (v/v) Triton X-100, 5 µg/ml aprotinin, 0.1 µg/ml pepstatin A, and 0.5 µg/ml antipain) using a Pellet Pestle™ Cordless Motor on ice. PFC tissue (stored after microdissection at -80°C) was homogenized in 104 µl of the above-described lysis. The homogenate was centrifuged at 2500 rpm for 30 min at 4°C. The supernatant was removed, and the total measured by Pierce™ BCA Protein Assay Kit (Thermo Fisher Scientific, Waltham, MA) following manufacturer's instructions. Samples were diluted to 2 mg/ml protein concentration in the above lysis buffer and stored at -80°C until testing. Samples were run on a Luminex® MAGPIX Multiplex ELISA system (LED) and quantified using MILLIPLEX® Analyst 5.1 software.

4.2.3. Data analysis and statistics

All Luminex® assay cytokine results are reported in pg/ml without normalization. Upon the completion of an assay all analyte data were inspected, and samples that were below the detectable limit of the assay within each analyte that did not meet minimum detection values (NAN) across all treatment groups (not in only 1 treatment group which would denote a true effect) were not included in analysis. Samples with high inter-plate variability were also excluded. Data that was near the lower limit was only considered as equal to the lower limit value if greater than half of all reported wells contained a valid reading. Results are presented as mean ± SEM. Statistical analysis was performed and graphed in GraphPad Prism 9 for macOS version 9.2.0 (GraphPad Software, LLC., San Diego, CA) with results presented as mean +/- SEM. The GraphPad online calculator was used for the outlier test (Grubbs' test or extreme studentized deviate (ESD) (https://www.graphpad.com/quickcalcs/grubbs1/) for each treatment condition removing at most 1 outlier per group based on the Alpha=0.05). Individual cytokines were analyzed by two-way ANOVA using treatment and sex as primary variables. Post hoc analysis for male and female comparisons was completed using Šídák's multiple comparisons test post hoc analysis and treatment differences were completed using Dunnett's multiple comparisons test post hoc analysis. The inter-cytokine correlation for all treatment groups in serum or protein was determined using a Pearson correlation analysis matrix.

4.3. Results and Discussion

4.3.1. An overview of protein detection used

In Chapter 3, we analyzed the mRNA expression of a number of chemokines and cytokines. In this chapter, we move from transcription to protein expression. While ELISA and Western blotting are gold standard approaches to quantitating protein, they are single antibody per analyte approaches. Working in mice means a limited amount of protein sample available due to the smaller brains, which decreases the number of individual antibodies one could assay. For this reason, we moved into flow cytometric multiplex arrays, a bead-based format to simultaneously analyze multiple chemokine and cytokine proteins using the Luminex® technology, which has higher throughput, requires small sample sizes, has a lower relative cost compared to ELISA or the cost of numerous antibodies, and most importantly provides high sensitivity and dynamic range [271, 272]. This assay was used in conjunction with a premade optimized mouse panel of 32 chemokines and cytokines (see Table 4.1 and Figure 4.1) and was performed in collaboration with the laboratory of Dr. Georgia Hodes (Virginia Polytechnic Institute and State University), which studies individual differences in stress, mood disorders, and neuroimmunity.

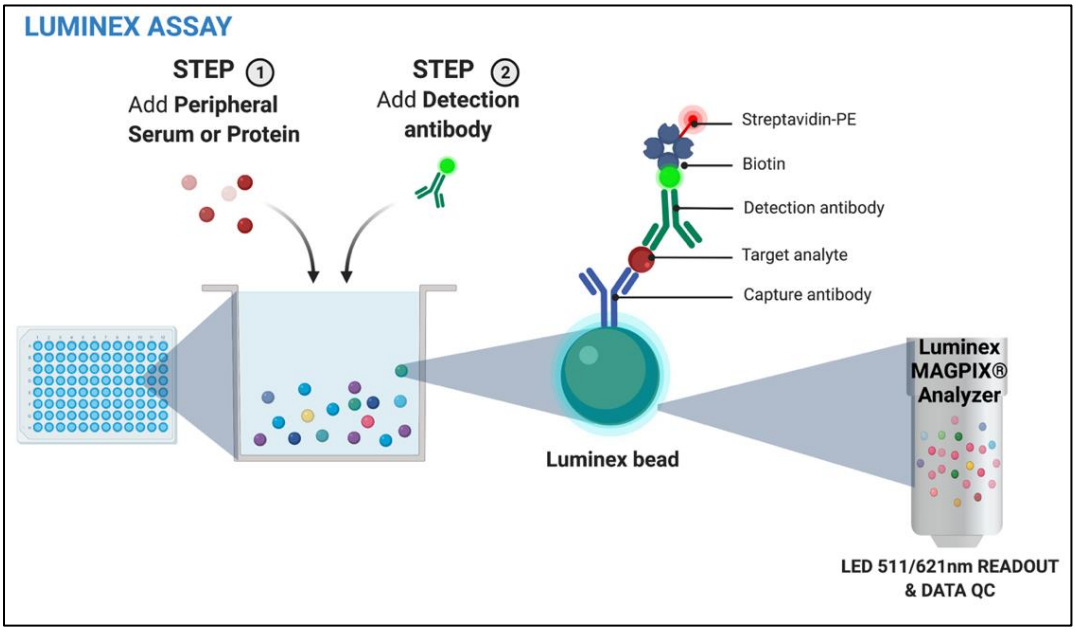

Figure 4.1. Schematic of the Luminex®® xMAP® bead-based technology for multiplex simultaneous analyte detection and quantification.

4.3.2. Synopsis of peripheral protein data

Initial protein assays were performed on peripheral mouse serum (mouse/treatment group n=14-18) and the overall assay results are listed in Table 4.2, with statistics listed in Table 4.3. A number of cytokines were discarded due to failure to meet detection limits (CXCL5, IFNG ,IL1A, IL1B, IL2, IL3, IL4, IL7, IL9, IL10, IL12B, IL15, IL17, MCSF, MCP1 (CCL2), MIP1B (CCL4), RANTES (CCL5), VEGF) and 3 not shown as they had no significant effects of sex or treatment (IL1A, IL1B, IL2). MCSF was rejected from the final set due to high intra-plate variability. Of the remaining set for analysis, 7 of the 14 to be analyzed are from a specific subset of cytokines called chemokines, including CXCL1 (KC), Eotaxin, IP10 (CXCL10), MCP1 (CCL2), MIG (CXCL9), MIP1A (CCL3), and MIP2 (CXCL2). Chemokines are cytokines that are secreted, producing signals for immune cell

migration. This is especially true for eosinophils that secrete chemokines as well as many cytokines [273].

Table 4.2. Mouse serum tested on and MILLIPLEX® MAP mouse cytokine/chemokine panel overall results. Chemokines in Bold.

Rejected Raw Data/ High Variability	No Significance	Main Effect and Post Hoc Significance
CXCL5 (LIX), IFNG, IL3, IL4, IL7, IL9, IL10, IL12B (p70), IL15, IL17, CXCL5 (LIX), MCSF (CSF1), MIP1B (CCL4), RANTES (CCL5), VEGF	IL1A, IL1B, IL2,	**CXCL1 (KC) (S,T), Eotaxin (CCL11) (S),** GCSF (I,T), GMCSF (significant post hoc), IL5 (T), IL6 (T), IL12B (T), IL13 (T), **IP10 (S,T), MCP1 (CCL2) (T), MIG (CXCL9) (S,T), MIP1A (CCL3) (S,T), MIP2 (CXCL2) (I,T),** TNFA (S,T)

Key: Interaction (I), Sex (S), Treatment (T) main effects, non-significant (ns)

Table 4.3. Luminex® assay of peripheral serum protein with main effect statistics.

Serum												
Gene	Sex	Sal pg/ml	Nic pg/ml	24Hr WD pg/ml	48Hr WD pg/ml	Mice/ group	Interaction	Sig	Main Effect: Sex	Sig	Main Effect: Treatment	Sig
CXCL1	M	17.47	20.49	9.80	9.46	14-18	F (3, 120) = 1.700	ns	F (1, 120) = 15.29	***	F (3, 120) = 3.49	*
	F	33.50	25.59	30.60	14.86		P=0.1706		P=0.0002		P=0.0180	
Eotaxin	M	305.40	331.50	304.40	203.20	14-18	F (3, 122) = 1.185	ns	F (1, 122) = 0.164	ns	F (3, 122) = 3.41	*
	F	275.70	329.70	295.30	276.10		P=0.3182		P=0.6858		P=0.0197	
GCSF	M	121.70	147.00	141.80	163.90	14-17	F (3, 119) = 3.222	*	F (1, 119) = 28.66	****	F (3, 119) = 1.97	ns
	F	474.70	411.10	370.90	173.40		P=0.0252		P<0.0001		P=0.1229	
GMCSF	M	6.95	3.94	4.53	3.07	14-17	F (3, 119) = 0.782	ns	F (1, 119) = 0.0002	ns	F (3, 119) = 2.26	ns
	F	5.10	4.97	4.87	3.59		P=0.5061		P=0.9893		P=0.0850	
IL5	M	3.73	2.90	5.15	2.32	14-18	F (3, 119) = 2.609	ns	F (1, 119) = 26.02	****	F (3, 119) = 1.35	ns
	F	11.19	10.66	5.99	7.17		P=0.0547		P<0.0001		P=0.2602	
IL6	M	8.10	8.10	7.10	4.25	14-18	F (3, 122) = 0.066	ns	F (1, 122) = 21.53	****	F (3, 122) = 1.24	ns
	F	15.41	16.99	16.09	11.72		P=0.9777		P<0.0001		P=0.2976	
IL12B	M	2.40	2.97	2.89	3.44	14-18	F (3, 121) = 1.934	ns	F (1, 121) = 29.38	****	F (3, 121) = 0.50	ns
	F	5.78	5.84	4.66	4.24		P=0.1276		P<0.0001		P=0.6855	
IL13	M	93.93	92.85	86.34	84.70	14-18	F (3, 120) = 0.150	ns	F (1, 120) = 17.89	****	F (3, 120) = 0.77	ns
	F	118.20	109.10	111.00	105.80		P=0.9298		P<0.0001		P=0.5136	
IP10	M	38.82	49.21	47.65	37.02	15-18	F (3, 123) = 0.733	ns	F (1, 123) = 10.21	**	F (3, 123) = 3.91	*
	F	55.62	57.8	54.41	42.64		P=0.5345		P=0.0018		P=0.0105	
MCP1	M	6.11	7.67	6.71	7.89	14-17	F (3, 119) = 0.813	ns	F (1, 119) = 19.06	****	F (3, 119) = 0.89	ns
	F	10.64	12.88	11.32	9.33		P=0.4891		P<0.0001		P=0.4507	
MIG	M	49.46	49.22	53.20	71.16	14-18	F (3, 121) = 0.660	ns	F (1, 121) = 29.87	****	F (3, 121) = 7.42	***
	F	75.22	74.76	72.61	110.30		P=0.5781		P<0.0001		P=0.0001	
MIP1A	M	19.51	21.89	21.63	17.40	14-18	F (3, 121) = 0.843	ns	F (1, 121) = 6.236	*	F (3, 121) = 3.01	*
	F	27.47	24.59	26.32	18.30		P=0.4730		P=0.0139		P=0.0330	
MIP2	M	40.27	56.59	61.98	61.84	14-18	F (3, 120) = 2.753	*	F (1, 120) = 17.30	****	F (3, 120) = 1.62	ns
	F	74.33	65.17	72.10	71.96		P=0.0456		P<0.0001		P=0.1881	
TNFA	M	3.36	3.27	3.30	2.51	14-17	F (3, 118) = 1.220	ns	F (1, 118) = 9.042	**	F (3, 118) = 4.09	**
	F	5.31	4.48	3.77	2.89		P=0.3056		P=0.0032		P=0.0084	

4.3.3. Sex as a biological variable in peripheral cytokine protein expression

Of the fourteen peripherally significant cytokines in Table 4.3, sex differences at baseline (saline control treatment group) were analyzed. Ten of the fourteen cytokines show significantly increased protein expression when analyzed for sex difference including the five of the above chemokines (CXCL1(KC), GCSF, IL5, IL12B, IP10 (CXCL10), MCP1 (CCL2), MIG (CXCL9), MIP1A (CCL3), MIP2 (CXCL2), TNFA) in Figure 4.2 and statistics table in Appendix Table A.12. Cytokine levels in plasma are often quite low and may be below detection in healthy subjects. Cytokines respond to insult such as drugs, trauma, injury, age, and disease with a strong immune response. This is evidenced when searching for cytokine biomarkers in sedation (non-human primates), autism spectrum disorder, bipolar disorder, treatment-resistant depression, and schizophrenia [274-280]. This response often shows a difference in sex as a biological variable with a higher response in women. Women are known to have higher incidence of autoimmune disease, produce more robust response to vaccines, and are less susceptible to infection as compared to men, and research is underway to see which contributions the X-chromosome genes, and which hormones, may be involved with respect to women's immunity and immune response [213-215].

It is important to study these biological differences and recognize that perhaps novel therapeutics could be targeted by sex as well as application. The high number of serum cytokines with increased protein expression in females to males (12 of 14) is quite striking. While the data spread in females tends to be greater than in males, the expression differences range from 28-58% greater. While this baseline level could be

due to differences in androgen and estrogen contributions that are not accounted for, we must also consider whether the effect of surgical minipump implantation affects the immune response in females more than males in certain cytokines.

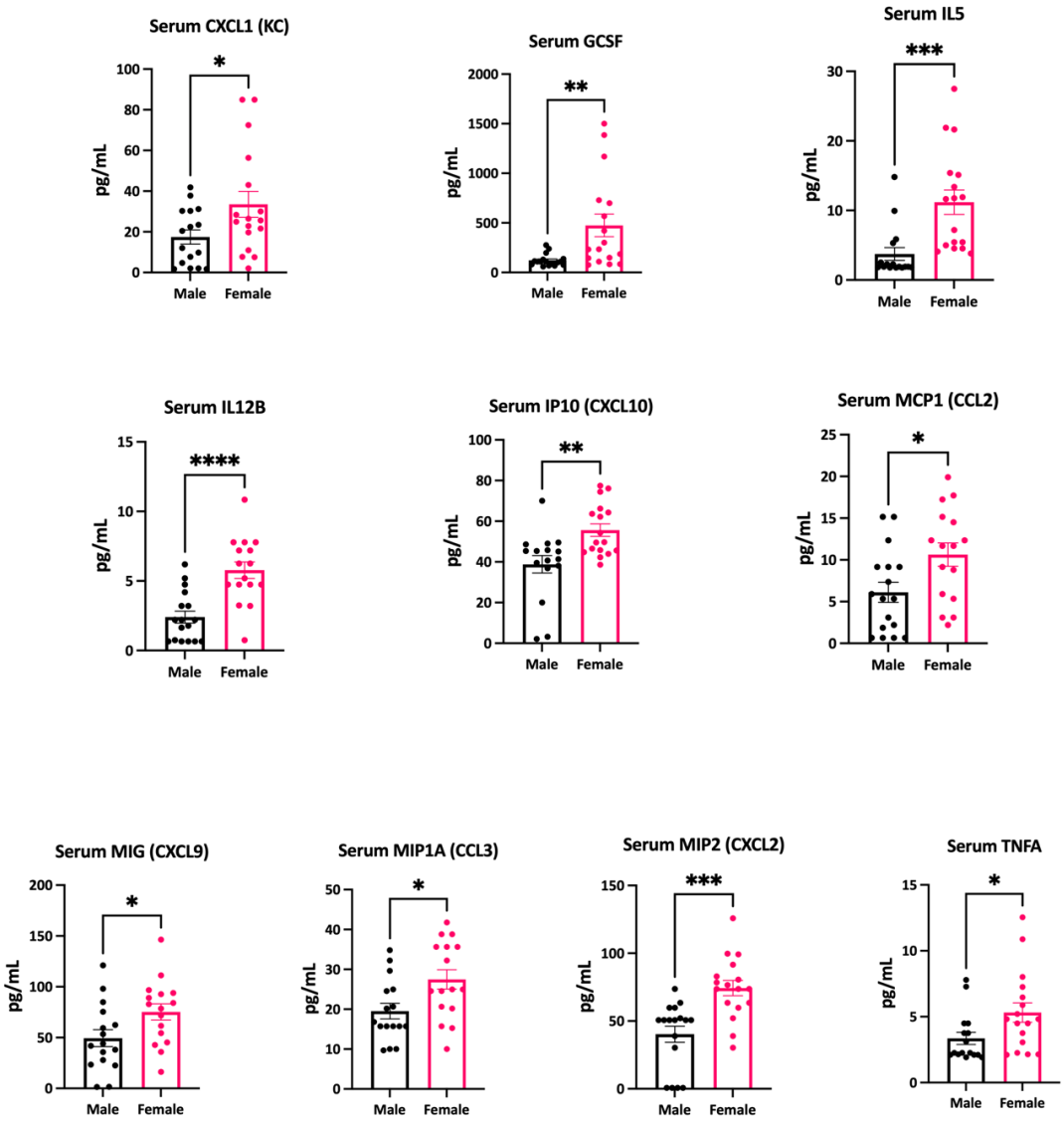

Figure 4.2. Serum (peripheral) cytokine protein expression of males compared to females in the saline control group (baseline control) two-tailed t-test. Increased expression in females over males, n=14-18, *P<0.05, **P<0.01, ***P<0.001, ****P<0.0001.

4.3.4. Both main effects and post hoc analysis in gene expression data

Only 1 cytokine, GMCSF, also known as colony stimulating factor 2 (CSF2), had no significance on any main effect but had a significant post hoc by Dunnett's multiple comparison test (see Figure 4.3). In the 48Hr WD group of males, the protein level, reported in pg/mL, as compared to the saline treated control decreased by 56%. This is the opposite effect seen during treatment at the mRNA level in the PFC male mice in many of the cytokines tested where there was an increase in gene expression in the 48Hr WD treatment group (see Chapter 3). This underscores the importance of analyzing both RNA and protein levels, as they do not always correlate. GMCSF is a growth factor that controls the production, differentiation, and function of granulocytes and macrophages. It is also an important mediator of innate immune response and the drop in the male 48Hr WD group only, while the 48Hr WD female group remains high. This type of higher level is seen in chronic inflammatory autoimmune diseases such as rheumatoid arthritis (RA) and systemic lupus erythematosus (SLE), making GMCSF a target for anti-inflammatory therapeutics [281, 282].

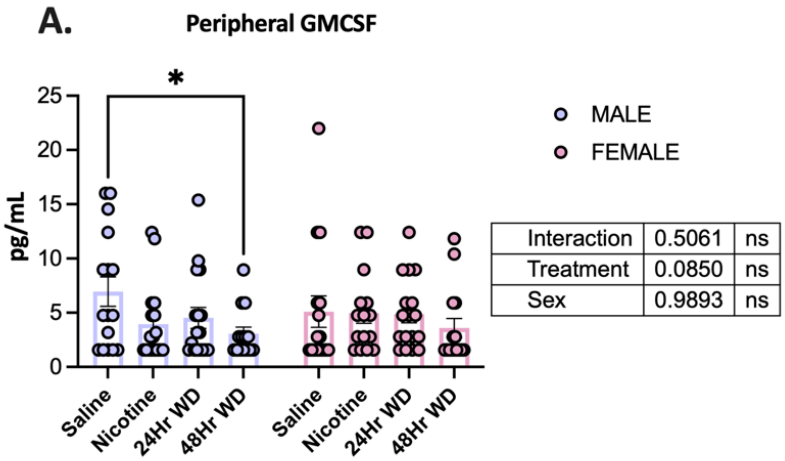

Figure 4.3. GMCSF (CSF2) is the only peripheral cytokine with no significant main effect but has a significant post hoc by Dunnett's multiple comparison test. This is after the two-way ANOVA within the males only at the 48HR WD group, n=14-18, *P<0.05.

Of the remaining 13 cytokines with significant main effects, Eotaxin (CCL11) was the lone peripheral cytokine exhibiting only a main effect for treatment (Figure 4.4). In the periphery, there is a significant drop in the protein level (33.3%) for males in the 48Hr WD group as compared to the male saline control group. This protein has been investigated in humans and has been shown to be a critical biomarker in a number of indications, such as aging, possibly neurodegeneration, alcohol use disorder (AUD) and cocaine use disorder (CUD) with comorbid mental disorders, ALS, bipolar disorder, schizophrenia, major depression, obsessive-compulsive disorder, and increases due to nicotine e-vapor as thirdhand exposure [283-286]. Eotaxin has been studied in C57BL/6, a parental background for our mouse strain, and was found to have high Eotaxin/CCL11 levels in response to the prototypical stimulator of inflammation, lipopolysaccharide (LPS). LPS has been investigated as a biomarker of BBB disruption and may show strain

dependent increases, thus showing the importance of verifiable lead targets in human plasma [287, 288].

A main effect of interaction and sex was found in peripheral GCSF and MIP2 with baseline sex differences already denoted above in Figure 4.2. GCSF, granulocyte colony–stimulating factor also studied in CUD, displayed a decrease in protein expression at the 48Hr WD group for females and had increased expression as compared to the males Figure 4.5 [289]. MIP2, a chemokine for neutrophil recruitment, had the previously noted sex difference, and significant protein increases in the nicotine, 24Hr WD, and 48Hr WD treatment groups compared to male saline. MIP2 MAb is being investigated as a possible therapeutic for myocarditis, a condition to which smokers are highly vulnerable [290].

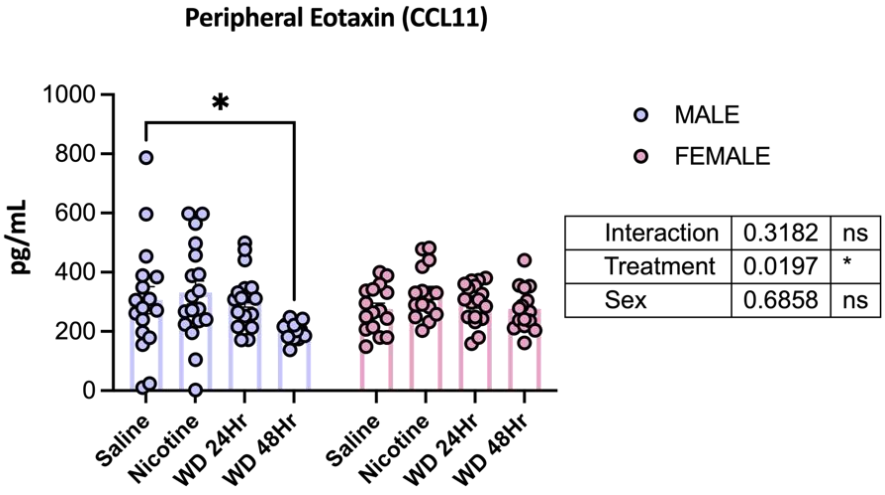

Figure 4.4. Peripheral serum protein level of Eotaxin (CCL11) denoting a main effect of treatment by two-way ANOVA and significant hoc by Dunnett's multiple comparison test. This is after the two-way ANOVA within the males only at the 48HR WD group, n=14-18,*P<0.05.

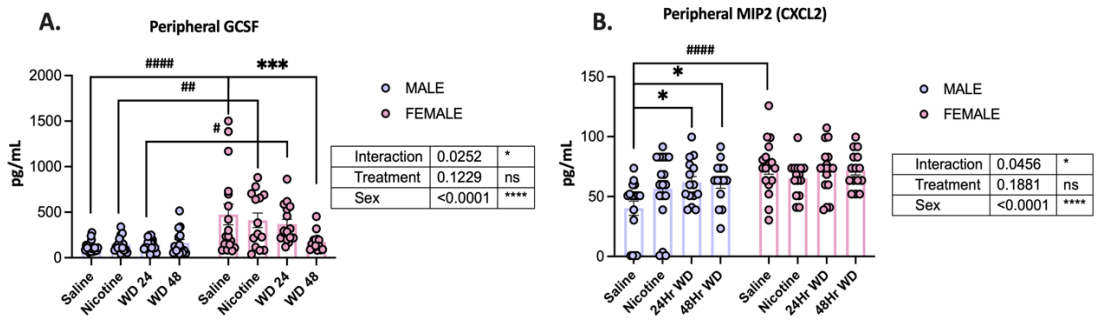

Figure 4.5. Peripheral cytokines (A) GCSF and (B) MIP2 which exhibit main effects of interaction by two-way ANOVA and with significant post hoc within sex by Dunnett's (*P<0.05, **P<0.01, ***P<0.001, ****P<0.0001) and between sex by Šídák's ($^{\#}$P<0.05, $^{\#\#}$P<0.01, $^{\#\#\#}$P<0.001, $^{\#\#\#\#}$P<0.0001) multiple comparison, n=14-18.

4.3.5. Both main effects and post hoc analysis in gene expression data

The remaining peripheral cytokine protein levels have main effects of both sex (IL5, IL6, IL12B, IL13, MCP1 (CCL2)) or sex and treatment (IP10, CXCL1, MIG, MIP1A, TNFA). These data may be found summarized in Appendix Figure A.13-Figure A.14. The overarching information gleaned from all the peripheral cytokine protein levels is that the females have an overall higher pg/mL level of a number of cytokines and the 48Hr WD group is the most likely of treatment groups to be altered. The key pro-inflammatory cytokines in the current literature are IL6 and TNFA levels which have been found to be dysregulated in smokers [291-293]. IL6, while often noted as pro-inflammatory, has pleiotropic activity and acts as a proinflammatory cytokine in chronic conditions but may be more of a defense mechanism [294]. It is important again to note that in healthy adults, gender usually has only a weak influence on plasma levels, where in our mice we observe an increased baseline in females [292].

4.3.6. Pearson correlation matrix analysis

In addition to looking at the individual treatment graphs, an important method of data visualization for large sample groups with a broad range of concentrations, is to view the data as a Pearson's correlation matrix. It becomes far easier to visualize the data en toto without data reduction, and it enables the visualization of patterns across the treatment groups and observation of the effect of nicotine treatment and withdrawal on inter-cytokine correlations Figure 4.6. The matrix has the cytokines along the Y and X axis such that a diagonal correlation value is 1 or a perfect correlation in dark blue squares while a -1 would be a bright red square. By looking at the cytokines with similar coloring, we gain insight as to which cytokines might be working in concert at any condition. In Figure 4.6, panels A-D are the matrices with male and female data combined for each treatment group (saline, nicotine, 24Hr WD, and 48Hr WD going left to right). Below the line in panes E-L are the data divided by sex; males are E-H and females are I-L. It becomes evident how crucial it is both to study males and females and to analyze the data separately as well as together. In panels A-D, there is little difference between the treatment group by visual inspection of the amount of blue and red squares. However, when the data is separated, clusters of cytokines group together: for instance, the large blue square on a field of red squares seen in panel E in the male saline group, compared to panel I, the female saline group, where there is a sea of blue squares. This simple visualization correlates to the saline treatment group sex differences noted above in Figure 4.2. The Pearson's r value, or correlation coefficient, measures the linear relationship between variables. In Table 4.4, the r values are

calculated at greater than 0.9 for very strongly correlated, greater than 0.7 for strongly correlated, and at greater than 0.5 for correlated cytokines. Within the table at an r greater than 0.9, the combined data for the saline treatment group exhibits zero cytokines as very strongly correlated. However, when the data is separated by sex both the males and females each have 2 different very strongly correlated cytokine pairs each, IL2 and IL5 for males, and RANTES and IL1B for females (raw data not shown). In comparison, in the nicotine treatment group, there is one pair of very strongly correlated cytokines in the combined data: IL1B and IL5, which corresponds to the identical very strongly correlated cytokine pair found within only the females. These differences reveal the importance of analyzing both sex and doing so independently as well as combined.

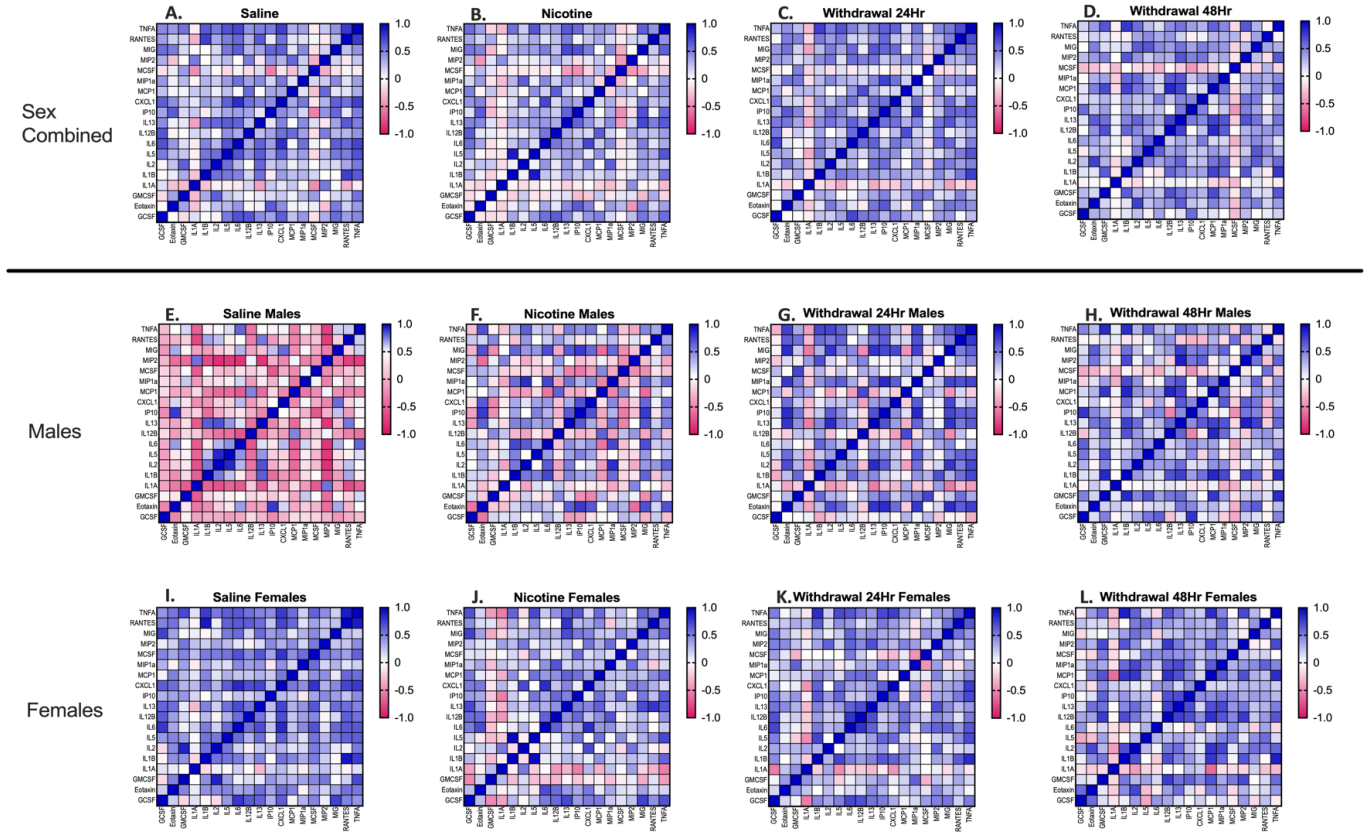

Figure 4.6. Effect of nicotine treatment and withdrawal on inter-cytokine correlations**:** Pairwise Pearson's correlations among cytokine levels in the peripheral serum of male and female mice treated with saline, nicotine, and withdrawal of 24 and 48 hours. Cytokines are rank ordered based on hierarchical clustering. Each square is a correlation with n = 13-18 mice/group. A-D are combined data for both sexes while E-H are males of the 4 treatment groups and I-L the females.

Table 4.4. Peripheral protein cytokines, Pearson correlation summary of treatment and sex. Highly correlated cytokine pairs, positive and negative, at r>0.9 very strongly correlated, r>0.7 strongly correlated, r>0.5 correlated.

		Saline		Nicotine		24Hr Wd		48Hr WD	
		+ correl. pairs	- correl. pairs	+ correl. pairs	- correl. pairs	+ correl. pairs	- correl. pairs	+ correl. pairs	- correl. pairs
r>0.9	M+F	0	0	2	0	0	0	0	0
	M	2	0	0	0	0	0	0	0
	F	2	0	2	0	0	0	0	0
r>0.7	M+F	10	0	6	0	8	0	14	0
	M	24	12	14	0	36	0	26	0
	F	10	0	16	0	14	0	26	0
r>0.5	M+F	86	2	42	0	88	0	74	0
	M	72	34	16	0	86	4	80	2
	F	86	0	68	4	72	2	82	2

Further investigation into the statistical significance of these groups of cytokines, which cluster together, requires additional statistical analysis, and data has been transferred to a collaborator in statistics at the University of Kentucky to model how the serum protein changes, and brain region protein changes (described below) can be used to predict important biomarkers and possible therapeutic targets. At this point, the data will be analyzed for Simpson's paradox, a phenomenon in which a trend appears in several groups of data but disappears or reverses when the groups are combined. We do not expect to see this arise as our data is normally distributed.

4.3.7. Sex as a biological variable (SABV) in PFC, CPU, and NAc cytokine protein expression

As the mRNA expression levels and serum protein cytokine levels had distinct baseline differences in the saline treatment (control), each of the cytokine proteins from the PFC, CPU, and NAc were analyzed for these differences. Of the 32 cytokines/chemokines in the multiplex array, 22 had significant protein level differences in at least one of the 3 brain regions. The region that had the highest number of cytokines with sex differences was in the PFC, where 12 of the 22 cytokines were significant with higher protein expression levels in the females as compared to the males and validates this region of the reward system as important when analyzing sex as a biological variable Table 4.5. Two cytokines were below detectable limits in this region and 8 were not significant. Due to pandemic constraints, a new cohort of animals was not generated for the protein extraction, but rather 5 animals originally earmarked for RNA extraction were used for Luminex®® analysis. However, as seen in the individual graphs, we had robust and significant signal with even the small cohort. The small sample number with this amount of significance evidences the degree of the protein expression disparity between the sexes. Graphs for individual cytokines in all brain regions are in Appendix Figure A.15-Figure A.22.

In the CPU, there were 5 cytokines that had a significant sex difference in protein expression Table 4.6. Interestingly, of these, only 1 cytokine, IL9, was higher in males than in females and was the only cytokine which exhibited this male specific pattern (69% greater). IL9 has been studied for its inflammatory role in autoimmune disease

such as SLE, asthma, MS, and experimental autoimmune encephalitis (EAE) in serum [295]. It is also known to protect neurons from developmental apoptosis and has been found predominantly in neurons [296]. However, there is little information as to the role of this protein in mice, or within the CPU, nor any noted CNS specific sex differences. There were 4 cytokines in the CPU whose protein expression was below detectable limits and 13 cytokines with no significant difference.

Table 4.5. Sex differences in protein levels as isolated from microdissected PFC brain region. Analysis by unpaired two-tailed t-test, P < 0.05, **P < 0.01, ***P < 0.001, ****P < 0.0001, n = 4-5.

A. PFC						
Gene	Male pg/ml	Female pg/ml	Significant	P value	t, df	Mice/group
CXCL5	11.82	104.20	****	<0.0001	t=11.36, df=8	5
Eotaxin	5.68	19.93	***	0.0005	t=5.620, df=8	5
GCSF	1.58	3.71	**	0.0069	t=3.607, df=8	5
GMCSF	4.99	14.80	*	0.0214	t=2.852, df=8	5
IFNG	1.91	2.82	*	0.0251	t=2.750, df=8	5
IL1A	42.29	139.80	***	0.0007	t=5.310, df=8	5
IL2	70.23	66.09	ns	0.838	t=0.2112, df=8	5
IL6	Below	detectable	limits			
IL7	4.43	8.98	**	0.0015	t=4.721, df=8	5
IL9	993.70	602.00	ns	0.2065	t=1.375, df=8	5
IL12B	1.88	5.10	*	0.0488	t=2.322, df=8	5
IL13	81.93	135.90	ns	0.205	t=1.380, df=8	5
IL15	39.30	101.20	***	0.0006	t=5.536, df=8	5
IL17	20.69	32.86	ns	0.1127	t=1.782, df=8	5
IP10	23.22	42.45	*	0.0228	t=2.812, df=8	5
MCP1	55.44	60.79	ns	8417	t=0.2072, df=7	5
MCP1A	97.71	53.99	ns	0.2341	t=1.287, df=8	5
MCP1B	Below	detectable	limits			
MCSF	4.16	10.84	****	<0.0001	t=7.551, df=8	5
MIG	3.45	5.25	ns	0.1875	t=1.441, df=8	5
MIP2	24.70	65.28	**	0.0044	t=3.924, df=8	5
VEGF	23.89	23.96	ns	0.9914	t=0.0112, df=8	5

Table 4.6. Sex differences in protein levels as isolated from microdissected CPU brain region. Analysis by unpaired two-tailed t-test. P < 0.05, **P < 0.01, ***P < 0.001, ****P < 0.0001, n = 4-5.

B. CPU						
Gene	Male pg/ml	Female pg/ml	Significant	P value	t, df	Mice/group
CXCL5	Below	detectable	limits			
Eotaxin	3.68	10.61	*	0.2016	t=2.847, df=8	5
GCSF	Below	detectable	limits			
GMCSF	10.25	15.03	ns	0.4104	t=0.8685, df=8	5
IFNG	3.85	4.49	ns	0.6426	t=0.4848, df=7	4-5
IL1A	50.94	71.53	*	0.0349	t=2.537, df=8	5
IL2	51.67	67.99	ns	0.4091	t=0.8711, df=8	5
IL6	Below	detectable	limits			
IL7	4.65	6.98	ns	0.1336	t=1.697, df=7	4-5
IL9	2942.00	896.90	***	0.0009	t=6.021, df=6	4
IL12B	2.26	9.74	ns	0.0908	t=1.922, df=8	5
IL13	236.50	166.60	ns	0.0973	t=1.877, df=8	5
IL15	44.71	80.63	*	0.0345	t=2.618, df=7	5
IL17	13.21	17.39	ns	0.2756	t=1.170, df=8	5
IP10	16.55	24.03	*	0.0214	t=2.851, df=8	5
MCP1	223.40	119.80	ns	0.0882	t=1.941, df=8	5
MCP1A	340.10	199.40	ns	0.1143	t=1.772, df=8	5
MCP1B	Below	detectable	limits			
MCSF	4.02	5.90	ns	0.0864	t=1.954, df=8	5
MIG	4.96	3.78	ns	0.2965	t=1.117, df=8	5
MIP2	25.14	47.29	ns	0.1352	t=1.661, df=8	5
VEGF	38.14	19.24	ns	0.0549	t=2.302, df=7	4-5

Table 4.7. Sex differences in protein levels as isolated from microdissected NAc brain region. Analysis by unpaired two-tailed t-test, P < 0.05, **P < 0.01, ***P < 0.001, ****P < 0.0001, n = 4-5.

C. NAc						
Gene	Male pg/ml	Female pg/ml	Significant	P value	t, df	Mice/group
CXCL5	2.03	28.04	ns	0.1508	t=1.589, df=8	5
Eotaxin	6.54	5.43	ns	0.3910	t=0.9143, df=7	4-5
GCSF	1.38	2.37	ns	0.0817	t=1.990, df=8	5
GMCSF	10.19	13.18	ns	0.1754	t=1.487, df=8	5
IFNG	2.92	8.82	*	0.0173	t=2.990, df=8	5
IL1A	70.64	79.84	ns	0.0573	t=2.218, df=8	5
IL2	59.05	82.89	***	0.0006	t=5.531, df=8	5
IL6	1.57	2.40	ns	0.0672	t=2.116, df=8	5
IL7	8.73	10.14	ns	0.0836	t=1.975, df=8	5
IL9	Below	detectable	limits			
IL12B	2.94	3.04	ns	0.1955	t=1.413, df=8	5
IL13	100.90	160.60	*	0.0325	t=2.582, df=8	5
IL15	Below	detectable	limits			
IL17	22.28	23.26	ns	0.7472	t=0.3337, df=8	5
IP10	23.18	23.86	ns	0.597	t=0.5538, df=7	5
MCP1	18.16	45.35	**	0.0025	t=4.319, df=8	5
MCP1A	62.22	186.60	**	0.0017	t=4.607, df=8	5
MCP1B	2.03	2.50	*	0.014	t=3.129, df=8	5
MCSF	6.22	6.31	ns	0.9201	t=0.1036, df=8	5
MIG	1.83	4.26	*	0.0265	t=2.714, df=8	5
MIP2	Below	detectable	limits			
VEGF	16.05	24.54	***	0.0001	t=6.824, df=8	5

In the NAc, there were 8 cytokines that exhibited a significant sex difference in protein expression all of which were higher in females as compared to males (Table 4.7). While 3 cytokines were below detectable levels, the other 11 cytokines were not significant vis a vis sex difference in this brain region. As the NAc is often studied for its role in the reward system, receiving neuronal inputs directly from the VTA but often

focusses on dopaminergic signaling. This data suggests that there could be interesting sex differences to follow closely upon treatment.

4.3.8. Both main effects and post hoc analysis in protein expression data

Protein was extracted from each of the brain regions of interest, the PFC, CPU, and NAc. There were 22/32 cytokines that had either a significant main effect in at least one of the brain regions. This data is summarized below in Table 4.8, while the statistics for the PFC are in Table 4.9, the CPU in Table 4.10 and the NAc in Table 4.11. Significant protein expression was predominant in the PFC during treatment groups as it was for saline control sex differences (Figure 4.6), see individual graphs in Appendix Figure A.23-Figure A.33 with 2 columns of figures with panes A and D representing the PFC region, B and E the CPU, and C and F the NAc. However, only 1 cytokine in the PFC has a significant main effect of treatment without also having one for sex, in interferon gamma (IFNG).

The Human Protein Atlas lists this protein as having very little brain region specificity, and the Brain RNA-seq database denotes almost undetectably low RNA levels in multiple cell types. In chronic nicotine and withdrawal, IFNG was significantly expressed in the PFC and NAc with the highest levels in the 48Hr WD group of both sexes (Figure 4.7) [297]. There is a distinct difference in the nicotine treatment groups in the PFC and NAc.

Table 4.8. Brain region derived protein cytokines with significant main effect and post hoc analysis.

	Main Effect and **post hoc significance**
PFC	**Eotaxin (S), GCSF (S**), GMCSF (S), **IFNG (T)**, **IL1A (I,S), IL2 (S), IL7 (S), IL9 (S), IL12B (S)**, **IL13 (I), IL15(S), IL17 (I), IP10 (I,S), CXCL5 (T,S), MCP1A (S), MCF (T,S), MIP2 (S), VEGF (S)**
CPU	**Eotaxin (S**), **IL9 (T,S), IL12B (I), IL13 (S), IL15 (S), IP10 (S), MCP1 (S**), **MCP1A (S),** MCSF (S), MIP2 (I), **VEGF (S)**
NAc	GMCSF (S), **IFNG (S),** IL2 (S), **IL6 (T,S), IL7 (T,S), IL12B (S), IL13 (S), MCP1 (S), MCP1A (S), MCP1B (T,S), MIG (S), VEGF (S)**

Key: Interaction (I), Sex (S), or Treatment (T) main effects

Significant post by Šídák's or Dunnett's multiple comparison in **Bold**

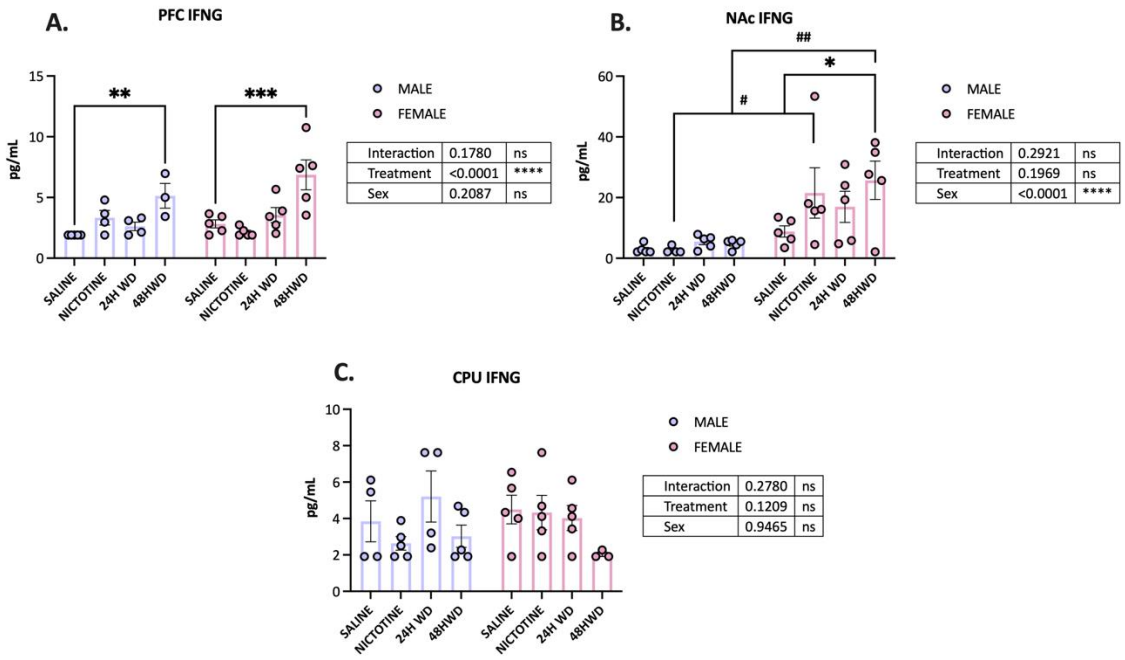

Figure 4.7. IFNG cytokine protein levels and main effect and post hoc significance evidenced in the (A) PFC and the (B) NAc while the (C) CPU below shows no significance of main effect. Analyzed by two-way ANOVA and with significant post hoc within sex by Dunnett's (*P<0.05, **P<0.01, ***P<0.001, ****P<0.0001) and between sex by Šídák's ($^{\#}$P<0.05, $^{\#\#}$P<0.01, $^{\#\#\#}$P<0.001, $^{\#\#\#\#}$P<0.0001) multiple comparison, n=4-5.

While it is not significant, there is an upward trend to IFNG protein expression in nicotine in males in the PFC that is decreased in nicotine in females. In the NAc, there is a significant difference in the expression levels of IFNG in the nicotine group between males and females with females having a 60% higher level than the female saline control. Much of the work discussing nicotine and IFNG is only in the periphery as opposed to tissue. However, IFNG has a proposed role for T-cell trafficking into the meningeal spaces and the choroid plexus, affecting behavior, and supporting a role for INFG in regulating neuronal connectivity in addition to its roles in brain development and function [297-300]. It has also been studied in AUD in the PFC as part of the IFNG-

PKR pathway regulating alcohol-induced neurotoxicity and alterations in plasticity [301]. With only this one cytokine and its diverse effects and changes in expression, we begin to see the complexity of the data generated via the multiplex array in our experimental model.

Table 4.9. Luminex® assay of PFC brain region derived protein (2mg/ml) with main effect statistics.

PFC												
Gene	Sex	Sal pg/ml	Nic pg/ml	24Hr WD pg/ml	48Hr WD pg/ml	Mice/ group	Interaction	Sig	Main Effect: Sex	Sig	Main Effect: Treatment	Sig
CXCL5	M	11.82	25.99	97.99	59.41	3-5	F (3, 29) = 1.464	ns	F (1, 29) = 22.15	****	F (3, 29) = 3.345	*
	F	104.20	100.70	119.00	114.10		P=0.2450		P<0.0001		P=0.0326	
Eotaxin	M	5.68	8.09	6.90	8.17	3-5	F (3, 28) = 1.538	ns	F (1, 28) = 49.67	****	F (3, 28) = 1.168	ns
	F	19.93	22.69	21.86	13.65		P=0.2266		P<0.0001		P=0.3397	
GCSF	M	1.58	1.53	1.85	1.53	3-5	F (3, 28) = 0.5444	ns	F (1, 28) = 35.45	****	F (3, 28) = 0.799	ns
	F	3.71	4.41	4.27	3.05		P=0.6560		P<0.0001		P=0.5047	
GMCSF	M	4.99	6.70	10.62	4.45	3-5	F (3, 28) = 0.5444	ns	F (1, 28) = 14.11	***	F (3, 28) = 0.605	ns
	F	14.80	12.40	15.00	14.86		P=0.6560		P=0.0008		P=0.6172	
IFNG	M	1.91	3.33	2.62	5.14	3-5	F (3, 28) = 1.758	ns	F (1, 28) = 1.656	ns	F (3, 28) = 11.69	****
	F	2.82	2.15	3.55	6.87		P=0.1780		P=0.2087		P<0.0001	
IL1A	M	42.29	80.10	125.70	85.84	3-5	F (3, 29) = 4.238	*	F (1, 29) = 28.19	****	F (3, 29) = 2.069	ns
	F	139.80	143.50	124.20	142.30		P=0.0134		P<0.0001		P=0.1261	
IL2	M	70.23	99.47	88.70	102.40	3-5	F (3, 29) = 2.102	ns	F (1, 29) = 23.00	****	F (3, 29) = 0.926	ns
	F	66.09	57.59	51.43	59.96		P=0.1217		P<0.0001		P=0.4406	
IL6	M	**Below**	**Lower**	**Limit**								
	F											
IL7	M	4.43	5.37	7.54	5.97	3-5	F (3, 28) = 1.775	ns	F (1, 28) = 51.99	****	F (3, 28) = 2.726	ns
	F	8.98	8.94	9.28	9.17		P=0.1749		P<0.0001		P=0.0630	
IL9	M	993.7	1225.0	870.2	1250.0	3-5	F (3, 29) = 0.4914	ns	F (1, 29) = 22.59	****	F (3, 29) = 0.993	ns
	F	602.0	584.7	481.9	574.7		P=0.6910		P<0.0001		P=0.4099	
IL12B	M	1.88	1.73	2.99	1.73	3-5	F (3, 28) = 1.278	ns	F (1, 28) = 9.937	**	F (3, 28) = 1.569	ns
	F	5.10	5.89	4.86	1.88		P=0.3010		P=0.0038		P=0.2190	
IL13	M	81.93	137.00	117.50	154.00	3-5	F (3, 29) = 4.077	*	F (1, 29) = 0.114	ns	F (3, 29) = 1.933	ns
	F	135.90	170.60	132.10	25.43		P=0.0156		P=0.7378		P=0.1462	
IL15	M	39.30	65.28	64.66	60.93	3-5	F (3, 29) = 1.162	ns	F (1, 29) = 48.62	****	F (3, 29) = 1.055	ns
	F	101.20	100.80	101.20	98.28		P=0.3411		P<0.0001		P=0.3832	
IL17	M	20.69	25.66	26.15	29.62	3-5	F (3, 28) = 5.264	**	F (1, 28) = 0.967	ns	F (3, 28) = 2.072	ns
	F	32.86	35.47	32.61	12.33		P=0.0052		P=0.3337		P=0.1266	

IP10	M	23.22	30.53	37.02	33.82	3-5	F (3, 28) = 3.263	*	F (1, 28) = 4.688	*	F (3, 28) = 1.242	ns
	F	42.45	41.57	39.78	27.21		P=0.0361		P=0.0390		P=0.3132	

PFC												
Gene	**Sex**	**Sal pg/ml**	**Nic pg/ml**	**24Hr WD pg/ml**	**48Hr WD pg/ml**	**Mice/ group**	**Interaction**	**Sig**	**Main Effect: Sex**	**Sig**	**Main Effect: Treatment**	**Sig**
MCP1	M	55.44	76.89	55.65	51.9	3-5	F (3, 28) = 0.9735	ns	F (1, 28) = 0.0787	ns	F (3, 28) = 2.319	ns
	F	60.79	85.44	86.55	21.05		P=0.4191		P=0.7812		P=0.0970	
MCP1A	M	97.71	121.00	102.80	137.90	3-5	F (3, 29) = 0.5618	ns	F (1, 29) = 20.48	****	F (3, 29) = 0.5178	ns
	F	53.99	65.69	49.17	45.50		P=0.6445		P<0.0001		P=0.6733	
MCP1B	M	**Below**	**Lower**	**Limit**								
	Fe											
MCSF	M	4.16	4.78	7.41	4.71	3-5	F (3, 28) = 0.3651	ns	F (1, 28) = 98.62	****	F (3, 28) = 3.827	*
	F	10.84	11.03	12.47	10.41		P=0.7787		P<0.0001		P=0.0205	
MIG	M	3.45	3.99	3.42	4.08	3-5	F (3, 28) = 1.163	ns	F (1, 28) = 1.416	ns	F (3, 28) = 0.3926	ns
	F	5.25	4.52	4.40	3.20		P=0.3414		P=0.2440		P=0.7593	
MIP2	M	24.70	33.21	44.98	29.69	3-5	F (3, 28) = 0.8648	ns	F (1, 28) = 30.46	****	F (3, 28) = 0.8178	ns
	F	65.28	57.65	63.94	60.37		P=0.4709		P<0.0001		P=0.4950	
VEGF	M	23.89	30.28	28.78	31.36	3-5	F (3, 28) = 1.648	ns	F (1, 28) = 11.24	**	F (3, 28) = 0.1106	ns
	F	23.96	20.49	22.02	18.50		P=0.2007		P=0.0023		P=0.9532	

Table 4.10. Luminex® assay of CPU brain region derived protein (2mg/ml) with main effect statistics.

CPU												
Gene	Sex	Sal pg/ml	Nic pg/ml	24Hr WD pg/ml	48Hr WD pg/ml	Mice/ group	Interaction	Sig	Main Effect: Sex	Sig	Main Effect: Treatment	Sig
CXCL5	M	**Below**	**Lower**	**Limit**								
	F											
Eotaxin	M	3.68	4.72	6.41	5.61	5	F (3, 32) = 1.988	ns	F (1, 32) = 26.12	****	F (3, 32) = 1.463	ns
	F	10.61	11.27	7.69	14.52		P=0.1355		P<0.0001		P=0.2431	
GCSF	M	**Below**	**Lower**	**Limit**								
	F											
GMCSF	M	10.25	9.44	11.94	12.59	5	F (3, 32) = 1.508	ns	F (1, 32) = 0.299	ns	F (3, 32) = 0.696	ns
	F	15.03	9.75	6.42	8.96		P=0.2313		P=0.5883		P=0.5612	
IFNG	M	3.85	2.64	5.21	3.02	3-5	F (3, 28) = 1.351	ns	F (1, 28) = 0.005	ns	F (3, 28) = 2.114	ns
	F	4.49	4.33	4.02	2.03		P=0.2780		P=0.9465		P=0.1209	
IL1A	M	50.94	45.71	82.36	64.99	4-5	F (3, 31) = 2.581	ns	F (1, 31) = 0.039	ns	F (3, 31) = 0.801	ns
	F	71.53	61.17	53.36	63.34		P=0.0712		P=0.8441		P=0.5028	
IL2	M	51.67	54.19	61.79	72.09	5	F (3, 32) = 2.261	ns	F (1, 32) = 2.194	ns	F (3, 32) = 1.455	ns
	F	67.99	45.17	35.90	54.81		P=0.1003		P=0.1483		P=0.2452	
IL6	M	**Below**	**Lower**	**Limit**								
	F											
IL7	M	4.65	5.02	6.92	5.42	4-5	F (3, 31) = 1.402	ns	F (1, 31) = 2.553	ns	F (3, 31) = 0.277	ns
	F	6.98	6.51	5.55	7.78		P=0.2607		P=0.1202		P=0.8418	
IL9	M	2942.00	2757.0	2869.0	3655.0	4-5	F (3, 27) = 0.6237	ns	F (1, 27) = 32.84	****	F (3, 27) = 3.350	*
	F	896.90	1596.0	1104.0	2428.0		P=0.6058		P<0.0001		P=0.0336	
IL12B	M	2.26	3.53	5.43	5.50	4-5	F (3, 31) = 4.289	*	F (1, 31) = 1.262	ns	F (3, 31) = 0.602	ns
	F	9.74	6.88	3.21	2.33		P=0.0121		P=0.2698		P=0.6186	
IL13	M	236.50	211.20	327.60	317.50	5	F (3, 32) = 1.807	ns	F (1, 32) = 17.29	***	F (3, 32) = 1.993	ns
	F	166.60	187.30	163.60	205.50		P=0.1657		P=0.0002		P=0.1348	
IL15	M	44.71	48.77	55.61	59.41	3-5	F (3, 28) = 1.734	ns	F (1, 28) = 13.22	**	F (3, 28) = 0.024	ns
	F	80.63	74.79	65.83	64.53		P=0.1828		P=0.0011		P=0.9950	
IL17	M	13.21	12.10	17.17	15.77	5	F (3, 28) = 5.264	ns	F (1, 28) = 0.967	ns	F (3, 28) = 2.072	ns
	F	17.39	16.37	18.70	19.30		P=0.0052		P=0.3337		P=0.1266	

IP10	M	16.55	16.18	20.55	20.15	5	F (3, 28) = 3.263	*	F (1, 28) = 4.688	*	F (3, 28) = 1.242	ns
	F	24.03	21.25	18.84	22.02		P=0.0361		P=0.0390		P=0.3132	

CPU												
Gene	**Sex**	**Sal pg/ml**	**Nic pg/ml**	**24Hr WD pg/ml**	**48Hr WD pg/ml**	**Mice/ group**	**Interaction**	**Sig**	**Main Effect: Sex**	**Sig**	**Main Effect: Treatment**	**Sig**
MCP1	M	223.40	259.90	309.50	265.10	5	F (3, 32) = 0.6507	ns	F (1, 32) = 13.61	***	F (3, 32) = 0.6126	ns
	F	119.80	154.70	119.70	195.40		P=0.5883		P=0.0008		P=0.6118	
MCP1A	M	340.10	367.60	474.60	417.70	5	F (3, 32) = 0.9621	ns	F (1, 32) = 21.33	****	F (3, 32) = 0.723	ns
	F	199.40	236.10	184.30	269.90		P=0.4225		P<0.0001		P=0.5458	
MCP1B	M	Below	Lower	Limit								
	F											
MCSF	M	4.02	3.42	4.76	4.26	5	F (3, 32) = 0.1301	ns	F (1, 32) = 14.93	***	F (3, 32) = 0.637	ns
	F	5.90	5.78	6.31	5.99		P=0.9415		P=0.0005		P=0.5965	
MIG	M	4.96	4.08	5.11	4.97	5	F (3, 32) = 1.265	ns	F (1, 32) = 3.119	ns	F (3, 32) = 1.176	ns
	F	3.78	3.88	3.02	5.20		P=0.3028		P=0.0869		P=0.3341	
MIP2	M	4.96	4.08	5.11	4.97	5	F (3, 32) = 1.265	ns	F (1, 32) = 3.119	ns	F (3, 32) = 1.176	ns
	F	3.78	3.88	3.02	5.20		P=0.3028		P=0.0869		P=0.3341	
VEGF	M	38.14	35.27	40.20	43.26	4-5	F (3, 31) = 0.2861	ns	F (1, 31) = 27.81	****	F (3, 31) = 0.687	ns
	F	19.24	21.43	17.43	25.36		P=0.8350		P<0.0001		P=0.5666	

Table 4.11. Luminex® assay of NAc brain region derived protein (2mg/ml) with main effect statistics.

NAc												
Gene	Sex	Sal pg/ml	Nic pg/ml	24Hr WD pg/ml	48Hr WD pg/ml	Mice/ group	Interaction	Sig	Main Effect: Sex	Sig	Main Effect: Treatment	Sig
CXCL5	M	2.03	10.13	13.79	12.67	4-5	F (3, 31) = 0.0851	ns	F (1, 31) = 7.812	**	F (3, 31) = 0.374	ns
	F	28.04	37.74	41.08	29.26		P=0.9677		P=0.0088		P=0.7724	
Eotaxin	M	6.54	5.91	7.03	7.79	4-5	F (3, 31) = 0.3459	ns	F (1, 31) = 0.028	ns	F (3, 31) = 1.143	ns
	F	5.43	6.90	7.68	7.78		P=0.7923		P=0.8682		P=0.3472	
GCSF	M	1.38	1.55	1.76	1.53	5	F (3, 32) = 0.5954	ns	F (1, 32) = 34.96	****	F (3, 32) = 2.373	ns
	F	2.37	2.49	3.32	2.54		P=0.6226		P<0.0001		P=0.0886	
GMCSF	M	10.19	10.96	14.55	12.54	5	F (3, 32) = 0.2527	ns	F (1, 32) = 8.746	**	F (3, 32) = 2.394	ns
	F	13.18	15.5	16.61	15.28		P=0.8588		P=0.0058		P=0.0866	
IFNG	M	2.92	2.69	5.47	4.70	4-5	F (3, 31) = 1.300	ns	F (1, 31) = 21.87	****	F (3, 31) = 1.655	ns
	F	8.82	21.54	16.96	25.69		P=0.2921		P<0.0001		P=0.1969	
IL1A	M	70.64	75.61	105.1	74.39	4-5	F (3, 32) = 2.130	ns	F (1, 32) = 0.013	ns	F (3, 32) = 0.724	ns
	F	79.84	83.32	74.66	91.13		P=0.1158		P=0.9116		P=0.5449	
IL2	M	59.05	60.81	70.39	55.66	5	F (3, 32) = 1.088	ns	F (1, 32) = 7.394	*	F (3, 32) = 0.878	ns
	F	82.89	66.93	73.54	72.69		P=0.3683		P=0.0105		P=0.4626	
IL6	M	1.57	1.55	2.04	1.77	5	F (3, 32) = 2.203	ns	F (1, 32) = 39.11	****	F (3, 32) = 5.126	**
	F	2.40	2.88	4.73	3.88		P=0.1068		P<0.0001		P=0.0052	
IL7	M	8.73	8.61	10.12	9.30	5	F (3, 32) = 0.6681	ns	F (1, 32) = 41.03	****	F (3, 32) = 6.534	**
	F	10.14	11.03	12.84	11.73		P=0.5779		P<0.0001		P=0.0014	
IL9	M	**Below**	**Lower**	**Limit**								
	F											
IL12B	M	2.94	2.89	3.11	3.01	4-5	F (3, 30) = 1.124	ns	F (1, 30) = 5.682	*	F (3, 30) = 2.869	ns
	F	3.04	3.06	3.09	3.10		P=0.3552		P=0.0237		P=0.0529	
IL13	M	100.90	133.00	121.20	86.38	5	F (3, 32) = 0.7990	ns	F (1, 32) = 13.88	***	F (3, 32) = 1.645	ns
	F	160.60	167.00	236.80	162.30		P=0.5036		P=0.0008		P=0.1985	
IL15	M	**Below**	**Lower**	**Limit**								
	F											
IL17	M	22.28	21.56	17.46	18.39	5	F (3, 32) = 0.9719	ns	F (1, 32) = 0.230	ns	F (3, 32) = 1.627	ns
	F	23.26	18.96	21.72	18.50		P=0.4181		P=0.6350		P=0.2025	

IP10	M	23.18	24.51	25.14	23.06	4-5	F (3, 31) = 0.2390	ns	F (1, 31) = 0.212	ns	F (3, 31) = 0.243	ns
	F	23.86	23.79	25.28	25.55		P=0.8685		P=0.6486		P=0.8654	

NAc												
Gene	**Sex**	**Sal pg/ml**	**Nic pg/ml**	**24Hr WD pg/ml**	**48Hr WD pg/ml**	**Mice/ group**	**Interaction**	**Sig**	**Main Effect: Sex**	**Sig**	**Main Effect: Treatment**	**Sig**
MCP1	M	18.16	19.57	50.93	30.54	4-5	F (3, 31) = 0.6861	ns	F (1, 31) = 10.62	**	F (3, 31) = 2.276	ns
	F	45.35	97.44	136.10	68.20		P=0.5674		P=0.0027		P=0.0993	
MCP1A	M	62.22	68.82	150.00	88.01	4-5	F (3, 30) = 1.072	ns	F (1, 30) = 44.98	****	F (3, 30) = 2.451	ns
	F	186.60	268.70	250.60	211.20		P=0.3758		P<0.0001		P=0.0827	
MCP1B	M	2.03	2.10	2.55	2.32	4-5	F (3, 31) = 0.6818	ns	F (1, 31) = 42.78	****	F (3, 31) = 6.231	**
	F	2.50	2.86	3.01	2.85		P=0.5699		P<0.0001		P=0.0019	
MCSF	M	6.22	5.73	7.01	8.03	5	F (3, 32) = 0.1301	ns	F (1, 32) = 14.93	***	F (3, 32) = 0.637	ns
	F	6.31	7.86	7.86	7.01		P=0.9415		P=0.0005		P=0.5965	
MIG	M	1.83	2.30	3.57	2.30	4-5	F (3, 31) = 0.1778	ns	F (1, 31) = 19.50	***	F (3, 31) = 1.972	ns
	F	4.26	4.00	5.70	4.98		P=0.9106		P=0.0001		P=0.1386	
MIP2	M	**Below**	**Lower**	**Limit**								
	F											
VEGF	M	16.05	16.67	23.14	16.58	4-5	F (3, 30) = 2.420	ns	F (1, 30) = 26.63	****	F (3, 30) = 1.621	ns
	F	24.54	24.04	24.89	29.55		P=0.0856		P<0.0001		P=0.2052	

Overall trends are increases of overall protein cytokine expression in the PFC for females over males with a few cytokines such as IL9, IL12B, MCP1A (CCL3), and VEGF exhibiting a lowered overall expression across treatment groups. MCP1A (CCL3) is a chemokine, IL9 and 12B are interleukins, and VEGF is a growth factor the decreased expression is not segregated to a specific type of cytokine. while the CPU has many more decreases in female protein expression. While anti-inflammatory cytokines such as IL6, IL13, and IGFN are significantly expressed, the majority of the cytokines are pro-inflammatory. With cytokines profiles changing by brain region and sex, we turn again to analysis by Pearson correlation matrix.

4.3.9. Brain region specific protein expression as analyzed by Pearson correlation matrix

The Pearson correlation will identify how strongly the cytokines are related to one another. This analysis was performed by treatment groups as either the sexes combined or separate in each brain region (Figure 4.8, Figure 4.9, Figure 4.10, Figure 4.11). Once again, the important observations to be made from these figures are that sex differences are important and should be considered (patterns of blue and red squares per region in a treatment group between males and females) and that there are numerous cytokines that are highly correlated and group together.

As opposed to the peripheral protein cytokines (Table 4.4), the protein expression in the specific brain regions of interest have many more very strongly correlated cytokine pairs (r greater than 0.9), and Table 4.12 contains only this correlation coefficient for each region. These cytokines are both positively and

negatively correlated to a greater extent than in the periphery. Also, the number of very strongly correlated cytokine pairs is more numerous by sex than in the combined data set underscoring the significance of testing and analyzing both sexes. Finally, the highest abundance of cytokine pairs is found in the PFC, followed by the NAc, and lastly the CPU, highlighting the significance of testing within various regions of the mesolimbic reward system separately. The next step will be to analyze which, if any, of the pairings of cytokines track together, what the downstream effects are, and whether there any combinations of the brain or periphery proteins are predictive for sex or treatment effects. This predictive information could then be combined with human data for translational efforts in finding possible novel therapeutics.

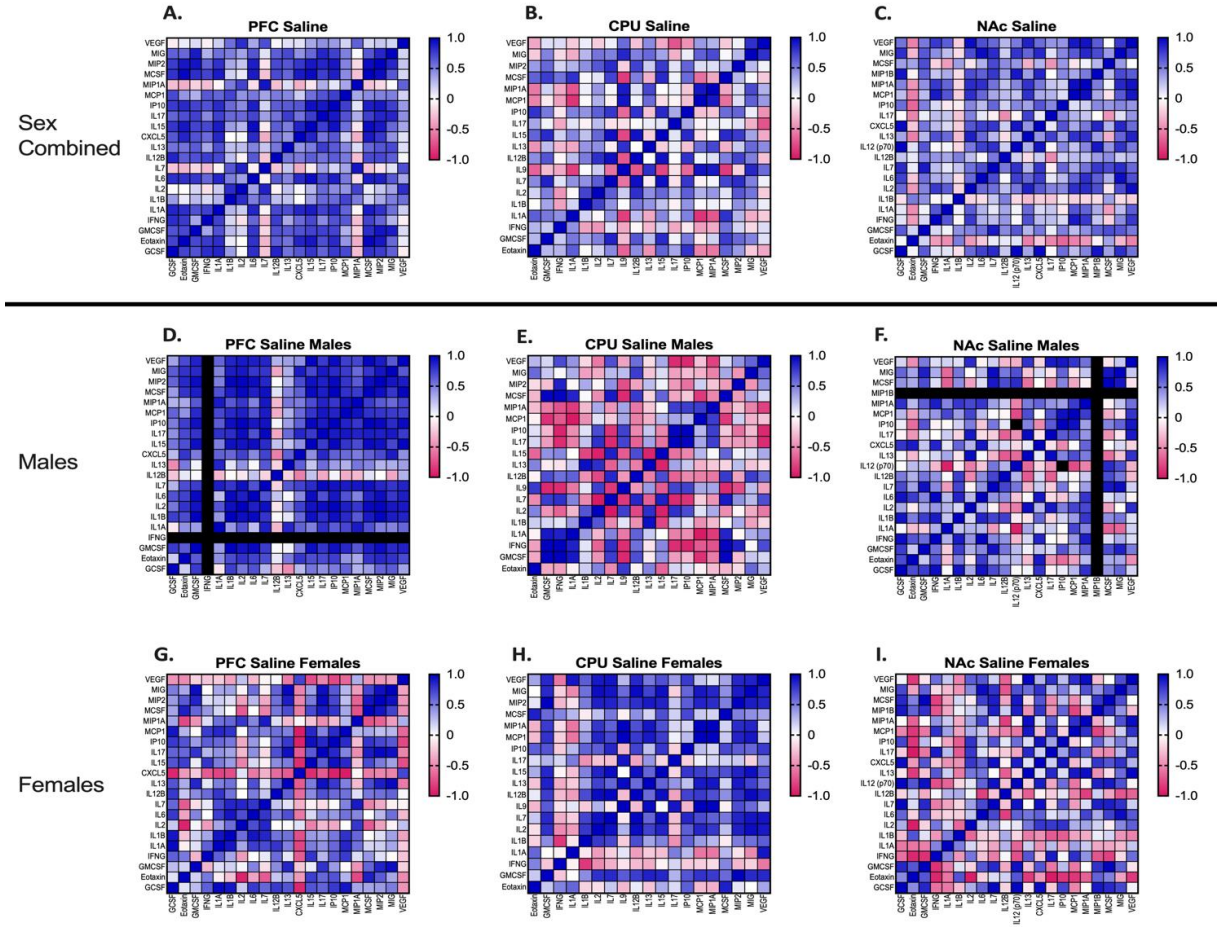

Figure 4.8. Effect of nicotine treatment and withdrawal on inter-cytokine correlations**:** Pairwise Pearson's correlations among cytokine brain region protein levels with sexes combined (A-C), males alone (D-F), and females alone (G-I). Each square is a correlation with n = 3-5 mice/group.

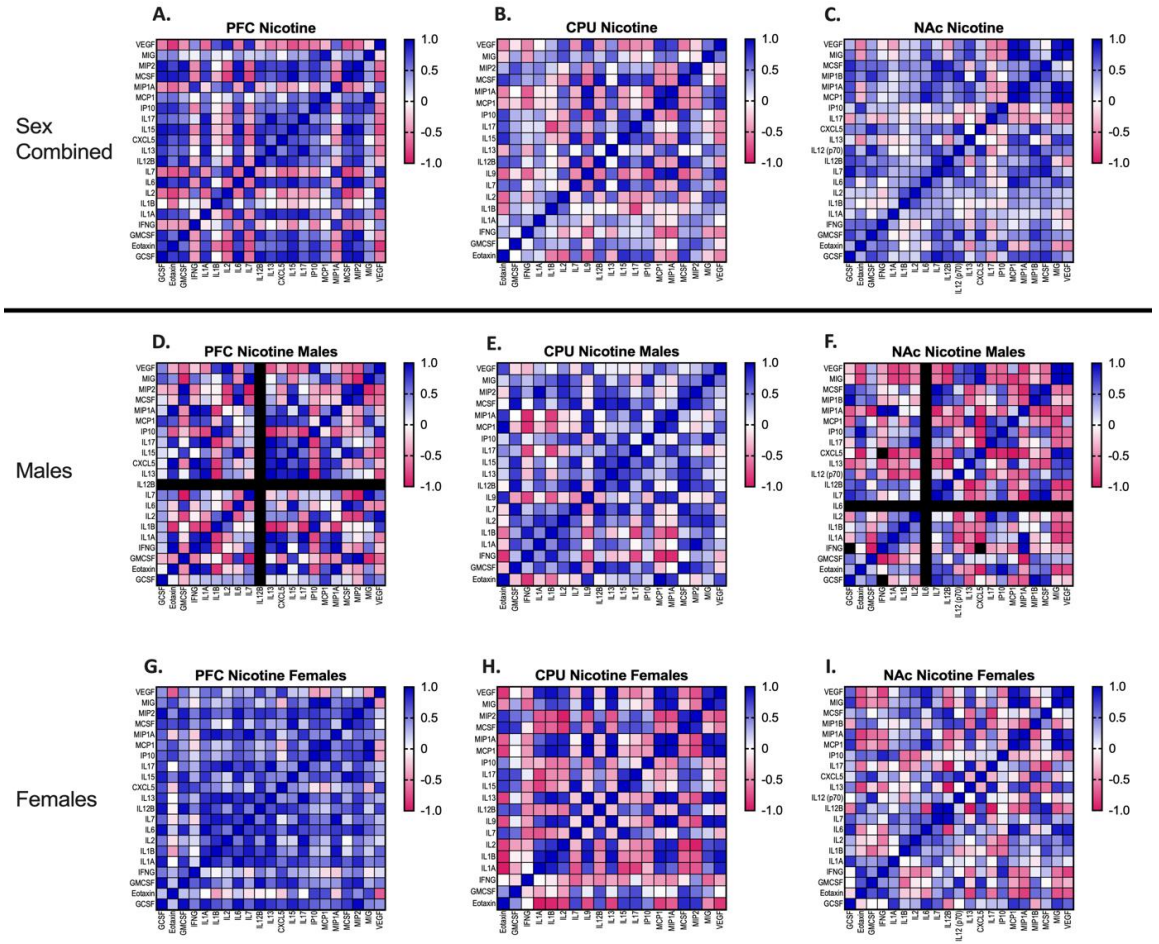

Figure 4.9. Effect of nicotine treatment and withdrawal on inter-cytokine correlations: Pairwise Pearson's correlations among cytokine brain region protein levels with sexes combined (A-C), males alone (D-F), and females alone (G-I). Each square is a correlation with n = 3-5 mice/group.

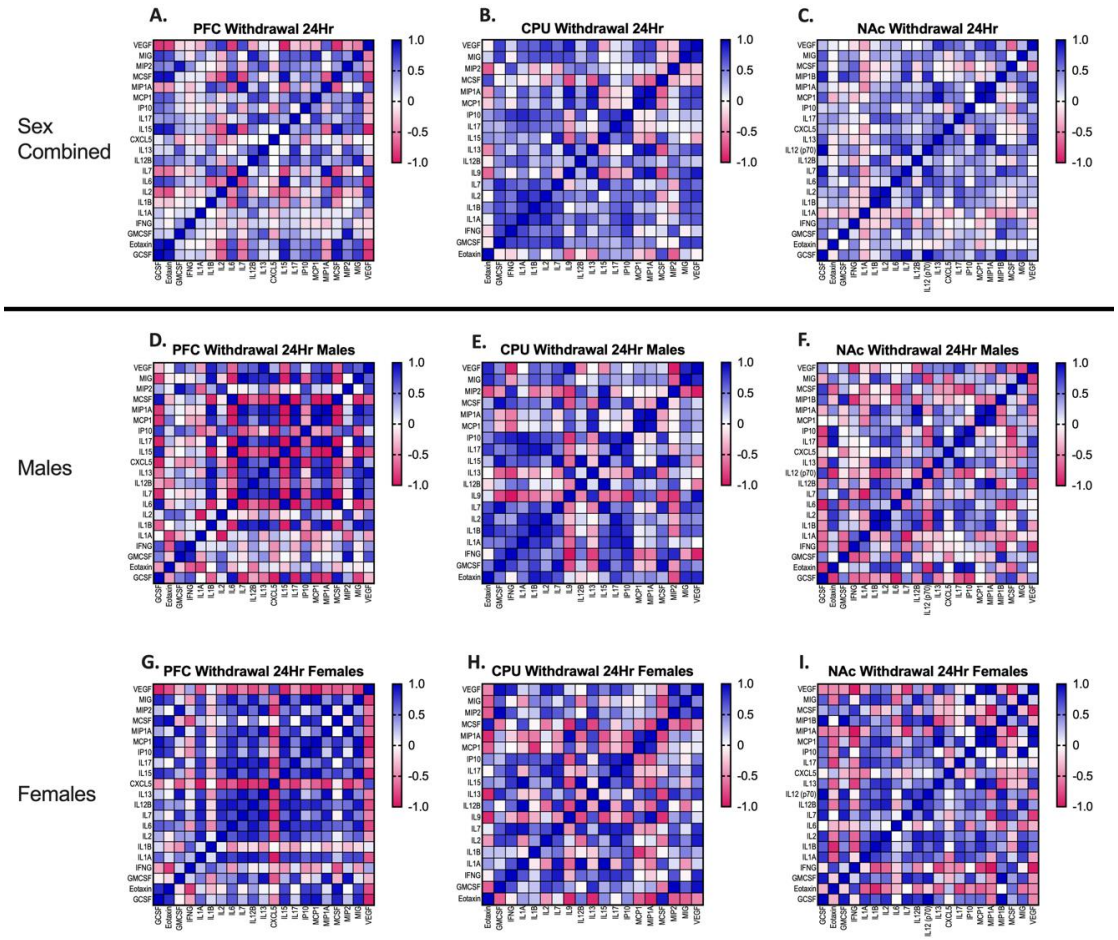

Figure 4.10. Effect of nicotine treatment and withdrawal on inter-cytokine correlations**:** Pairwise Pearson's correlations among cytokine brain region protein levels with sexes combined (A-C), males alone (D-F), and females alone (G-I). Each square is a correlation with n = 3-5 mice/group.

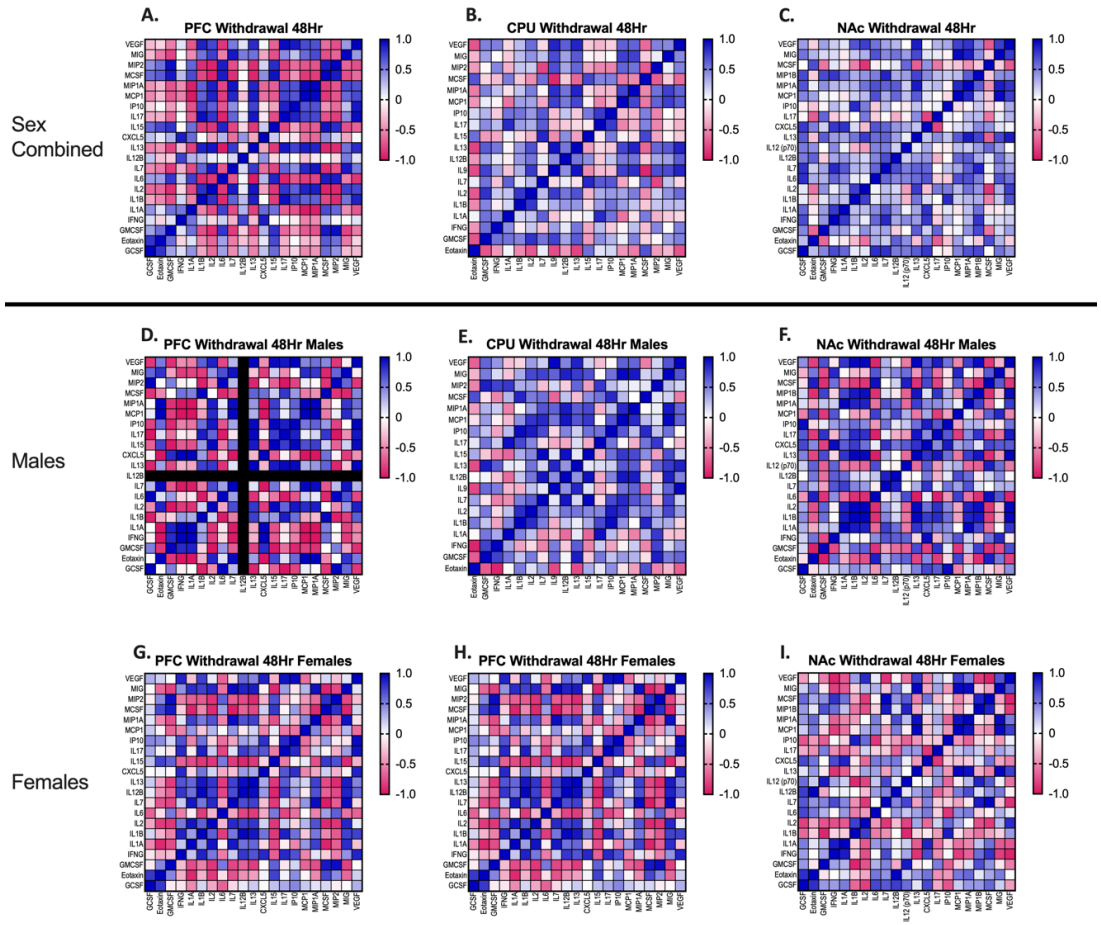

Figure 4.11. Effect of nicotine treatment and withdrawal on inter-cytokine correlations: Pairwise Pearson's correlations among cytokine brain region protein levels with sexes combined (A-C), males alone (D-F), and females alone (G-I). Each square is a correlation with n = 3-5 mice/group.

Table 4.12. Brain Region protein cytokines, Pearson correlation summary of treatment and Sex. Highly correlated cytokine pairs, positive and negative, all at r>0.9 for very strongly correlated.

PFC	Saline		Nicotine		24Hr Wd		48Hr WD	
	+ correl. pairs	- correl. pairs	+ correl. pairs	- correl. pairs	+ correl. pairs	- correl. pairs	+ correl. pairs	- correl. pairs
M+F	24	0	34	0	16	2	26	16
M	74	0	36	10	46	42	46	50
F	26	8	40	0	50	10	24	0
CPU	Saline		Nicotine		24Hr Wd		48Hr WD	
	+ correl. pairs	- correl. pairs	+ correl. pairs	- correl. pairs	+ correl. pairs	+ correl. pairs	- correl. pairs	+ correl. pairs
M+F	10	0	12	0	12	0	2	2
M	12	18	24	2	24	6	18	2
F	42	0	36	0	20	6	44	38
NAc	Saline		Nicotine		24Hr Wd		48Hr WD	
	+ correl. pairs	- correl. pairs	+ correl. pairs	- correl. pairs	+ correl. pairs	+ correl. pairs	- correl. pairs	+ correl. pairs
M+F	22	0	20	0	8	0	2	0
M	28	2	18	18	10	4	32	8
F	30	6	16	4	20	10	20	8

4.4. Conclusion

Understanding how the immune system functionally contributes to nicotine use disorder is necessary to understand how nicotine can be both therapeutic and disadvantageous in the brain, and to understand the mechanisms that affect withdrawal. This avenue could be crucial to developing sensitive bioassays and effective new therapeutics. In analyzing RNA in Chapter 3, multiple genes were altered by both sex and treatment at the mRNA level and this trend continued for protein expression

levels in the peripheral serum and brain tissue. There were numerous sex differences seen with many cytokines having higher expression in females over males. A total microglial density higher in females, as shown in Chapter 2, would likely not account for all the expression changes, as not all the genes are expressed only via microglia. The correlation matrices demonstrate the interconnectedness of the cytokines to one another. It is not a matter of a few cytokines or a class of cytokines but many working in concert. This makes future statistical modeling invaluable in searching for new therapeutic targets for inflammation as a therapeutic biomarker could be combined with related cytokines when optimizing a panel for diagnostic accuracy.

Chapter 5. Conclusions and Future Directions

There are 3 FDA approved frontline therapies for nicotine substance use disorder. Two are centered on nicotinic receptors (nicotine replacement therapy and varenicline), while the third drug, bupropion, is a dopamine reuptake inhibitor that boosts dopamine actions in the brain. However, with cessation success rates hovering at ~5%, the need for effective cessation therapies is still high. This suggests that there is an aspect of nicotine withdrawal that is not targeted by these mechanisms. This study aimed to explore microglia and their cytokine production as a possible new path forward for therapeutic development. By better understanding how the neuroinflammatory process contributes to nicotine dependence and withdrawal, we may be able to find better biomarkers for risk assessment, monitor cessation attempts, and select personalized therapeutics with predictive response.

5.1. Chapter 2 Experimental Design and Microglial Morphology Summary

In Chapter 2, the experimental model and its validation was discussed in depth. The upregulation of nicotinic receptors in response to the chronic nicotine treatment validated that the experimental design worked in our hands and in our lab. The rationale for the specific brain regions chosen from the mesolimbic reward system were examined. For example, it was important to look at microglial morphology in the nucleus accumbens shell. The literature has shown the shell, not the core, was linked to increased dopamine release from the afferents from the ventral tegmental area in

response to nicotine [302]. Thus, there would be environmental changes in this area which could affect microglial activation during treatment or withdrawal. This was the first *a priori* work investigating sex as a biological variable in neuroinflammatory contributors to nicotine dependence; my work found that female mice have a higher microglial density as compared to males under many treatment conditions in the PFC and the CPU, but there were no density changes found in the nucleus accumbens core or shell. Analysis of individual microglial morphology demonstrated that female mice were affected by both treatment and withdrawal very differently from the male mice. When gauging whether the changes indicated more surveillance or activation, the males overall appeared to be more surveilling than the female microglia, which took on many hallmarks of activated microglia.

5.1.1. Chapter 2 future directions

In future studies, there are numerous considerations that could increase the translatability of these experiments. For example, rather than using an osmotic minipump with a continuous steady state delivery of nicotine, a Lynch coil could be employed. The Lynch coil is an external coil of tubing that is alternately filled with either nicotine or saline, and then mineral oil in a banded pattern, and then attached to a saline filled pump. This allows for nicotine to be delivered intermittently to better model the habits of nicotine smokers who smoke intermittently throughout the day and provides a stronger nicotine response [303]. If money were not an object, there are also programmable implantable pumps such as the iPRECIO pumps by Alzet. In this system, nicotine would be not only delivered intermittently, but could be paused for a long

duration to mimic cessation due to sleep. This extended daily withdrawal period would better match the desensitization patterns in nicotinic receptors found in humans.

Lastly, when considering morphology analysis, the IHC platform could be exchanged for immunofluorescence, which would make microglial morphology analysis more readily automated. Methods for skeletonization of the individual cells are different in IHC, as the staining can create a background that makes it difficult to differentiate from cells of interest. Also, in addition to the commercial programs like Neurolucida, there are many open-source protocols available for skeletonization of the individual cells that work with IF images. Finally, by using a 3D z-stacks approach would allow for full cell reconstruction and volumetric analysis, increasing the detail of information gleaned from alterations in morphology at baseline and in treatment [304].

5.2. Chapter 3 Summary

Morphology changes found in Chapter 2 led us to question what is happening at the molecular level within these cells. We used RNA isolated from brain regions evaluated in chapter 2 to investigate potential genes pertinent to the neuroinflammatory cascade via a qPCR microarray of mouse chemokine and cytokines. This data was combined with information from literature to ensure mouse orthologs to human genes as well as use of the Brain RNA-seq online repository to find genes highly expressed in microglia. RNA expression was found to be both sex and treatment dependent. One quarter of our genes demonstrated increased expression by females over males in the saline control group in the PFC, CPU, or NAc. While 16/20 had significant main effects of interaction, treatment, or sex when analyzed across

treatment groups and by sex. Also, many of the genes analyzed in the 48Hr WD group of males were significantly increased in the PFC. This gene expression data was striking, as the brain has many mechanisms to ensure homeostasis and, while only 1/3 of human genes are enriched in mouse microglia, changes within this core set could be quite meaningful [236, 305]. The data provided confidence that the next step should be investigation at the translational level.

5.2.1. Chapter 3 future directions

While the Brain RNA-seq database is a powerful tool for researching the gene expression levels within mouse and humans in various cell types, it relies on data solely from the cortex. It has been shown that microglia vary by their local environment and brain regions and thus the database may not be accurate to the level we wish. There are drawbacks in using flow cytometry and magnetic activated cell sorting (MACS) to isolate microglia for RNA-seq. These processes must be performed on pooled mice tissues, and the act of enzymatically or mechanically dissociating the cells from tissue may alter the mRNA expression of the cells [306-308]. The new spatial transcriptomics may be the ideal tool. It would allow for use of the current or modified experimental design, but sequencing would occur via a brain slice on a special slide with capture probes. The sequences, once derived, could then be mapped back to a location in the tissue and specific markers used to assess in situ gene expression from various cell types.

5.3. Chapter 4 Summary

After the sex differences and treatment differences were found in the mRNA data in Chapter 3, the protein expression levels were analyzed. This was done in

peripheral serum as well as in protein isolated from the brain regions of interest. We employed a MILLIPLEX® multiplex assay approach to analyze 32 different chemokines and cytokines. The data from the periphery demonstrated that at baseline (saline control), 71% of the proteins were significantly upregulated in females over males. Upon analysis of the Pearson correlation matrix, only 2 pair of cytokines were very strongly correlated: Il2 and IL5 in males and IL1B and RANTES in females. Overall, within the periphery, the correlations for sex and treatment found at the *r* cutoffs of 0.7 and 0.5. When compared to the brain region data by sex, there were numerous cytokines that were very strongly correlated by t-test. The PFC contained the highest number of cytokines that had significant correlation at 12/22, then the NAc with 8/22 and finally the CPU with 5/22 cytokines with very strong correlations. This data became more complex when analyzing main effects of interaction, sex, and treatment (see Table 4.8) but overall, the brain regions contained very strongly correlated cytokines in all treatment groups and all regions. The next step of analysis is described in the following Chapters 5.5.2 and 5.5.3.

5.3.1. Chapter 4 future directions

The cytokine proteins discovered in Chapter 4 future directions are already in progress and are presented below in Chapters 5.5.2 and 5.5.3.

5.4. Further Experimentation in Progress

While this thesis denotes a demarcation of experimental data for presentation, this is an ongoing project that will be prepared for publication after the following are complete.

5.4.1. Microglial knockdown and radioligand assays

While we have very strong indications that microglial inflammation is involved in the cytokine expression we analyzed, the best way to verify that the nicotinic effect on the microglia is to delete them and examine the effect. A common methodology for this approach is to target the colony-stimulating factor 1 receptor (CSF1R), whose signaling is required for microglial survival. We currently have this experiment in progress using the highly selective and brain penetrant CSF1R inhibitor, PLX5622, which can be given orally via chow and can deplete 99% of microglia within 7 days. PLX5622 depletes the microglia but allows for regrowth without the inhibitor. Of interest to many researchers is that, if microglia are allowed to repopulate, they repopulate into a non-inflammatory state with no alterations in learning or behavior [261, 309, 310]. We have 2 cohorts of mice that follow the original experimental design with n=3 per group (48 mice total); one cohort was given control chow, while the second was given chow with the inhibitor for microglial depletion. Animals were sacked and cryosectioned for film autoradiography in concert with the Dr. James Pauly lab at the University of Kentucky.

Two different radioligands are in process. The first uses [^{125}I]epibatidine, which has higher specific activity as compared to [^{3}H]EB form used in the receptor binding assay found in Chapter 2. The [^{125}I]EB boosts signal ~100 fold and and allows for rapid quantification of the autoradiographic images, making it more appropriate to verify the nicotine nAChR upregulation in the brain slices and validate the experimental design [311]. The second radioligand is [^{3}H]PK11195, which selectively binds the 18 kDa translocator protein (TSPO, also known as the peripheral benzodiazepine receptor).

Increases in TSPO are associated with altered microglia density as well as activated microglia and has been used as a clinical biomarker in human PET scans (using a carbon-11 isotope tag and validated by IHC) in inflammatory brain diseases such as recent onset schizophrenia, Alzheimer's disease (AD), and Parkinson's disease (PD) [312-316]. Increases in microglial activation have also demonstrated in patients with conditions such as obsessive-compulsive disorder, complex regional pain syndrome, and major depressive disorder [317-319]. Thus, TSPO will be used as a proxy for microglial induced activation and subsequent neuroinflammation.

5.4.2. Statistical modeling and predictions

The Pearson's correlation matrices used to analyze cytokines in the periphery and within specific brain regions is a data visualization method for large data sets. There is, however, predictive value to this data that is not teased out by this statistical method. It does not encompass the totality of the number and types of cytokines working in concert under each treatment condition. Working with Dr. Richard Charnigo, a biostatistics professor at the University of Kentucky, we are hoping to use advanced statistical analysis to create a model of peripheral cytokines as predictors of brain region levels for use as translational biomarkers for personalized medicine.

5.4.3. Human sample cytokine analysis

In this vein, we are collaborating with Dr. Penni Black and the Kentucky Research Registry and Specimen Bank and have obtained human serum samples. Our data set consists of 180 samples equally divided by sex and smoking status as smokers, former smokers and never smokers. These samples will be assayed in the human kit equivalent

of our mouse Luminex kits by Dr. Lilian Gonçalves Custódio, also at UKY. This data will then be analyzed with our statistical predictive model.

5.5. Future Directions

There is great interest in the area of neuroinflammation and research is increasing exponentially. It is being studied in multiple substance use disorders, mental illnesses, autoimmune diseases, complex regional pain syndrome, glioblastoma, neurodegeneration, and aging [208, 261, 309, 310, 318-323]. The gut-brain axis and the role of the microbiome is also being studied for its influence on microglia [305]. NASA has even recently begun studying the effects of temporary microglial depletion after cosmic radiation in preparation for long space travel using the same PLX5622 compound used in our studies [324]. Outside of the many areas of interest noted above, and considering the studies that need SABV added, below are other avenues that this research could take moving forward.

5.5.1. Blood brain barrier

There is interest in the blood brain barrier as many of the cytokines can cross into the brain from the periphery. The question of macrophage intrusion from the periphery during nicotine or nicotine withdrawal is also of interest. While our data demonstrated only a small percent of macrophages within the brain during this type of experiment, the data was only from male mice and was a small sampling. Unpublished research from our lab has also demonstrated a sex specific effect in females where there was a breach of the BBB in only female brains at a 48Hr WD timepoint and affected tight junction proteins at the BBB interface. Alterations in the BBB could alter

cytokine and macrophage levels within the brain. Adding in the newest addition of capillary-associated microglia (CAMs), which make up ~30% of the brain's microglia, regulates microvascular tone and may exert influence over cerebral blood flow [152]. There are current studies underway examining whether the amount of vasculature in females is different than males. New data in BioRxiv suggests sex specific BBB alterations in chronic stress and depression and will be valuable to follow in the future [325].

5.5.2. Quad-partite communication

Microglia are no longer considered merely "brain glue" or for solely the purpose of phagocytosis of cell debris. As new roles are discovered, the communication between the microglia and other cell types must be considered. Their direct interaction with neurons for synaptic remodeling is a direct communication, but the microglia secrete numerous signals that may affect other cells. The interactions between neurons and astrocytes, once viewed as a tripartite synapse with bidirectional communication between them must be updated to include microglia. This results in a quad-partite synapse, a term coined by Schafer et al. in 2013, see Figure 5.1 [111]. This model better exemplifies the complication of crosstalk between multiple partners, including the BBB, vasculature, and pericytes. Astrocytes, like microglia, may also be activated and undergo morphology changes and release signals altering the local environment. Microglia activation has been shown to trigger an astrocyte-mediated neuronal excitatory neurotransmission [326]. There is also evidence of microglia communicating directly with astrocytes as well [327, 328, [Badimon, 2020 #11004]]. Here, spatial

transcriptomics may be a good tool to analyze treatment effects on various cell types in situ and would be an important pathway for future study.

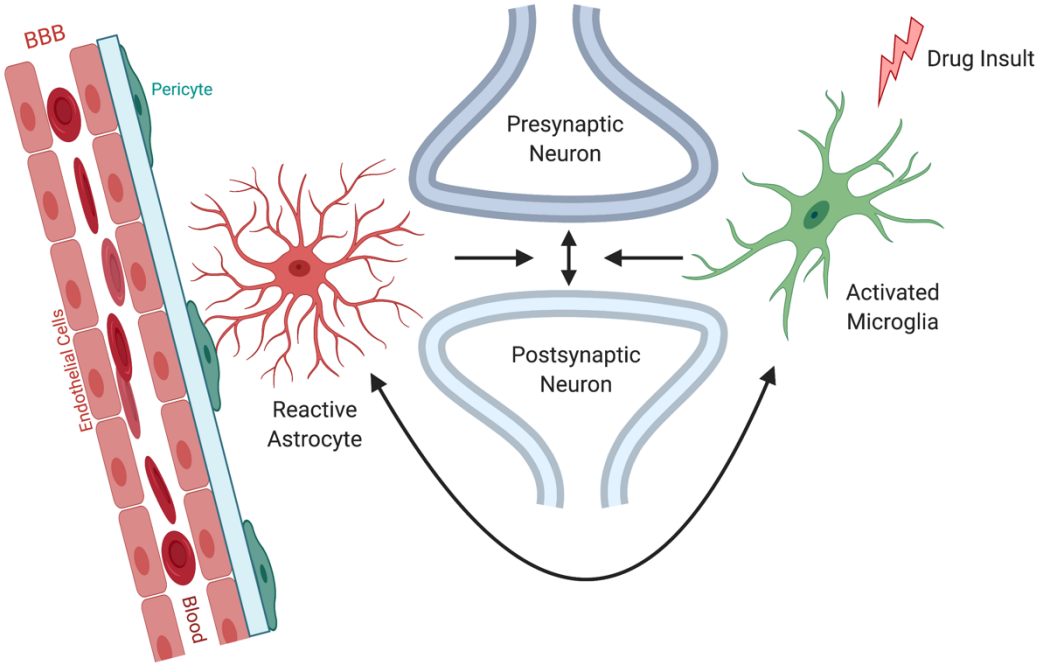

Figure 5.1. A schematic model of the quad-partite synapse. This includes neurons, microglia, astrocytes, the blood brain barrier, vasculature, and pericytes.

Within the quad-partite synapse, the communication could also include the study of purinergic receptors on microglia, such as P2Y6, P2Y12, and P2Y14. Microglia are known to be activated by ATP released from dying neurons and triggers the phagocytic response. There are also P2X and P2Y receptors on astrocytes. The role of these P2 receptors could be investigated in the context of cell-to-cell communication [327-329].

Overall, neuroinflammation and the role of microglia in neuroimmunity is an exciting field that is still at its early stages and promises to bring exciting new information to the field of neuroscience.

References

1. Hong, S., et al., *Complement and microglia mediate early synapse loss in Alzheimer mouse models.* Science, 2016. **352**(6286): p. 712-716.
2. Paolicelli, R.C., et al., *TDP-43 Depletion in Microglia Promotes Amyloid Clearance but Also Induces Synapse Loss.* Neuron, 2017. **95**(2): p. 297-308.e6.
3. Vasek, M.J., et al., *A complement–microglial axis drives synapse loss during virus-induced memory impairment.* Nature, 2016. **534**(7608): p. 538-543.
4. Werneburg, S., et al., *Targeted Complement Inhibition at Synapses Prevents Microglial Synaptic Engulfment and Synapse Loss in Demyelinating Disease.* Immunity, 2020. **52**(1): p. 167-182.e7.
5. Bachtell, R.K., et al., *Glial and neuroinflammatory targets for treating substance use disorders.* Drug and Alcohol Dependence, 2017. **180**: p. 156-170.
6. WHO, *WHO report on the global tobacco epidemic, 2017*.
7. Reitsma, M.B., et al., *Smoking prevalence and attributable disease burden in 195 countries and territories, 1990–2015: a systematic analysis from the Global Burden of Disease Study 2015.* The Lancet, 2017. **389**(10082): p. 1885-1906.
8. HHS, *2014 Surgeon General's Report: The Health Consequences of Smoking—50 Years of Progress*.
9. Hughes, J.R., J. Keely, and S. Naud, *Shape of the relapse curve and long-term abstinence among untreated smokers.* Addiction, 2004. **99**(1): p. 29-38.

10. Borland, R., et al., *How much unsuccessful quitting activity is going on among adult smokers? Data from the International Tobacco Control Four Country cohort survey: Prevalence of quitting activity among smokers.* Addiction, 2012. **107**(3): p. 673-682.

11. Ng, M., et al., *Smoking Prevalence and Cigarette Consumption in 187 Countries, 1980-2012.* JAMA, 2014. **311**(2): p. 183.

12. Rose, J.E., et al., *Kinetics of brain nicotine accumulation in dependent and nondependent smokers assessed with PET and cigarettes containing 11C-nicotine.* Proceedings of the National Academy of Sciences of the United States of America, 2010. **107**(11): p. 5190-5195.

13. Zhou, Y., et al., *Human α4β2 Acetylcholine Receptors Formed from Linked Subunits.* The Journal of Neuroscience, 2003. **23**(27): p. 9004-9015.

14. Fenster, C.P., et al., *Influence of Subunit Composition on Desensitization of Neuronal Acetylcholine Receptors at Low Concentrations of Nicotine.* The Journal of Neuroscience, 1997. **17**(15): p. 5747-5759.

15. Ramirez-Latorre, J., et al., *Functional contributions of α5 subunit to neuronal acetylcholine receptor channels.* Nature, 1996. **380**(6572): p. 347-351.

16. D'Souza, M.S. and A. Markou, *Neuronal mechanisms underlying development of nicotine dependence: implications for novel smoking-cessation treatments.* Addiction Science & Clinical Practice, 2011. **6**(1): p. 4-16.

17. Govind, A.P., P. Vezina, and W.N. Green, *Nicotine-induced upregulation of nicotinic receptors: Underlying mechanisms and relevance to nicotine addiction.* Biochemical Pharmacology, 2009. **78**(7): p. 756-765.

18. Amador, M. and J. Dani, *Mechanism for modulation of nicotinic acetylcholine receptors that can influence synaptic transmission.* The Journal of Neuroscience, 1995. **15**(6): p. 4525-4532.

19. Benowitz, N.L., *Nicotine Addiction.* New England Journal of Medicine, 2010. **362**(24): p. 2295-2303.

20. Markou, A., *Neurobiology of nicotine dependence.* Philosophical Transactions of the Royal Society B: Biological Sciences, 2008. **363**(1507): p. 3159-3168.

21. Barrett, S.P., et al., *The hedonic response to cigarette smoking is proportional to dopamine release in the human striatum as measured by positron emission tomography and [11C]raclopride.* Synapse, 2004. **54**(2): p. 65-71.

22. Watkins, S.S., G.F. Koob, and A. Markou, *Neural mechanisms underlying nicotine addiction: acute positive reinforcement and withdrawal.* Nicotine & Tobacco Research, 2000. **2**(1): p. 19-37.

23. Singer, S., et al., *Nicotine-Induced Changes in Neurotransmitter Levels in Brain Areas Associated with Cognitive Function.* Neurochemical Research, 2004. **29**(9): p. 1779-1792.

24. Hegadoren, K.M., et al., *The role of β-endorphin in the pathophysiology of major depression.* Neuropeptides, 2009. **43**(5): p. 341-353.

25. Nuss, P., *Anxiety disorders and GABA neurotransmission: a disturbance of modulation.* Neuropsychiatric Disease and Treatment, 2015. **11**: p. 165-175.

26. Turner, B.D., et al., *Synaptic Plasticity in the Nucleus Accumbens: Lessons Learned from Experience.* ACS Chemical Neuroscience, 2018. **9**(9): p. 2114-2126.

27. Benowitz, N.L., *NICOTINE ADDICTION.* Primary Care: Clinics in Office Practice, 1999. **26**(3): p. 611-631.

28. McEntee, W.J. and T.H. Crook, *Glutamate: its role in learning, memory, and the aging brain.* Psychopharmacology, 1993. **111**(4): p. 391-401.

29. Berger, M., J.A. Gray, and B.L. Roth, *The Expanded Biology of Serotonin.* Annual Review of Medicine, 2009. **60**(1): p. 355-366.

30. Feduccia, A.A., S. Chatterjee, and S.E. Bartlett, *Neuronal nicotinic acetylcholine receptors: neuroplastic changes underlying alcohol and nicotine addictions.* Frontiers in Molecular Neuroscience, 2012. **5**.

31. Picciotto, M.R., et al., *Mood and anxiety regulation by nicotinic acetylcholine receptors: A potential pathway to modulate aggression and related behavioral states.* Neuropharmacology, 2015. **96**: p. 235-243.

32. Volkow, N.D. and T.-K. Li, *Drug addiction: the neurobiology of behaviour gone awry.* Nature Reviews Neuroscience, 2004. **5**(12): p. 963-970.

33. Volkow, Nora D. and M. Morales, *The Brain on Drugs: From Reward to Addiction.* Cell, 2015. **162**(4): p. 712-725.

34. Dani, J.A. and M. De Biasi, *Mesolimbic Dopamine and Habenulo-Interpeduncular Pathways in Nicotine Withdrawal.* Cold Spring Harbor Perspectives in Medicine, 2013. **3**(6): p. a012138-a012138.

35. Hyman, S.E., R.C. Malenka, and E.J. Nestler, *NEURAL MECHANISMS OF ADDICTION: The Role of Reward-Related Learning and Memory.* Annual Review of Neuroscience, 2006. **29**(1): p. 565-598.

36. Zhou, F.-M., C.J. Wilson, and J.A. Dani, *Cholinergic interneuron characteristics and nicotinic properties in the striatum.* Journal of Neurobiology, 2002. **53**(4): p. 590-605.

37. Yager, L.M., et al., *The ins and outs of the striatum: Role in drug addiction.* Neuroscience, 2015. **301**: p. 529-541.

38. Reid, M.S., et al., *Nicotine stimulation of extracellular glutamate levels in the nucleus accumbens: neuropharmacological characterization.* Synapse (New York, N.Y.), 2000. **35**(2): p. 129-136.

39. Mao, D., K. Gallagher, and D.S. McGehee, *Nicotine Potentiation of Excitatory Inputs to Ventral Tegmental Area Dopamine Neurons.* Journal of Neuroscience, 2011. **31**(18): p. 6710-6720.

40. Bamford, N.S., R.M. Wightman, and D. Sulzer, *Dopamine's Effects on Corticostriatal Synapses during Reward-Based Behaviors.* Neuron, 2018. **97**(3): p. 494-510.

41. Jones, I.W., *Precise Localization of 7 Nicotinic Acetylcholine Receptors on Glutamatergic Axon Terminals in the Rat Ventral Tegmental Area.* Journal of Neuroscience, 2004. **24**(50): p. 11244-11252.

42. Wang, W., et al., *Regulation of prefrontal excitatory neurotransmission by dopamine in the nucleus accumbens core: Corticoaccumbal neurotransmission.* The Journal of Physiology, 2012. **590**(16): p. 3743-3769.

43. D'Souza, M.S. and A. Markou, *The "Stop" and "Go" of Nicotine Dependence: Role of GABA and Glutamate.* Cold Spring Harbor Perspectives in Medicine, 2013. **3**(6): p. a012146-a012146.

44. Lewis, A.S. and M.R. Picciotto, *High-affinity nicotinic acetylcholine receptor expression and trafficking abnormalities in psychiatric illness.* Psychopharmacology, 2013. **229**(3): p. 477-485.

45. Richards, C.I., et al., *Live-Cell Imaging of Single Receptor Composition Using Zero-Mode Waveguide Nanostructures.* Nano Letters, 2012. **12**(7): p. 3690-3694.

46. Brody, A.L., et al., *Cigarette Smoking Saturates Brain α4β2 Nicotinic Acetylcholine Receptors.* Archives of General Psychiatry, 2006. **63**(8): p. 907.

47. Brody, A.L., et al., *Differences between smokers and nonsmokers in regional gray matter volumes and densities.* Biological Psychiatry, 2004. **55**(1): p. 77-84.

48. Grieder, T.E., et al., *Phasic D1 and tonic D2 dopamine receptor signaling double dissociate the motivational effects of acute nicotine and chronic nicotine withdrawal.* Proceedings of the National Academy of Sciences, 2012. **109**(8): p. 3101-3106.

49. Hilario, M.R.F., J.R. Turner, and J.A. Blendy, *Reward Sensitization: Effects of Repeated Nicotine Exposure and Withdrawal in Mice.* Neuropsychopharmacology, 2012. **37**(12): p. 2661-2670.

50. Hildebrand, B.E., et al., *Reduced dopamine output in the nucleus accumbens but not in the medial prefrontal cortex in rats displaying a mecamylamine-precipitated nicotine withdrawal syndrome.* Brain Research, 1998. **779**(1-2): p. 214-225.

51. Gould, T.J., et al., *Dissociation of tolerance and nicotine withdrawal-associated deficits in contextual fear.* Brain Research, 2014. **1559**: p. 1-10.

52. Picciotto, M., et al., *It is not "either/or": Activation and desensitization of nicotinic acetylcholine receptors both contribute to behaviors related to nicotine addiction and mood.* Progress in Neurobiology, 2008. **84**(4): p. 329-342.

53. Heishman, S.J. and J.E. Henningfield, *Tolerance to repeated nicotine administration on performance, subjective, and physiological responses in nonsmokers.* Psychopharmacology, 2000. **152**(3): p. 321-333.

54. McLaughlin, I., J.A. Dani, and M. De Biasi, *Nicotine Withdrawal*, in *The Neuropharmacology of Nicotine Dependence*, D.J.K. Balfour and M.R. Munafò, Editors. 2015, Springer International Publishing: Cham. p. 99-123.

55. Cosci, F., *Nicotine dependence and psychological distress: outcomes and clinical implications in smoking cessation.* Psychology Research and Behavior Management, 2011: p. 119.

56. Adeluyi, A., et al., *Microglia morphology and proinflammatory signaling in the nucleus accumbens during nicotine withdrawal.* Science Advances, 2019. **5**(10): p. eaax7031.

57. Hussmann, G.P., et al., *Chronic sazetidine-A maintains anxiolytic effects and slower weight gain following chronic nicotine without maintaining increased density of nicotinic receptors in rodent brain.* Journal of Neurochemistry, 2014. **129**(4): p. 721-731.

58. Turner, J.R., et al., *Divergent Functional Effects of Sazetidine-A and Varenicline During Nicotine Withdrawal.* Neuropsychopharmacology, 2013. **38**(10): p. 2035-2047.

59. Yohn, N.L., J.R. Turner, and J.A. Blendy, *Activation of a4b2/a6 b2 Nicotinic Receptors Alleviates Anxiety during Nicotine Withdrawal Without Upregulating Nicotinic Receptors.* Journal of Pharmacology and Experimental Therapeutics, 2014. **349**(2): p. 348-354.

60. Salas, R., et al., *Nicotinic Receptors in the Habenulo-Interpeduncular System Are Necessary for Nicotine Withdrawal in Mice.* Journal of Neuroscience, 2009. **29**(10): p. 3014-3018.

61. Zhao-Shea, R., et al., *Activation of GABAergic Neurons in the Interpeduncular Nucleus Triggers Physical Nicotine Withdrawal Symptoms.* Current Biology, 2013. **23**(23): p. 2327-2335.

62. George, O., et al., *CRF CRF1 system activation mediates withdrawal-induced increases in nicotine self-administration in nicotine-dependent rats.* Proceedings of the National Academy of Sciences, 2007. **104**(43): p. 17198-17203.

63. Panagis, G., et al., *Selective c-fos induction and decreased dopamine release in the central nucleus of amygdala in rats displaying a mecamylamine-precipitated nicotine withdrawal syndrome.* Synapse (New York, N.Y.), 2000. **35**(1): p. 15-25.

64. Addicott, M.A., et al., *Smoking withdrawal is associated with increases in brain activation during decision making and reward anticipation: a preliminary study.* Psychopharmacology, 2012. **219**(2): p. 563-573.

65. Cole, R.D., et al., *Cognitive rigidity and BDNF-mediated frontostriatal glutamate neuroadaptations during spontaneous nicotine withdrawal.* Neuropsychopharmacology, 2020. **45**(5): p. 866-876.

66. Gipson, C.D., et al., *Reinstatement of nicotine seeking is mediated by glutamatergic plasticity.* Proceedings of the National Academy of Sciences, 2013. **110**(22): p. 9124-9129.

67. Morud, J., et al., *Progressive modulation of accumbal neurotransmission and anxiety-like behavior following protracted nicotine withdrawal.* Neuropharmacology, 2018. **128**: p. 86-95.

68. Balfour, D.J.K., *The psychobiology of nicotine dependence.* European Respiratory Review, 2008. **17**(110): p. 172-181.

69. Armitage, A.K., et al., *Absorption and metabolism of nicotine from cigarettes.* BMJ, 1975. **4**(5992): p. 313-316.

70. Matta, S.G., et al., *Guidelines on nicotine dose selection for in vivo research.* Psychopharmacology, 2007. **190**(3): p. 269-319.

71. Services., U.D.o.H.a.H., *2014 Surgeon General's Report: The Health Consequences of Smoking—50 Years of Progress.* US Department of Health and Human Services, 2014.

72. Lee, K.-H., et al., *Cigarette Smoke Extract Enhances IL-17A-Induced IL-8 Production via Up-Regulation of IL-17R in Human Bronchial Epithelial Cells.* Molecules and Cells, 2018. **41**(4): p. 282-289.

73. Levänen, B., et al., *Impact of tobacco smoking on cytokine signaling via interleukin-17A in the peripheral airways.* International Journal of Chronic Obstructive Pulmonary Disease, 2016. **Volume 11**: p. 2109-2116.

74. Shu, H., et al., *Acute Nicotine Treatment Alleviates LPS-Induced Impairment of Fear Memory Reconsolidation Through AMPK Activation and CRTC1 Upregulation in Hippocampus.* International Journal of Neuropsychopharmacology, 2020. **23**(10): p. 687-699.

75. Wang, J., et al., *Genome-Wide Expression Analysis Reveals Diverse Effects of Acute Nicotine Exposure on Neuronal Function-Related Genes and Pathways.* Frontiers in Psychiatry, 2011. **2**.

76. Turner, M.D., et al., *Cytokines and chemokines: At the crossroads of cell signalling and inflammatory disease.* Biochimica et Biophysica Acta (BBA) - Molecular Cell Research, 2014. **1843**(11): p. 2563-2582.

77. Besedovsky, H.O., et al., *Cytokines as modulators of the hypothalamus-pituitary-adrenal axis.* The Journal of Steroid Biochemistry and Molecular Biology, 1991. **40**(4-6): p. 613-618.

78. Krueger, J., *The Role of Cytokines in Sleep Regulation.* Current Pharmaceutical Design, 2008. **14**(32): p. 3408-3416.

79. Bourgognon, J.-M. and J. Cavanagh, *The role of cytokines in modulating learning and memory and brain plasticity.* Brain and Neuroscience Advances, 2020. **4**: p. 239821282097980.

80. Yang, H.S., et al., *Plasma IL-12/IFN-γ axis predicts cognitive trajectories in cognitively unimpaired older adults.* Alzheimer's & Dementia, 2021: p. alz.12399.

81. Albert, P., *Why is depression more prevalent in women?* Journal of Psychiatry & Neuroscience, 2015. **40**(4): p. 219-221.

82. Hodes, G.E., et al., *Neuroimmune mechanisms of depression.* Nature Neuroscience, 2015. **18**(10): p. 1386-1393.

83. Dowlati, Y., et al., *A Meta-Analysis of Cytokines in Major Depression.* Biological Psychiatry, 2010. **67**(5): p. 446-457.

84. Isung, J., et al., *High interleukin-6 and impulsivity: determining the role of endophenotypes in attempted suicide.* Translational Psychiatry, 2014. **4**(10): p. e470-e470.

85. Simão, F., V. Habekost Oliveira, and M.L. Nunes, *Enhanced susceptibility to seizures modulated by high interleukin-1β levels during early life malnutrition.* Developmental Neurobiology, 2016. **76**(10): p. 1150-1159.

86. Galic, M.A., K. Riazi, and Q.J. Pittman, *Cytokines and brain excitability.* Frontiers in Neuroendocrinology, 2012. **33**(1): p. 116-125.

87. Dorfman, M.D., et al., *Sex differences in microglial CX3CR1 signalling determine obesity susceptibility in mice.* Nature Communications, 2017. **8**(1): p. 14556.

88. Banks, W.A., A.J. Kastin, and R.D. Broadwell, *Passage of Cytokines across the Blood-Brain Barrier.* Neuroimmunomodulation, 1995. **2**(4): p. 241-248.

89. Alfonso-Loeches, S., et al., *Ethanol-Induced TLR4/NLRP3 Neuroinflammatory Response in Microglial Cells Promotes Leukocyte Infiltration Across the BBB.* Neurochemical Research, 2016. **41**(1-2): p. 193-209.

90. Gonçalves, J., et al., *Extended-access methamphetamine self-administration elicits neuroinflammatory response along with blood-brain barrier breakdown.* Brain, Behavior, and Immunity, 2017. **62**: p. 306-317.

91. Pimentel, E., et al., *Effects of Drugs of Abuse on the Blood-Brain Barrier: A Brief Overview.* Frontiers in Neuroscience, 2020. **14**: p. 513.

92. Wolburg, H. and A. Lippoldt, *Tight junctions of the blood–brain barrier.* Vascular Pharmacology, 2002. **38**(6): p. 323-337.

93. Dudek, K.A., et al., *Molecular adaptations of the blood–brain barrier promote stress resilience vs. depression.* Proceedings of the National Academy of Sciences, 2020. **117**(6): p. 3326-3336.

94. Lotrich, F.E., *Major depression during interferon-alpha treatment: vulnerability and prevention.* Dialogues in Clinical Neuroscience, 2009. **11**(4): p. 417-425.

95. Moon, Y., et al., *Sex-Related Differences in Regional Blood–Brain Barrier Integrity in Non-Demented Elderly Subjects.* International Journal of Molecular Sciences, 2021. **22**(6): p. 2860.

96. Namba, M.D., et al., *Neuroimmune Mechanisms as Novel Treatment Targets for Substance Use Disorders and Associated Comorbidities.* Frontiers in Neuroscience, 2021. **15**: p. 650785.

97. Lockman, P.R., et al., *Chronic nicotine exposure alters blood-brain barrier permeability and diminishes brain uptake of methyllycaconitine.* Journal of Neurochemistry, 2005. **94**(1): p. 37-44.

98. Saravia, R., et al., *Anti-inflammatory agents for smoking cessation? Focus on cognitive deficits associated with nicotine withdrawal in male mice.* Brain, Behavior, and Immunity, 2019. **75**: p. 228-239.

99. Salter, M.W. and B. Stevens, *Microglia emerge as central players in brain disease.* Nature Medicine, 2017. **23**(9): p. 1018-1027.

100. Réu, P., et al., *The Lifespan and Turnover of Microglia in the Human Brain.* Cell Reports, 2017. **20**(4): p. 779-784.

101. Zhan, L., et al., *Proximal recolonization by self-renewing microglia re-establishes microglial homeostasis in the adult mouse brain.* PLOS Biology, 2019. **17**(2): p. e3000134.

102. Nimmerjahn, A., *Resting Microglial Cells Are Highly Dynamic Surveillants of Brain Parenchyma in Vivo.* Science, 2005. **308**(5726): p. 1314-1318.

103. George, J., et al., *Microglia-derived purines modulate mossy fibre synaptic transmission and plasticity through P2X $_4$ and A $_1$ receptors.* European Journal of Neuroscience, 2016. **43**(10): p. 1366-1378.

104. Sipe, G.O., et al., *Microglial P2Y12 is necessary for synaptic plasticity in mouse visual cortex.* Nature Communications, 2016. **7**(1): p. 10905.

105. Wake, H., et al., *Resting Microglia Directly Monitor the Functional State of Synapses In Vivo and Determine the Fate of Ischemic Terminals.* Journal of Neuroscience, 2009. **29**(13): p. 3974-3980.

106. Lenz, K.M., et al., *Microglia Are Essential to Masculinization of Brain and Behavior.* Journal of Neuroscience, 2013. **33**(7): p. 2761-2772.

107. Consortium, S.W.G.o.t.P.G., et al., *Schizophrenia risk from complex variation of complement component 4.* Nature, 2016. **530**(7589): p. 177-183.

108. Parkhurst, Christopher N., et al., *Microglia Promote Learning-Dependent Synapse Formation through Brain-Derived Neurotrophic Factor.* Cell, 2013. **155**(7): p. 1596-1609.

109. Torres, L., et al., *Dynamic microglial modulation of spatial learning and social behavior.* Brain, Behavior, and Immunity, 2016. **55**: p. 6-16.

110. Paolicelli, R.C., et al., *Synaptic Pruning by Microglia Is Necessary for Normal Brain Development.* Science, 2011. **333**(6048): p. 1456-1458.

111. Schafer, D.P., E.K. Lehrman, and B. Stevens, *The "quad-partite" synapse: Microglia-synapse interactions in the developing and mature CNS.* Glia, 2013. **61**(1): p. 24-36.

112. Inoue, K., et al., *Chapter 12 P2Y6-Evoked Microglial Phagocytosis*, in *International Review of Neurobiology*. 2009, Elsevier. p. 159-163.

113. De, S., et al., *Two distinct ontogenies confer heterogeneity to mouse brain microglia.* Development, 2018. **145**(13): p. dev152306.

114. Ginhoux, F., et al., *Fate Mapping Analysis Reveals That Adult Microglia Derive from Primitive Macrophages.* Science, 2010. **330**(6005): p. 841-845.

115. Tay, T.L., et al., *A new fate mapping system reveals context-dependent random or clonal expansion of microglia.* Nature Neuroscience, 2017. **20**(6): p. 793-803.

116. Biber, K., et al., *Expression and Signaling of Group I Metabotropic Glutamate Receptors in Astrocytes and Microglia.* Journal of Neurochemistry, 2001. **72**(4): p. 1671-1680.

117. Bsibsi, M., et al., *Broad expression of Toll-like receptors in the human central nervous system.* Journal of Neuropathology and Experimental Neurology, 2002. **61**(11): p. 1013-1021.

118. Färber, K., U. Pannasch, and H. Kettenmann, *Dopamine and noradrenaline control distinct functions in rodent microglial cells.* Molecular and Cellular Neuroscience, 2005. **29**(1): p. 128-138.

119. Hagino, Y., et al., *Heterogeneity and potentiation of AMPA type of glutamate receptors in rat cultured microglia.* Glia, 2004. **47**(1): p. 68-77.

120. Kigerl, K.A., et al., *Pattern recognition receptors and central nervous system repair.* Experimental Neurology, 2014. **258**: p. 5-16.

121. Kuhn, S.A., et al., *Microglia express GABA B receptors to modulate interleukin release.* Molecular and Cellular Neuroscience, 2004. **25**(2): p. 312-322.

122. Maduna, T., et al., *Microglia Express Mu Opioid Receptor: Insights From Transcriptomics and Fluorescent Reporter Mice.* Frontiers in Psychiatry, 2019. **9**: p. 726.

123. Noda, M., et al., *Expression and function of bradykinin receptors in microglia.* Life Sciences, 2003. **72**(14): p. 1573-1581.

124. Noda, M., et al., *AMPA–Kainate Subtypes of Glutamate Receptor in Rat Cerebral Microglia.* The Journal of Neuroscience, 2000. **20**(1): p. 251-258.

125. Taylor, D.L., et al., *Activation of group II metabotropic glutamate receptors underlies microglial reactivity and neurotoxicity following stimulation with chromogranin A, a peptide up-regulated in Alzheimer's disease: Microglial metabotropic glutamate receptors.* Journal of Neurochemistry, 2004. **82**(5): p. 1179-1191.

126. Taylor, D.L., L.T. Diemel, and J.M. Pocock, *Activation of Microglial Group III Metabotropic Glutamate Receptors Protects Neurons against Microglial Neurotoxicity.* The Journal of Neuroscience, 2003. **23**(6): p. 2150-2160.

127. Wang, Q., et al., *Substance P enhances microglial density in the substantia nigra through neurokinin-1 receptor/NADPH oxidase-mediated chemotaxis in mice.* Clinical Science, 2015. **129**(8): p. 757-767.

128. Wohleb, E.S., *Neuron–Microglia Interactions in Mental Health Disorders: "For Better, and For Worse".* Frontiers in Immunology, 2016. **7**.

129. Hanisch, U.-K., *Microglia as a source and target of cytokines.* Glia, 2002. **40**(2): p. 140-155.

130. Limatola, C. and R.M. Ransohoff, *Modulating neurotoxicity through CX3CL1/CX3CR1 signaling.* Frontiers in Cellular Neuroscience, 2014. **8**.

131. Aw, E., Y. Zhang, and M. Carroll, *Microglial responses to peripheral type 1 interferon.* Journal of Neuroinflammation, 2020. **17**(1): p. 340.

132. Yamada, T. and I. Yamanaka, *Microglial localization of α-interferon receptor in human brain tissues.* Neuroscience Letters, 1995. **189**(2): p. 73-76.

133. De Biase, L.M., et al., *Local Cues Establish and Maintain Region-Specific Phenotypes of Basal Ganglia Microglia.* Neuron, 2017. **95**(2): p. 341-356.e6.

134. Cherry, J.D., J.A. Olschowka, and M. O'Banion, *Neuroinflammation and M2 microglia: the good, the bad, and the inflamed.* Journal of Neuroinflammation, 2014. **11**(1): p. 98.

135. Butovsky, O. and H.L. Weiner, *Microglial signatures and their role in health and disease.* Nature Reviews Neuroscience, 2018. **19**(10): p. 622-635.

136. Nakagawa, Y. and K. Chiba, *Diversity and plasticity of microglial cells in psychiatric and neurological disorders.* Pharmacology & Therapeutics, 2015. **154**: p. 21-35.

137. Orihuela, R., C.A. McPherson, and G.J. Harry, *Microglial M1/M2 polarization and metabolic states: Microglia bioenergetics with acute polarization.* British Journal of Pharmacology, 2016. **173**(4): p. 649-665.

138. Tang, Y. and W. Le, *Differential Roles of M1 and M2 Microglia in Neurodegenerative Diseases.* Molecular Neurobiology, 2016. **53**(2): p. 1181-1194.

139. Yao, K. and H.-b. Zu, *Microglial polarization: novel therapeutic mechanism against Alzheimer's disease.* Inflammopharmacology, 2020. **28**(1): p. 95-110.

140. Gustin, A., et al., *NLRP3 Inflammasome Is Expressed and Functional in Mouse Brain Microglia but Not in Astrocytes.* PLOS ONE, 2015. **10**(6): p. e0130624.

141. Moore, C.S., et al., *P2Y12 expression and function in alternatively activated human microglia.* Neurology - Neuroimmunology Neuroinflammation, 2015. **2**(2): p. e80.

142. Stratoulias, V., et al., *Microglial subtypes: diversity within the microglial community.* The EMBO Journal, 2019. **38**(17).

143. Chiu, Isaac M., et al., *A Neurodegeneration-Specific Gene-Expression Signature of Acutely Isolated Microglia from an Amyotrophic Lateral Sclerosis Mouse Model.* Cell Reports, 2013. **4**(2): p. 385-401.

144. Consortium, T.I.G., et al., *Gene-expression profiles and transcriptional regulatory pathways that underlie the identity and diversity of mouse tissue macrophages.* Nature Immunology, 2012. **13**(11): p. 1118-1128.

145. Hammond, T.R., et al., *Single-Cell RNA Sequencing of Microglia throughout the Mouse Lifespan and in the Injured Brain Reveals Complex Cell-State Changes.* Immunity, 2019. **50**(1): p. 253-271.e6.

146. Hickman, S.E., et al., *The microglial sensome revealed by direct RNA sequencing.* Nature Neuroscience, 2013. **16**(12): p. 1896-1905.

147. Masuda, T., et al., *Spatial and temporal heterogeneity of mouse and human microglia at single-cell resolution.* Nature, 2019. **566**(7744): p. 388-392.

148. Zeisel, A., et al., *Cell types in the mouse cortex and hippocampus revealed by single-cell RNA-seq.* Science, 2015. **347**(6226): p. 1138-1142.

149. Friedman, B.A., et al., *Diverse Brain Myeloid Expression Profiles Reveal Distinct Microglial Activation States and Aspects of Alzheimer's Disease Not Evident in Mouse Models.* Cell Reports, 2018. **22**(3): p. 832-847.

150. Bennett, M.L., et al., *New tools for studying microglia in the mouse and human CNS.* Proceedings of the National Academy of Sciences, 2016. **113**(12): p. E1738-E1746.

151. Tremblay, M.-E., et al., *The Role of Microglia in the Healthy Brain.* Journal of Neuroscience, 2011. **31**(45): p. 16064-16069.

152. Bisht, K., et al., *Capillary-associated microglia regulate vascular structure and function through PANX1-P2RY12 coupling in mice.* Nature Communications, 2021. **12**(1): p. 5289.

153. Long, J.M., et al., *Stereological analysis of astrocyte and microglia in aging mouse hippocampus.* Neurobiology of Aging, 1998. **19**(5): p. 497-503.

154. McCarthy, M.M., *Location, Location, Location: Microglia Are Where They Live.* Neuron, 2017. **95**(2): p. 233-235.

155. Egea, J., et al., *Anti-inflammatory role of microglial alpha7 nAChRs and its role in neuroprotection.* Biochemical Pharmacology, 2015. **97**(4): p. 463-472.

156. De Simone, R., et al., *Activation of α7 nicotinic acetylcholine receptor by nicotine selectively up-regulates cyclooxygenase-2 and prostaglandin E2 in rat microglial cultures.* Journal of Neuroinflammation, 2005. **2**(1): p. 4.

157. King, J.R., T.C. Gillevet, and N. Kabbani, *A G protein-coupled α7 nicotinic receptor regulates signaling and TNF-α release in microglia.* FEBS Open Bio, 2017. **7**(9): p. 1350-1361.

158. Mencel, M., M. Nash, and C. Jacobson, *Neuregulin Upregulates Microglial α7 Nicotinic Acetylcholine Receptor Expression in Immortalized Cell Lines: Implications for Regulating Neuroinflammation.* PLoS ONE, 2013. **8**(7): p. e70338.

159. Suzuki, T., et al., *Microglial α7 nicotinic acetylcholine receptors drive a phospholipase C/IP3 pathway and modulate the cell activation toward a neuroprotective role.* Journal of Neuroscience Research, 2006. **83**(8): p. 1461-1470.

160. Shytle, R.D., et al., *Cholinergic modulation of microglial activation by α7 nicotinic receptors: Cholinergic modulation of microglial activation.* Journal of Neurochemistry, 2004. **89**(2): p. 337-343.

161. Godin, J.-R., et al., *A silent agonist of α7 nicotinic acetylcholine receptors modulates inflammation ex vivo and attenuates EAE.* Brain, Behavior, and Immunity, 2020. **87**: p. 286-300.

162. Noda, M. and A. Kobayashi, *Nicotine inhibits activation of microglial proton currents via interactions with α7 acetylcholine receptors.* The Journal of Physiological Sciences, 2017. **67**(1): p. 235-245.

163. Thomsen, M.S. and J.D. Mikkelsen, *The α7 nicotinic acetylcholine receptor ligands methyllycaconitine, NS6740 and GTS-21 reduce lipopolysaccharide-induced TNF-α release from microglia.* Journal of Neuroimmunology, 2012. **251**(1-2): p. 65-72.

164. Jaikhan, P., et al., *Design and Synthesis of Nicotinic Acetylcholine Receptor Antagonists and their Effect on Cognitive Impairment.* Chemical Biology & Drug Design, 2016. **87**(1): p. 39-56.

165. Guan, Y.-Z., et al., *Nicotine Inhibits Microglial Proliferation and Is Neuroprotective in Global Ischemia Rats.* Molecular Neurobiology, 2015. **51**(3): p. 1480-1488.

166. Ohnishi, M., et al., *Long-term treatment with nicotine suppresses neurotoxicity of, and microglial activation by, thrombin in cortico-striatal slice cultures.* European Journal of Pharmacology, 2009. **602**(2-3): p. 288-293.

167. Linker, K.E., et al., *Microglial activation increases cocaine self-administration following adolescent nicotine exposure.* Nature Communications, 2020. **11**(1).

168. Fiore, M.C., *A Clinical Practice Guideline for Treating Tobacco Use and Dependence: 2008 Update.* American Journal of Preventive Medicine, 2008. **35**(2): p. 158-176.

169. Prochaska, J.J. and N.L. Benowitz, *The Past, Present, and Future of Nicotine Addiction Therapy.* Annual Review of Medicine, 2016. **67**(1): p. 467-486.

170. de Villiers, S.H.L., et al., *Nicotine hapten structure, antibody selectivity and effect relationships: Results from a nicotine vaccine screening procedure.* Vaccine, 2010. **28**(10): p. 2161-2168.

171. Goniewicz, M.L. and M. Delijewski, *Nicotine vaccines to treat tobacco dependence.* Human Vaccines & Immunotherapeutics, 2013. **9**(1): p. 13-25.

172. Pravetoni, M., et al., *Structurally distinct nicotine immunogens elicit antibodies with non-overlapping specificities.* Biochemical Pharmacology, 2012. **83**(4): p. 543-550.

173. Garvey, A.J., et al., *Predictors of smoking relapse among self-quitters: A report from the normative aging study.* Addictive Behaviors, 1992. **17**(4): p. 367-377.

174. Latt, N., *Addiction medicine*. Oxford specialist handbooks. 2009, Oxford ; New York: Oxford University Press. 459.

175. Picciotto, M., R., *Neuroprotection via nAChRs: the role of nAChRs in neurodegenerative disorders such as Alzheimer's and Parkinson's disease.* Frontiers in Bioscience, 2008. **13**(13): p. 492.

176. Quik, M., X.A. Perez, and T. Bordia, *Nicotine as a potential neuroprotective agent for Parkinson's disease.* Movement Disorders, 2012. **27**(8): p. 947-957.

177. Flurkey, K., *The Jackson laboratory handbook of genetically standardized mice: ask for the j*. 6. ed., 1. printing ed. 2009, Bar Harbor, Me: The Jackson Laboratory. 380.

178. Fisher, M.L., et al., *Distinct Roles of CREB Within the Ventral and Dorsal Hippocampus in Mediating Nicotine Withdrawal Phenotypes.* Neuropsychopharmacology, 2016.

179. Turner, J.R., et al., *Evidence from mouse and man for a role of neuregulin 3 in nicotine dependence.* Molecular Psychiatry, 2014. **19**(7): p. 801-810.

180. Franklin, K.B.J. and G. Paxinos, *Paxinos and Franklin's The mouse brain in stereotaxic coordinates*. Fourth edition ed. 2013, Amsterdam: Academic Press, an imprint of Elsevier. 1.

181. Schindelin, J., et al., *The ImageJ ecosystem: An open platform for biomedical image analysis: T HE I MAGEJ E COSYSTEM.* Molecular Reproduction and Development, 2015. **82**(7-8): p. 518-529.

182. Schindelin, J., et al., *Fiji: an open-source platform for biological-image analysis.* Nature Methods, 2012. **9**(7): p. 676-682.

183. Benowitz, N.L., J. Hukkanen, and P. Jacob, *Nicotine Chemistry, Metabolism, Kinetics and Biomarkers*, in *Nicotine Psychopharmacology*, J.E. Henningfield, E.D. London, and S. Pogun, Editors. 2009, Springer Berlin Heidelberg: Berlin, Heidelberg. p. 29-60.

184. Fung, Y.K. and Y.-S. Lau, *Receptor mechanisms of nicotine-induced locomotor hyperactivity in chronic nicotine-treated rats.* European Journal of Pharmacology, 1988. **152**(3): p. 263-271.

185. Fung, Y.K. and Y.S. Lau, *Chronic effects of nicotine on mesolimbic dopaminergic system in rats.* Pharmacology Biochemistry and Behavior, 1992. **41**(1): p. 57-63.

186. Sanderson, E.M., et al., *Upregulation of nicotinic receptors following continuous infusion of nicotine is brain-region-specific.* Brain Research, 1993. **617**(2): p. 349-352.

187. Slotkin, T.A., et al., *Chronic prenatal nicotine exposure sensitizes rat brain to acute postnatal nicotine challenge as assessed with ornithine decarboxylase.* Life Sciences, 1991. **49**(9): p. 665-670.

188. Mathieu-Kia, A., et al., *Nicotine addiction: insights from recent animal studies.* Psychopharmacology, 2002. **162**(2): p. 102-118.

189. Picciotto, M., *Nicotinic Receptors in the Brain Links between Molecular Biology and Behavior.* Neuropsychopharmacology, 2000. **22**(5): p. 451-465.

190. Merali, Z., C. Levac, and H. Anisman, *Validation of a simple, ethologically relevant paradigm for assessing anxiety in mice.* Biological Psychiatry, 2003. **54**(5): p. 552-565.

191. Nakajima, M. and M. Al'Absi, *Nicotine withdrawal and stress-induced changes in pain sensitivity: A cross-sectional investigation between abstinent smokers and nonsmokers: Smoking withdrawal and pain.* Psychophysiology, 2014. **51**(10): p. 1015-1022.

192. Breese, C.R., et al., *Effect of smoking history on [3H]nicotine binding in human postmortem brain.* The Journal of Pharmacology and Experimental Therapeutics, 1997. **282**(1): p. 7-13.

193. Mukhin, A.G., et al., *Greater Nicotinic Acetylcholine Receptor Density in Smokers Than in Nonsmokers: A PET Study with 2-* ^{18} *F-FA-85380.* Journal of Nuclear Medicine, 2008. **49**(10): p. 1628-1635.

194. Turner, J.R., L.M. Castellano, and J.A. Blendy, *Parallel Anxiolytic-Like Effects and Upregulation of Neuronal Nicotinic Acetylcholine Receptors Following Chronic Nicotine and Varenicline.* Nicotine & Tobacco Research, 2011. **13**(1): p. 41-46.

195. Sihver, W., B. Långström, and A. Nordberg, *Ligands for in vivo imaging of nicotinic receptor subtypes in Alzheimer brain: Imaging of nicotinic receptors in Alzheimer brain.* Acta Neurologica Scandinavica, 2000. **102**: p. 27-33.

196. Spande, T.F., et al., *Epibatidine: a novel (chloropyridyl)azabicycloheptane with potent analgesic activity from an Ecuadoran poison frog.* Journal of the American Chemical Society, 1992. **114**(9): p. 3475-3478.

197. Pauly, J.R., et al., *An autoradiographic analysis of cholinergic receptors in mouse brain after chronic nicotine treatment.* The Journal of Pharmacology and Experimental Therapeutics, 1991. **258**(3): p. 1127-1136.

198. Utsugisawa, K., et al., *Changes with aging and ischemia in nicotinic acetylcholine receptor subunit α7 mRNA expression in postmortem human frontal cortex and putamen.* Neuroscience Letters, 1999. **270**(3): p. 145-148.

199. Wüllner, U., et al., *Smoking upregulates α4β2* nicotinic acetylcholine receptors in the human brain.* Neuroscience Letters, 2008. **430**(1): p. 34-37.

200. Nguyen, M.D., J.-P. Julien, and S. Rivest, *Innate immunity: the missing link in neuroprotection and neurodegeneration?* Nature Reviews Neuroscience, 2002. **3**(3): p. 216-227.

201. Lull, M.E. and M.L. Block, *Microglial activation and chronic neurodegeneration.* Neurotherapeutics, 2010. **7**(4): p. 354-365.

202. Riikonen, J., *INTERMITTENT ETHANOL EXPOSURE INCREASES THE NUMBER OF CEREBELLAR MICROGLIA.* Alcohol and Alcoholism, 2002. **37**(5): p. 421-426.

203. Sekine, Y., et al., *Methamphetamine Causes Microglial Activation in the Brains of Human Abusers.* Journal of Neuroscience, 2008. **28**(22): p. 5756-5761.

204. Miyamoto, A., et al., *Microglia contact induces synapse formation in developing somatosensory cortex.* Nature Communications, 2016. **7**(1): p. 12540.

205. Carr, D.B. and S.R. Sesack, *Projections from the Rat Prefrontal Cortex to the Ventral Tegmental Area: Target Specificity in the Synaptic Associations with Mesoaccumbens and Mesocortical Neurons.* The Journal of Neuroscience, 2000. **20**(10): p. 3864-3873.

206. De Biasi, M. and J.A. Dani, *Reward, Addiction, Withdrawal to Nicotine.* Annual Review of Neuroscience, 2011. **34**(1): p. 105-130.

207. Pignatelli, M. and A. Bonci, *Role of Dopamine Neurons in Reward and Aversion: A Synaptic Plasticity Perspective.* Neuron, 2015. **86**(5): p. 1145-1157.

208. Badimon, A., et al., *Negative feedback control of neuronal activity by microglia.* Nature, 2020. **586**(7829): p. 417-423.

209. Nisell, M., et al., *Differential effects of acute and chronic nicotine on dopamine output in the core and shell of the rat nucleus accumbens.* Journal of Neural Transmission, 1997. **104**(1): p. 1-10.

210. Sellings, L.H.L., et al., *Rewarding and aversive effects of nicotine are segregated within the nucleus accumbens.* European Journal of Neuroscience, 2008. **28**(2): p. 342-352.

211. Butovsky, O., et al., *Identification of a unique TGF-β–dependent molecular and functional signature in microglia.* Nature Neuroscience, 2014. **17**(1): p. 131-143.

212. Young, K.F., et al., *Can quantifying morphology and TMEM119 expression distinguish between microglia and infiltrating macrophages after ischemic stroke and reperfusion in male and female mice?* Journal of Neuroinflammation, 2021. **18**(1): p. 58.

213. Fairweather, D., S. Frisancho-Kiss, and N.R. Rose, *Sex Differences in Autoimmune Disease from a Pathological Perspective.* The American Journal of Pathology, 2008. **173**(3): p. 600-609.

214. Ngo, S.T., F.J. Steyn, and P.A. McCombe, *Gender differences in autoimmune disease.* Frontiers in Neuroendocrinology, 2014. **35**(3): p. 347-369.

215. Quintero, O.L., et al., *Autoimmune disease and gender: Plausible mechanisms for the female predominance of autoimmunity.* Journal of Autoimmunity, 2012. **38**(2-3): p. J109-J119.

216. Barbieri, R.L., J. Gochberg, and K.J. Ryan, *Nicotine, cotinine, and anabasine inhibit aromatase in human trophoblast in vitro.* Journal of Clinical Investigation, 1986. **77**(6): p. 1727-1733.

217. Biegon, A., et al., *Nicotine Blocks Brain Estrogen Synthase (Aromatase): In Vivo Positron Emission Tomography Studies in Female Baboons.* Biological Psychiatry, 2010. **67**(8): p. 774-777.

218. Zhu, D., et al., *Relationships between intensity, duration, cumulative dose, and timing of smoking with age at menopause: A pooled analysis of individual data from 17 observational studies.* PLOS Medicine, 2018. **15**(11): p. e1002704.

219. Baker, A.E., V.M. Brautigam, and J.J. Watters, *Estrogen Modulates Microglial Inflammatory Mediator Production via Interactions with Estrogen Receptor β.* Endocrinology, 2004. **145**(11): p. 5021-5032.

220. Bruce-Keller, A.J., et al., *Antiinflammatory Effects of Estrogen on Microglial Activation [1].* Endocrinology, 2000. **141**(10): p. 3646-3656.

221. d'Adesky, N., et al., *Nicotine Alters Estrogen Receptor-Beta-Regulated Inflammasome Activity and Exacerbates Ischemic Brain Damage in Female Rats.* International Journal of Molecular Sciences, 2018. **19**(5): p. 1330.

222. Hara, Y., et al., *Estrogen Effects on Cognitive and Synaptic Health Over the Lifecourse.* Physiological Reviews, 2015. **95**(3): p. 785-807.

223. Vegeto, E., et al., *Estrogen receptor- mediates the brain antiinflammatory activity of estradiol.* Proceedings of the National Academy of Sciences, 2003. **100**(16): p. 9614-9619.

224. Caligioni, C.S., *Assessing Reproductive Status/Stages in Mice.* Current Protocols in Neuroscience, 2009. **48**(1).

225. Alia-Klein, N., et al., *Gene × Disease Interaction on Orbitofrontal Gray Matter in Cocaine Addiction.* Archives of General Psychiatry, 2011. **68**(3): p. 283.

226. Das, D., et al., *Lifetime cigarette smoking is associated with striatal volume measures: Smoking and striatal volume.* Addiction Biology, 2012. **17**(4): p. 817-825.

227. Liao, Y., et al., *Differences between smokers and non-smokers in regional gray matter volumes: a voxel-based morphometry study: Gray matter changes in smokers.* Addiction Biology, 2012. **17**(6): p. 977-980.

228. Breschi, A., T.R. Gingeras, and R. Guigó, *Comparative transcriptomics in human and mouse.* Nature Reviews Genetics, 2017. **18**(7): p. 425-440.

229. Hanamsagar, R. and S.D. Bilbo, *Sex differences in neurodevelopmental and neurodegenerative disorders: Focus on microglial function and neuroinflammation during development.* The Journal of Steroid Biochemistry and Molecular Biology, 2016. **160**: p. 127-133.

230. Lopez-Lee, C., L. Kodama, and L. Gan, *Sex Differences in Neurodegeneration: The Role of the Immune System in Humans.* Biological Psychiatry, 2021: p. S0006322321000391.

231. Livak, K.J. and T.D. Schmittgen, *Analysis of Relative Gene Expression Data Using Real-Time Quantitative PCR and the 2−ΔΔCT Method.* Methods, 2001. **25**(4): p. 402-408.

232. Ye, J., et al., *Primer-BLAST: A tool to design target-specific primers for polymerase chain reaction.* BMC Bioinformatics, 2012. **13**(1): p. 134.

233. Untergasser, A., et al., *Primer3Plus, an enhanced web interface to Primer3.* Nucleic Acids Research, 2007. **35**(Web Server): p. W71-W74.

234. Rivest, S., *Regulation of innate immune responses in the brain.* Nature Reviews Immunology, 2009. **9**(6): p. 429-439.

235. Zhang, Y., et al., *An RNA-sequencing transcriptome and splicing database of glia, neurons, and vascular cells of the cerebral cortex.* The Journal of Neuroscience: The Official Journal of the Society for Neuroscience, 2014. **34**(36): p. 11929-11947.

236. Zhang, Y., et al., *Purification and Characterization of Progenitor and Mature Human Astrocytes Reveals Transcriptional and Functional Differences with Mouse.* Neuron, 2016. **89**(1): p. 37-53.

237. Schwarz, J.M., P.W. Sholar, and S.D. Bilbo, *Sex differences in microglial colonization of the developing rat brain: Sex differences in microglial colonization.* Journal of Neurochemistry, 2012: p. no-no.

238. Makinson, R., et al., *Intrauterine inflammation induces sex-specific effects on neuroinflammation, white matter, and behavior.* Brain, Behavior, and Immunity, 2017. **66**: p. 277-288.

239. Arnò, B., et al., *Neural progenitor cells orchestrate microglia migration and positioning into the developing cortex.* Nature Communications, 2014. **5**(1): p. 5611.

240. Hattori, Y. and T. Miyata, *Microglia extensively survey the developing cortex via the CXCL12/CXCR4 system to help neural progenitors to acquire differentiated properties.* Genes to Cells, 2018. **23**(10): p. 915-922.

241. (IFGC), I.F.-G.C., et al., *CXCR4 involvement in neurodegenerative diseases.* Translational Psychiatry, 2018. **8**(1): p. 73.

242. Guo, L., et al., *Sex Differences in Alzheimer's Disease: Insights From the Multiomics Landscape.* Biological Psychiatry, 2021: p. S0006322321010982.

243. Sanfilippo, C., et al., *Postsynaptic damage and microglial activation in AD patients could be linked CXCR4/CXCL12 expression levels.* Brain Research, 2020. **1749**: p. 147127.

244. Yamamori, T., *Localization of cholinergic differentiation factor/leukemia inhibitory factor mRNA in the rat brain and peripheral tissues.* Proceedings of the National Academy of Sciences, 1991. **88**(16): p. 7298-7302.

245. Rensink, A.A., et al., *Expression of the cytokine leukemia inhibitory factor and pro-apoptotic insulin-like growth factor binding protein-3 in Alzheimer's disease.* Acta Neuropathologica, 2002. **104**(5): p. 525-533.

246. Soilu-HÃ¤nninen, M., et al., *Expression of LIF and LIF receptor beta in Alzheimer's and Parkinson's diseases: LIF and LIFR in Alzheimer's and Parkinson's diseases.* Acta Neurologica Scandinavica, 2010. **121**(1): p. 44-50.

247. Borgesius, N.Z., et al., *Accelerated Age-Related Cognitive Decline and Neurodegeneration, Caused by Deficient DNA Repair.* Journal of Neuroscience, 2011. **31**(35): p. 12543-12553.

248. Kerr, N., et al., *Sexually dimorphic microglia and ischemic stroke.* CNS Neuroscience & Therapeutics, 2019. **25**(12): p. 1308-1317.

249. Villapol, S., D.J. Loane, and M.P. Burns, *Sexual dimorphism in the inflammatory response to traumatic brain injury.* Glia, 2017. **65**(9): p. 1423-1438.

250. Liao, S.-L., W.-Y. Chen, and C.-J. Chen, *Estrogen attenuates tumor necrosis factor-α expression to provide ischemic neuroprotection in female rats.* Neuroscience Letters, 2002. **330**(2): p. 159-162.

251. Clarner, T., et al., *CXCL10 Triggers Early Microglial Activation in the Cuprizone Model.* The Journal of Immunology, 2015. **194**(7): p. 3400-3413.

252. Whitman, B.A., et al., *The Cytokine mRNA Increase Induced by Withdrawal from Chronic Ethanol in the Sterile Environment of Brain is Mediated by CRF and HMGB1 Release.* Alcoholism: Clinical and Experimental Research, 2013. **37**(12): p. 2086-2097.

253. Hsieh, C.L., et al., *A role for TREM2 ligands in the phagocytosis of apoptotic neuronal cells by microglia.* Journal of Neurochemistry, 2009. **109**(4): p. 1144-1156.

254. Cantoni, C., et al., *TREM2 regulates microglial cell activation in response to demyelination in vivo.* Acta Neuropathologica, 2015. **129**(3): p. 429-447.

255. Blednov, Y., et al., *Perturbation of chemokine networks by gene deletion alters the reinforcing actions of ethanol.* Behavioural Brain Research, 2005. **165**(1): p. 110-125.

256. Smith, P.H., et al., *Gender Differences in Medication Use and Cigarette Smoking Cessation: Results From the International Tobacco Control Four Country Survey.* Nicotine & Tobacco Research, 2015. **17**(4): p. 463-472.

257. McKee, S.A., et al., *Sex Differences in Varenicline Efficacy for Smoking Cessation: A Meta-Analysis.* Nicotine & Tobacco Research, 2016. **18**(5): p. 1002-1011.

258. Ebbert, J., M.V. Burke, and J.T. Hays, *Varenicline for smoking cessation: a narrative review of efficacy, adverse effects, use in at-risk populations, and adherence.* Patient Preference and Adherence, 2016: p. 435.

259. Singh, K.P., et al., *Systemic biomarkers in electronic cigarette users: implications for noninvasive assessment of vaping-associated pulmonary injuries.* ERJ Open Research, 2019. **5**(4): p. 00182-2019.

260. Arnson, Y., Y. Shoenfeld, and H. Amital, *Effects of tobacco smoke on immunity, inflammation and autoimmunity.* Journal of Autoimmunity, 2010. **34**(3): p. J258-J265.

261. Han, T., et al., *Nicotine Induced Neurocognitive Protection and Anti-inflammation Effect by Activating α 4β 2 Nicotinic Acetylcholine Receptors in Ischemic Rats.* Nicotine & Tobacco Research, 2020. **22**(6): p. 919-924.

262. Jiang, W., et al., *Infiltration of CCR2 $^{+}$ Ly6C ^{high} Proinflammatory Monocytes and Neutrophils into the Central Nervous System Is Modulated by Nicotinic Acetylcholine Receptors in a Model of Multiple Sclerosis.* The Journal of Immunology, 2016. **196**(5): p. 2095-2108.

263. Lakhan, S.E. and A. Kirchgessner, *Anti-inflammatory effects of nicotine in obesity and ulcerative colitis.* Journal of Translational Medicine, 2011. **9**(1): p. 129.

264. Johnson, G.J., J. Cosnes, and J.C. Mansfield, *Review article: smoking cessation as primary therapy to modify the course of Crohn's disease.* Alimentary Pharmacology and Therapeutics, 2005. **21**(8): p. 921-931.

265. Sajja, R.K., S. Rahman, and L. Cucullo, *Drugs of abuse and blood-brain barrier endothelial dysfunction: A focus on the role of oxidative stress.* Journal of Cerebral Blood Flow & Metabolism, 2016. **36**(3): p. 539-554.

266. Shi, F.-D., et al., *Nicotinic Attenuation of Central Nervous System Inflammation and Autoimmunity.* The Journal of Immunology, 2009. **182**(3): p. 1730-1739.

267. Pan, W., et al., *Cytokine signaling modulates blood-brain barrier function.* Current Pharmaceutical Design, 2011. **17**(33): p. 3729-3740.

268. Pan, W., et al., *Neuroinflammation facilitates LIF entry into brain: role of TNF.* American Journal of Physiology-Cell Physiology, 2008. **294**(6): p. C1436-C1442.

269. Vogel, C. and E.M. Marcotte, *Insights into the regulation of protein abundance from proteomic and transcriptomic analyses.* Nature Reviews Genetics, 2012. **13**(4): p. 227-232.

270. Hodes, G.E., et al., *Individual differences in the peripheral immune system promote resilience versus susceptibility to social stress.* Proceedings of the National Academy of Sciences, 2014. **111**(45): p. 16136-16141.

271. Dossus, L., et al., *Validity of multiplex-based assays for cytokine measurements in serum and plasma from "non-diseased" subjects: Comparison with ELISA.* Journal of Immunological Methods, 2009. **350**(1-2): p. 125-132.

272. Leng, S.X., et al., *ELISA and Multiplex Technologies for Cytokine Measurement in Inflammation and Aging Research.* The Journals of Gerontology Series A: Biological Sciences and Medical Sciences, 2008. **63**(8): p. 879-884.

273. Hughes, C.E. and R.J.B. Nibbs, *A guide to chemokines and their receptors.* The FEBS Journal, 2018. **285**(16): p. 2944-2971.

274. Ashwood, P., et al., *Elevated plasma cytokines in autism spectrum disorders provide evidence of immune dysfunction and are associated with impaired behavioral outcome.* Brain, Behavior, and Immunity, 2011. **25**(1): p. 40-45.

275. Hocum Stone, L., et al., *Serum cytokine profiles in healthy nonhuman primates are blunted by sedation and demonstrate sexual dimorphism as detected by a validated multiplex immunoassay.* Scientific Reports, 2021. **11**(1): p. 2340.

276. Howes, O.D. and R. McCutcheon, *Inflammation and the neural diathesis-stress hypothesis of schizophrenia: a reconceptualization.* Translational Psychiatry, 2017. **7**(2): p. e1024-e1024.

277. Kiraly, D.D., et al., *Altered peripheral immune profiles in treatment-resistant depression: response to ketamine and prediction of treatment outcome.* Translational Psychiatry, 2017. **7**(3): p. e1065-e1065.

278. Munkholm, K., M. Vinberg, and L. Vedel Kessing, *Cytokines in bipolar disorder: A systematic review and meta-analysis.* Journal of Affective Disorders, 2013. **144**(1-2): p. 16-27.

279. Panizzutti, B., et al., *Increased serum levels of eotaxin/CCL11 in late-stage patients with bipolar disorder: An accelerated aging biomarker?* Journal of Affective Disorders, 2015. **182**: p. 64-69.

280. Potvin, S., et al., *Inflammatory Cytokine Alterations in Schizophrenia: A Systematic Quantitative Review.* Biological Psychiatry, 2008. **63**(8): p. 801-808.

281. Fiehn, C., et al., *Plasma GM-CSF concentrations in rheumatoid arthritis, systemic lupus erythematosus and spondyloarthropathy.* Zeitschrift Fur Rheumatologie, 1992. **51**(3): p. 121-126.

282. Lee, K.M., A.A. Achuthan, and J.A. Hamilton, *GM-CSF: A Promising Target in Inflammation and Autoimmunity.* ImmunoTargets and Therapy, 2020. **Volume 9**: p. 225-240.

283. Chen, H., et al., *Evidence from a mouse model on the dangers of thirdhand electronic cigarette exposure during early life.* ERJ Open Research, 2020. **6**(2): p. 00022-2020.

284. Fontenelle, L.F., et al., *A cytokine study of adult patients with obsessive-compulsive disorder.* Comprehensive Psychiatry, 2012. **53**(6): p. 797-804.

285. Simon, N.M., et al., *A detailed examination of cytokine abnormalities in Major Depressive Disorder.* European Neuropsychopharmacology, 2008. **18**(3): p. 230-233.

286. Teixeira, A.L., et al., *Increased serum levels of CCL11/eotaxin in schizophrenia.* Progress in Neuro-Psychopharmacology and Biological Psychiatry, 2008. **32**(3): p. 710-714.

287. Erickson, M.A., et al., *Genetics and sex influence peripheral and central innate immune responses and blood-brain barrier integrity.* PLOS ONE, 2018. **13**(10): p. e0205769.

288. Erickson, M.A., et al., *Rapid Transport of CCL11 across the Blood-Brain Barrier: Regional Variation and Importance of Blood Cells.* Journal of Pharmacology and Experimental Therapeutics, 2014. **349**(3): p. 497-507.

289. Galván, S.T., et al., *Plasma concentrations of granulocyte colony-stimulating factor (G-CSF) in patients with substance use disorders and comorbid major depressive disorder.* Scientific Reports, 2021. **11**(1): p. 13629.

290. Detorakis, E., et al., *Role of smoking in the evolution of cardiovascular magnetic resonance and laboratory findings of acute myocarditis.* Heart Views, 2020. **21**(1): p. 22.

291. Elisia, I., et al., *The effect of smoking on chronic inflammation, immune function and blood cell composition.* Scientific Reports, 2020. **10**(1): p. 19480.

292. Himmerich, H., et al., *TNF-alpha, soluble TNF receptor and interleukin-6 plasma levels in the general population.* European Cytokine Network, 2006. **17**(3): p. 196-201.

293. Voican, C., *Tumor necrosis factor-α serum levels in healthy smokers and nonsmokers.* International Journal of Chronic Obstructive Pulmonary Disease, 2010: p. 217.

294. Tanaka, T., M. Narazaki, and T. Kishimoto, *IL-6 in Inflammation, Immunity, and Disease.* Cold Spring Harbor Perspectives in Biology, 2014. **6**(10): p. a016295-a016295.

295. Ouyang, H., et al., *Increased interleukin-9 and CD4+IL-9+ T cells in patients with systemic lupus erythematosus.* Molecular Medicine Reports, 2013. **7**(3): p. 1031-1037.

296. Fontaine, R.H., et al., *IL-9/IL-9 receptor signaling selectively protects cortical neurons against developmental apoptosis.* Cell Death & Differentiation, 2008. **15**(10): p. 1542-1552.

297. Uhlen, M., et al., *Tissue-based map of the human proteome.* Science, 2015. **347**(6220): p. 1260419-1260419.

298. Filiano, A.J., et al., *Unexpected role of interferon-γ in regulating neuronal connectivity and social behaviour.* Nature, 2016. **535**(7612): p. 425-429.

299. Kunis, G., et al., *IFN-γ-dependent activation of the brain's choroid plexus for CNS immune surveillance and repair.* Brain, 2013. **136**(11): p. 3427-3440.

300. Steinman, L., *Inflammatory Cytokines at the Summits of Pathological Signal Cascades in Brain Diseases.* Science Signaling, 2013. **6**(258): p. pe3-pe3.

301. Johnson, S., et al., *The IFNG-PKR Pathway in the Prefrontal Cortex Reactions to Chronic Excessive Alcohol Use.* Alcoholism: Clinical and Experimental Research, 2015. **39**(3): p. 476-484.

302. Lee, A.M., et al., *Sex Differences in the Ventral Tegmental Area and Nucleus Accumbens Proteome at Baseline and Following Nicotine Exposure.* Frontiers in Molecular Neuroscience, 2021. **14**: p. 657064.

303. Brynildsen, J.K., et al., *A novel method to induce nicotine dependence by intermittent drug delivery using osmotic minipumps.* Pharmacology Biochemistry and Behavior, 2016. **142**: p. 79-84.

304. York, E.M., et al., *3DMorph Automatic Analysis of Microglial Morphology in Three Dimensions from Ex Vivo and In Vivo Imaging.* eneuro, 2018. **5**(6): p. ENEURO.0266-18.2018.

305. Thion, M.S., et al., *Microbiome Influences Prenatal and Adult Microglia in a Sex-Specific Manner.* Cell, 2018. **172**(3): p. 500-516.e16.

306. Haimon, Z., et al., *Re-evaluating microglia expression profiles using RiboTag and cell isolation strategies.* Nature Immunology, 2018. **19**(6): p. 636-644.

307. Marsh, S.E., et al., *Single Cell Sequencing Reveals Glial Specific Responses to Tissue Processing & Enzymatic Dissociation in Mice and Humans*. 2020, Neuroscience.

308. Ocañas, S.R., et al., *Minimizing the ex vivo confounds of cell-isolation techniques on transcriptomic -profiles of purified microglia*. 2021, Neuroscience.

309. Ali, S., et al., *CSF1R inhibitor PLX5622 and environmental enrichment additively improve metabolic outcomes in middle-aged female mice.* Aging, 2020. **12**(3): p. 2101-2122.

310. Elmore, M.R.P., et al., *Replacement of microglia in the aged brain reverses cognitive, synaptic, and neuronal deficits in mice: XXXX.* Aging Cell, 2018. **17**(6): p. e12832.

311. Whiteaker, P., et al., *Identification of a novel nicotinic binding site in mouse brain using [^{125} I]-epibatidine: A novel mouse brain nicotinic receptor subtype.* British Journal of Pharmacology, 2000. **131**(4): p. 729-739.

312. Zhou, R., et al., *PET Imaging of Neuroinflammation in Alzheimer's Disease.* Frontiers in Immunology, 2021. **12**: p. 739130.

313. van der Doef, T.F., et al., *In vivo (R)-[11C]PK11195 PET imaging of 18kDa translocator protein in recent onset psychosis.* npj Schizophrenia, 2016. **2**(1): p. 16031.

314. Shen, Z., X. Bao, and R. Wang, *Clinical PET Imaging of Microglial Activation: Implications for Microglial Therapeutics in Alzheimer's Disease.* Frontiers in Aging Neuroscience, 2018. **10**: p. 314.

315. Conen, S., et al., *Neuroinflammation as measured by positron emission tomography in patients with recent onset and established schizophrenia: implications for immune pathogenesis.* Molecular Psychiatry, 2020.

316. Banati, R.B., et al., *The peripheral benzodiazepine binding site in the brain in multiple sclerosis.* Brain, 2000. **123**(11): p. 2321-2337.

317. Setiawan, E., et al., *Association of translocator protein total distribution volume with duration of untreated major depressive disorder: a cross-sectional study.* The Lancet Psychiatry, 2018. **5**(4): p. 339-347.

318. Jeon, S.Y., et al., *[11C]-(R)-PK11195 positron emission tomography in patients with complex regional pain syndrome: A pilot study.* Medicine, 2017. **96**(1): p. e5735.

319. Attwells, S., et al., *Inflammation in the Neurocircuitry of Obsessive-Compulsive Disorder.* JAMA Psychiatry, 2017. **74**(8): p. 833.

320. Rice, R.A., et al., *Microglial repopulation resolves inflammation and promotes brain recovery after injury: RICE et al.* Glia, 2017. **65**(6): p. 931-944.

321. Spangenberg, E., et al., *Sustained microglial depletion with CSF1R inhibitor impairs parenchymal plaque development in an Alzheimer's disease model.* Nature Communications, 2019. **10**(1): p. 3758.

322. Zhang, L., J. Zhang, and Z. You, *Switching of the Microglial Activation Phenotype Is a Possible Treatment for Depression Disorder.* Frontiers in Cellular Neuroscience, 2018. **12**: p. 306.

323. Walter, T.J. and F.T. Crews, *Microglial depletion alters the brain neuroimmune response to acute binge ethanol withdrawal.* Journal of Neuroinflammation, 2017. **14**(1).

324. Krukowski, K., et al., *Temporary microglia-depletion after cosmic radiation modifies phagocytic activity and prevents cognitive deficits.* Scientific Reports, 2018. **8**(1): p. 7857.

325. Dion-Albert, L., et al., *Sex-specific blood-brain barrier alterations and vascular biomarkers underlie chronic stress responses in mice and human depression*. 2021, Neuroscience.

326. Pascual, O., et al., *Microglia activation triggers astrocyte-mediated modulation of excitatory neurotransmission.* Proceedings of the National Academy of Sciences, 2012. **109**(4): p. E197-E205.

327. Inoue, K., S. Koizumi, and M. Tsuda, *The role of nucleotides in the neuron-glia communication responsible for the brain functions: Role of nucleotides in the neuron-glia communication.* Journal of Neurochemistry, 2007. **102**(5): p. 1447-1458.

328. Matejuk, A. and R.M. Ransohoff, *Crosstalk Between Astrocytes and Microglia: An Overview.* Frontiers in Immunology, 2020. **11**: p. 1416.

329. Bianco, F., et al., *Pathophysiological roles of extracellular nucleotides in glial cells: differential expression of purinergic receptors in resting and activated microglia.* Brain Research Reviews, 2005. **48**(2): p. 144-156.

Appendix A: Supplementary Figures and Tables

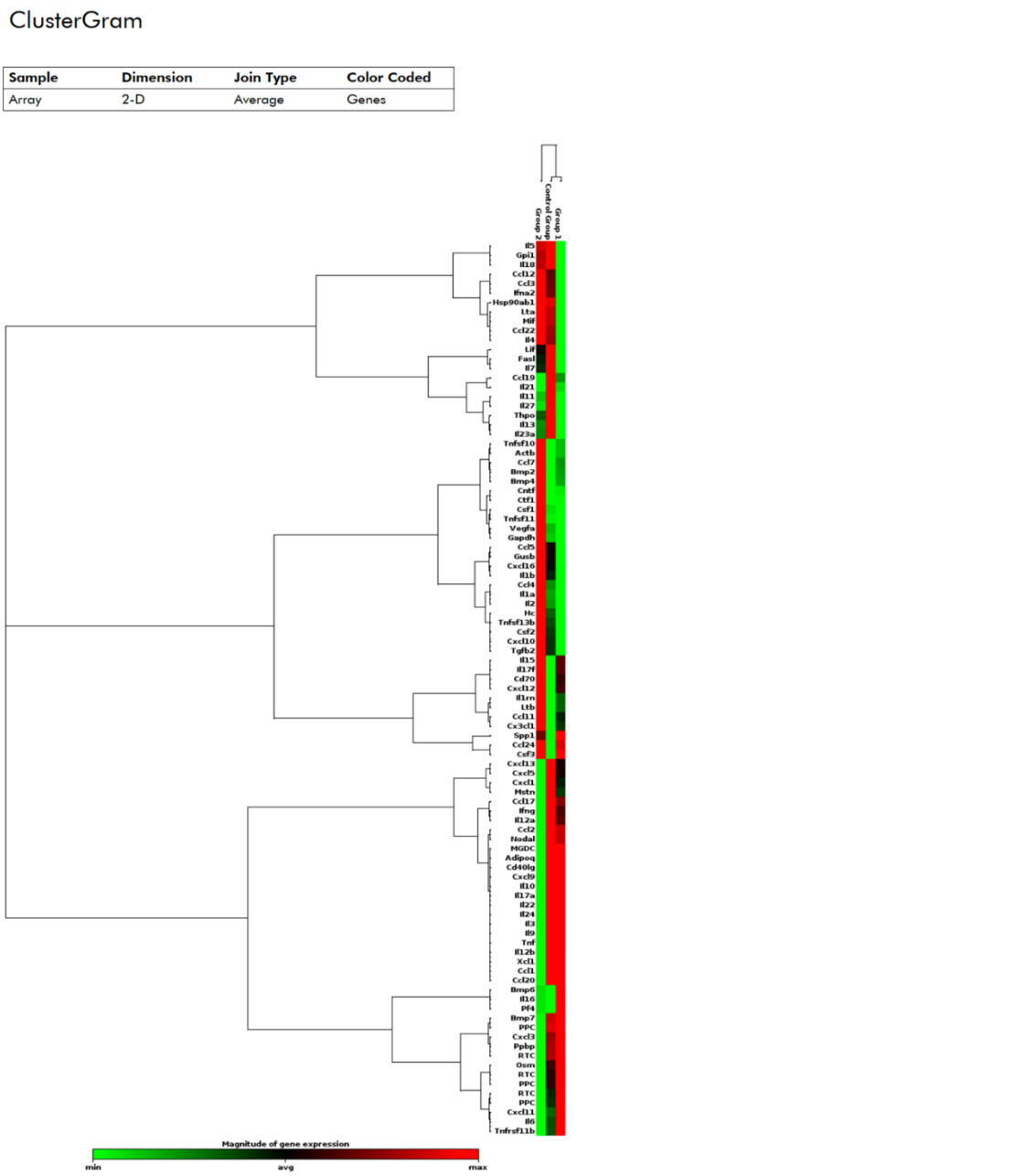

Figure A.1. Qiagen clustergram full analysis of pilot data from Chapter 3.

Table A.2. Primers designed by NCBI and Primer3Plus.

Primer Name	Primer Sequence	Target Template
TNFa_F	CCCACTCTGACCCCTTTACTC	NM_013693.3
TNFa_R	AAGCCCATTTGAGTCCTTGAT	
IL1b_F	CATGGAATCCGTGTCTTCCTA	NM_008361.4
IL1b_R	CAGAATGTGCCATGGTTTCTT	
TBP_F	GCACAGGACTTACTCCACAGC	NM_013684.3
TBP_R	GTGGGTTGCTGAGATGTTGAT	
BMP4_F	TCTCTGAGCCTTTCCAGCAAG	NM_007554.3
BMP4_R	AAAGCAGAGCTCTCACTGGTC	
CCL2_F	ACCTGCTGCTACTCATTCACC	NM_011333.3
CCL2_R	TGCTGGTGATCCTCTTGTAGC	
CCL3_F	CCTGACTAAGAGAAACCGGCA	NM_011337.2
CCL3_R	CAGGCATTCAGTTCCAGGTCA	
CCL4_F	AAACCTAACCCCGAGCAACA	NM_013652.2
CCL4_R	CCATTGGTGCTGAGAACCCT	
CXCR4_F	GCCATGGCTGACTGGTACTT	NM_009911.3
CXCR4_R	AGGGCCTCTGTGATGGAGAT	
IL1a_F	GAAGCTCGTCAGGCAGAAGT	NM_010554.4
IL1a_R	GTGCAAGTGACTCAGGGTGA	
IL10_F	TCTATTCTAAGGCTGGCCACA	NM_010548.2
IL10_R	GCAGGAATGATCATCAAAGGA	
TREM2_F	CTCAATCCAGGAGCACAGTTC	NM_001272078.1
TREM2_R	GTGATCAGCAGCAGGAGAAAC	
TLR4_F	AACAAAACTCTGGGGCCTAAA	NM_021297.3
TLR4_R	AGGCCTTAGCCTCTTCTCCTT	
CXCL10_F	TCCCCATCAGCACCATGAAC	NM_021274.2
CXCL10_R	CCACTTGAGCGAGGACTCAG	
CXCL12_F	TCTCTGAGTAGTGGCTCCCC	NM_013655.4
CXCL12_R	GCAGGGCTCTTTCCATGACT	
IBA1_L	GTTCCCAAGACCCACCTAGAG	NM_001361501.1
IBA1_R	GTGTGACATCCACCTCCAATC	
CD68_F	CTTGGGGCATATCTGTTTTGA	NM_001291058
CD68_R	ATTGTATTCCACCGCCATGTA	
OCLN_F	TACTCCTCCAATGGCAAAGTG	NM_008756.2
OCLN_R	CCCACCTGTCGTGTAGTCTGT	
TGFB1_F	CGCCATCTATGAGAAAACCAA	NM_011577.2
TGFB1_R	GTCAAAAGACAGCCACTCAGG	
TMEM119_F	GGATGCCTCACAGCTACAAAG	NM_146162
TMEM119_R	AGGGTTGCTTGACACTTGAGA	
NOX2_F	CCA ACT GGG ATA ACG AGT TCA	NM_007807.5
NOX2_R	GGA CAT TTG GCA GCA TAC ACT	

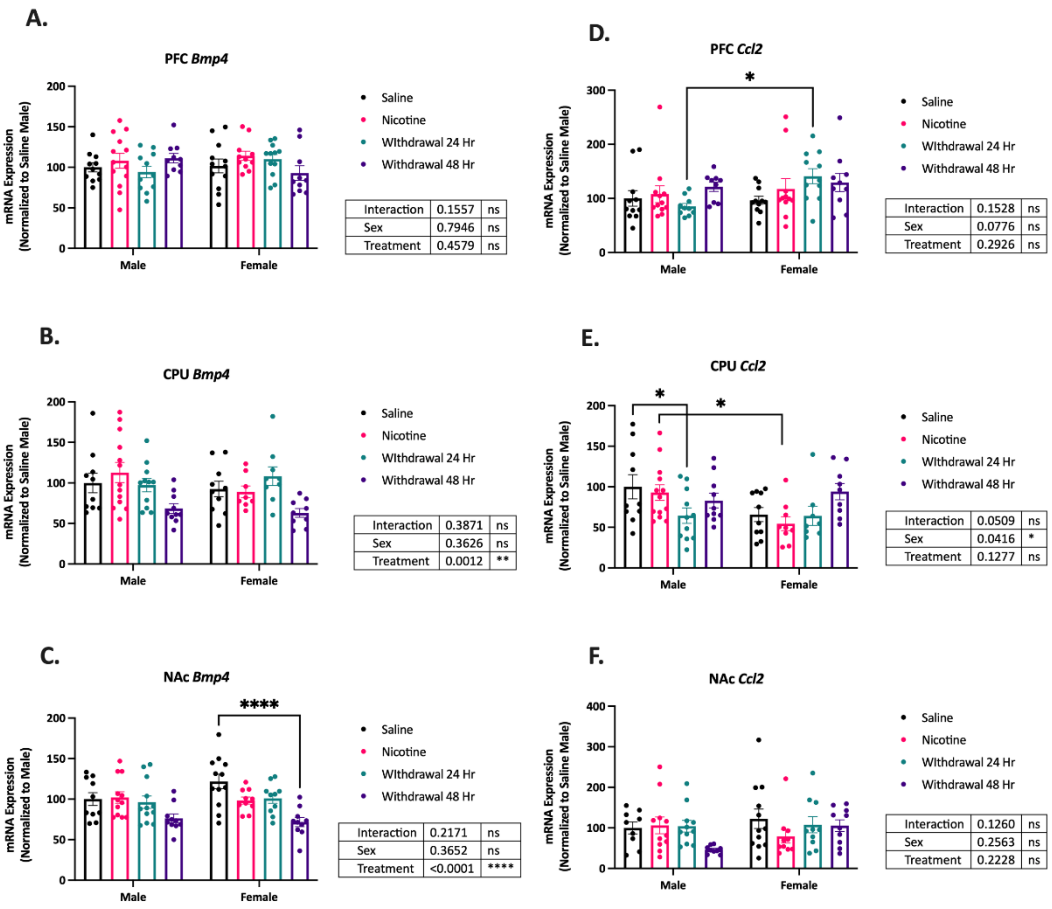

Figure A.3. Cytokine mRNA expression levels in the PFC (A & D), CPU (B & E), and NAc (C & E) among sex and treatment. A. *Bmp4* mRNA expression PFC, (B) CPU main effect of treatment and (C) in the NAc with a main effect of treatment and significant post hoc in females (saline to 48Hr WD), n=10-13. D. *Ccl2* mRNA expression PFC with no main effect but sex differences in the 24Hr WD group, and (E) CPU with main effect of sex and individually in males on (saline to 24Hr WD group) and between sexes in the nicotine group and (F) NAc no significant findings, n=8-13. Post hoc analysis between sexes by Šídák's ($^{\#}$P<0.05, $^{\#\#}$P<0.01, $^{\#\#\#}$P<0.001, $^{\#\#\#\#}$P<0.0001) and within sex Dunnett's multiple comparisons test (*P<0.05, **P<0.01, ***P<0.001, ****P<0.0001) after two-way ANOVA.

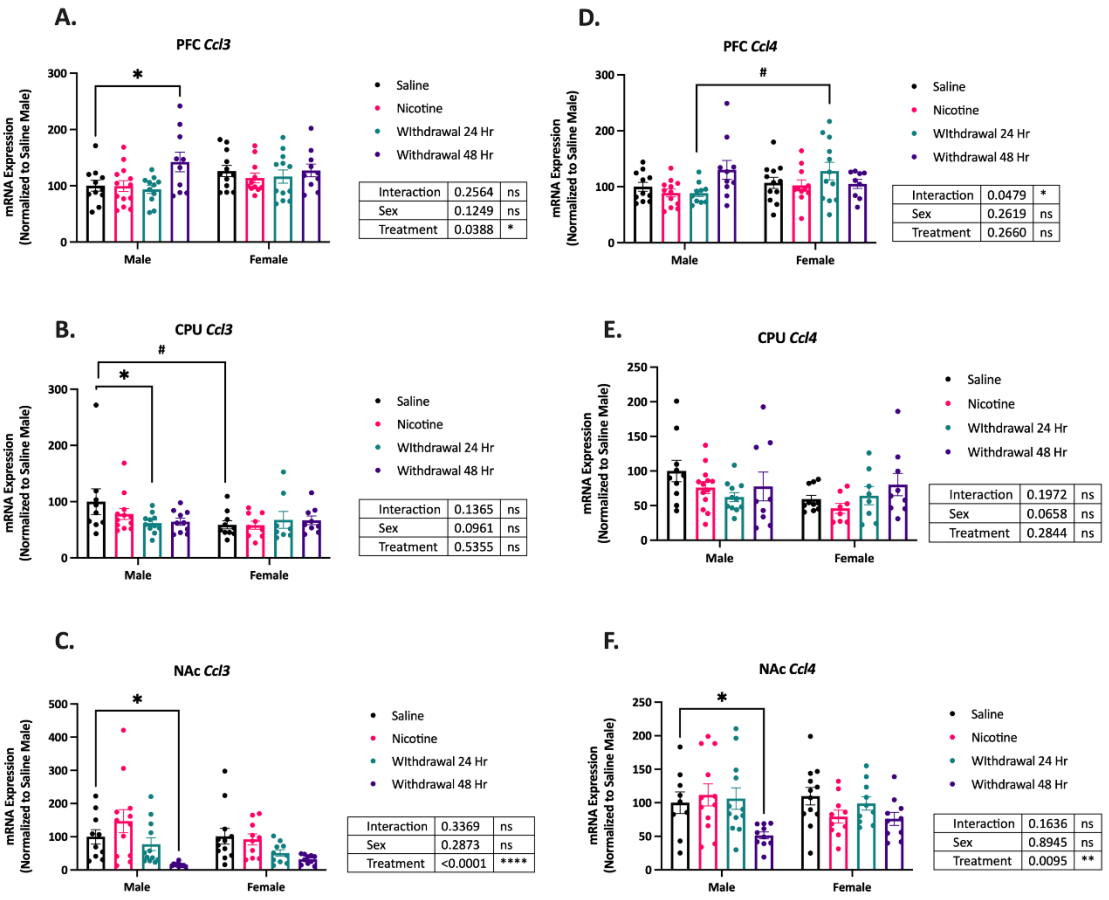

Figure A.4. Cytokine mRNA expression levels in the PFC (A & D), CPU (B & E), and NAc (C & E) among sex and treatment. A. *Ccl3* mRNA expression PFC with main effect of treatment, (B) CPU with no main effect but significant individual treatments, (C) NAc with main effect of treatment and significant individual treatment (male saline to48Hr WD), n=10-13. D. *Ccl4* mRNA expression PFC with main effect of interaction and an individual effect at 24Hr WD male to female (E) CPU with no significant findings, and (F) NAc with a main treatment effect and significance in males (saline to 48Hr WD), at an n=8-13. Post hoc analysis between sexes by Šídák's ($^{\#}$P<0.05, $^{\#\#}$P<0.01, $^{\#\#\#}$ P<0.001, $^{\#\#\#\#}$P<0.0001) and within sex Dunnett's multiple comparisons test (*P<0.05, **P<0.01, ***P<0.001, ****P<0.0001) after two-way ANOVA.

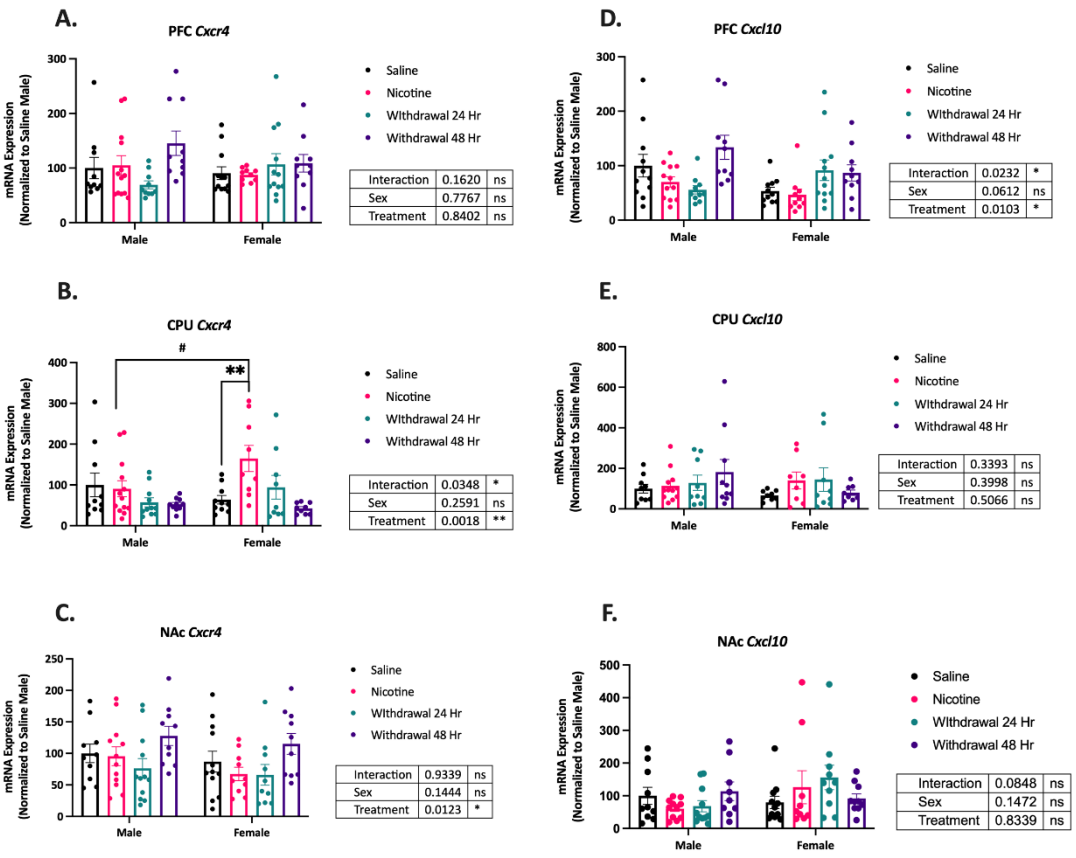

Figure A.5. Cytokine mRNA expression levels in the PFC (A & D), CPU (B & E), and NAc (C & E) among sex and treatment. (A) *Cxcr4* mRNA expression PFC with no significance, (B) CPU main effect of interaction and treatment with significant increase in female nicotine and dividual treatments significant(C) NAc also with a main effect of treatment only, n=10-13. (D) *Cxcl10* mRNA expression PFC with a main effect of interaction and treatment only (E) CPU no significant findings, and (F) NAc no significant findings, n=8-13. Post hoc analysis between sexes by Šídák's ($^{\#}P<0.05$, $^{\#\#}P<0.01$, $^{\#\#\#}P<0.001$, $^{\#\#\#\#}P<0.0001$) and within sex Dunnett's multiple comparisons test (*P<0.05, **P<0.01, ***P<0.001, ****P<0.0001) after two-way ANOVA.

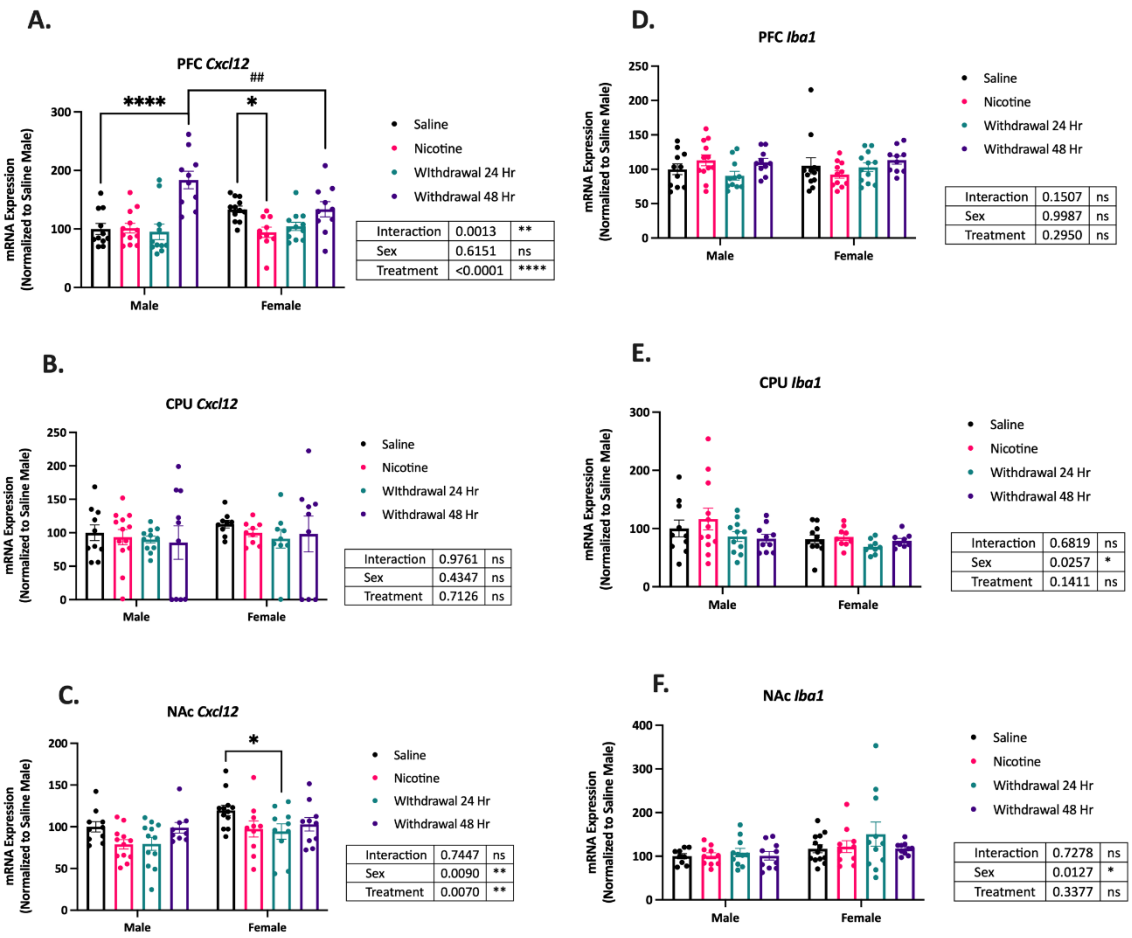

Figure A.6. Cytokine mRNA expression levels in the PFC (A & D), CPU (B & E), and NAc (C & E) among sex and treatment with (A-C) *Cxcl12* and (D-E) *Iba1* expression. Post hoc analysis between sexes by Šídák's ($^{\#}$P<0.05, $^{\#\#}$P<0.01, $^{\#\#\#}$ P<0.001, $^{\#\#\#\#}$P<0.0001) and within sex Dunnett's multiple comparisons test (*P<0.05, **P<0.01, ***P<0.001, ****P<0.0001) after two-way ANOVA.

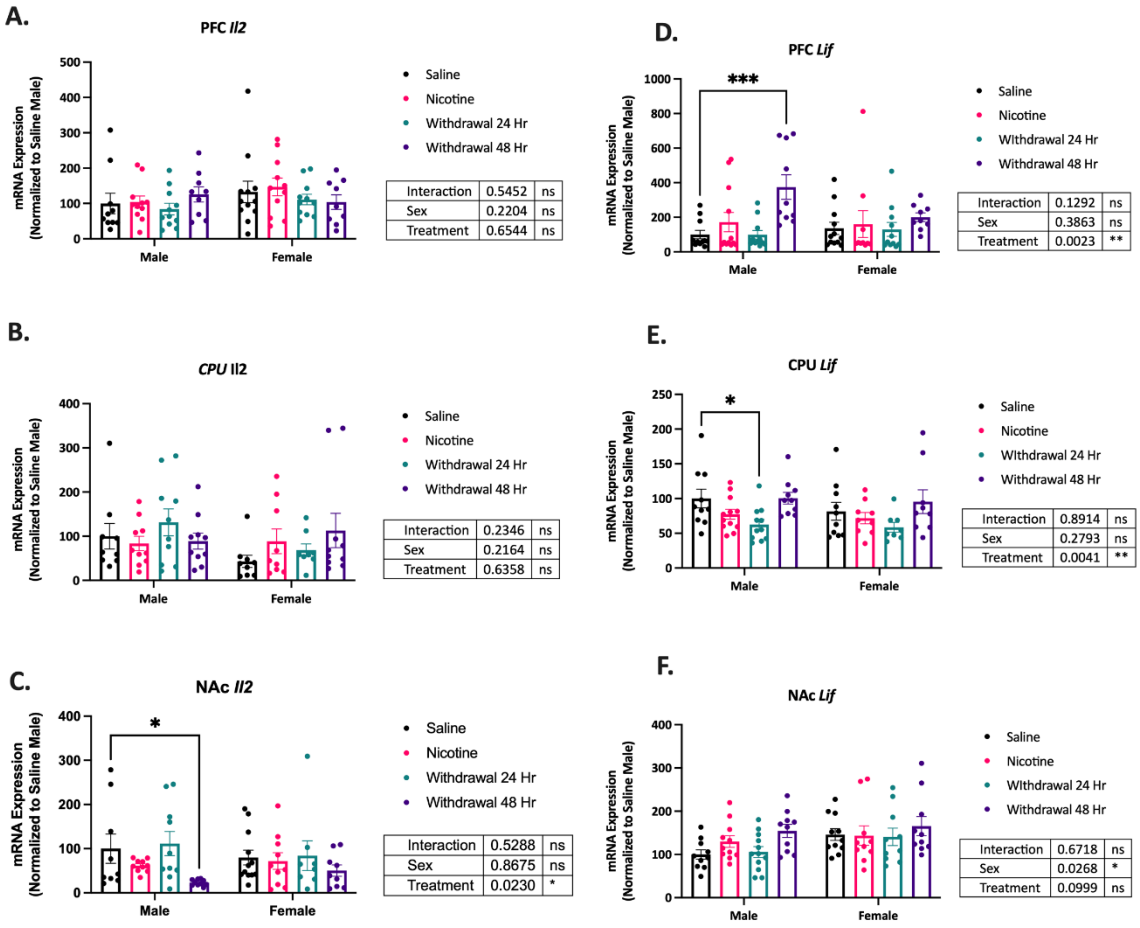

Figure A.7. Cytokine mRNA expression levels in the PFC (A & D), CPU (B & E), and NAc (C & E) among sex and treatment with (A-C) *Il2* and (D-E) *Lif* expression. Post hoc analysis between sexes by Šídák's ($^{\#}$P<0.05, $^{\#\#}$P<0.01, $^{\#\#\#}$ P<0.001, $^{\#\#\#\#}$P<0.0001) and within sex Dunnett's multiple comparisons test (*P<0.05, **P<0.01, ***P<0.001, ****P<0.0001) after two-way ANOVA.

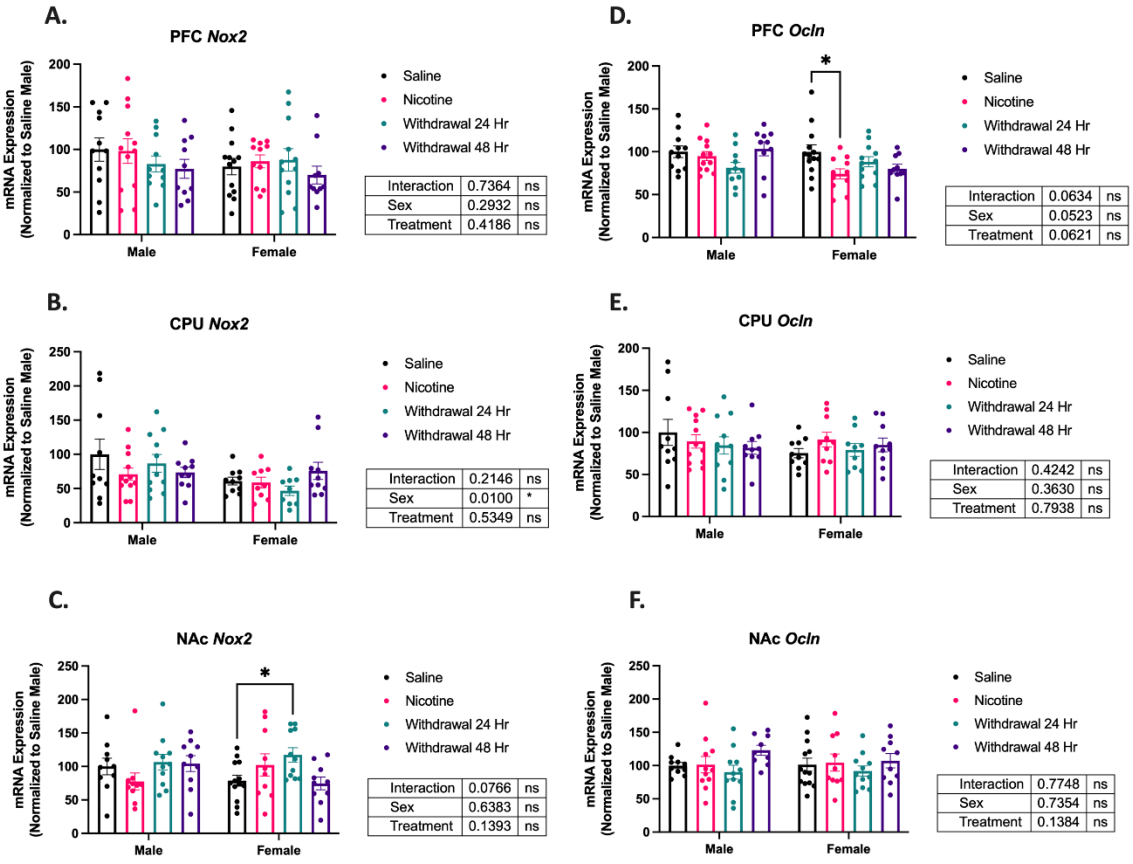

Figure A.8. Cytokine mRNA expression levels in the PFC (A & D), CPU (B & E), and NAc (C & E) among sex and treatment with (A-C) *Nox2* and (D-E) *Ocln* expression. Post hoc analysis between sexes by Šídák's ($^{\#}$P<0.05, $^{\#\#}$P<0.01, $^{\#\#\#}$ P<0.001, $^{\#\#\#\#}$P<0.0001) and within sex Dunnett's multiple comparisons test (*P<0.05, **P<0.01, ***P<0.001, ****P<0.0001) after two-way ANOVA.

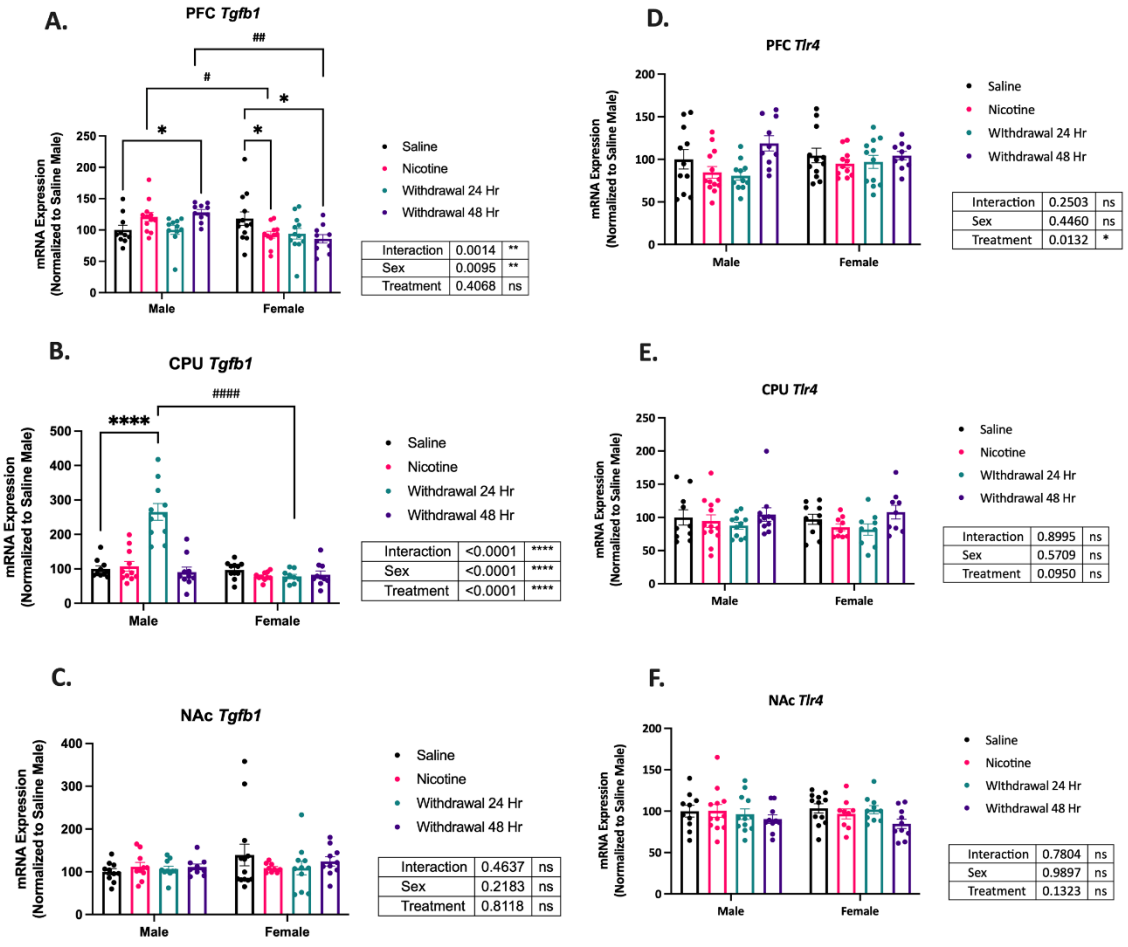

Figure A.9. Cytokine mRNA expression levels in the PFC (A & D), CPU (B & E), and NAc (C & E) among sex and treatment with (A-C) *Tgfb1* and (D-E) *Tlr4* expression. Post hoc analysis between sexes by Šídák's ($^{\#}$P<0.05, $^{\#\#}$P<0.01, $^{\#\#\#}$ P<0.001, $^{\#\#\#\#}$P<0.0001) and within sex Dunnett's multiple comparisons test (*P<0.05, **P<0.01, ***P<0.001, ****P<0.0001) after two-way ANOVA.

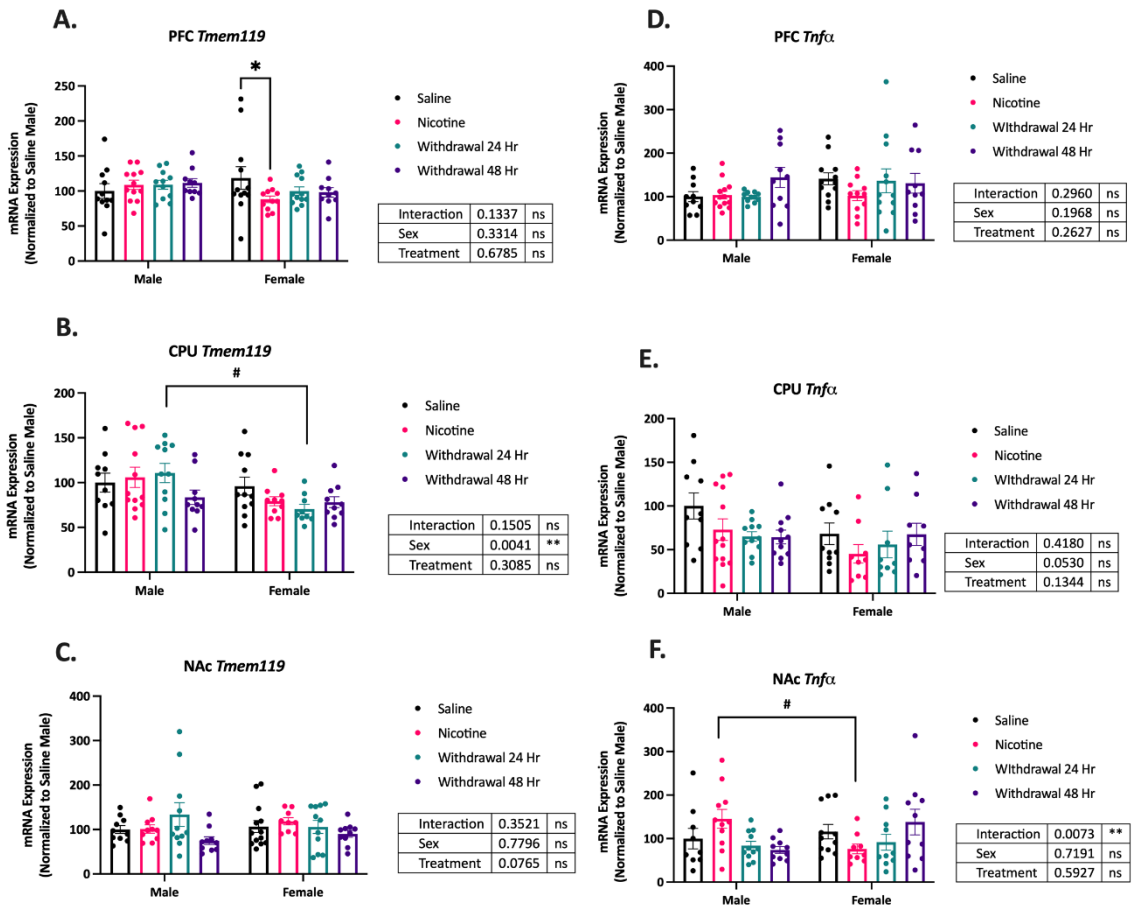

Figure A.10. Cytokine mRNA expression levels in the PFC (A & D), CPU (B & E), and NAc (C & E) among sex and treatment with (A-C) *Tmem119* and (D-E) *Tnfα* expression. Post hoc analysis between sexes by Šídák's ($^{\#}$P<0.05, $^{\#\#}$P<0.01, $^{\#\#\#}$ P<0.001, $^{\#\#\#\#}$P<0.0001) and within sex Dunnett's multiple comparisons test (*P<0.05, **P<0.01, ***P<0.001, ****P<0.0001) after two-way ANOVA.

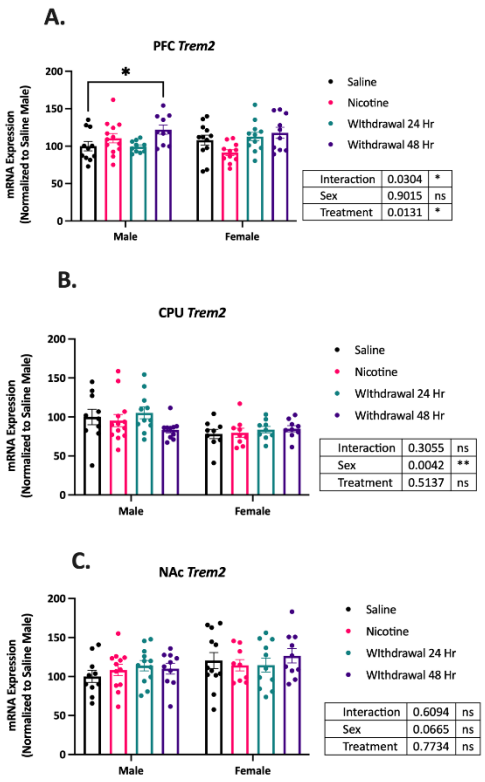

Figure A.11. Cytokine mRNA expression levels in the PFC (A & D), CPU (B & E), and NAc (C & E) of chronic nicotine and 24Hr and 48Hr WD animals. Post hc analysis between sexes by Šídák's (#P<0.05, ##P<0.01, ####P<0.0001) and within sex Dunnett's multiple comparisons test (*P<0.05, **P<0.01, ***P<0.001, ****P<0.0001) after two-way ANOVA.

Table A.12. Sex differences in protein expression of the saline treatment group for analysis of sex differences. Analysis by unpaired two-tailed t-test. $P < 0.05$, $^{**}P < 0.01$, $^{***}P < 0.001$, $^{****}P < 0.0001$, n = 16-17. Chemokines in Bold.

Peripheral	**Saline**					
Gene	**Male pg/ml**	**Female pg/ml**	**Significant**	**P value**	**t, df**	**Mice/group**
CXCL1	17.47	33.50	*	0.0371	t=2.178, df=31	16-17
GCSF	121.70	474.70	**	0.0043	t=3.069, df=32	17
IL5	3.73	11.19	***	0.0009	t=3.682, df=31	16-17
IL12B	2.40	5.78	****	<0.0001	t=4.621, df=31	16-17
IP10	38.82	55.62	**	0.0032	t=3.195, df=31	16-17
MCP1	6.11	100.64	*	0.0193	t=2.469, df=31	16-17
MIG	49.46	75.22	*	0.0333	t=2.231, df=30	16
MIP1A	19.51	27.47	*	0.0158	t=2.560, df=30	16
MIP2	40.27	74.33	***	0.00002	t=2.231, df=30	17
TNFA	3.36	5.31	*	0.0334	t=2.226, df=31	16-17

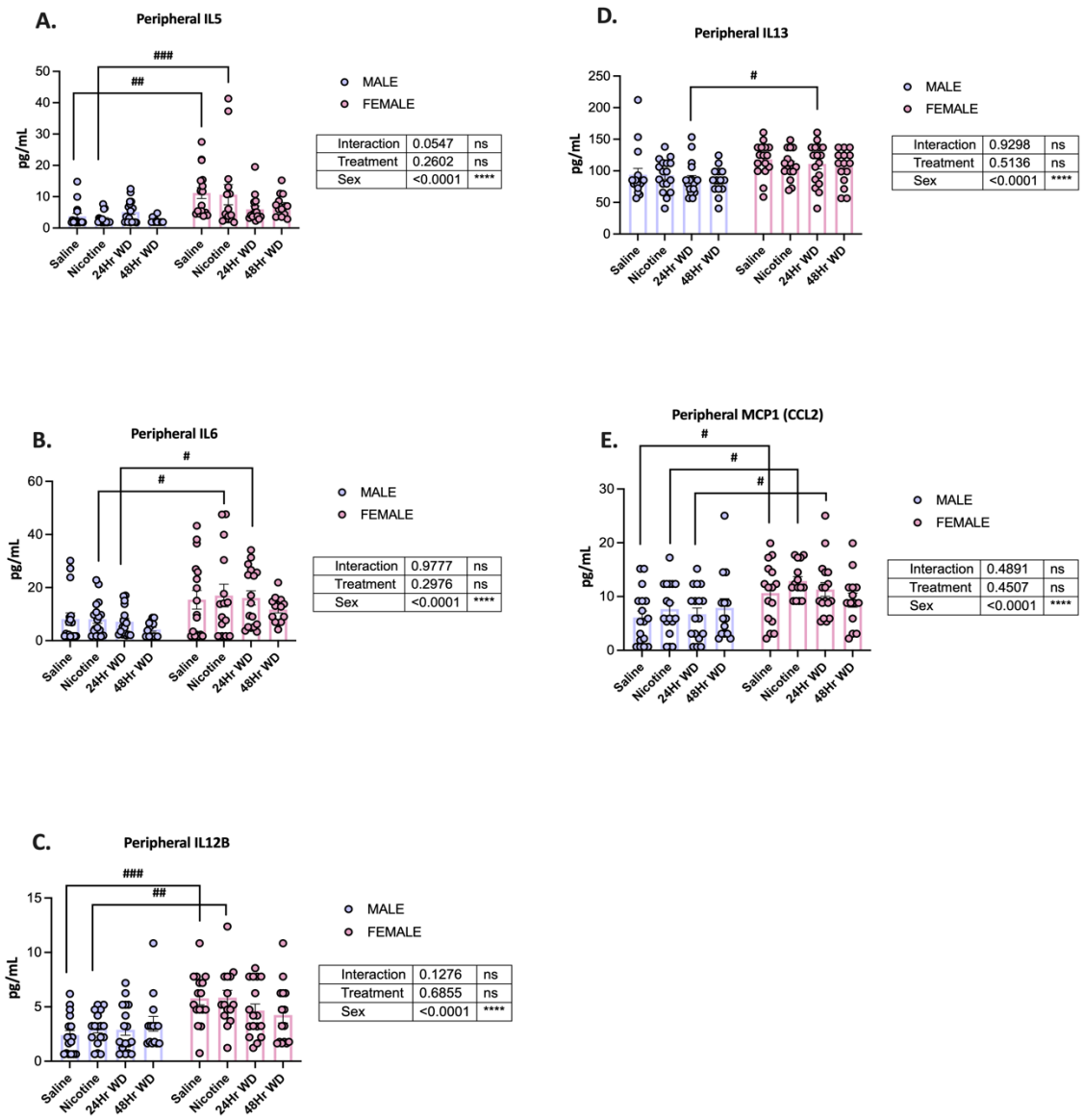

Figure A.13. Peripheral protein cytokine levels with main effects of treatment and sex by two-way ANOVA (A-E). With previously noted sex differences in the saline groups (A, C, E). Post hoc analysis between sexes by Šídák's ($^{\#}P<0.05$, $^{\#\#}P<0.01$, $^{\#\#\#}P<0.001$, $^{\#\#\#\#}P<0.0001$) and within sex Dunnett's multiple comparisons test (*P<0.05, **P<0.01, ***P<0.001, ****P<0.0001) after two-way ANOVA.

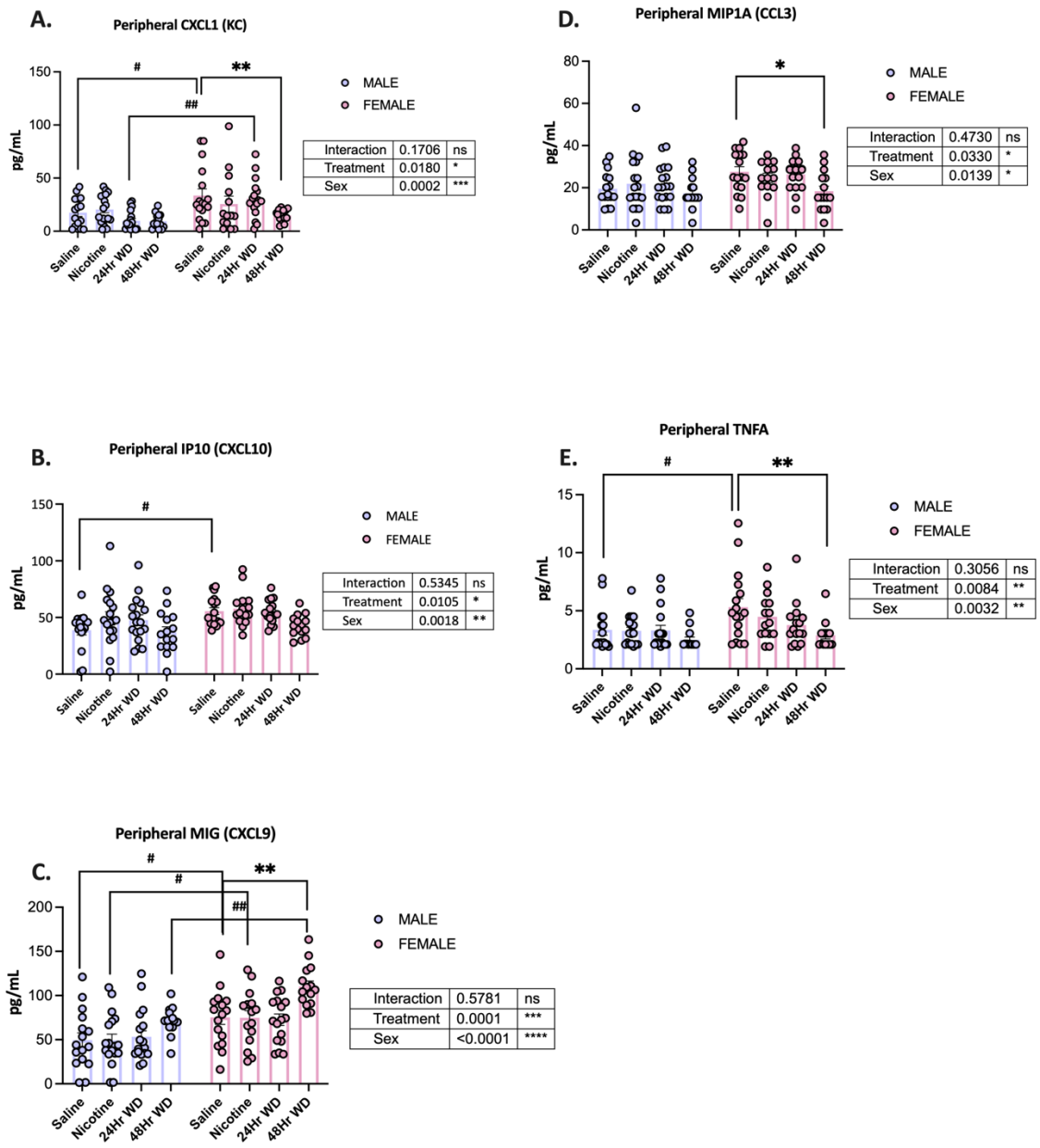

Figure A.14. Peripheral protein cytokine levels with main effects of treatment and sex by two-way ANOVA (A-E). With previously noted sex differences in the saline groups (A, B, C, E). Post hoc analysis between sexes by Šídák's ($^{\#}$P<0.05, $^{\#\#}$P<0.01, $^{\#\#\#}$ P<0.001, $^{\#\#\#\#}$P<0.0001) and within sex Dunnett's multiple comparisons test (*P<0.05, **P<0.01, ***P<0.001, ****P<0.0001) after two-way ANOVA.

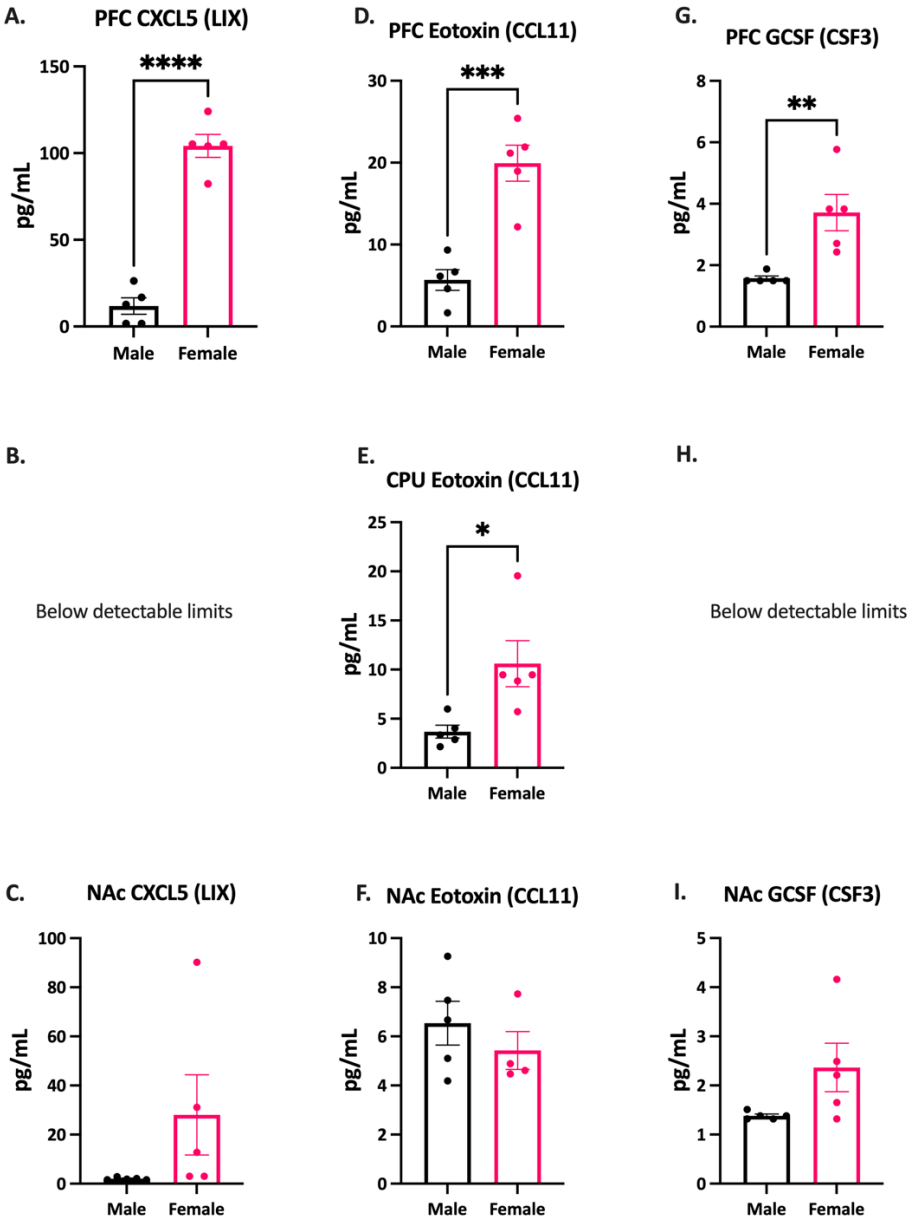

Figure A.15. Peripheral cytokine levels protein expression of males compared to females in the saline control group (baseline control) two-tailed t-test, n=16-17. (A, D & G) PFC, (B, E & H) CPU, and (C, F, & I) NAc portions with cytokine levels. Increased expression in females over males, *P<0.05, **P<0.01, ***P<0.001, ****P<0.0001.

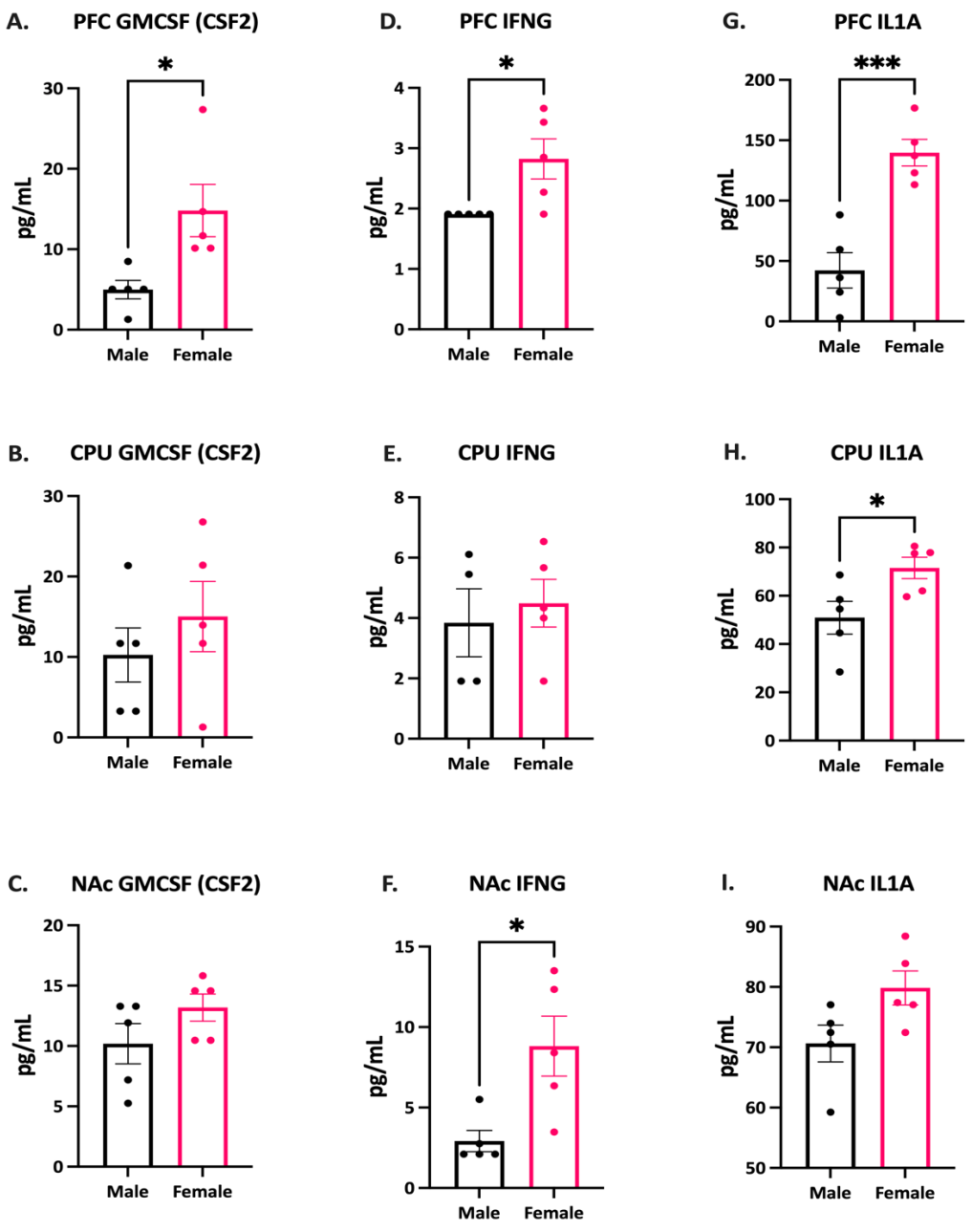

Figure A.16. Peripheral cytokine levels protein expression of males compared to females in the saline control group (baseline control) two-tailed t-test, n=16-17. (A, D & G) PFC, (B, E & H) CPU, and (C, F, & I) NAc portions with cytokine levels. Increased expression in females over males, *P<0.05, **P<0.01, ***P<0.001, ****P<0.0001.

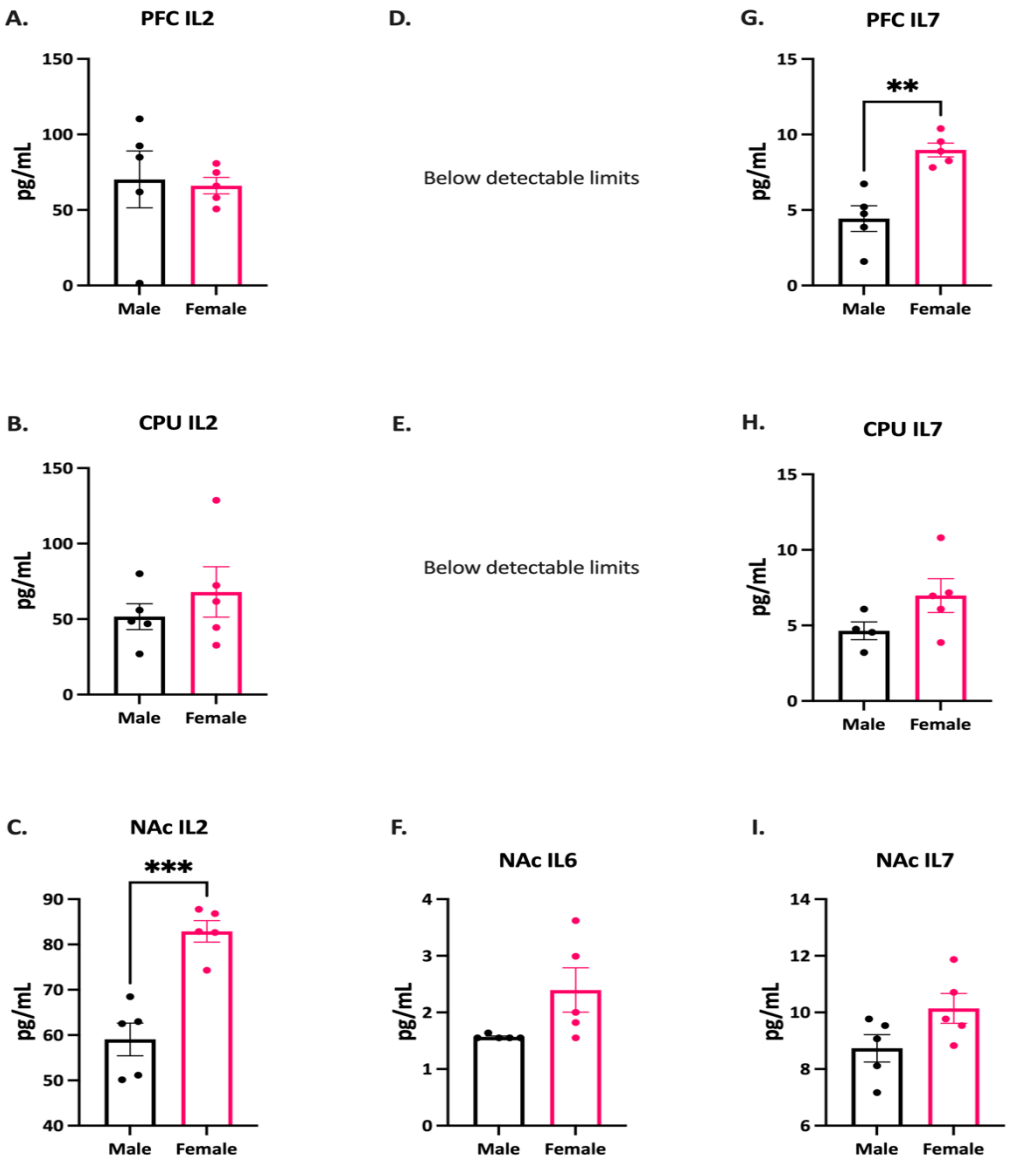

Figure A.17. Peripheral cytokine levels protein expression of males compared to females in the saline control group (baseline control) two-tailed t-test, n=16-17. (A, D & G) PFC, (B, E & H) CPU, and (C, F, & I) NAc portions with cytokine levels. Increased expression in females over , *P<0.05, **P<0.01, ***P<0.001, ****P<0.0001.

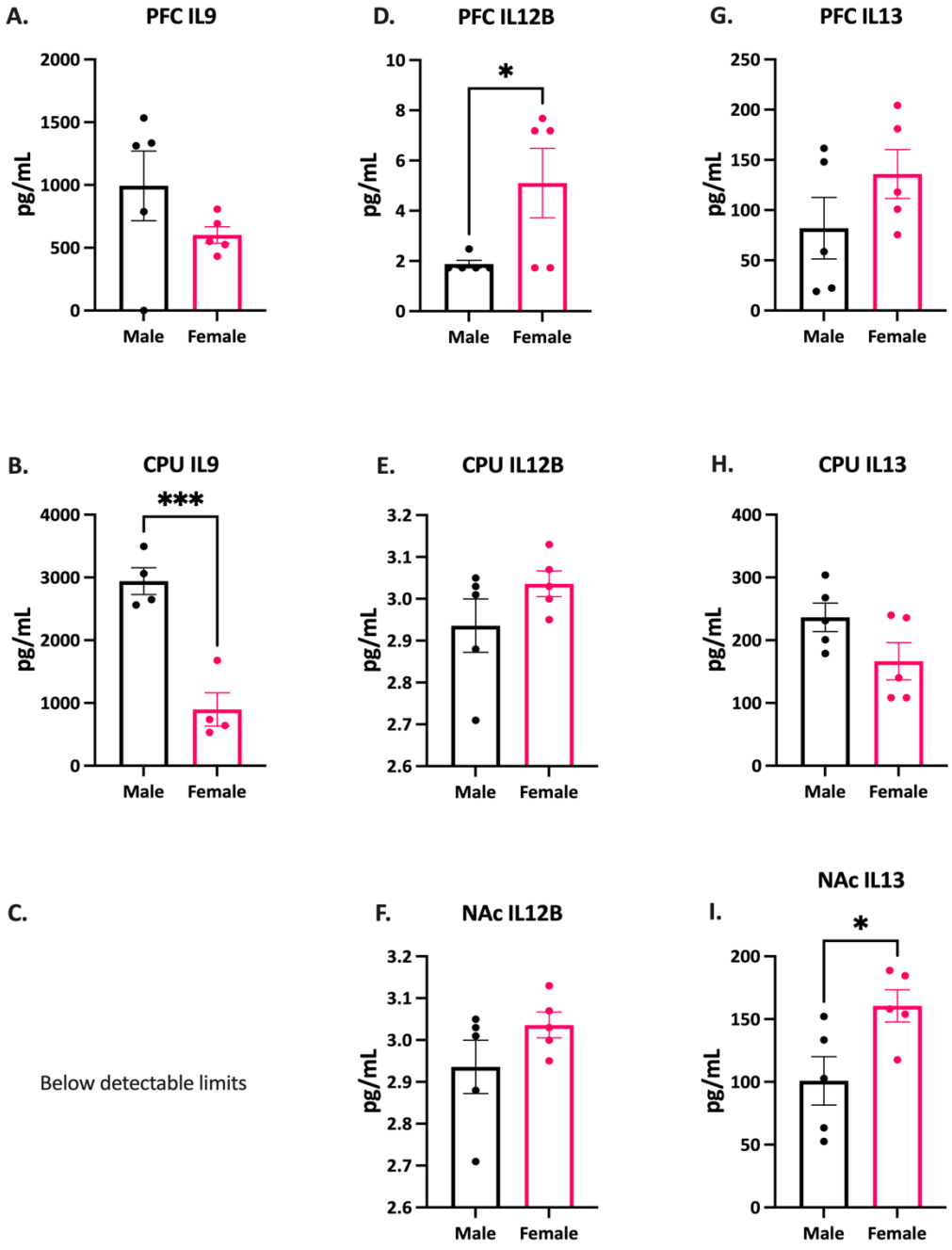

Figure A.18. Peripheral cytokine levels protein expression of males compared to females in the saline control group (baseline control) two-tailed t-test, n=16-17. (A, D & G) PFC, (B, E & H) CPU, and (C, F, & I) NAc portions with cytokine levels. Increased expression in females over , *P<0.05, **P<0.01, ***P<0.001, ****P<0.0001.

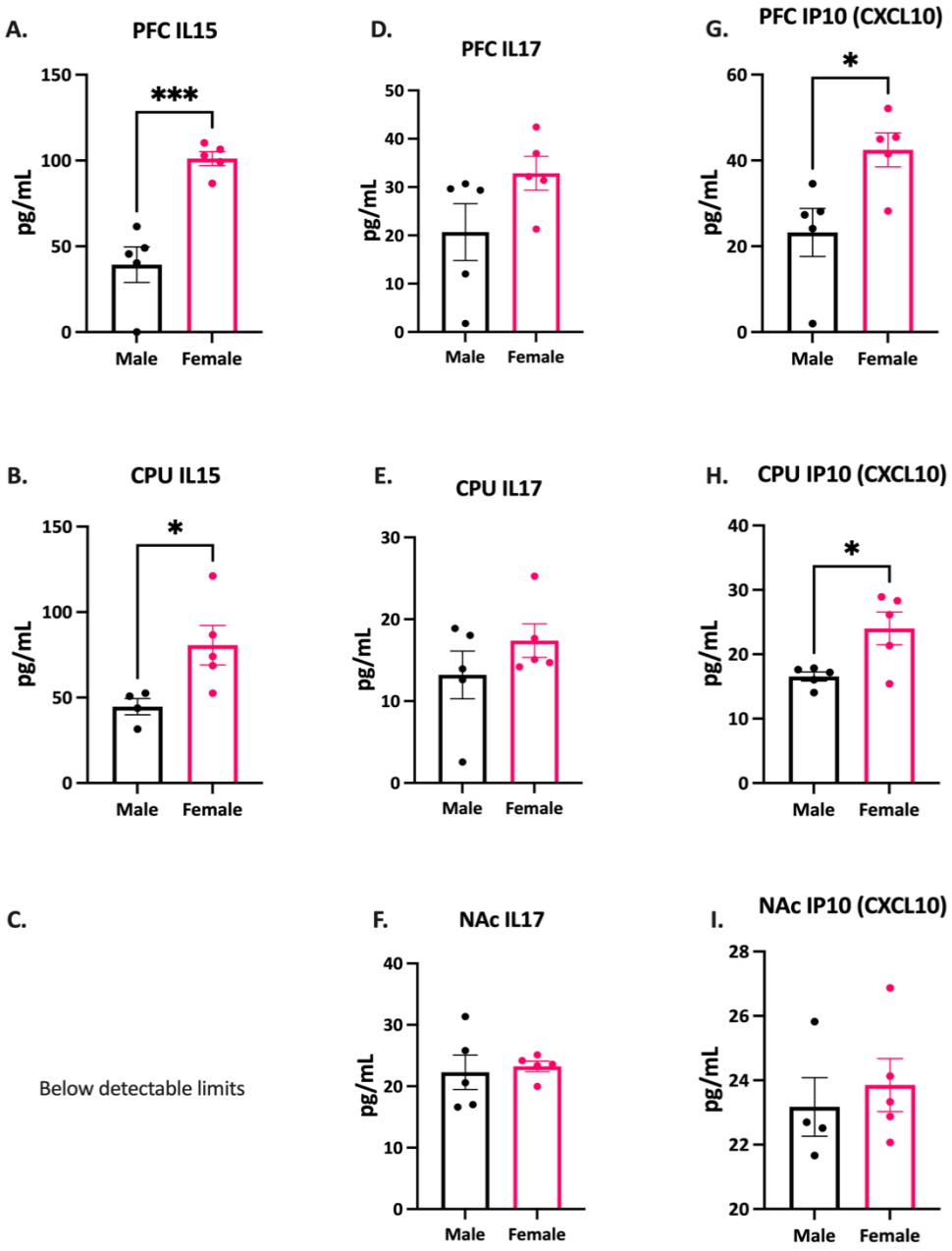

Figure A.19. Peripheral cytokine levels protein expression of males compared to females in the saline control group (baseline control) two-tailed t-test, n=16-17. (A, D & G) PFC, (B, E & H) CPU, and (C, F, & I) NAc portions with cytokine levels. Increased expression in females over males, *P<0.05, **P<0.01, ***P<0.001, ****P<0.0001.

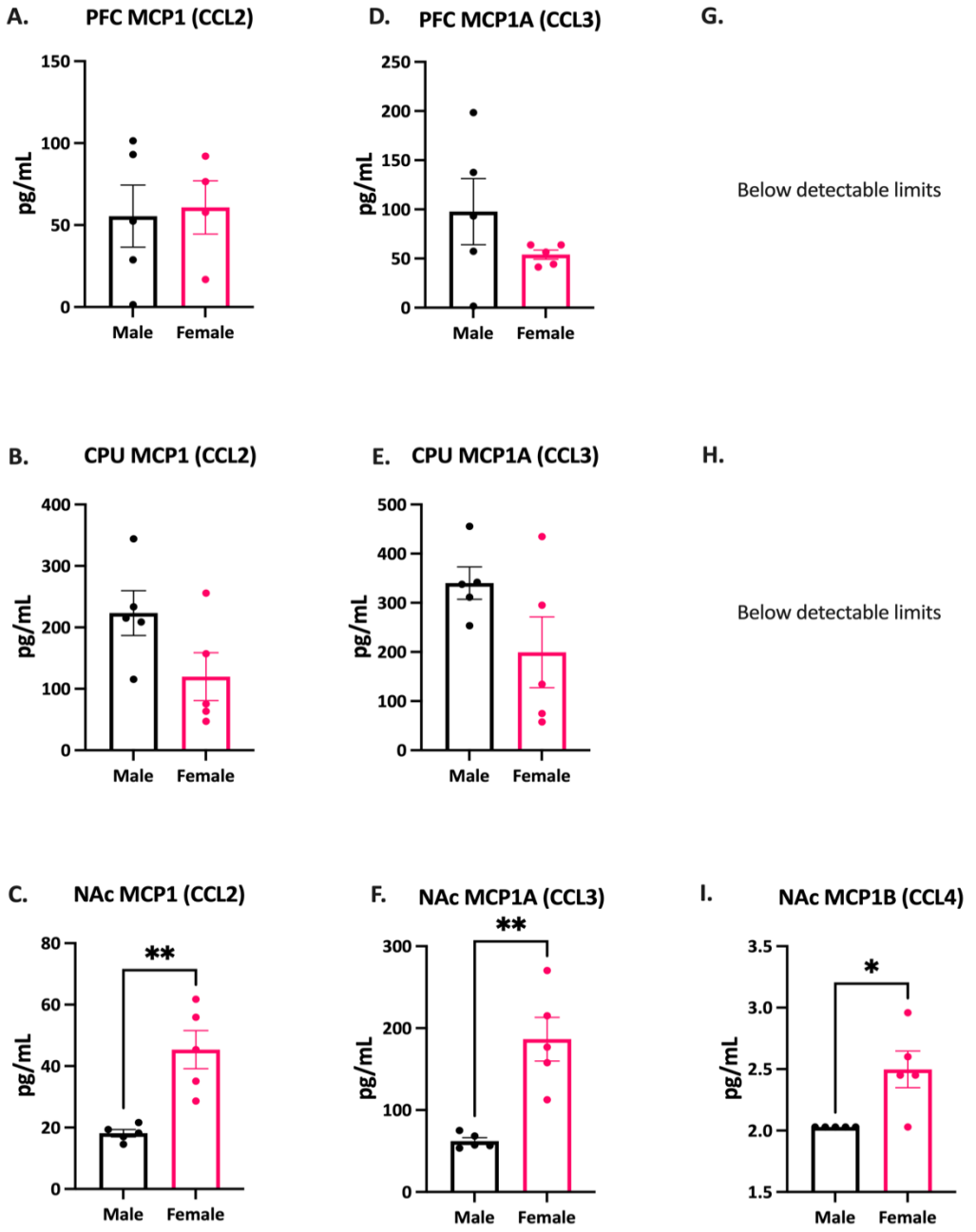

Figure A.20. Peripheral cytokine levels protein expression of males compared to females in the saline control group (baseline control) two-tailed t-test, n=16-17. (A, D & G) PFC, (B, E & H) CPU, and (C, F, & I) NAc portions with cytokine levels. Increased expression in females over males, *P<0.05, **P<0.01, ***P<0.001, ****P<0.0001.

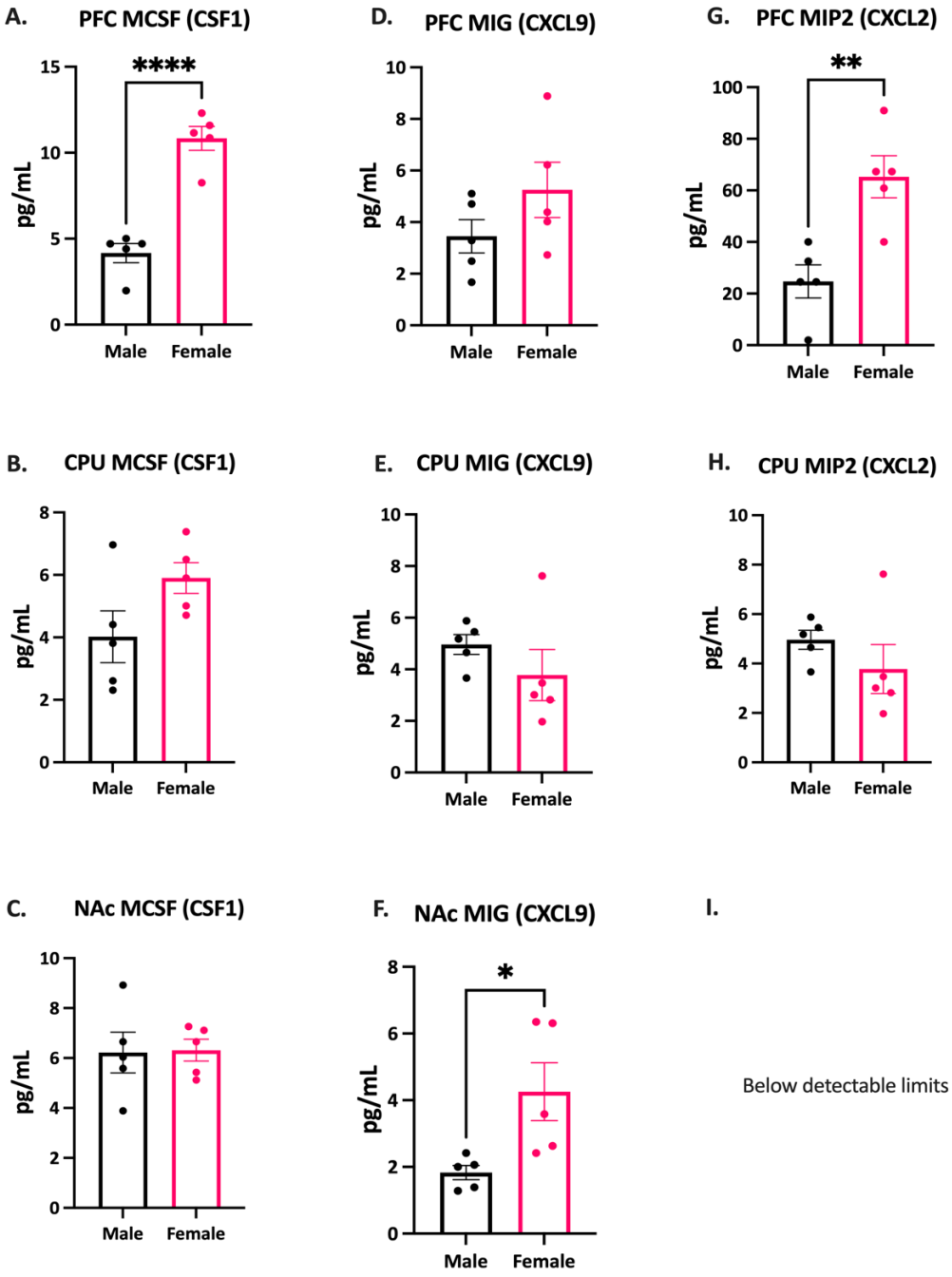

Figure A.21. Peripheral cytokine levels protein expression of males compared to females in the saline control group (baseline control) two-tailed t-test, n=16-17. (A, D & G) PFC, (B, E & H) CPU, and (C, F, & I) NAc portions with cytokine levels. Increased expression in females over males, *P<0.05, **P<0.01, ***P<0.001, ****P<0.0001.

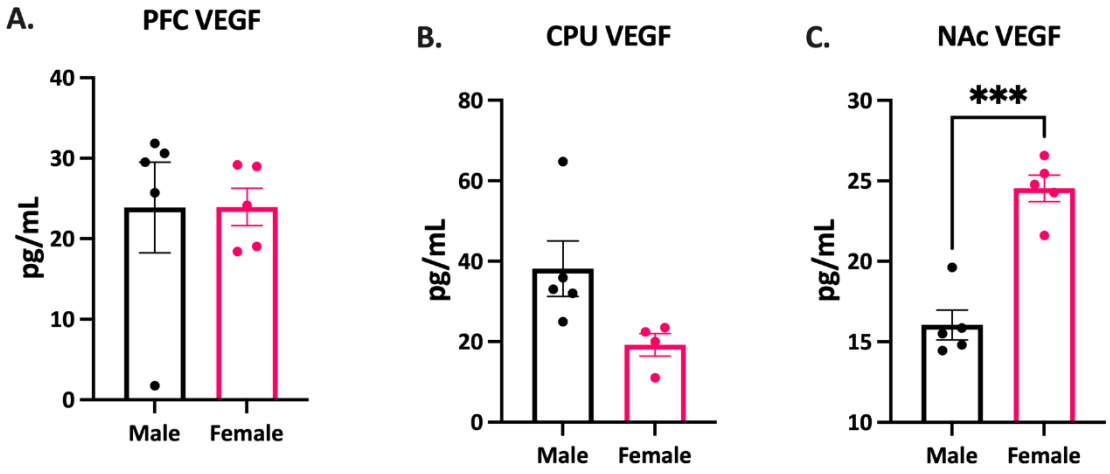

Figure A.22. Peripheral cytokine levels protein expression of males compared to females in the saline control group (baseline control) two-tailed t-test, n=16-17. (A, D & G) PFC, (B, E & H) CPU, and (C, F, & I) NAc portions with cytokine levels. Increased expression in females over males, *P<0.05, **P<0.01, ***P<0.001, ****P<0.0001.

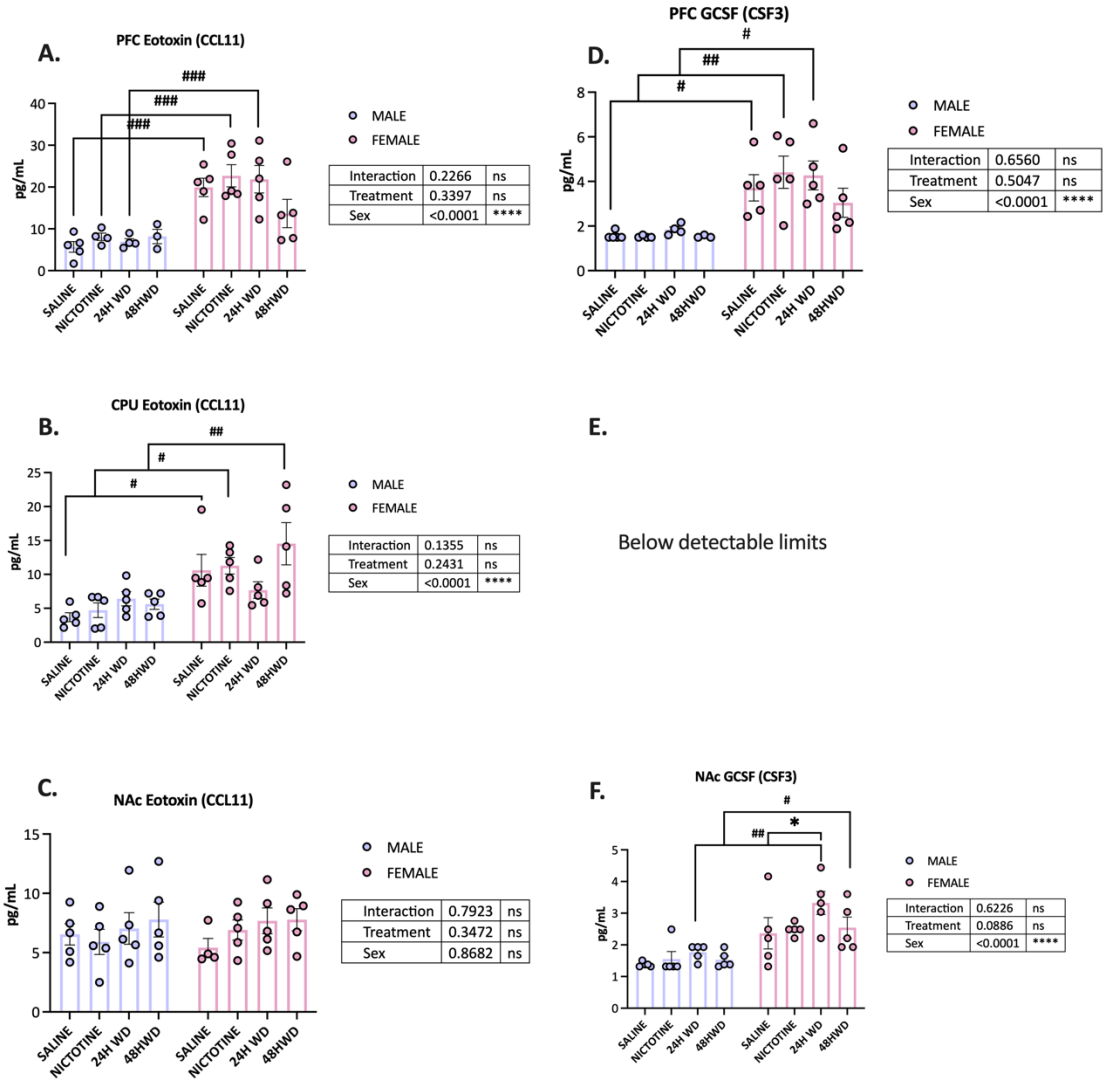

Figure A.23. Mouse brain region extracted protein assayed via Luminex®. (A & D) PFC, (B & E) CPU, and (C & F) NAc portions with cytokine levels. Post hoc analysis between sexes by Šídák's ($^{\#}P<0.05$, $^{\#\#}P<0.01$, $^{\#\#\#}P<0.001$, $^{\#\#\#\#}P<0.0001$) and within sex Dunnett's multiple comparisons test (*P<0.05, **P<0.01, ***P<0.001, ****P<0.0001) after two-way ANOVA.

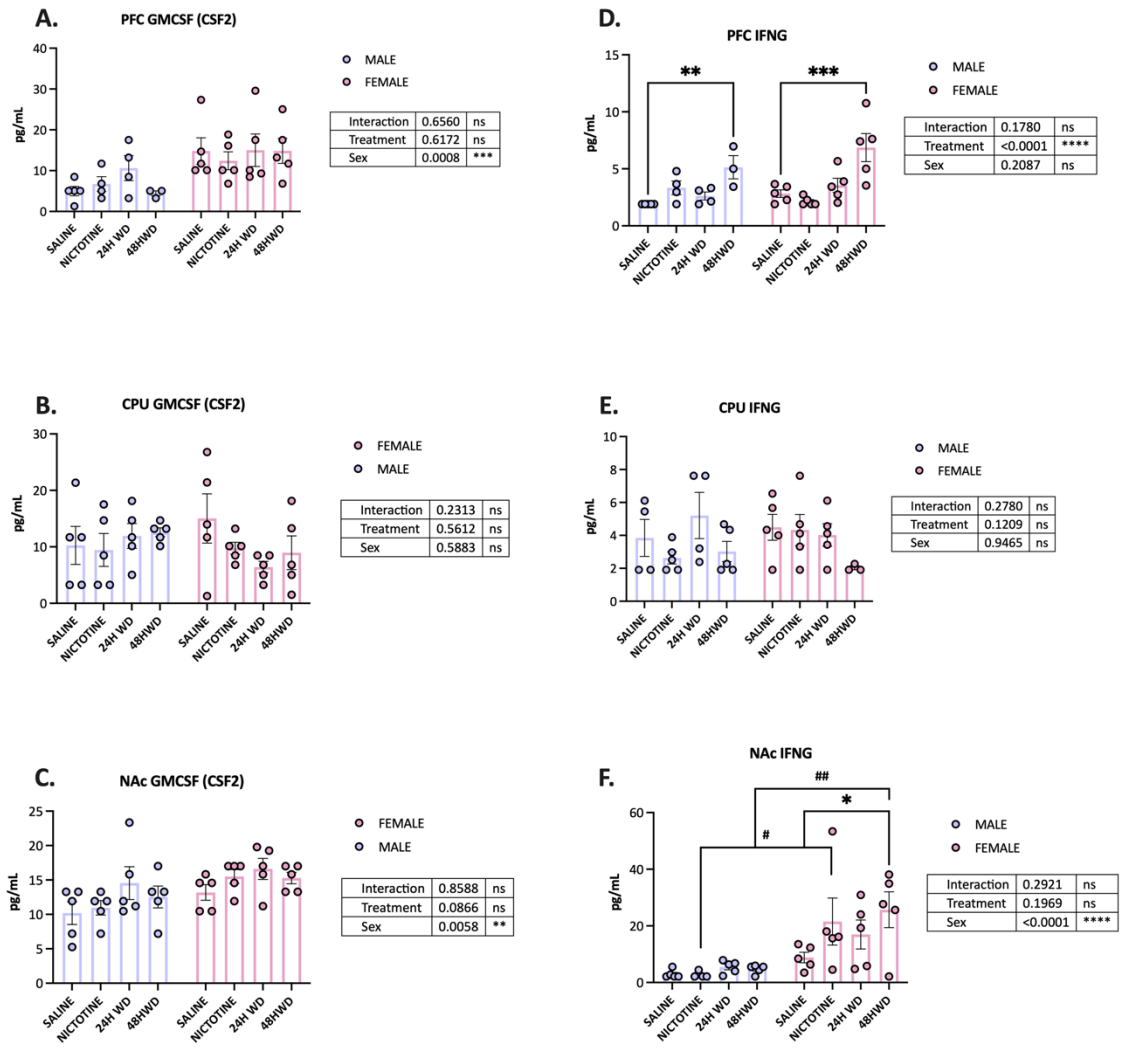

Figure A.24. Mouse brain region extracted protein assayed via Luminex®. A & D) PFC, (B & E) CPU, and (C & F) NAc portions with cytokine levels. Post hoc analysis between sexes by Šídák's ($^{\#}$P<0.05, $^{\#\#}$P<0.01, $^{\#\#\#}$ P<0.001, $^{\#\#\#\#}$P<0.0001) and within sex Dunnett's multiple comparisons test (*P<0.05, **P<0.01, ***P<0.001, ****P<0.0001) after two-way ANOVA.

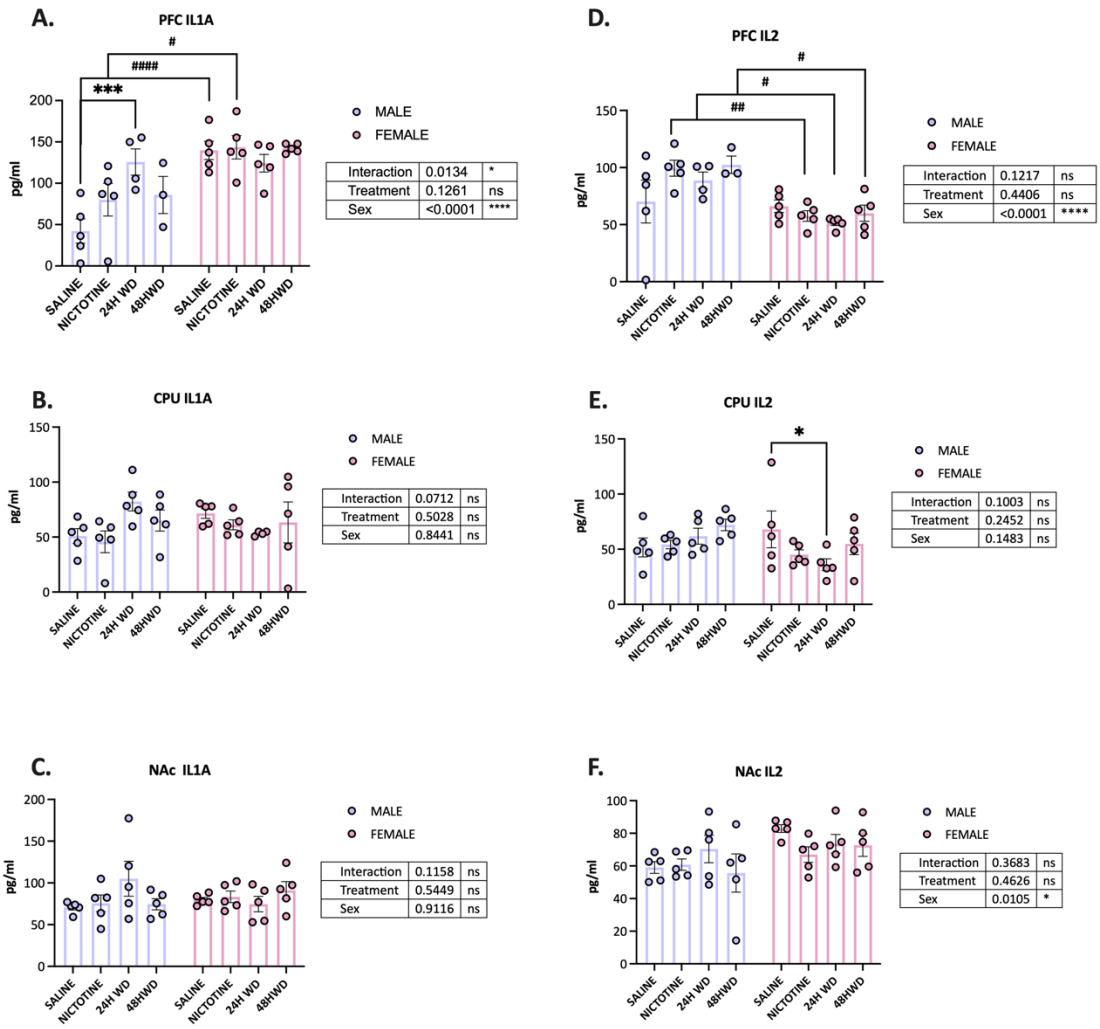

Figure A.25. Mouse brain region extracted protein assayed via Luminex®. A & D) PFC, (B & E) CPU, and (C & F) NAc portions with cytokine levels. Post hoc analysis between sexes by Šídák's ($^{\#}$P<0.05, $^{\#\#}$P<0.01, $^{\#\#\#}$ P<0.001, $^{\#\#\#\#}$P<0.0001) and within sex Dunnett's multiple comparisons test (*P<0.05, **P<0.01, ***P<0.001, ****P<0.0001) after two-way ANOVA.

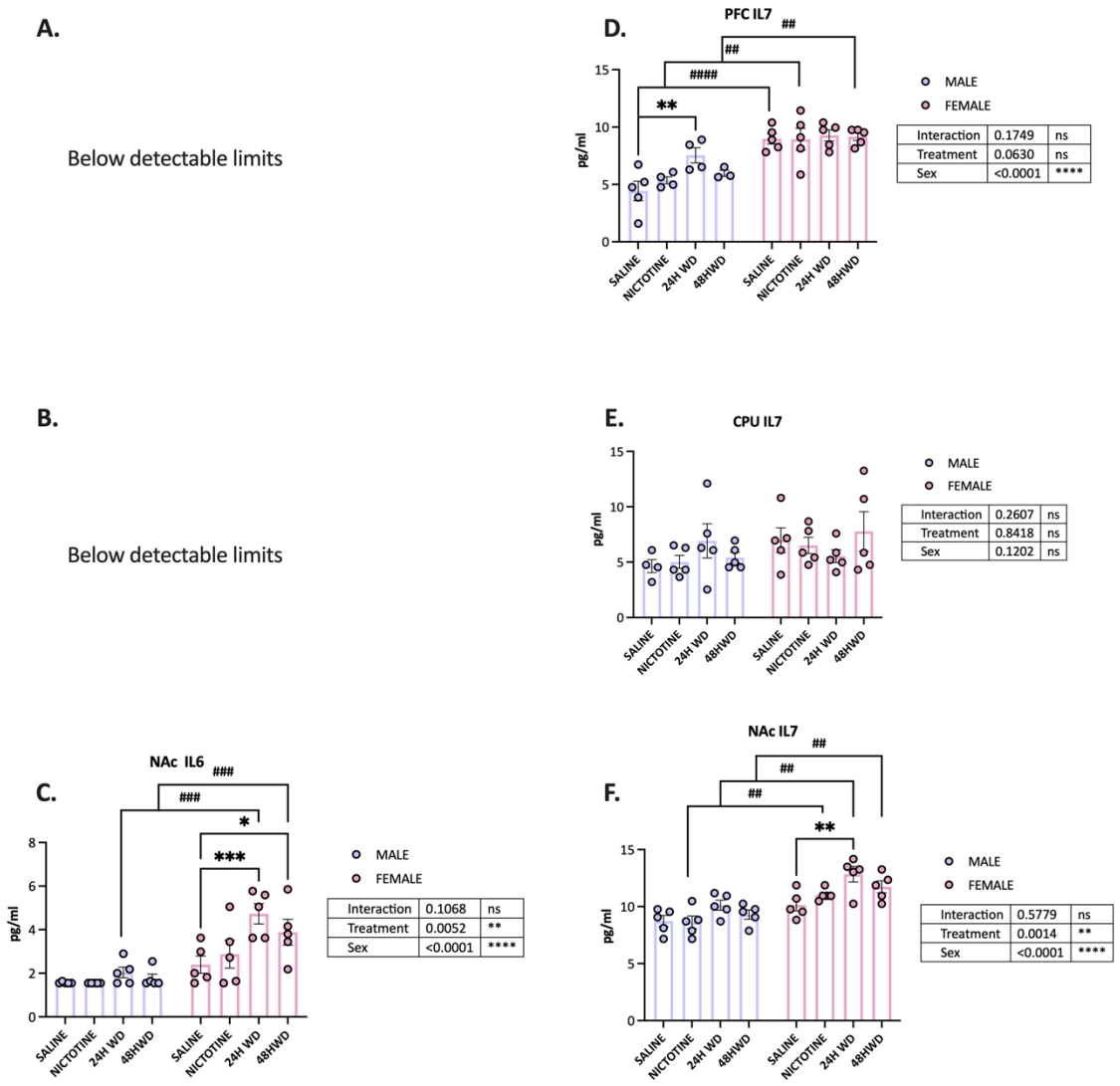

Figure A.26. Mouse brain region extracted protein assayed via Luminex®. A & D) PFC, (B & E) CPU, and (C & F) NAc portions with cytokine levels. Post hoc analysis between sexes by Šídák's ($^{\#}$P<0.05, $^{\#\#}$P<0.01, $^{\#\#\#}$ P<0.001, $^{\#\#\#\#}$P<0.0001) and within sex Dunnett's multiple comparisons test (*P<0.05, **P<0.01, ***P<0.001, ****P<0.0001) after two-way ANOVA.

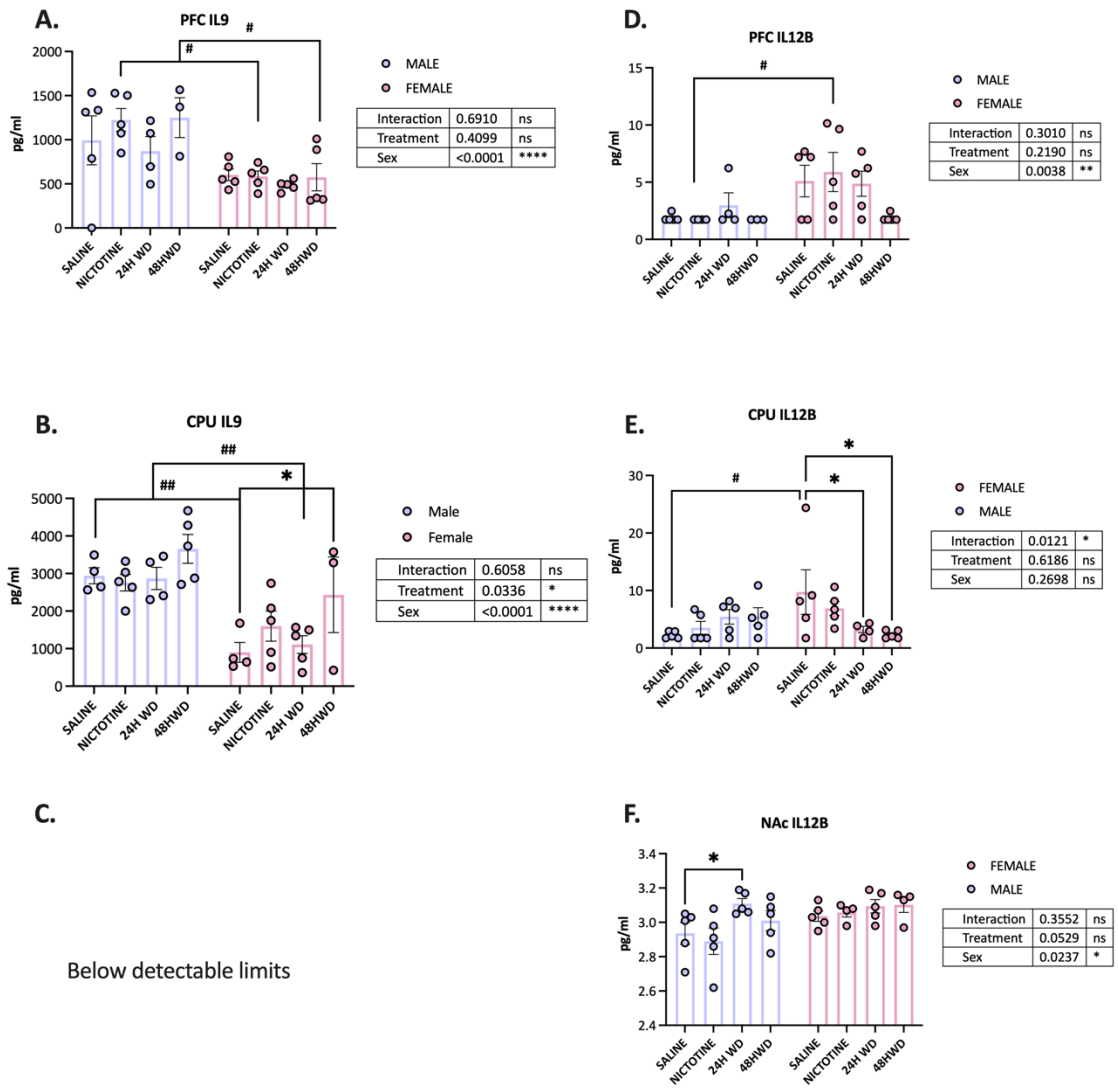

Figure A.27. Mouse brain region extracted protein assayed via Luminex®. A & D) PFC, (B & E) CPU, and (C & F) NAc portions with cytokine levels. Post hoc analysis between sexes by Šídák's ($^{\#}P<0.05$, $^{\#\#}P<0.01$, $^{\#\#\#}P<0.001$, $^{\#\#\#\#}P<0.0001$) and within sex Dunnett's multiple comparisons test (*P<0.05, **P<0.01, ***P<0.001, ****P<0.0001) after two-way ANOVA.

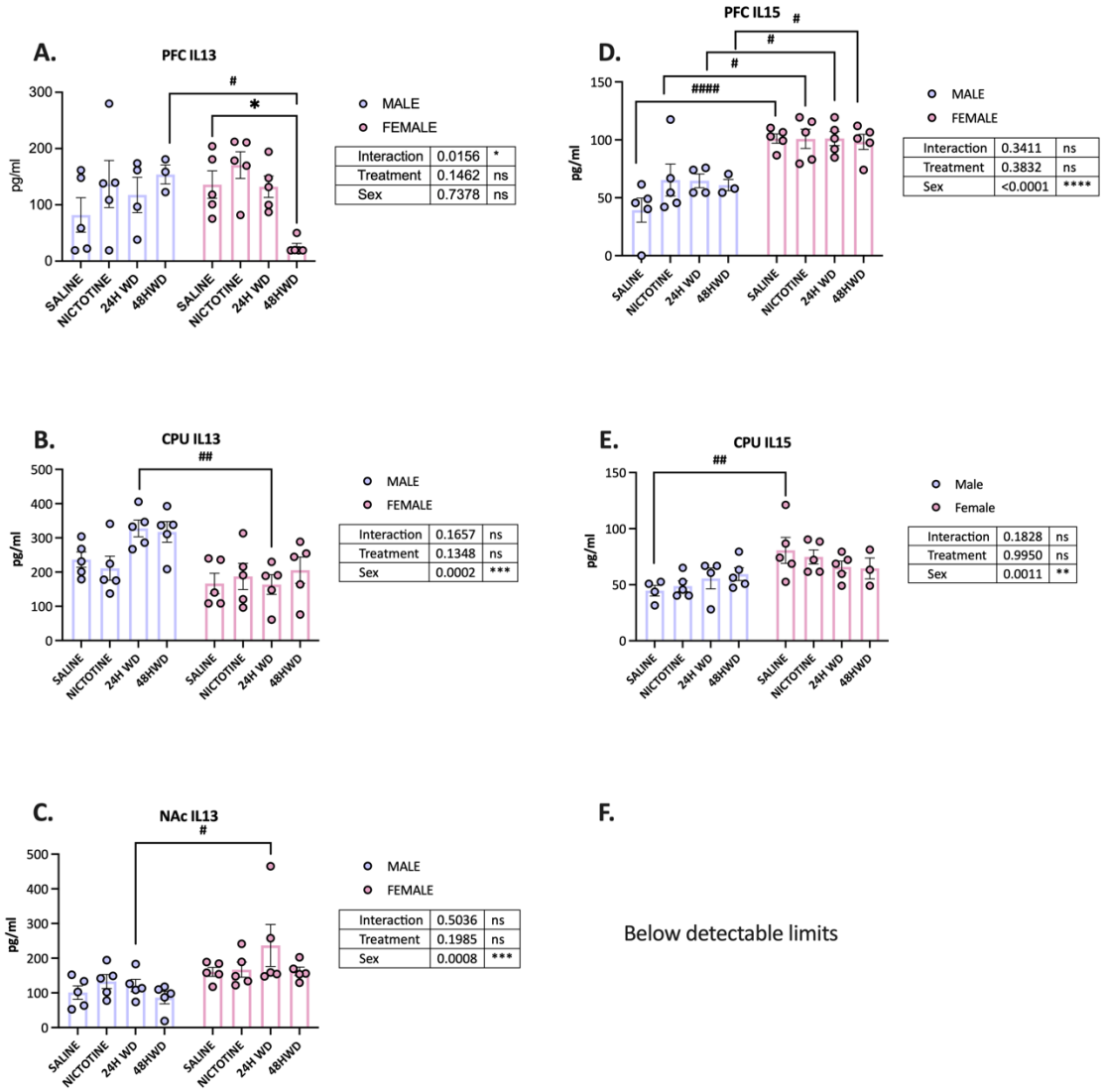

Figure A.28. Mouse brain region extracted protein assayed via Luminex®. A & D) PFC, (B & E) CPU, and (C & F) NAc portions with cytokine levels. Post hoc analysis between sexes by Šídák's ($^{\#}$P<0.05, $^{\#\#}$P<0.01, $^{\#\#\#}$ P<0.001, $^{\#\#\#\#}$P<0.0001) and within sex Dunnett's multiple comparisons test (*P<0.05, **P<0.01, ***P<0.001, ****P<0.0001) after two-way ANOVA.

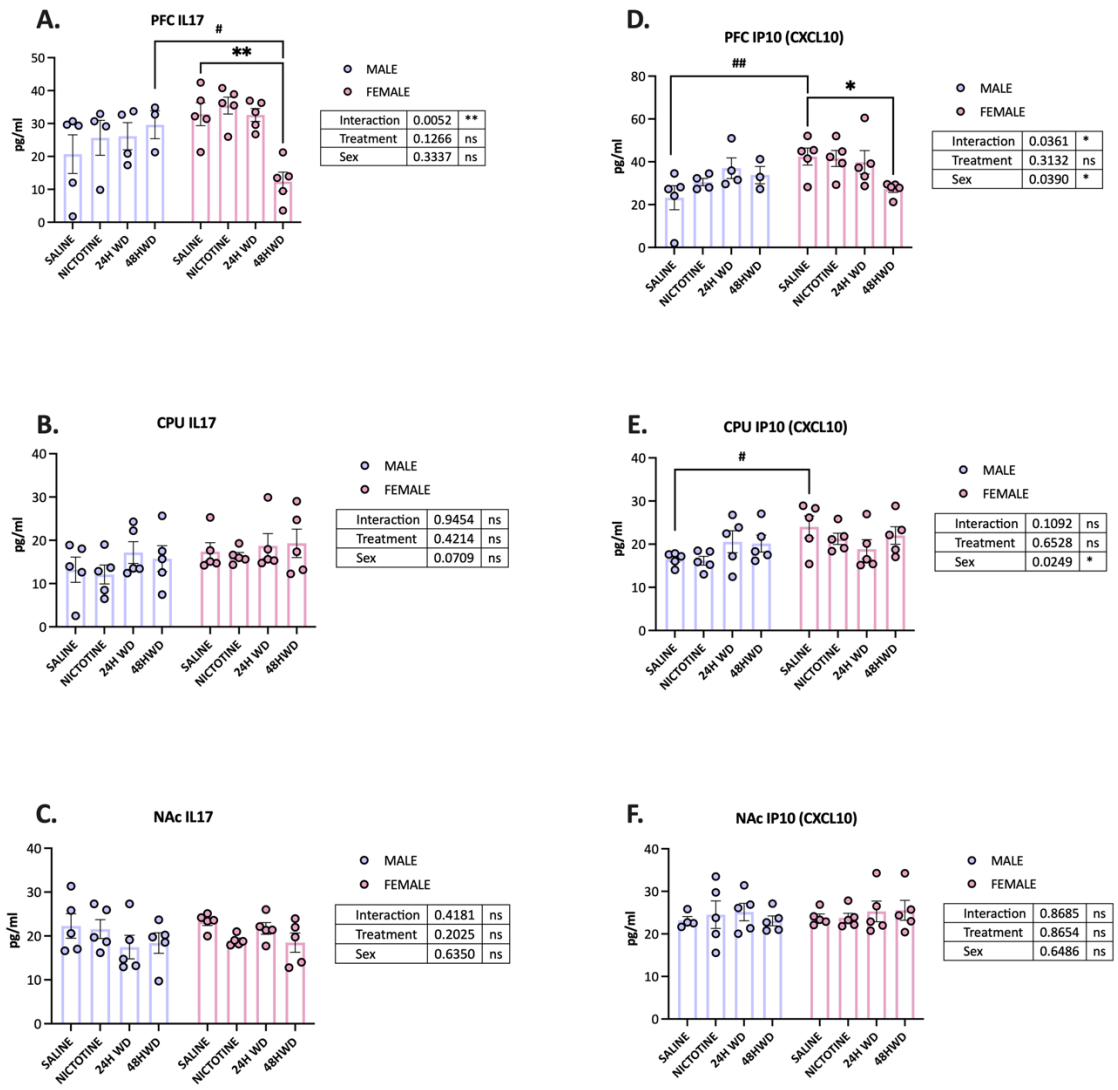

Figure A.29. Mouse brain region extracted protein assayed via Luminex®. A & D) PFC, (B & E) CPU, and (C & F) NAc portions with cytokine levels. Post hoc analysis between sexes by Šídák's ($^{\#}P<0.05$, $^{\#\#}P<0.01$, $^{\#\#\#}P<0.001$, $^{\#\#\#\#}P<0.0001$) and within sex Dunnett's multiple comparisons test (*P<0.05, **P<0.01, ***P<0.001, ****P<0.0001) after two-way ANOVA.

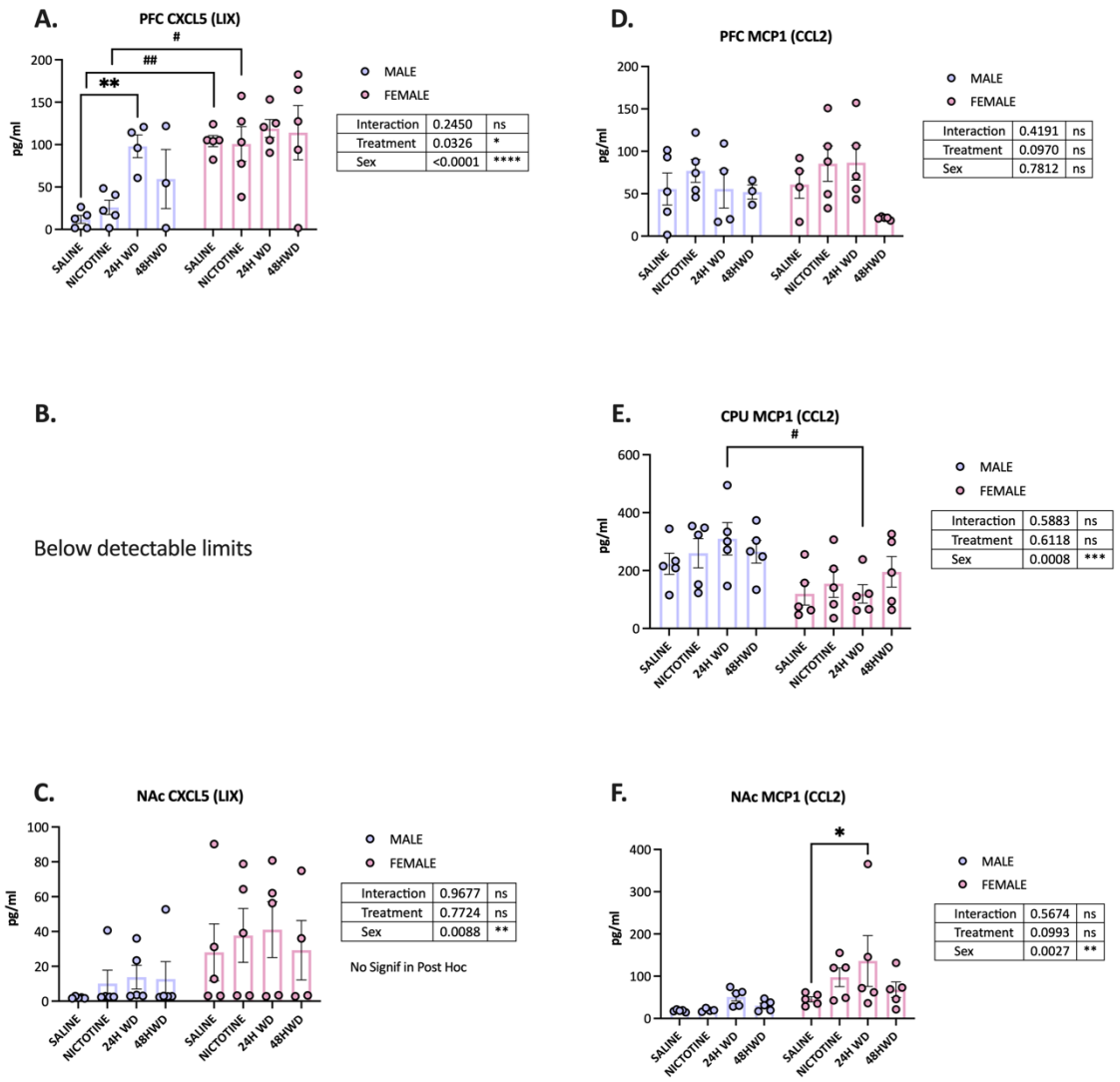

Figure A.30. Mouse brain region extracted protein assayed via Luminex®. A & D) PFC, (B & E) CPU, and (C & F) NAc portions with cytokine levels. Post hoc analysis between sexes by Šídák's ($^{\#}P<0.05$, $^{\#\#}P<0.01$, $^{\#\#\#}P<0.001$, $^{\#\#\#\#}P<0.0001$) and within sex Dunnett's multiple comparisons test (*P<0.05, **P<0.01, ***P<0.001, ****P<0.0001) after two-way ANOVA.

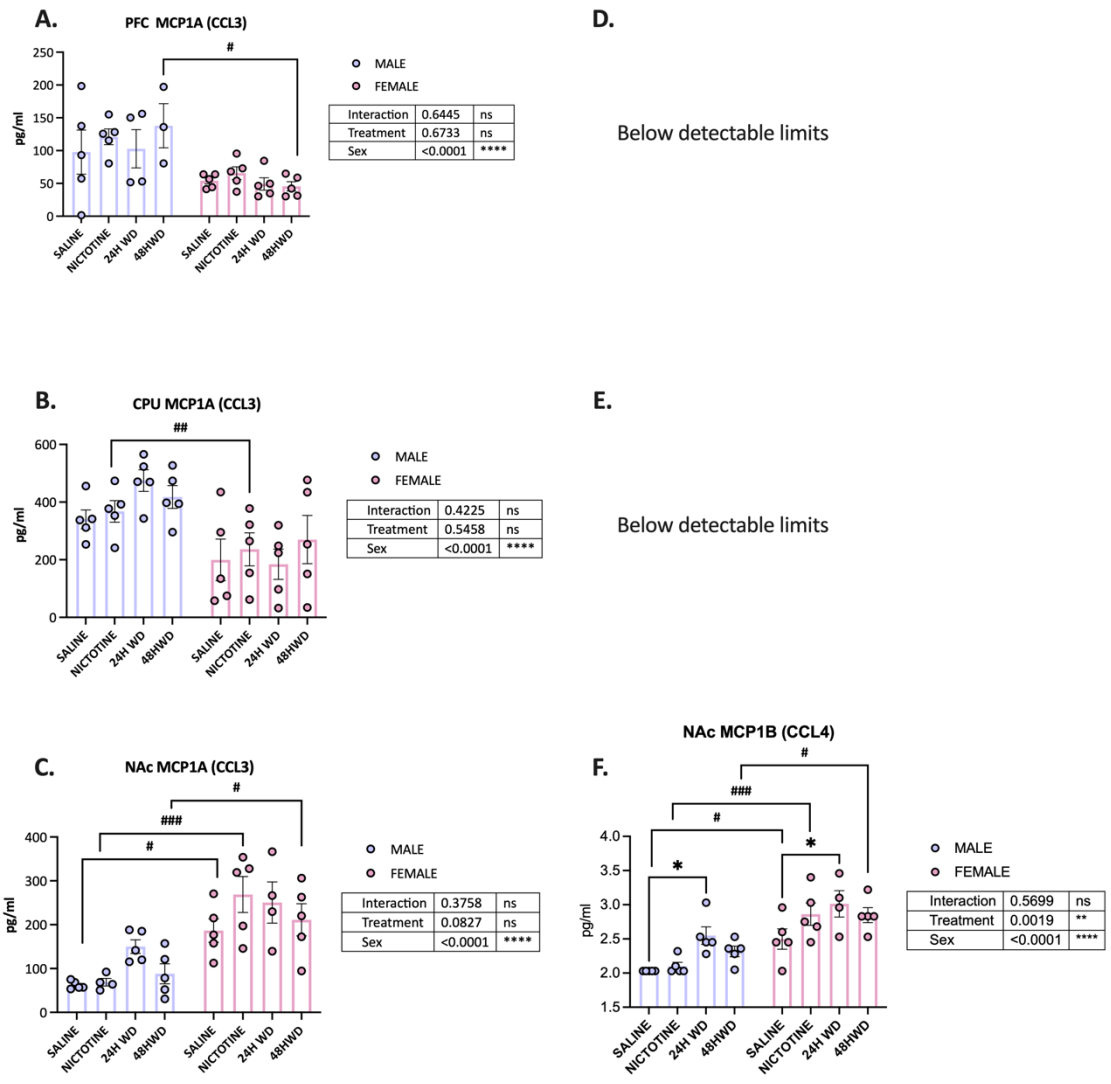

Figure A.31. Mouse brain region extracted protein assayed via Luminex®. A & D) PFC, (B & E) CPU, and (C & F) NAc portions with cytokine levels. Post hoc analysis between sexes by Šídák's ($^{\#}$P<0.05, $^{\#\#}$P<0.01, $^{\#\#\#}$ P<0.001, $^{\#\#\#\#}$P<0.0001) and within sex Dunnett's multiple comparisons test (*P<0.05, **P<0.01, ***P<0.001, ****P<0.0001) after two-way ANOVA.

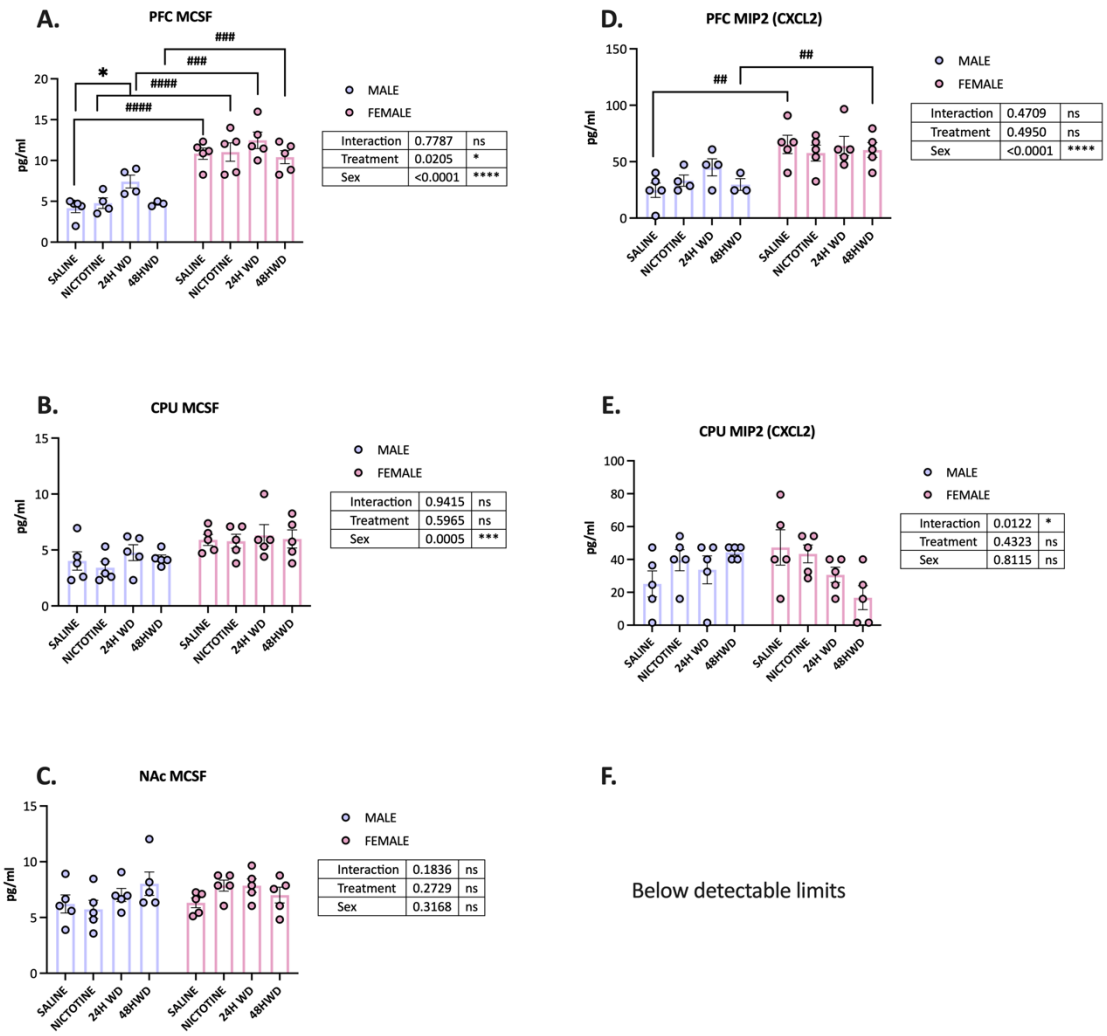

Figure A.32. Mouse brain region extracted protein assayed via Luminex®. A & D) PFC, (B & E) CPU, and (C & F) NAc portions with cytokine levels. Post hoc analysis between sexes by Šídák's ($^{\#}$P<0.05, $^{\#\#}$P<0.01, $^{\#\#\#}$ P<0.001, $^{\#\#\#\#}$P<0.0001) and within sex Dunnett's multiple comparisons test (*P<0.05, **P<0.01, ***P<0.001, ****P<0.0001) after two-way ANOVA.

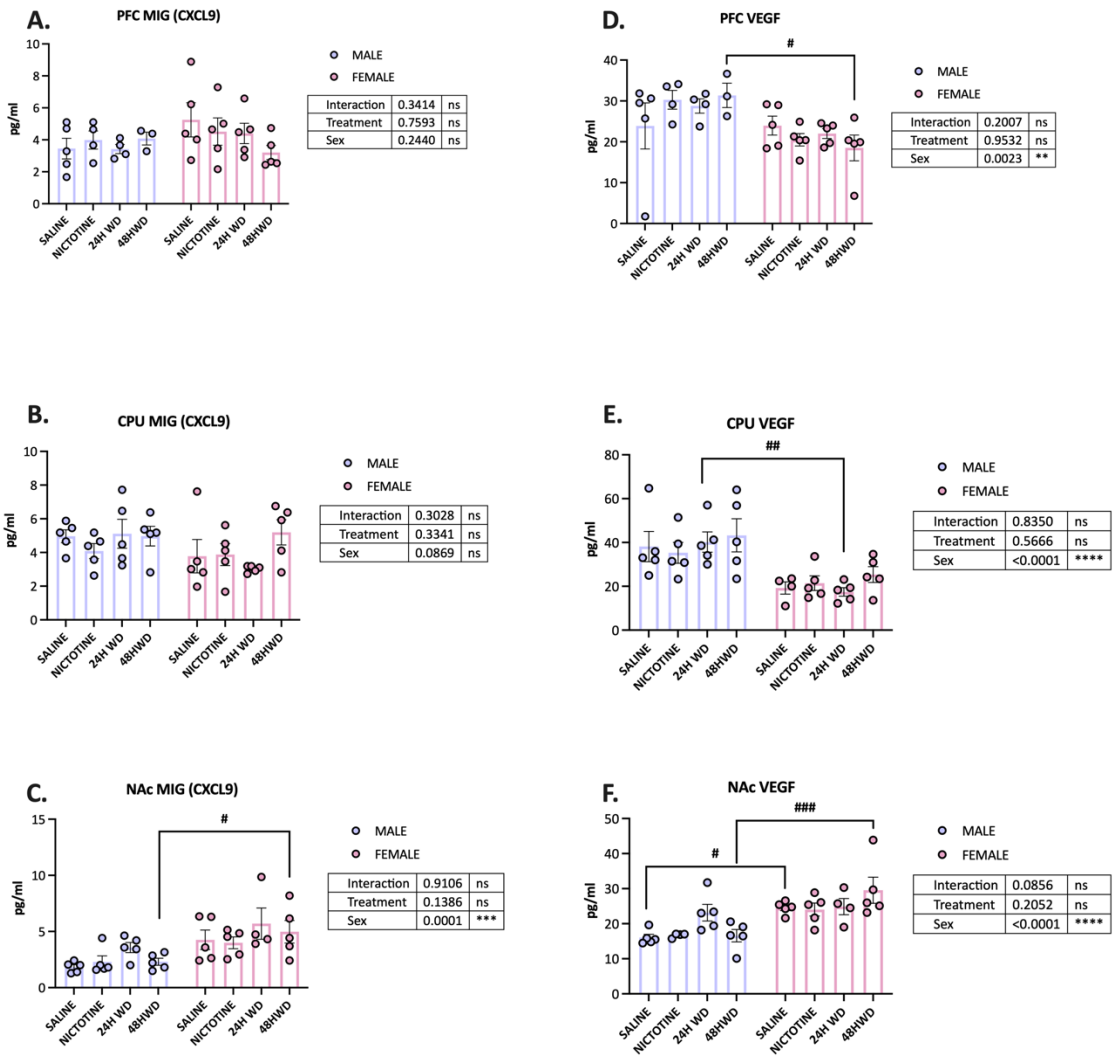

Figure A.33. Mouse brain region extracted protein assayed via Luminex®. A & D) PFC, (B & E) CPU, and (C & F) NAc portions with cytokine levels. Post hoc analysis between sexes by Šídák's ($^{\#}$P<0.05, $^{\#\#}$P<0.01, $^{\#\#\#}$ P<0.001, $^{\#\#\#\#}$P<0.0001) and within sex Dunnett's multiple comparisons test (*P<0.05, **P<0.01, ***P<0.001, ****P<0.0001) after two-way ANOVA.